Imperial College London

Microscopy of Interactions at the Cell-Material and Cell-Matrix Interface

by Catherine Sarah Hansel

Supervisors: Professor Molly Stevens & Professor Tony Cass

Submitted in Accordance with the Requirements for the Degree of Doctor of Philosophy and the Diploma of Imperial College

The Department of Chemistry

Imperial College London

September 2017

Abstract

This PhD project investigates how mechanical and biochemical cues from the microenvironment regulate fundamental aspects of cell behaviour, using both synthetically and naturally derived systems, and places a particular emphasis on the application of microscopy as a means to elucidate these interactions.

Firstly, porous silicon nanoneedle (nN) arrays are used as a synthetic material to study cellular mechanotransduction; the mechanism by which cells transduce mechanical forces into biochemical signals. Nanoneedles are able to tightly interface with cells and can therefore act as a tool to directly probe and manipulate cells. The interaction between nN and two primary human cell types is assessed: human umbilical vein endothelial cells (HUVECs) and human mesenchymal stem cells (hMSCs). In this work, nN are shown to interact with multiple organelles in primary human cells and these findings have implications for the design of nanomaterial biointerfaces to study and influence cell behaviour and to administer cargo.

Secondly, a naturally-cleaved extracellular matrix (ECM) protein fragment (laminin-β1 fragment) is used to explore how cryptic ECM sites affect biochemical signalling pathways in cells. The epithelial-to-mesenchymal transition (EMT) is initiated by transforming growth factor beta (TGF-β) in normal murine mammary gland epithelial (NMuMG) cells in the presence and absence of a laminin β1-fragment, and the effects of the laminin β1-fragment on EMT are explored. This includes an assessment of the biochemical signalling pathways involved in EMT, and cell migration studies. By studying the molecular basis of EMT through a range of microscopy techniques, insight can be provided into a process that is pivotal in cancer metastasis and that is a feature of inflammatory and fibrotic responses.

Declaration of originality

I, Catherine Sarah Hansel, declare that the original scientific content contained within this thesis was acquired and analysed by myself at either Imperial College London, UK or at the Karolinksa Institutet, Stockholm, Sweden, unless otherwise stated. All collaborative efforts are noted by name and affiliation in the text.

The copyright of this thesis rests with the author and is made available under a Creative Commons Attribution Non-Commercial No Derivatives license. Researchers are free to copy, distribute or transmit the thesis on the condition that they attribute it, that they do not use it for commercial purposes and that they do not alter, transform or build upon it. For any reuse or redistribution, researchers must make clear to others the license terms of this work

Acknowledgements

I would like to thank Professor Molly Stevens for inspiring and supporting me throughout my PhD at Imperial College London. It has been a pleasure to work for the Stevens' group, and I have enjoyed collaborating with many of the creative, lively and intelligent members of the group. Special thanks go to Dr. Spencer Crowder, Dr. Ciro Chiappini, Dr. Christine-Maria Horejs, Dr. Carolyn Schutt Ibsen and Dr. Subinoy Rana for guiding me during my PhD. I would also like to thank Sabrina Skeete and Dr. Benjamin Pierce for their administrative support. Further mention goes to the staff at Imperial College Facility for Light Microscopy (FILM), Stephen Rothery and Dr. Debora Keller, who ignited my passion for microscopy, and to Petter Ranefall at Uppsala Universitet, Sweden, for helping me with image analysis software. Importantly, I acknowledge my secondary supervisor Professor Tony Cass, who has offered me pearls of wisdom over the course of my PhD and who has always been available when help was required.

I would also like to thank my many friends in the Stevens Group and beyond, especially Sahana Gopal; I will miss our lunch breaks where we discussed Science and much more. Finally, I'd like to thank my Dad, for teaching me how research is a search for the truth, and always encouraging me to think outside the box. In addition, I thank my Mum for moral support, and my Swedish boyfriend Wiking who has kept me sane while preparing this thesis!

Funding for this PhD has come from the Engineering and Physical Sciences Research Council (EPSRC) as part of the Institute of Chemical Biology Centre for Doctoral Training.

Table of Contents

1. Introduction: cells and the extracellular space 21
1.1 The extracellular matrix 22
1.2 Organelles connected to the extracellular matrix 23
1.2.1 Integrins 25
1.2.2 Focal adhesions 26
1.2.3 The actomyosin cytoskeleton 28
1.2.4 The nucleus 32
1.3 Mechanotransduction and the cellular response to extracellular cues 35
1.3.1 The tensegrity model 36
1.3.2 Force and the extracellular matrix-integrin-cytoskeleton link 36
1.3.3 Force and the nucleus 38
1.3.4 Extracellular matrix stiffness 40
1.4 Methods to study mechanotransduction and cell-matrix interactions 44
1.4.1 Materials to assess surface chemistry 45
1.4.2 Materials to assess topographical cues 46
1.4.3 Materials to assess mechanotransduction 47
1.4.4 Methods to assess mechanotransduction and cell-matrix interactions 50
1.4.5 Limitations of mechanobiology and cell-matrix interaction studies 54
1.5 Scope of the thesis 57

2 Microscopy of the interactions at the cell-nanoneedle interface 58
2.1 Introduction 59
2.1.1 Nanoneedle fabrication 59
2.1.2 Functionalisation of nanoneedles 62
2.1.3 Intracellular access 63
2.1.4 Biological applications of nanoneedles 68
2.1.5 Cell properties on nanoneedle interfacing 71
2.1.6 Porous silicon nanoneedle arrays 75
2.2 Chapter aims 78
2.3 Materials and Methods 78
2.3.1 Nanoneedle preparation 78
2.3.2 Cell culture 79
2.3.3 Latrunculin B treatment 80
2.3.4 Immunofluorescent labelling and imaging 80
2.3.5 Cytoskeleton stabilisation buffer treatment 81
2.3.6 Live cell imaging 81
2.3.7 Scanning electron microscopy 82
2.3.8 Quantitative real-time polymerase chain reaction (qRT-PCR) 82
2.3.9 Quantification of lamin signal 83
2.3.10 Quantitative cell morphology analysis 84
2.3.11 Feature extraction 85
2.3.12 Linear discriminant analysis 87
2.3.13 Quantifying actin stress fibres 87
2.3.14 Focal adhesion quantification 87
2.3.15 YAP localisation analysis 88
2.3.16 Statistical analysis 89
2.4 Results 90
2.4.1 Cell viability 90
2.4.2 Cell morphology and the actin cytoskelton 91
2.4.3 Focal adhesions and phosphorylated myosin light chain 96

2.4.4 YAP/TAZ mechanosensors 101
2.4.5 The nucleus 104
2.4.6 Nuclear lamins 106
2.4.7 Lamin quantification 108
2.4.8 Nanoneedle degradation 110
2.5 Discussion 112
2.6 Conclusion 115
2.7 Future directions 115

3 Microscopy of the cell-matrix interface 117
3.1 Introduction 118
3.1.1 The epithelial-to-mesenchymal transition 118
3.1.2 The basement membrane 119
3.1.3 Matrix metalloproteinases 127
3.1.4 α3β1-integrin 131
3.1.5 TGF-β1 induced epithelial-to-mesenchymal transition 133
3.1.6 The laminin β1-fragment 142
3.2 Chapter Aims 144
3.3 Materials and Methods 145
3.3.1 TGF-β1 reporter cells 145
3.3.2 TGF-β1 reconsitution 146
3.3.3 Cell culture 146
3.3.4 Recombinant laminin β1-fragment production 146
3.3.5 Confocal and high content imaging 147
3.3.6 Laminin β1-fragment labelling 149
3.3.7 Live cell imaging 149
3.3.8 Immunoblotting 150
3.3.9 Nuclear and cytoplasmic extraction 151
3.3.10 Statistical analysis 151
3.4 Results 152
3.4.1 System verification and optimisation 152
3.4.2 α3β1–integrin and laminin β1-fragment interactions 153
3.4.3 TGF-β1/Smad canonical signalling 156
3.4.4 NF-κB p65 signalling 159
3.4.5 Cell migration 161
3.4.6 Focal adhesions 162
3.4.7 Matrix metalloproteinases and basement membrane breakdown 165
3.4.8 YAP and lamin-A 168
3.5 Discussion 170
3.6 Conclusion 173
3.7 Future directions 173

4 Final conclusions and future directions 177
4.1 Porous silicon nanoneedle arrays as a novel tool to manipulate cell mechanobiology 177
4.2 The laminin β1-fragment and its effect on TGF- β1 signalling and EMT pathways 181
4.3 Concluding remarks 185

5 References 187

6 Appendices 233
6.1 Figure reproduction permissions 233
6.2 List of publications 267

List of Figures

Figure 1.1: Cell-extracellular matrix interactions 22
Figure 1.2: The extracellular matrix is physically connected to the cell nucleus..... 24
Figure 1.3: Integrin activation 26
Figure 1.4: The molecular architecture of focal adhesion complexes..... 28
Figure 1.5: Matrix stiffness affects cell signalling pathways and cell phenotype..... 41
Figure 2.1: Fabrication strategies for nanoneedles..... 60
Figure 2.2: The cell–nanoneedle interface..... 65
Figure 2.3: Representative images of cell behaviour on nanoneedle arrays. 72
Figure 2.4: Porous silicon nanoneedle arrays strongly interface with the cell and can deliver cargo in vitro and in vivo 77
Figure 2.5: Nanoneedle arrays minimally affect cell viability..... 91
Figure 2.6: Nanoneedle arrays interact with cells and affect cell morphology..... 93
Figure 2.7: Linear discriminant analysis can distinguish cells on flat and nanoneedle substrates. 94
Figure 2.8: Nanoneedle arrays remodel the actin cytoskeleton 95
Figure 2.9: Actin rings form at the sites of nN interaction. 96
Figure 2.10: Nanoneedle arrays affect vinculin focal adhesion formation 98
Figure 2.11: Nanoneedle arrays affect paxillin focal adhesion formation. 100
Figure 2.12: Nanoneedle arrays affect phosphorylated myosin light chain levels..... 101
Figure 2.13: Nanoneedle arrays affect yes-associated protein (YAP) localisation and activity 102
Figure 2.14: Nanoneedle arrays cause a reduction in YAP correlation with cell area..... 103
Figure 2.15: YAP localisation is controlled by the actomyosin machinery on nN arrays..... 104
Figure 2.16: Nanoneedle arrays interact with the nucleus. 105
Figure 2.17: Nanoneedle arrays do not cause nuclear leakage..... 106
Figure 2.18: Nanoneedle arrays increase levels of *LMNA* but not *LMNB* 107
Figure 2.19: Lamin-A protein levels increase at nanoneedle locations, but lamin-B levels do not 108
Figure 2.20: Quantification of lamin-A vs. lamin-B localisation. 109
Figure 2.21: Nanoneedles degrade at 48 hours 110
Figure 2.22: Following 48 hours of culture on nN, the flat phenotype is restored 111
Figure 2.23: Quantification of YAP localisation and focal adhesion density following 48 hours of cell culture on nN. 112
Figure 3.1: The epithelial to mesenchymal transition..... 119
Figure 3.2: The structure of the basement membrane..... 121
Figure 3.3: Canonical TGF-β Smad signalling..... 136
Figure 3.4: TGF-β nuclear factor kappa-light-chain-enhancer of activated B cells (NF-κB) signalling 141
Figure 3.5: The laminin β1-fragment..... 142
Figure 3.6: TGF-β1 and NMuMg cell proliferation and phenotype 153
Figure 3.7: α3-integrin immunofluorescence labelling optimisation 155
Figure 3.8: Laminin β1-fragment labelling. 156
Figure 3.9: pSmad3 localisation in response to the laminin β1-fragment 157
Figure 3.10: E-cadherin response to the laminin β1-fragment. 158
Figure 3.11: Smad7 localisation and intensity in response to the laminin β1-fragment..... 159

Figure 3.12: NF-κB p65 localisation in response to the laminin β1-fragment 160
Figure 3.13: Cell migration in response to the laminin β1-fragment. 161
Figure 3.14: Focal adhesion number on laminin β1-fragment addition 163
Figure 3.15: Focal adhesion kinase and its interaction with vinculin and the laminin β1-fragment 164
Figure 3.16: Membrane type 1 matrix metalloproteinase immunofluorescence optimisation 166
Figure 3.17: Cortactin response to the laminin β1-fragment. 167
Figure 3.18: Basement membrane breakdown in response to TGF-β1 treatment 168
Figure 3.19: Yes associated protein (YAP) response to the laminin β1-fragment 169
Figure 3.20: Lamin-A response to the laminin β1-fragment. 170
Figure 4.1: Summary of chapter 2 results: nN arrays alter primary human cell mechanobiology 178
Figure 4.2: Summary of chapter 3 results: The laminin β1-fragment and its effect on TGF-β1 signalling 182

List of Tables

Table 1.1: The properties of membrane protrusion structures 29
Table 2.1: Cell-nanoneedle interfacing strategies 66
Table 2.2: Antibody information for immunofluorescent labelling 81
Table 2.3: qRT-PCR primer sequences 83
Table 3.1: Antibody information for immunofluorescent labelling 149

List of Movies

Movie 2.1: Actin rings form at various heights along the nN 95
Movie 2.2: Actin rings are dynamic and short-lived 95
Movie 3.1: Cell migration in response to the laminin β1-fragment 161

List of Abbreviations

Abl	Abelson kinase
AEC	alveolar epithelial cells
AFM	atomic force microscopy
Akt	protein kinase B
ANKRD1	ankyrin repeat domain-1
ANOVA	one-way analysis of variance
AP1	activator protein-1
APTES	3-amino-propyltriEthoxysilane
APTMS	3-amino-propyltriMethoxysilane
ATP	adenosine triphosphate
BIT-FET	branched intracellular nanotube field effect transistor
BM	basement membrane
BMP	bone morphogenetic protein
BSA	bovine serum albumin
CAM 120/80	calcium dependent adhesion protein
CBP	cAMP-regulated-enhancer-binding protein
CD147/EMMPRIN	extracellular matrix metalloproteinase inducer
Cdc42	cell division control protein 42 homolog
CH3	cadherin homology region 3
CHO	Chinese hamster ovary
CSK	cytoskeletal stabilisation buffer
CT-B	cholera toxin B
CTGF	connective tissue growth factor
Dab2	disabled-2
DAPI	4',6-diamidino-2-phenylindole
DNA	deoxyribonucleic acid
DPPC	Dipalmitoylphosphatidylcholine
DRIE	deep reactive ion etch
E-cadherin	epithelial cadherin

ECM	extracellular matrix
EGF	epidermal growth factor
EGFP	enhanced green fluorescent protein
EHS	Engelbreth-Holm-Swarm
EMMPRIN	extracellular matrix metalloproteinase inducer
EMT	epithelial to mesenchymal transition
ERK	extracellular signal-regulated kinase
ESC	embryonic stem cells
FA	focal adhesion
FAK	focal adhesion kinase
FET	field effect transistor
FGF	fibroblast growth factor
FIB	focused ion beam
FIB-SEM	focused-ion beam scanning electron microscopy
FITC	fluorescein isothiocyanate
Fragment	laminin β1-fragment
FRAP	fluorescence recovery after photobleaching
FRET	fluorescence resonance energy transfer
Fz	frizzled
GAGs	glycosaminoglycans
GAPDH	glyceraldehyde-3-phosphate dehydrogenase
GBR2	growth factor receptor bound protein 2
GFP	green fluorescent protein
GOI	gene of interest
GPI	glycosylphosphatidylinocitol
GRB2	growth factor receptor bound protein 2
GSD	ground state depletion
HCI	high content imaging
HEK293	human embryonic kidney 293 cell
HELA	Henrietta Lacks cervical cancer-derived cell line
HGPS	Hutchinson-Gilford progeria syndrome

HKG	housekeeping gene
hMSC	human mesenchymal stem cell
hnRNP	heterogeneous nuclear ribonucleoprotein
HUVEC	human umbilical vein endothelial cell
IF	intermediate filament
Ig	immunoglobulin
IKK	inhibitor of IκB kinase
IL-1	interleukin-1
ILK	integrin-linked kinase
INM	inner nuclear membrane
IRSp53	insulin receptor substrate protein of 53 kDa
IκB	inhibitor of κB kinases
JNKs	c-Jun amino-terminal kinases
KASH	Klarsicht, ANC-1, Syne Homology
LAP	latency-associated peptide
LatB	latrunculin B
LATS 1/2	large tumour suppressor kinase ½
Lef	lymphocyte enhancer factor
LINC	linker of nucleoskeleton and cytoskeleton
LMNA	lamin-A
LMNB	lamin-B
LN	laminin
LRP	lipoprotein receptor-related protein
LSPR	localised surface plasmon resonance
MACE	metal-assisted chemical etch
MAL	T-cell differentiation protein
MALDI	matrix-assisted laser desorption/ionisation
MAP2	microtubule-associated protein 2
MAPK	mitogen-activated protein kinase
MKL1	megakaryoblastic acute leukaemia factor-1
MLC	myosin-light-chain

MMP	matrix metalloproteinases
MOMENT	MOlecular MEter with nanowire Technology
MPC	magnetic pulling cytometry
MPCD/ JMD	membrane proximal cytoplasmic/conserved domain
mRNA	messenger ribonucleic acid
MSC	mouse stromal cell
MSCs	mesenchymal stem cells
MST 1/2	MEN-SIN-TAN family 1/2
MT1-MMP	membrane type 1 matrix metalloproteinase
MTC	magnetic twisting cytometry
mTOR1	mechanistic target of rapamycin-1
MTT	3-(4,5-dimethylthiazol-2-yl)-2,5-diphenyltetrazolium bromide
N-cadherin	neural cadherin
NF-κB	nuclear factor kappa-light-chain-enhancer of activated B cells
NIR	near infrared
NMuMg	normal mouse mammary gland epithelial cell line
nN	nanoneedle
nN-B	nanoneedle bottom technique
nN-T	nanoneedle top technique
NPC	neural progenitor cell
NS	nanostructure
NW	nanowire
n-WASP	neural-Wiskott-Aldrich syndrome
ONM	outer nuclear membrane
PAK2	p21 activated kinase
PALM	photoactivation localisation microscopy
PAX	paxillin
PBS	phosphate-buffered saline
PCL	poly(e-caprolactone)
PDGF	platelet-derived growth factor
PDMS	poly(dimethylsiloxane)

PG	proteoglycan
PI	phosphoinositide
PI3K	phosphatidylinositol-3-kinase
PIP2	phosphatidylinositol 4,5-bisphosphate
PKC	protein kinase C
pPax	phosphorylated paxillin
QD	quantum dot
qPCR	quantitative polymerase chain reaction
qRT-PCR	quantitative real-time polymerase chain reaction
Rac1	ras-related C3 botulinum toxin substrate 1
Raf	rapidly accelerated fibrosarcoma
RAF6	receptor-associated factor 6
RAP1	ras-related protein 1
RARG	transcription factor retinoic acid receptor γ
Ras	GTP-binding switch protein
RESOLFT	reversible saturable optical fluorescent transitions
RGD	Arg-Gly-Asp
RhoA	ras homolog gene family, member A
RNA	ribonucleic acid
ROCK	rho-associated protein kinase
ROS	reactive oxygen species
RSD	relative standard deviation
SAM	self-assembled monolayer
SAPK	stress activated protein kinase
SAV1	Salvador family WW domain containing protein 1
SECM	scanning electron confocal microscopy
SEM	scanning electron microscopy
SHCA	Src homology 2 domain containing transformin A
SIM	structured illumination microscopy
SIP-1	smad-interacting protein
SLRP	small leucine-rich repeat proteoglycan

Smad	small mothers against decapentaplegic
snai1	snail
snai2	slug
SOS	son of sevenless
SRF	serum response factor
SRI	super-resolution imaging
SRM	super-resolution microscopy
STAT	signal transducer and activator of transcription
STED	stimulated emission depletion microscopy
SUN	Sad1p, UNC-84
SYNE1	nesprin-1
SYNE2	nesprin-2
TAILS	terminal amine isotopic labelling of substrates
TAK1	transforming growth factor-beta-activated kinase-1
TAMRA	5 carboxy-tetramethylrhodamine N-succinimidyl ester
TAZ	transcriptional coactivator with PDZ-binding motif/ WWTR1
TCF	T-cell transcription factor
TEAD	TEA domain family member 1
TEM	transmission electron microscopy
TF	transcription factor
TFM	traction force microscopy
TGF-β	transforming growth factor-beta
TGF-βR	transforming growth factor-beta receptor
TIMP	tissue inhibitor of metalloproteinases
TIRF	total internal reflection fluorescence microscopy
TNF-α	tumour necrosis factor-α
TOF	time-of-flight
TRAF6	TNF receptor-associated factor 6
UDP-GalNAz	UDP-*N*-azidoacetylgalactosamine
uPAR	urokinase receptor
UV	ultra-violet

VASP	vasodilator-stimulated phosphoprotein
WASP	Wiskott-Aldrich syndrome protein
VCL	vinculin
WGA	wheat germ agglutinin
WIP	WASP-interacting protein
VLS	vapour-liquid-solid
VNEA	vertical nanowire electrode array
YAP	yes-associated protein
ZO1	zonula occludens-1 or tight junction protein-1
ZYX	zyxin

1. Introduction: cells and the extracellular space

Cells and the extracellular matrix (ECM) have a reciprocal relationship[1]. Cells deposit, maintain and remodel the ECM in order to maintain tissue-level structural integrity and functionality[2,3]. In return, the ECM exhibits physical and chemical cues which influence many cellular functions; such as cell survival, proliferation, and differentiation[4,5]. Transmembrane integrin proteins interact with the ECM, inducing a number of biochemical and mechanical signalling cascades involving focal adhesion (FA) complexes and the actomyosin cytoskeleton. Some of these structures can also act as mechanotransducers[6], converting the applied force into biochemical signals (**Figure 1.1**). Misregulation of matrix-cell crosstalk plays a major role in disease, such as in cancer and fibrosis[3,7], and it is therefore important that the mechanisms involved in cell-matrix crosstalk are understood.

In this introduction, the ECM and the organelles which are connected to, and affected by, the ECM are described. These organelles include integrins, FAs, the actin cytoskeleton, the linker of nucleoskeleton and cytoskeleton (LINC) complex, the nuclear lamina and the nucleus. Next, mechanotransduction, the mechanism by which cells sense and transduce mechanical forces into biochemical signals[8], is explained in the context of these organelles. Mechanical forces originating from the ECM can be propagated through the cell to the nucleus via the ECM-integrin-cytoskeleton link and certain proteins and structures unfold or change shape in response to this force, changing their binding affinities and altering signalling pathways as a result. Finally, the methods to study mechanotransduction and cell-matrix interactions are reviewed.

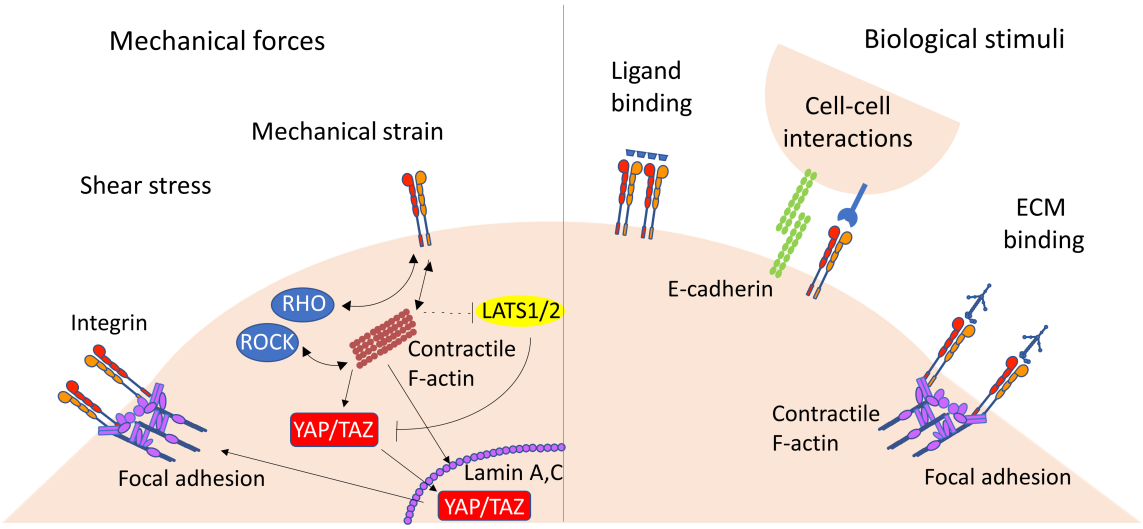


Figure 1.1: Cell-extracellular matrix interactions. Cell fate and function can be controlled by extracellular mechanical forces and extracellular biological stimuli. Mechanical forces, such as fluid shear stress and mechanical strain, can activate specific cell signaling pathways. For example, mechanical force can activate Rho/ROCK, inducing contractile F-actin which results in nuclear translocation of YAP/TAZ and focal adhesion formation[9], and increased levels of A-type lamins (lamin A,C)[10]. Extracellular biological stimuli consist of stimuli such as ligand binding, cell-cell and cell-extracellular matrix (ECM) interactions. Transmembrane integrins play a key role in cell-ECM interactions and ligand binding. They can activate, cluster, and recruit focal adhesion proteins to form focal adhesion complexes which can bind to the actin cytoskeleton. Cell-cell interactions involve cell adhesion molecules such as cadherins, as well as integrins.

1.1 The extracellular matrix

The extracellular matrix (ECM) is composed of a variety of proteins and polysaccharides secreted by cells and organised into a meshwork that is closely associated with the cells that produced them. The ECM acts as a physical support for cells, and is also involved in the establishment and maintenance of differentiated tissues since it regulates growth factor and receptor levels, hydration levels and local tissue pH[11,12]. Moreover, the ECM contains growth factor- and chemokine-binding domains, acts as a complex adhesion surface and provides diffusion barriers between different cellular layers. Therefore the ECM is a specialised supramolecular structure which functions as a support for cells but can also directly participate in cell signalling[13,14]. Indeed, the ECM plays an important role in regulating cell development, function and homeostasis[3,11,15], and tissue-specific cell behaviour is dictated by the mechanical and biochemical properties of the ECM. The basement membrane (BM) is a

specialised form of ECM which covers almost all organs and body cavities and provides both structural and functional roles[16–18].

The ECM consists of over 300 proteins, 200 glycoproteins, and 30 proteoglycans[19]. The ECM is primarily composed of two main classes of macromolecules: fibrous proteins (such as collagens and elastin) and glycoproteins (such as fibronectin, proteoglycans (PGs) and laminin)[11]. These molecules can be assembled in different ways to produce ECMs with unique compositions and topographies, reflecting the requirements for particular tissues[20]. The structural properties of the ECM are mainly a result of elastic fibres and fibrillar collagens[2]. Elastic fibres are made up of an elastin core which is surrounded by a sheath of microfibrils, and they enable tissues to be able to extend and recoil, as well as providing chemical and biological stability[21,22]. Collagen fibres provide tissues with stiffness and strength, and they are able to remodel under stress. Proteoglycans provide the higher order ECM structures around cells. A basic proteoglycan unit is made up of a core protein covalently bound to one or more glycosaminoglycan (GAG) chains. GAGs consist of a long negatively-charged chain of repeating disaccharide units with attached sulphate and carboxyl groups, they have biochemical and hydrodyanamic characteristics which sequestrate grown factors and bind water molecules, providing the ECM with hydration and compressive resistance[20]. Major GAGs include heparan sulphate, chondroitin sulphate, dermatan sulphate, hyaluronan and keratin sulphate[20]. Adhesive glycoproteins such as fibronectin and laminins enable cells to bind to the ECM, act as bridges to connect to the supportive ECM network and also connect the ECM to soluble molecules within the extracellular space[20].

1.2 Organelles connected to the extracellular matrix

A number of organelles are indirectly connected to the ECM through integrins, that are transmembrane proteins which bind to the ECM and the cell cytoskeleton. Integrins are physically coupled to the actin cytoskeleton with the help of focal adhesion (FA) proteins. The actin cytoskeleton is linked to the nucleus via the linker of nucleoskeleton and cytoskeleton (LINC) complex and nuclear lamins **(Figure 1.2)**[23]. Therefore, the nucleus is mechanically linked to the ECM. Changes in ECM physical and biochemical properties can therefore affect

these organelles leading to altered cellular phenotype. Moreover, these organelles can directly influence the ECM in return[1].

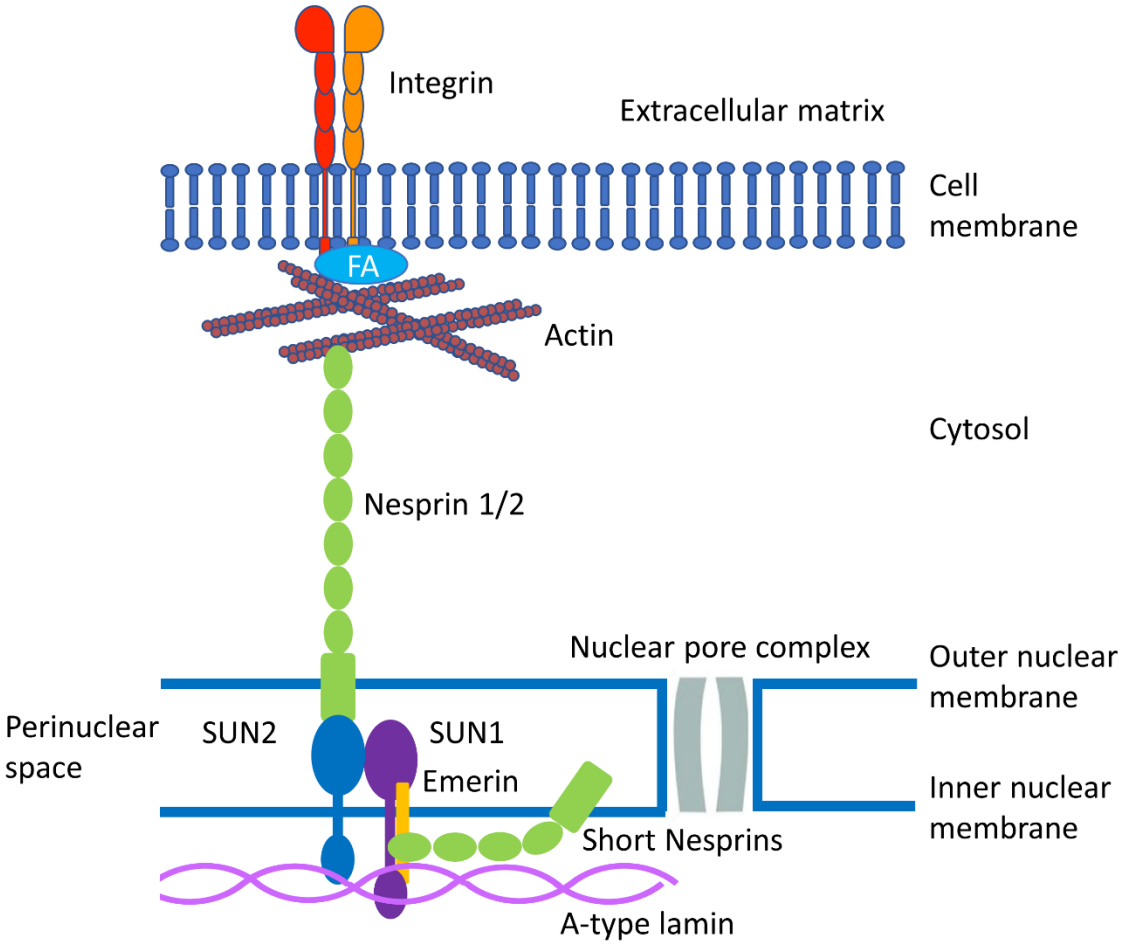


Figure 1.2: The extracellular matrix is physically connected to the cell nucleus, adapted from P. Meinke *et al*. *Biochem. Soc. Trans.* **39,** (2011). The cell can directly interact with the extracellular matrix (ECM) via integrins. Integrins can recruit focal adhesion (FA) complexes which can bind to the actin cytoskeleton. The nuclear envelope consists of an inner and outer membrane separated by perinuclear space. The nuclear pore complex (NPC) spans the inner and outer membrane. The inner nuclear membrane contains proteins such as emerin, A-type lamins, SUN1, SUN2, nesprin-1 and nesprin-2. These proteins form the LINC complex which tethers the nucleoskeleton to the cytoskeleton via the nuclear envelope. Thus, there is a continuous transmission of tension from the cytoskeleton to both the nucleus and ECM receptors.

1.2.1 Integrins

Integrins are the main cell surface receptors involved in the assembly and recognition of a functional ECM. Integrins are mechanically-functioning proteins which attach the cytoskeleton to the ECM, and thus transmit signals between the cell and the ECM. Integrins interact with a variety of cell surface receptors, including growth factor receptors and G-protein coupled receptors, to regulate intracellular signalling pathways that control cell polarisation, spreading, migration, survival, and gene expression[24]. An integrin is made up of two transmembrane glycoprotein subunits known as the α- and β- subunits, these provide a ligand binding head and two legs in the extracellular region, connected to a single transmembrane helix and a short cytoplasmic domain. When present, the A-domain contains the binding site for extracellular ligands[25,26]. There are a total of 25 integrins, made up of different combinations of 18 α- and 8 β-subunits. Integrin composition in a cell determines which ECM components that cell can bind to.

Inactive integrin heterodimers are in a bent V-shape with the head close to the membrane-proximal regions of the legs[27]. This conformation is maintained by an α/β salt bridge at the inner membrane region and helix packing of the transmembrane region[28]. Integrin activation involves rapid, reversible conformational changes to increase ligand affinity[29–31]. This involves the complete extension of the extracellular domains and the separation of the cytoplasmic leg domains[32,33]. Integrin activity is controlled by conformational changes[34] as a result of bidirectional signal transmission across the cell membrane ("inside-out" and "outside-in" signalling) (**Figure 1.3**). "Inside-out" signalling regulates integrin-ECM ligand binding, whilst "outside-in" signalling is activated on adhesion and transduces signals from the ECM into the cell[34–37]. "Inside-out" signalling, describes how intracellular signals can be transmitted to the outside of cells to regulate the adhesive capacity of integrins. Integrin activation is an example of inside-out signalling and this is initiated by disrupting the non-covalent clasp between the integrin α and β cytoplasmic tails[34]. The head domain of the cytoskeletal protein talin binds to the integrin β cytoplasmic tails and induces integrin activation by separating the α and β cytoplasmic tails[38–40]. During "outside-in" signalling, the ECM presents multiple integrin-binding sites, inducing integrin clustering. This clustering then activates a number of signalling kinases (e.g. focal adhesion kinase (FAK) and Src) by increasing the local concentration of their signalling components. "Outside-in" integrin signalling is dependent on adaptors or scaffold

proteins to link integrins to these kinases because the cytoplasmic tails of integrins have no known enzymatic activity [41,42]. In addition, ligand binding can cause conformational change in integrins, separating the α and β cytoplasmic tails, enabling the recruitment of cytoplasmic proteins[43–50]. Therefore, "outside in" signalling can be transmitted by integrin clustering and/or conformational change[51].

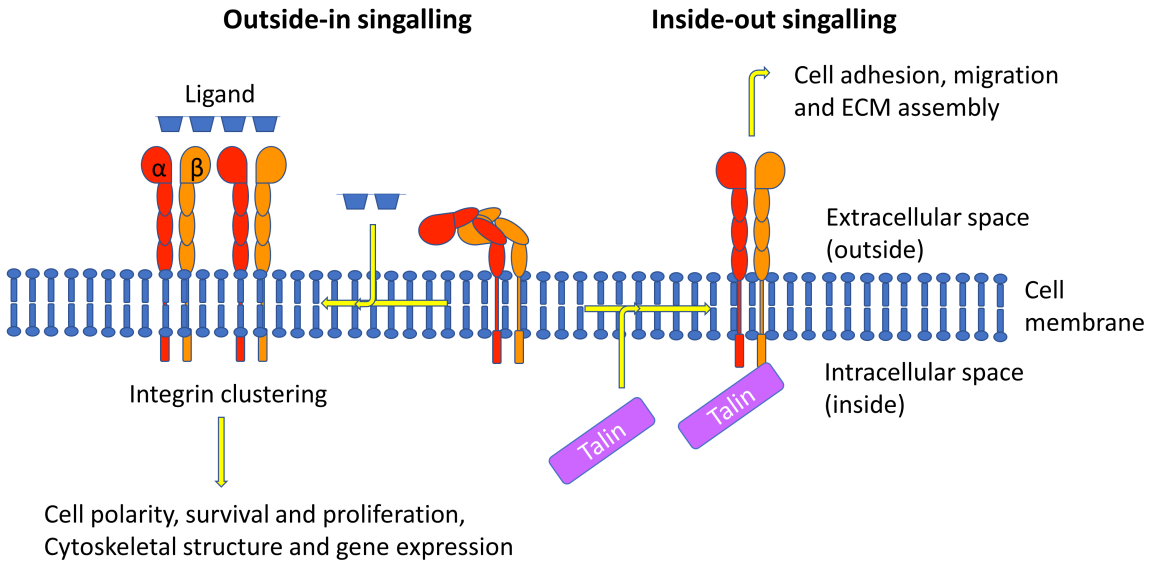


Figure 1.3: Integrin activation, modified from Shattil *et al*., *Nat. Rev. Mol. Cell Biol.* **11,** 288–300 (2010)[52], with permission from Macmillan Publishers Ltd., copyright 2010. Integrins can perform "outside-in" and "inside-out" signalling. "Outside-in" signalling involves extracellular ligand binding, which changes the conformation of the integrin, and since many ligands are multivalent, contributes to integrin clustering. Integrin conformation change and clustering leads to intracellular signalling pathways which control cell polarity, cytoskeletal structure, gene expression and cell survival and proliferation. "Inside-out" signalling involves an intracellular activator (e.g. talin or kindlins) which binds to the β-integrin tail. This causes a conformational change which results in the integrin having increased affinity for extracellular ligands; the integrin has been "activated". "Inside–out" signalling controls adhesion strength and allows enough interaction between integrins and extracellular matrix (ECM) proteins to enable forces to be transmitted by integrins necessary for cell migration and ECM remodelling and assembly.

1.2.2 Focal adhesions

Since integrins lack enzymatic activity, signalling is induced by the assembly of signalling complexes on the cytoplasmic face of the cell membrane, known as focal adhesions (FAs),

once they have matured. Focal adhesions are extremely complex, with 2,412 proteins identified within integrin adhesion complexes so far, and with many of these proteins exhibiting multiple protein-protein interactions[53–55]. Focal adhesions assemble, disassemble or mature at the leading edge of a cell and disassemble at the retracting cell rear to enable migration[56]. Focal adhesion assembly is highly regulated, with proteins being recruited sequentially[57]. The activated integrins cluster into unstable nascent adhesion structures[58] which progress to dot-like focal complexes which can mature into larger FA and eventually result in fibrillary adhesions which connect the integrins to the actin cytoskeleton[59]. Some key FA proteins include focal adhesion kinase (FAK), talin, vinculin, and paxillin. Other FA proteins include α-actinin and zyxin **(Figure 1.4)**.

Integrins initially recruit FAK and talin to nascent adhesions. The ordering of these events has been debated, with canonical models supporting a role of talin in mediating FAK localisation and activation at adhesions[60–62]. However there is also evidence that FAK promotes talin recruitment to nascent adhesions, occurring independently of talin binding to β1-integrins[63]. Focal adhesion kinase is an intracellular protein-tyrosine kinase which acts as a central mediator of signalling in integrins and other cell surface receptors, when associated with the Src tyrosine protein kinase[64]. Talin provides the initial integrin-cytoskeleton linkage by a 2-pN slip bond following fibronectin binding[65]. The integrin-cytoskeleton linkage is followed by the rapid recruitment of proteins to the nascent adhesion. For example, talin induces conformational changes in vinculin, which activates vinculin and enables it to target FAs[66,67] and is also required for paxillin recruitment to FAs[68]. Vinculin is a key scaffolding protein which, to date, has been shown to have 19 binding partners including talin, α-actinin, paxillin, fibrous (F)-actin, vasodilator-stimulated phosphoprotein (VASP), Arp 2/3, vinexin-α/β, catenin-α/β, and phosphatidylinositol 4,5-bisphosphate (PIP_2)[69]. Paxillin serves as a docking protein recruiting signalling proteins to FAs and regulates cell spreading and motility[70].

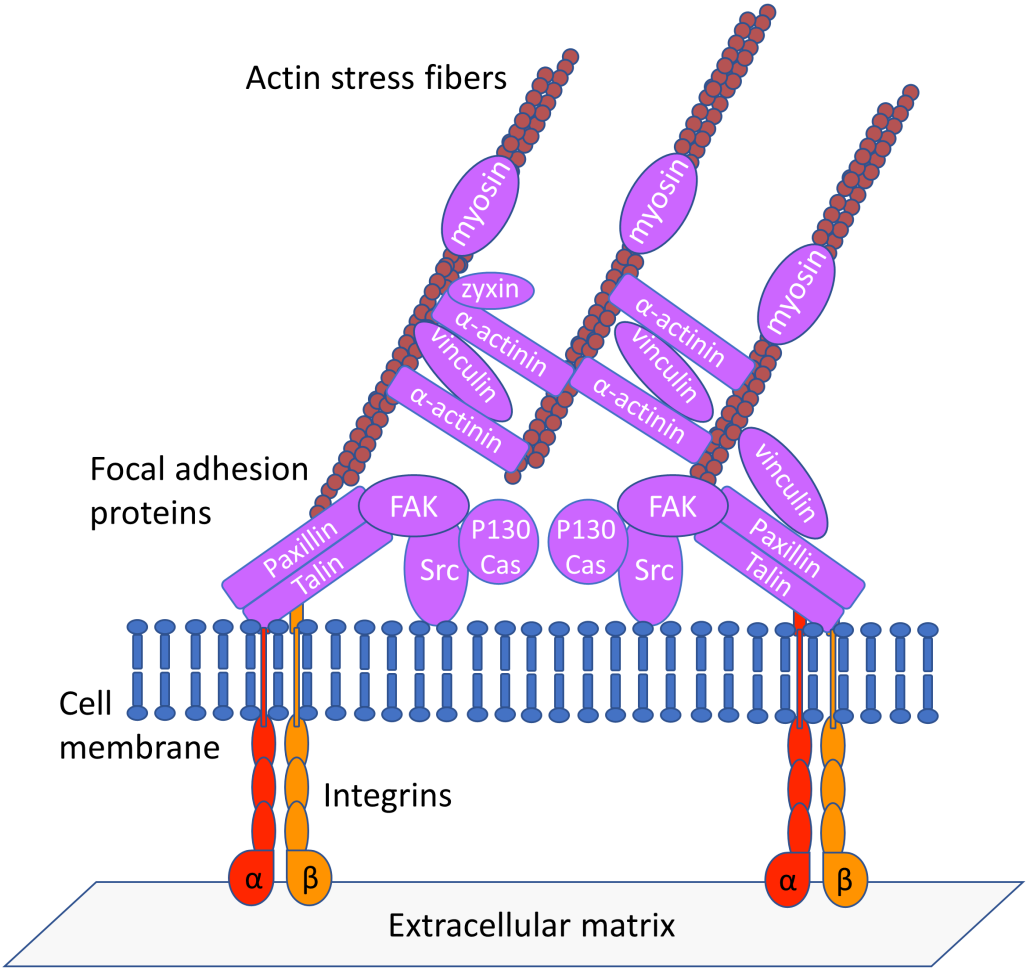


Figure 1.4: The molecular architecture of focal adhesion complexes, modified from S. K. Mitra *et al.*, *Nat. Rev. Mol. Cell Biol.* **6,** 56–68 (2005)[64], with permission from Macmillan Publishers Ltd., copyright 2005. The extracellular matrix (ECM), integrins and the cell cytoskeleton interact at focal adhesion (FA) sites. Focal adhesions are dynamic groups of structural and regulatory proteins which can transduce extracellular signals to the cell interior, and they can also activate integrins by relaying intracellular signals. Focal adhesion kinase (FAK) and talin are initially recruited to focal adhesions and these proteins then enable vinculin and paxillin to be recruited. α-actinin binds to vinculin and crosslinks actomyosin fibres, causing them to be tethered to focal adhesion sites. Zyxin is an α-actinin and cytoskeletal-binding protein that is present in mature contacts. The membrane-associated protein tyrosine kinase Src and the adaptor proteins p130Cas only associate with focal adhesions following integrin clustering.

1.2.3 The actomyosin cytoskeleton

The actin cytoskeleton is connected to the ECM through integrins and FAs. This is necessary for control of cell protrusions and is required for cellular sensing of the ECM as well as cell migration. Cell migration is a highly integrated multistep process regulated by multiple

signalling pathways which is essential in embryonic morphogenesis and tissue repair, and drives disease progression in cancer, atherosclerosis, arthritis and mental retardation[71]. Cell migration can be viewed as a cyclic process[72] in which the cell first polarises and extends protrusions in the direction of migration. Migrating and invading cells form a number of protrusive structures termed filopodia, lamellipodia, invadopodia and podosomes (**Table 1.1**) [73]. These protrusions require dynamic actin remodelling and this is controlled by regulatory proteins including nucleation-promoting factors, capping proteins and polymerases[74,75]. Global structural rearrangements of the actin cytoskeleton in response to external signals are triggered though a variety of cell-surface receptors which tend to converge on the Rho GTPases[76]. The most commonly studied mammalian Rho GTPases are Ras-related C3 botulinum toxin substrate 1 (Rac1), Cell division control protein 42 homolog (Cdc42) and Ras homolog gene family, member A (RhoA)[77]. RhoA is involved in FAs and is a regulator of cell contractility, Rac1 is involved in lamellipodium formation whereas Cdc42 promotes filopodia formation[78].

Table 1.1: The properties of membrane protrusion structures, modified from D. A. Murphy and S. A. Courtneidge, *Nat. Rev. Mol. Cell Biol*. **12,** 413–426 (2011)[79], with permission from Macmillan Publishers Ltd., copyright 2011.

Name	**Description**	**Location**	**Dimension**	**Pericellular proteolysis**	**Duration**
Filopodia[80,81]	Finger-like projections of parallel actin filament bundles	Regions of lamellipodia	Width: 0.1–0.3 µm Length: 3 –10 µm	No	Minutes
Lamellipodia[80,81]	Surface-attached, sheet-like. Branched actin filament protrusions	Leading edge of the cell	Width: 0.1–0.2 µm	Minimal[82]	Minutes[83]
Podosome[84]	Actin rich protrusions containing branched and unbranched actin[85]	Ventral cell surface, *leading edge* of the cell	Width: 0.5–2 µm Length: > 2 µm	Yes[86,87]	Minutes
Invadopodia[84,88]	Actin rich protrusions with branched actin at the cell surface and unbranched actin filaments through the protrusion tip[89]	Ventral cell surface, *under the nucleus*	Width: 0.5–2 µm Length: > 2 µm	Yes[84,90–92]	Hours

Filopodia and lamellipodia are found at the leading edge of migrating cells and they control the direction of migration[80,93]. Filopodia are thin (0.1-0.3 μm) plasma membrane-rich protrusions consisting of tight parallel bundles of F-actin which cells use as an antennae to interact with their environment[80]. They play a role in migration, adhesion to the ECM, wound healing, guidance towards chemoattractants, neuronal growth-cone pathfinding and embryonic development[94]. Filopodia formation is induced by the small GTPases Cdc42 and RIF. RIF activates actin polymerisation through Dia2 formin, whereas Cdc42 might regulate filopodia formation by activating actin-filament nucleation through Wiskott-Aldrich syndrome protein/neural-Wiskott-Aldrich syndrome (WASP/N-WASP) protein and membrane deformation through insulin receptor substrate protein of 53 kDa (IRSp53)[95,96]. WASP proteins have an active open and an inactive folded conformation. WASP is activated on association with Cdc42 enabling it to bind to the Arp2/3 complex and enhancing the actin-nucleating activity of the Arp2/3 complex[97]. During filopodia formation, capping of actin filaments is protected and their barbed ends are clustered together by tip-complex proteins, such as ENA/VASPs, Dia2 formin and myosin-X[80]. Filopodia contain receptors for signalling and ECM molecules; the tips and shaft of filopodia often contain integrins and cadherins[98–101]. When a cell spreads, the initial adhesion sites are provided by filopodia containing integrins. Following this, other focal adhesion complex components (e.g. talin, FAK, vinculin, paxillin) are recruited to these sites, forming mature FAs[98].

Lamellipodia are another type of protrusive actin structure at the leading edge of a motile cell and filopodia are often found protruding from the lamellipodial actin network. A lamellipodium is a thin 0.1-0.2 μm sheet-like protrusion that is composed of a branched F-actin meshwork[93]. As with filopodia protrusions, the fast-barbed end of actin filaments are oriented towards the plasma membrane. The elongation of filopodia and lamellipodia by growth of the barbed end of actin filaments pushes the leading edge forward, promoting cell migration[80]. Lamellipodia are formed via Rac activation of WASP family members, alongside PI(4)P-5 kinase, which generates PI(4,5)P_2 (a form of PIP_2) which can cause the uncapping of filaments who have their plus end bound by gelsolin or CapZ[102,103]. This provides more sites for actin assembly near the cell membrane and results in the formation of lamellipodia and membrane ruffles.

Podosomes and invadopodia arise on the ventral surface of the cell membrane. They act as sites of attachment to the ECM and are involved in matrix degradation[79]. Specifically, invadopodia are found in cancer cells whereas podosomes are found in highly motile cells (e.g. mesenchymal cells). Growth factors such as platelet-derived growth factor (PDGF), TGFβ, and epidermal growth factor (EGF) can induce podosome or invadopodia formation[104–107], often via pathways involving Src tyrosine kinase and protein kinase C (PKC)[106,108]. Reactive oxygen species (ROS) signalling[109], integrin signalling[86,110], and microRNA control[111,112] have also been shown to be involved in podosome and invadopodia formation[79].

Since podosomes and invadopodia play a role in ECM degradation, podosomes are found in cell types involved in tissue remodelling and immune surveillance, and the invadopodia levels are correlated cancer cell metastasis and invasion[79]. These structures contain three main classes of proteases which assist with membrane degradation: MMPs, the cathepsin cysteine proteases, and the serine proteases seprase and urokinase plasminogen activator[113,114]. Although podosomes and invadopodia are similar in structure and function, invadopodia protrude further into the ECM and are stable for hours, whereas podosomes tend to show minimal protrusions (dendritic cells can form long podosomes[86]) and are rapidly turned over; the explains why cancer show higher degradative properties[88]. Key proteins in podosomes and invadopodia include the adaptor proteins Tks4 and Tks5, the actin regulators cortactin and (N)-WASP, the tyrosine kinase Src, and the membrane type 1 matrix metalloproteinase (MT1-MMP, also known as MMP-14)[84,90–92].

RhoA induces myosin light chain phosphorylation, leading to the formation of actin stress fibres, the major contractile structures in many cultured animal cells[115,116]. Stress fibres consist of bundles of 10-30 actin filaments cross-linked by α-actinin and anchored to FAs[116]. It has been debated as to whether stress fibres are an *in vitro* artefact since they are often seen in cells grown on tissue culture whereas they are rarely seen in intact tissues. However, evidence does suggest that stress fibres are seen in tissues. For example stress fibres have been observed in would granulation tissues[117,118], and in endothelial cells which are exposed to high velocity flow[119] or from hypertensive animals[120]. Therefore, stress fibres are rarely found *in vivo* but do appear to arise in situations when cells experience high levels of mechanical force.

Most cellular movements depend on myosin interacting with actin stress filaments. There are at least 24 classes in the myosin family, and myosin I and II are the most abundant, present in almost all eukaryotic cells[121,122]. Myosin I and V are involved in interactions between the cytoskeleton and the cell membrane (e.g. transport of membrane vesicles)[123,124]. Myosin II is involved in muscle contraction and cytokinesis, the last stage of mitosis when the two daughter cells separate[125,126]. Myosin is an adenosine triphosphate (ATP)ase that moves along actin filaments and causes conformational changes by hydrolysing ATP[127]. Myosin is therefore a motor protein since it converts chemical energy into mechanical energy. The microtubule motors kinesin and dynein have similar properties to myosin[128]. Myosins are composed of one or two heavy chains and several light chains. The heavy chains have a globular head domain which contains actin and ATP binding sites and which is responsible for force generation. The head domain is connected to the α-helical neck region which associates with the light chains. The light chains control the activity of the head domain and contain binding sites that determine the specificity of the myosin since the head domain is conserved among the myosin family members[127].

1.2.4 The nucleus

The cytoskeleton is connected to the LINC complex which is attached to the lamina in the nuclear envelope (NE) (**Figure 1.2**). The nuclear envelope consists of an inner nuclear membrane (INM) and outer nuclear membrane (ONM) separated by a 40-50 nm perinuclear space. This perinuclear space is interconnected at the nuclear pores and through a dense protein network known as the nuclear lamina[129]. Nuclear pore complexes are multiprotein channels which control macromolecular trafficking across the nuclear envelope and the nuclear lamina lines the nuclear face of the INM.

The nucleus is connected to the cell cytoskeleton by the LINC complex[130], and disruption of the LINC complex has been shown to affect the organisation of the actin cytoskeleton as well as cell mechanics[131–133]. Moreover, the LINC complex controls nuclear positioning during processes in which the nuclear position varies[130,134] such as cell division, migration and differentiation[135,136]. The LINC complex is a complex of proteins composed of Sad1p, UNC-84 (SUN)-domain and Klarsicht, ANC-1, Syne Homology (KASH)-domain proteins which is

associated with both the INM and ONM[137]. SUN domain proteins associate with nuclear lamins and chromatin and cross the INM. KASH-domain proteins interact with SUN domain proteins and are located in the perinuclear space and also cross the ONM, interacting with the cytoskeleton and cytoplasmic organelles. Nesprin 1 and nesprin 2 (also known as SYNE1 and SYNE2) are rod-like nuclear membrane proteins which have an amino terminus with an actin-binding domain, a central spectrin-like domain and a carboxyl terminal KASH domain which binds to SUN proteins[138]. Nesprin 1 and 2 connect actin filaments to SUN1 and SUN2 on the ONM and on the INM SUN1 binds to lamin-A and the nuclear pore complexes. Nesprin 3, which lacks the actin-binding domain found in nesprin 1 and 2 connects to the cytosplasmic intermediate filaments by associating with plectin 1, SUN 1 and SUN 2[139,140]. ANC-1 attaches nuclei to the cell cytoskeleton by interacting with the SUN member UNC-84.

The nuclear lamins are type V intermediate filament proteins which have a small "head" domain connected to four coiled-coil regions (1A, 1B, 2A, 2B) connected a large non-helical tail domain which is organised around an immunoglobulin (Ig)-like β-fold. The tail domain usually contains a nuclear localisation sequence[141]. Nuclear lamins provide structural integrity to the nuclear envelope, acting as "nuclear shock absorbers"[142], contributing to nuclear stiffness[143,144] and nuclear stability[145]. Lamins are found in nearly all cell nuclei and are involved in nuclear assembly and disassembly during mitosis[146–148]. They are also involved in transcriptional regulation since they provide anchoring sites for chromatin domains[149] and a number of regulatory proteins such as signalling molecules and transcription factors[141].

Lamins can be described as A- or B- type lamins. A-type mammalian lamins include lamin-A, lamin-C, lamin-C2 and lamin-AΔ10 are encoded by a single gene. Proteomics and transcriptomics have shown that there are about 10^7 copies of A-type lamin proteins in a mouse fibroblast cell, which accounts for roughly 0.7% of the cell's protein mass, and around 200 copies of the *LMNA* transcript. Deoxyribonucleic acid (DNA) methylation is not a major mechanism to control *LMNA* levels[10], *LMNA* transcription is thought to be regulated by retinoic-acid receptor family transcription factors (RAR and RXR family proteins[10,150–153]), and the resulting mRNA is alternatively spliced, giving the lamin-A and truncated lamin-C forms. Lamin-A expression is essential for maturation and survival against stress; by matching to the level of stress, *LMNA* can favour a pre-specified lineage[10]. Indeed *LMNA* knockout mice are

able to develop all tissues but they have growth retardation of connective tissues, a severe form of muscular dystrophy and die weeks after birth[154–156]. Mutations in A-type lamin genes (truncations or single amino acid substitutions) result in laminopathies which can lead to serious disorders such as muscular dystrophy, cardiomyopathies, lipodystraphies and Hutchinson–Gilford progeria syndrome (HGPS)[157,158]. The three mammalian B-type lamins include lamin-B1, lamin-B2 and lamin-B3[141]. Although weakly modulated, the B-type lamins are important in embryonic development however *LMNB* knockout mice do survive embryogenesis[159], and show neuron apoptosis[159] when the nucleus is stretched in the dense midcortex[143]. Interestingly, embryonic stem cells containing no lamins can be cultured and differentiated[160] and lamins are not expressed in yeast and plants[161].

The lamin types share structural features and show some similarities in amino acid sequence, but they have different post-translational modifications; B-type lamins have a permanently attached farnesyl group whereas this is cleaved from mature lamin-A[162,163]. The A- and B-type lamins have different turnover rates and provide different structural and functional roles in the nucleus[164]. For example, lamins -A and -C are important contributors to the mechanical stiffness of nuclei whilst lamin-B1 contributes to the nuclear integrity[144]. Moreover, lamin-A has been shown to exhibit a viscous response to resist deformation whereas lamin-B exhibits an elastic response[10,153,165]. When aspirated into micropipettes at stresses of kPa (similar to the tension found in cells[166]), nuclei in a diverse range of cell types extend in a viscoelastic manner within just ~10 seconds, and a greater lamin A:B stoichiometry was shown to increase the effective viscosity of the nucleus more rapidly than the effective elasticity. Moreover, when lamin-B is the dominant isoform in U251 cells, the nucleus recovers following migration through a 3 μm pore, whereas when lamin-A is the dominant isoform the nucleus remains deformed[165]. This suggests that there is a physical distinction between the two isoforms, with lamin-A providing viscosity and lamin-B providing elasticity to the nucleus. This observation is supported by fluorescence correlation spectroscopy which has shown lamin-A to be mobile and lamin-B to be immobile[149].

Successful migration requires cells to survive large distortions, but the nucleus, the largest organelle in the cell, tends to be stiff[143,144,167]. It has been shown that nuclear dynamics is the rate limiting factor when cells are forced to squeeze through constrictions which are smaller

in size than the nucleus[168,169]. Interestingly, lamin-A-deficient cells have more deformable nuclei[170] and have been shown to pass through narrow constrictions significantly faster than wild type cells during active migration and passive perfusion[169]. When lamin-A is knocked down in granulocytes/monocytes their migration increases several-fold through Transwell filters with smaller-sized micropores but not through larger pores[153]. However, these results should be treated with caution since lamin perturbations result in altered differentiation state and can also alter the cytoskeletal factors involved in migration[10,153,171]. Interestingly, cancer cells have been shown to transverse through constrictions more easily than normal cells, and this is because they have softer nuclei and are often associated with lamin mutations (e.g. low lamin-A has been shown to correlate with the recurrence of colon cancer)[169,172]. Although A-type lamins impede 3D migration, they also help cells survive against the stresses induced by migration: deep lamin-A knockdown results in a broad range of defects associated with stress resistance. For example, HSP90, which contributes to repair of DNA damage[173], can be down-regulated when lamin-A is repressed[165].

1.3 Mechanotransduction and the cellular response to extracellular cues

Mechanotransduction describes how cells sense their physical 3D environment, by translating mechanical forces and deformations into biochemical signals. These biochemical signals elicit a cellular response, for example a change in migration, proliferation or differentiation[174,175]. Dysfunctional mechanotransduction results in a number of diseases including atherosclerosis, hypertension, asthma, osteoporosis, and cancer[176].

Mechanotransduction has been described by means of an architectural model of cell function called “tensegrity”, in which there is a continuous transmission of tension from the cytoskeleton to both the nucleus and ECM receptors[177]. Force has also been shown to initiate signals by unfolding individual protein domains and changing binding affinities, and the nucleus has been described as a mechanosensor[178]. Finally, mechanotransduction can be investigated by seeding cells on materials of different extracellular stiffness and it has been shown *in vitro* that factors such as cell spreading, Yes-associated protein (YAP) and

transcriptional coactivator with PDZ-binding motif (TAZ, also known as WWTR1) activity, FAs, myosin contractility, lamin-A levels, migration, and cell cycle progression are sensitive to extracellular stiffness[4,10,166,179–184]. These are all examples of cell mechanotransduction since the cell changes its phenotype in response to altered extracellular stiffness, and thus altered extracellular force.

1.3.1 The tensegrity model

It has been proposed that the cytoskeleton acts as a tensegrity structure within the cell, and that cells consist of a network of tense cables (contractile microfilaments and intermediate filaments) which are stabilised by compressed struts (microtubules and cross-linked actin bundles) and anchors (adhesions to the ECM and neighbouring cells), rather like a tent[185,186]. The tensegrity model predicts that the cytoskeleton is in a state of tensional "prestress", to enable a mechanical force balance between cytoskeletal traction forces and the resistance force from the ECM. The "hard-wired" tensegrity network enables mechanical force at the cell membrane to be propagated to the nucleus via the actin cytoskeleton in the absence of protein polymerisation and chemical based diffusion[174,187,188]. Compressive[189] or elongational forces[187] applied at the cell membrane can then lead to the immediate displacement of internal organelles[187] and deformation of the nucleus, altering nuclear morphology, chromatin organisation, and epigenetic status[4,10,190–195].

Indeed studies have shown that pulling on integrins induces molecular realignment of the actin cytoskeleton and the nucleus, with the nucleoli reorienting along the field lines of the applied tension[187]. Moreover, a force that is applied to an integrin can displace mitochondria and nuclei 20 μm away[196] and this is lost when intermediate filaments are disrupted[187]. When mesenchymal stem cells (MSCs) are cultured on soft substrates, they show a wrinkled and relaxed nucleus whereas the nuclei are taut, smooth and flattened on stiff substrates due to the pull from stress fibres[10].

1.3.2 Force and the extracellular matrix-integrin-cytoskeleton link

Forces acting across ECM–integrin–cytoskeletal linkages are thought to initiate signals by unfolding protein domains and changing binding affinities. For example, force exposes

fibronectin binding sites which results in it self-assembling into fibrils on stretching[197], and it has been shown by fluorescence resonance energy transfer (FRET) that actomyosin-dependent forces cause fibronectin to unfold within fibrils[198,199]. This unfolding process potentially regulates cell signalling processes since fibronectin displays a large number of molecular recognition site which may be altered by protein unfolding. The integrins themselves undergo conformational changes under force; pulling forces enhance transition rates to high affinity conformations that stabilise the integrin-ligand bond[200] and also enable the binding of new ligands[201,202]. Interestingly the increase in binding affinity is even more efficient under rapidly applied force, and is further enhanced under cyclic forces[203], which is important for rigidity sensing.

Lamellipodia at the edge of the cell become lamella towards the centre of the cells and these structures show different magnitudes of force transmission. Cells initially adhere to the ECM by forming nascent adhesions within the lamellipodia or filopodia at the cell periphery. A small number of nascent adhesions at the lamellipodium-lamella boundary undergo a force-dependent maturation process, where they become more stably connected to the ECM, increase in size and become elongated[58,204]. Examples of force-dependent maturation include the stretching of talin which enables it to unfold and bind to vinculin[205,206], which then binds actin and reinforces the integrin-actin link[207,208]. Vinculin binding sites within the rod are buried within helix bundles, but the *in vitro* stretching of these domains exposes the binding sites[205], enabling vinculin to bind to F-actin contributing to tension-induced adhesion stabilisation[207]. Moreover, tension causes actin filament stabilisation by decreasing the rate of spontaneous depolymerisation[209] and by reducing its sensitivity to cofilin severing[210] which can influence FA lifetime since FA stability requires actin scaffolds[211].

Mature FAs elongate in the direction of the attached stress fibres, most likely due to the force transmitted through the stress fibres[212–215]. It has been debated whether focal complexes mature into FAs in response to external force[216–219] or the actin cross-linking that is induced in response to force via α-actinin and myosin II[58]. Upon maturation, FAs decrease propulsive forces[220] and no longer grow under tension[221]. Instead, they become passive anchorage tools for the maintenance of a spread cell morphology[220] and can sustain up to a six-fold increase in external force load without elongating[221].

The actin cytoskeleton is highly important in the cellular response to mechanical loads, and this response is sensitive to the size, timing and direction of the loading. Force induces polymerisation of the actin cytoskeleton and the fibrous/globular actin ratio causing nuclear translocation of the G-actin-associated transcriptional cofactor, megakaryoblastic acute leukaemia factor-1 (MKL1)[222]. MKL1 is bound to G-actin in the cytoplasm, preventing MKL1 from translocating to the nucleus. MKL1 is able to translocate to the nucleus when G-actin polymerises into F-actin, since this causes it to dissociate from G-actin. MKL1 interacts with SRF in the nucleus and this activates fibrotic gene programming, such as α-SMA gene expression, enabling myofibroblast differentiation[223,224]. The actin cytoskeleton exhibits viscoelasticity; stress application causes temporary deformation if it is removed quickly, but permanent deformation if it is maintained. It initially shows strain stiffening to resist deformation and then relaxes passively via viscoelastic mechanisms[225–227]. When cyclic loading is applied to cells, the cytoskeleton is actively remodelled and reoriented and this is dependent on the magnitude and frequency of the applied load[228]. It must be noted that realignment does not occur on highly compliant substrates[229].

1.3.3 Force and the nucleus

The nucleus has been proposed to act as a cellular mechanosensor, with extracellular forces causing changes in nuclear shape resulting in a change in cell phenotype and function. The nucleus has an elastic modulus of 1 − 10 kPa (the exact result depending on the type of cell and experimental technique used to obtain the measurements[230–233]) and has consistently been shown to be 2 to more than 10 times stiffer than the surrounding cytoskeleton. For example, when endothelial cells are compressed between two parallel plates and the nuclear and cytoskeletal deformation is measured, the nucleus is shown to have an effective elasticity of 8 kPa compared to just 0.5 kPa for the cytoplasm[230]. Although the nucleus is the stiffest organelle in the cell, extracellular forces and strain result in clear nuclear deformations[187,189,231]. Nuclear size and shape can change drastically when the actin cytoskeleton is disrupted, suggesting that the nucleus is mechanically constrained in cells.

Strong correlations between nuclear shape and cellular phenotype have been shown. Indeed collagen synthesis correlates more strongly with nuclear shape than with cell shape[234], and

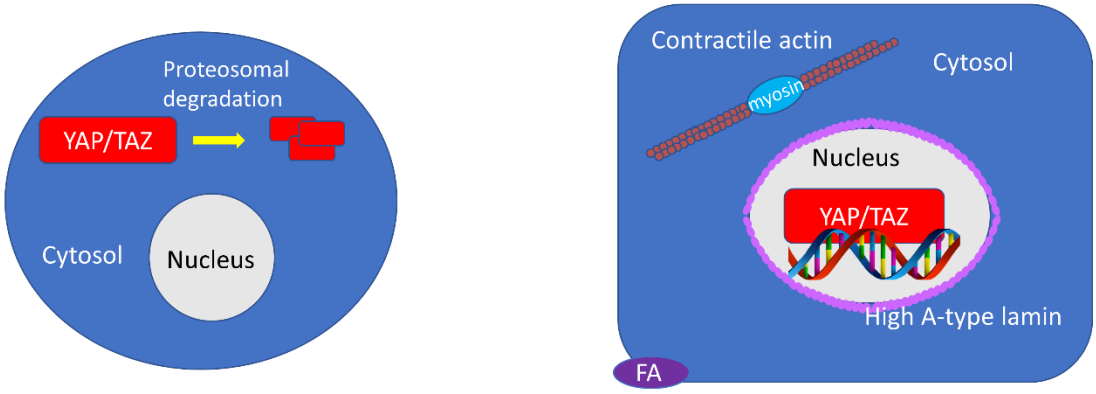
chondrocyte nuclear shape correlates with changes in cartilage composition and density[189]. Moreover, cells have been shown to undergo dramatic nuclear shape change during differentiation and maturation[235]. The cell phenotype changes during differentiation correlate with reduced chromatin movement[236], upregulation of A-type lamin components[237] and alterations in nuclear shape and stiffness[143]. Changes in gross nuclear morphology is often used to identify cancerous tissue[238,239], and many cancers correlate with changes in nuclear structural proteins. For example, lamin-A is overexpressed in ovarian cancers[240]; lamin-B levels are increased when prostate cancer tumours differentiate[241]; and changes in nuclear stiffness can be used to mark increased mobility of tumour cells and metastatic potential[242,243]. It has been proposed that changes in nuclear shape causes conformational changes in chromatin structure and organisation, directly affecting transcriptional regulation[235]. Indeed, on the single-molecule and macromolecular levels, force has been shown to induce remodelling and disassembly of purified DNA, chromatin and chromosomes, which may be required for transcription[244,245]. A modification in chromatin structure may increase and/ or decrease the accessibility of certain genes to enable differentiation.

The nucleus is able to adapt and reorder its shape and mechanics when cells are exposed to force. For example, micropipette aspiration of isolated nuclei and AFM studies show that nuclei exposed to shear stress have a reduced height and increased stiffness compared to non-sheared controls[246,247]. These results suggest that cells actively change their nuclear structural elements in response to force, however the mechanisms involved are not fully understood. It remains unclear whether direct force or lamin reorganisation results in the reorganisation of genes within the nucleus. This is because almost all INM proteins directly bind to A- and/or B-type lamins[248,249], and the lamins have been implicated in chromatin organisation and regulation since they are physically linked to DNA[159,250–254]. As well as being located at the nuclear periphery, lamins can form intra-nuclear structures which can modulate chromatin organisation[255,256]: several *LMNA* mutations are linked to a loss of heterochromatin[257]; loss of lamin-B1 can alter the positioning of chromosome territories in the nucleus[258]; and it has been suggested that a lamin-B1-dependent nucleoskeleton is necessary for RNA synthesis[259]. Moreover, lamin-A mutation has been shown to affect YAP-dependent mechanosensing in myoblasts[260], there is a correlation between lamin-A levels

and matrix rigidity[10], and A-type lamin knockdown can result in impaired NF-κB-regulated transcription[170]. Finally, lamin-A interacts with the cell cycle regulator and tumour suppressor retinoblastoma protein (pRb)[261,262], and lamin-A expression levels correlate with the DNA-binding and transcriptional activity of activating protein 1 (AP-1), which in turn affects cellular proliferation[263]. Finally, it has been shown that lamin-A and emerin regulate MLK1 nuclear localisation and SRF dependent transcription[171].

1.3.4 Extracellular matrix stiffness

Extracellular matrix stiffness has been shown to affect cell signalling pathways, cell phenotype and cell fate (**Figure 1.5**). Indeed, when cells are seeded on softer gels that mimic the compliance of brain or fat, neurogenesis or adipogenesis are maximised, respectively[4,264,265]; when cells are cells are seeded on gels that are moderately stiff, mimicking muscle, myogenesis is promoted[266–268]; and when cells are seeded on gels that are firm mimicking pre-calcified bone, osteogenesis is optimised[182,269,270]. This is thought to be driven by cell shape, which can influence cell fate by modulating RhoA activity[190], since cells are balled up on soft substrates and well-spread on stiffer substrates. Moreover, the nuclear lamins also play a role in controlling cell fate[10]. On soft hydrogels, the extent of adipogenesis is doubled with lamin-A knockdown, and when stiff cells are combined with lamin-A overexpression, they cooperate and osteogenesis is enhanced. Stiff substrates also cause YAP translocation to the nucleus[4], and increase the protein levels of cytoskeletal components, which is consistent with greater activity of T-cell differentiation protein (MAL) and its binding to serum response factor (SRF)[171,271], increasing cytoskeletal tension.



Soft Matrix	Stiff Matrix
Balled up cell Reduced RhoA/ROCK activity	Cell Spreading[166,272] Increased RhoA/ROCK activity[9]
Phosphorylated Myosin-IIA Unpolarised myosin-IIB Low myosin contractility/ cytoskeletal tension	Dephosphorylated Myosin-IIA[273] Polarised myosin-IIB[274] High myosin contractility/ cytoskeletal tension[273]
Increased A-type lamin turnover Low A-type lamin Less spread nucleus, nuclear softening	Reduced A-type lamin turnover[10] High A-type lamin[10] More spread nucleus, stiffer nucleus[10]
Low serum response factor activity Cytosolic RARG and YAP/TAZ	High serum response factor activity[171,271] Nuclear RARG[10] and YAP/TAZ[166]
Minimal focal adhesion formation	Focal adhesion formation[9]
Adipogenesis	Osteogenesis[166]

Figure 1.5: Matrix stiffness affects cell signalling pathways and cell phenotype. In going from a soft to stiff matrix, cells spread and show increased RhoA/ROCK activity with higher myosin contractility and cytoskeletal tension. This is correlated with reduced turnover and thus higher levels of A-type lamin which causes the nucleus to become stiffer. Stiff matrices also cause higher activity of serum response factor, RARG and YAP/TAZ. YAP activity has been linked to focal adhesion formation on stiffer matrices. Finally, matrix stiffness can determine cell fate, for example, soft matrices promote adipogenesis and stiff matrices promote osteogeneis.

1.3.4.1 YAP/TAZ cellular mechanotransducers

YAP and TAZ have been shown to act as cellular mechanotransducers, as well as transducers of the Hippo pathway[275], allowing cells to sense and adapt to their physical environment[4]. ECM stiffness and cell geometry can regulate YAP/TAZ activity and YAP/TAZ can sense cytoskeletal tension and mediate cellular mechanoresponses independent from the Hippo pathway[4]. The Hippo pathway controls organ size by regulating cell proliferation, apoptosis,

and self-renewal of stem cells. It involves a key kinase cascade, where MEN-SIN-TAN family 1/2 (Mst1/2, ortholog of Drosophila Hippo) kinases and Salvador Family WW Domain Containing Protein 1 (SAV1) form a complex to phosphorylate and activate Large Tumor Suppressor Kinase 1/2 (LATS1/2). LATS1/2 kinases in turn phosphorylate and inhibit YAP and TAZ. YAP/TAZ are able to translocate to the nucleus when they are dephosphorylated, and here they interact with TEA domain family member 1-4 (TEAD1-4) and other transcription factors to induce expression of genes that promote cell proliferation and inhibit apoptosis[276].

YAP/TAZ transcriptional activity has been monitored in human mesenchymal stem cells (hMSCs) grown on hydrogels of various stiffness (elastic moduli ranging from 0.7-40 kPa, as found in natural tissues)[166]. The YAP/TAZ regulated genes connective tissue growth factor (*CTGF)* and Ankyrin Repeat Domain 1 (*ANKRD1)* were monitored by real-time PCR and it was shown that YAP/TAZ activity correlated with substrate stiffness. Moreover, YAP/TAZ were localised in the cytosol on soft substrates whereas they were localised in the nucleus on stiffer substrates. Thus, YAP/TAZ activity and subcellular location is regulated by ECM stiffness.

ECM stiffness also affects cell spreading[166,272]. Micro-patterned fibronectin islands of defined size were used to control cell spreading, and it was shown that YAP/TAZ was nuclear in spread cells and cytoplasmic in confined cells. The use of adhesive islands allowed single cell analysis and showed that cell-cell contacts were not involved in YAP localisation (cell-cell contacts lead to activation of Hippo/LATS signalling)[277]. Moreover, by seeding hMSCs on micropillars, where they have controlled contact to ECM levels, it was shown that YAP/TAZ are primarily regulated by cell spreading imposed by the ECM[4]. Since cell spreading activates Rho GTPase and remodelling of the actin cytoskeleton[8,278], Rho and actin were inhibited and it was shown that Rho and the actin cytoskeleton are required to maintain nuclear YAP/TAZ in hMSCs[4].

A model has been suggested for YAP/TAZ mechanosensing which involves two upstream pathways partially overlapping with the Hippo pathway. Firstly, it is believed that small GTPase Rho indirectly controls YAP/TAZ nuclear localisation by promoting the formation of actin bundles and stress fibres in response to cell spreading[190,279]. Moreover, YAP/TAZ upstream kinase LATS is targeted by integrin-FAK signalling through Src[280]. It has recently been demonstrated that YAP localisation is controlled by cell area through Rho/ROCK

activation and is independent of FA formation. YAP then transcriptionally controls FA formation and cytoskeleton stability, which determines cell mechanics and cell adhesion to the ECM[9].

1.3.4.2 A-type lamins

A-type lamins have been shown to act as mechanosensors. Swift *et al.* have used proteomic profiling to examine whether the nuclear lamina is involved in sensing tissue elasticity in differentiation by culturing cells on soft and stiff gels. This was also investigated *in vivo* by growing human-derived U251 glioblastoma tumours in the brain and in subcutaneous flank sites of nude mice[10]. Proteomic analysis has shown that A-type lamin protein levels are upregulated on stiff substrates (40 kPa)[10]. Indeed, lamin-A was found to increase systematically 30-fold from soft to stiff tissue, lamin-B1 differed by less than threefold, and lamin-B2 varied even less. This is consistent with B-type lamins being constitutively expressed[281].

In addition, the extent of A-type lamin phosphorylation is decreased at four sites on a stiff substrate. Intermediate filament proteins use phosphorylation as a key method to alter their conformation, organisation and solubility[282]. For example, lamins are highly phosphorylated during mitosis, which enables lamina disassembly in preparation for chromosomal separation[148,283]. The decreased phosphorylation of A-type lamins on stiff substrates decreases their solubility and strengthens the lamina as a result. Indeed, A-type lamins show greater phosphorylation on soft substrates (0.3 kPa), which promotes its disassembly[284] and turnover[285]. A-type lamins are rapidly phosphorylated in response to reduced cytoskeletal tension and thus levels of A-type lamin and myosin-IIA are co-regulated in response to matrix elasticity. Tension-dependent stabilisation of A-type lamin and myosin-IIA can therefore couple nuclear and cell morphology downstream of matrix mechanics. It has been argued that a feedback mechanism occurs by which lamin can promote its own transcription since lamin-A levels have been shown to drive the translocation of the lamin-promoting transcription factor retinoic acid receptor γ (RARG) to the nucleus, activating the retinoic acid signalling pathway[10].

Extracellular matrix stiffness has also been shown to affect A-type lamin accessibility[192]. At least two N- and C-terminal A-type lamin epitopes are not accessible at the basal side of the nuclear envelope under environmental conditions known to upregulate cell contractility[192]. Other lamin-type antibodies (A, C and B1) showed no preference in basal or apical staining. The conformational epitope on the Ig-domain of A-type lamins is more buried in the basal than apical nuclear envelope of hMSCs undergoing osteogenesis, and in fibroblasts adhering to rigid polyacrylamide hydrogels. This is not seen in hMSCs undergoing adipogenesis or fibroblast adhering to soft gels. This phenomenon was shown to emerge during cell spreading, was promoted by compressive forces, and it required A-type lamin multimerisation, an intact LINC complex, and apical-actin stress-fibre assembly[192]. The C-terminal A-type lamin epitope overlaps with emerin, DNA and histone binding sites, and has mutation sites responsible for various laminopathies (e.g. muscular dystrophy, lypodystrophy and generalised metabolic syndrome), and A-type lamin is key in tethering peripheral heterochromatin to the nuclear envelope during differentiation[250,286–288]. Therefore, the nuclear envelope may make A-type lamin epitopes inaccessible, as part of the mechanoregulation of transcription processes.

1.4 Methods to study mechanotransduction and cell-matrix interactions

In vivo, cells are continually responding to a dynamic environment. For example, cells can reorganise their cytoskeleton and modify their function in response to physical and chemical stimuli. Cells can sense their environment by exerting minute forces at sites of cell adhesion and this leads to the transduction of signalling pathways which result in altered cell phenotype. An absence of appropriate physical cues also leads to altered cell function, and this can be observed when isolated cells are seeded on tissue culture plastic *in vitro*; a number of cell types dedifferentiate, and stem cells have been shown to lose their self-renewal capacity[289].

Therefore, materials have been designed to assess cell-environment interactions. Such materials include 2D gels, 3D hydrogels, arrays of one dimensional micro- and nano-structures, and microcontact printing. As well as designing materials to understand cell-

matrix interactions, bioengineered devices have also been designed to investigate the biophysical parameters that control cell mechanotransduction, and cellular interactions with surface chemistry and surface topography. Devices have been developed to assess and manipulate cell adhesion as well as to apply and/or detect pico-Newton forces that mimic the forces experienced by cell receptors. Commonly used techniques include optical tweezers, magnetic tweezers, atomic force microscopy (AFM), magnetic twisting cytometry (MTC) and magnetic pulling cytometry (MPC), traction force microscopy (TFM), arrays of one dimensional micro- and nano-structures, and super-resolution microscopy[290].

1.4.1 Materials to assess surface chemistry

Cells are sensitive to the surface chemistry of a material, with surface chemistry affecting cell adhesion and cell differentiation pathways. Cell adhesion depends on the hydrophobicity of the chemical structures at the surface of a material. This is because hydrophobicity dictates the adhesion of serum proteins to the surface, and the serum proteins' chemical groups can impact cell behaviour. Indeed, cell adhesion and cell fate have been directed using simple functionalities on silane surfaces[291,292]. It has been demonstrated that -NH_2 functionalised surfaces show the greatest level of cell adhesion and favour osteogenesis. In comparison, -COOH functionalised surfaces showed different cell morphology, altered fibronectin and vitronectin spatial distributions, and favoured chondrogenic differentiation, since there was an increase in Collagen II expression[291]. Following 28 days of hMSC incubation on the different surface chemistries in basal, chondrogenic and osteogenic stimulated media, the CH-3 surface and clean glass control maintained an MSC phenotype; the -NH_2 and -SH surfaces promoted and maintained osteogenesis both in the presence and absence of biological stimuli, and the -OH and -COOH-modified surfaces promoted and maintained chondrogenesis under both basal and chondrogenic stimulated conditions[292]. In addition, simple chemical group incorporation (–NH_2, t-butyl, phosphate, –F, and –COOH) into a polymer hydrogel can influence stem cell differentiation, and hydrophobic functional groups such as t-butyl have been shown to induce an adipogenic phenotype, whereas charged functional groups such as the phosphate group promoted osteogenesis, and acid functionalisation favoured chondrogenesis[293]. Finally, large arrays of polymers have been functionalised on glass slides to assess polymers with differentiation inducing properties[294,295], and this has been used to

demonstrate that human embryonic stem cells favour substrates generated from monomers with high acrylate content, with a moderate wettability and which utilise αVβ3 and αVβ5 integrin engagement with adsorbed vitronectin[295]. A next step will be to synthesise 3D scaffolds with spatially controlled chemical functionalities in order to control stem cell fate in a more *in vivo*-like environment.

1.4.2 Materials to assess topographical cues

Topographical cues have also been shown to affect cell adhesion and stem cell fate *in vitro*. For example, endothelial cells spread to a greater extent on nanometrically high polymer de-mixed islands of 13, 35 and 95 nm compared to flat surfaces of similar chemistry[296]. Moreover, vertebrate cell adhesions have been shown to react to silica with fabricated nanometric features; with enhanced adhesion at cliff edges and decreased cell adhesion on ordered arrays of pits or pillars[297]. In line with this, fibroblast cells also show reduced adhesion and spread area on ordered nano pits compared to flat substrate controls, with a disruption in cytoskeletal organisation and a decrease in the size and number of FA[298].

Indeed, highly ordered topographical surface patterns tend to show low cell adhesion whereas random sub-μm roughened substrates can control MSC differentiation relative to flat controls[299]. Flat controls and random and ordered pits (120 nm diameter and 100 nm depth) do not impact MSC differentiation, whereas disordered pits in a square arrangement (±20 and ±50 nm offset) show bone differentiation to a similar extent as MSCs treated with soluble chemical (dexamethasone and ascorbate) treatment[300]. Interestingly, high control of order in pitted features has been shown to maintain MSC growth for over eight weeks, and this could be utilised in the production of large numbers of high-quality stem cells[301,302].

Topography has also been used to differentiate MSCs towards a neural lineage. Engineered nanochannels cause cells to spread directionally, and have been shown to increase MSC expression of the neuronal marker microtubule-associated protein 2 (MAP2)[303]. Moreover, parallel microgrooves have been shown to enhance the directed differentiation of cardiac progenitors into cardiomyocyte-like cells using a lentivirus-mediated direct reprogramming approach[304]. The cells aligned with the microgrooved substrate, mimicking the native ventricular myocardium, and the microgrooved substrate caused an increase in histone H3

acetylation, favouring "stemness" factors for reprogramming, and also stimulated the myocardin sumoylation post-translational modification necessary for the transcriptional function of this crucial co-activator.

1.4.3 Materials to assess mechanotransduction

1.4.3.1 2D gels and 3D hydrogels

Matrix stiffness has been shown to control stem cell differentiation, with softer matrices favouring adipogenesis and harder matrices favouring osteogenesis[166]. Materials with tunable stiffness have been designed to assess this, including ECM protein-based gels, polysaccharide-based alginate gels, and non-natural polymeric gels (e.g. polyacrylamide) coated with ECM proteins. Non-natural polymeric gels are chemically inert and they therefore need to be coated with ECM proteins to enable cell adhesion. The stiffness of these gels is controlled by altering the density of crosslinkers, however this also alters surface geometry, porosity and ligand binding[305]. As a result, polyacrylamide gels of constant stiffness with varying porosity and ligand-substrate tethering have been synthesised. These gels have been used to show that differentiation is not affected by porosity or tethering, and that stiffness is the factor that directs cell differentiation[306].

Cells have also been cultured in 3D hydrogels, which better mimic an *in vivo* environment compared to 2D gels. As with 2D polyacrylamide gels, 3D alginate gels with different stiffness have been shown to direct stem cell differentiation[270]. However, further work in 3D covalently crosslinked hyaluronic acid (HA) hydrogels has suggested that cell fate depends on the cell's ability to degrade its surrounding matrix and the resultant cellular traction, rather than matrix stiffness[307]. When cells were seeded on HA hydrogels with equivalent stiffness but altered cell-mediated degradation capacities (permissive and restrictive hydrogels), cells seeded on permissive hydrogels demonstrated high degrees of cell spreading and high tractions and favoured osteogenesis whereas cells seeded on restrictive hydrogels showed low levels of cell spreading, low tractions and favoured adipogenesis. Cell traction was shown to be responsible for cell fate, since a switch in permissive to restrictive hydrogel properties by delayed secondary crosslinking suppressed cell traction and caused a switch from osteogenesis to adipogenesis without a change in cell morphology. Moreover, inhibition of

tension-mediated signalling in the permissive hydrogel showed similar effects on the hydrogels with delayed secondary crosslinking, whereas an upregulation of tension induced osteogenesis even on the restrictive hydrogel.

1.4.3.2 Arrays of one dimensional micro- and nano-structures

When cells are grown on one dimensional micro- and nano-structure (NS) arrays cellular mechanobiology has been shown to be altered. For example, FA formation and cell attachment is altered on InAs nanowire (NW) arrays compared to flat InAs controls[308]. Rinsing assays were used to show that cell detachment is reduced on the NW arrays compared to flat controls. When the cell cytoskeleton was labelled, the actin-rich extremities of the cells were colocalised with the NW, demonstrating an interaction between the actin cytoskeleton and the NW. This interaction may be the reason why cell attachment was stronger on the NW. Next, FA position, density and morphology were investigated. Focal adhesions were localised on the NW but also in the space between NW; FA were more elongated in morphology; and the FA area and density was increased on NW compared to flat controls. Increased cellular adhesion on nanostructured arrays compared to flat controls has also been shown by centrifugation forces[309] and cells have been shown to migrate less on rings of vertical NW[310]. On the other hand, cells have shown decreased adhesion levels to zinc oxide (ZnO) nanorods compared to their corresponding ZnO flat substrate controls[311]. Indeed, cells on ZnO nanorods were rounded and were unable to form FA, stress fibres, and lamellipodia. This example of conflicting adhesion levels on NS highlights how the cellular response to NS arrays is highly varied. This is most likely due to the variety of different NS arrays (displaying varying surface chemistries, geometries, topographies, and fabrication methods) and the variety of cell types which are seeded onto them.

Nanostructured arrays have also been shown to influence stem cell fate[312,313]. Liu *et al.* have shown that when MSCs are seeded onto silicon NS arrays in the absence of growth factors, they preferentially differentiate into osteoblasts and chondrocytes[313]. Moreover, Ca^{2+} ion channels were transiently activated which led to the activation of Ras/ rapidly accelerated fibrosarcoma (Raf) / mitogen-activated protein (MEK) / extracellular signal-regulated kinase (ERK) signalling cascades to regulate processes such as adhesion, proliferation, and differentiation of the MSCs. Interestingly, hMSC osteogenic gene

expression of *COL1A1* and *Runx2* has been shown to be higher on shorter NS arrays, compared to longer NS arrays and flat controls[312].

1.4.3.3 Micro-patterned materials

Microcontact printing is a form of lithography which uses poly(dimethylsiloxane) (PDMS) as a flexible mould that can retain the surface chemistry of silicon masters which have been patterned using standard photolithography techniques[314,315]. In this way, multiple replica substrates with specific transfer patterns can be made. Microcontact printing with patterns of ECM molecules and well-defined shapes on the micrometre scale have been developed. These can be used to hold single cells in particular configurations since adherent cells tend to take on the shape of the micro-engineered islands they are seeded on. Therefore, microcontact printing has been used to assess the relationship between cell shape and cell function. For example, it has shown that capillary epithelial cells proliferated on large (2500 mm^2) islands in the presence of soluble growth factors, but differentiated to form hollow tubes when cultured on smaller islands that promote moderate spreading (1000–2000 mm^2) in the same medium[316–318]. Moreover, microcontact printing has been used to show that reduced cell spreading and round patterns promote adipogenesis, whereas larger spread areas or concave edged-shaped cells which promote actin cable formation promote osteogenesis in stem cells[271,319–321]. These cell fate decisions are associated with the modulation of the cytoskeleton via Ras homolog gene family, member A (RhoA) and rho-associated, coiled-coil containing protein kinase 1 (ROCK) signalling[190,320]. Thus, microfabricated ECM islands enable researchers to discriminate between signals introduced by soluble factors, direct binding of ECM molecules and cell shape change.

Microcontact printing has also been useful in assessing cell-ECM adhesions. For example, microarrays of multiple small (3-5 mm diameter) ECM islands have shown that FA assembly depends on the degree to which the cell can spread, and the FA structure depended on the island size and its location beneath the cell, along with the level of cytoskeletal tension[322]. When cells are cultured on square ECM islands covering their entire surface, stress fibres predominantly align along the diagonals of the square and FA tend to form at the corners[323,324]. When motility factors were added the cells formed actin projections at their corners, whereas on circular islands filopodia/lamellipodia/microspikes formed over the

entire circumference of the cell[324]. It has also been shown that cells prefer to extend motile processes from corners with acute, rather than obtuse angles[323] and that cells also exert the greatest traction forces in these corner regions[325].

1.4.4 Methods to assess mechanotransduction and cell-matrix interactions

1.4.4.1 Atomic force microscopy

Atomic force microscopy (AFM) can mechanically stimulate cells and simultaneously measure their elastic response. AFM works by pushing the sample against a soft elastic cantilever and measuring the resultant probe deflection. Since the spring constant of the cantilever is known, the contact force between the probe and the sample can be determined and this is related to the mechanical properties of the sample. The AFM can perform mechanical testing on soft biological samples[326] and cells[327]. AFM has proven to be a powerful tool to study the rupture of molecular bonds, ranging from covalent bonds[328], to the unfolding of proteins[329] and nucleic acids[330]. For example, it has been used to discover the unfolding intermediates of the actin-crosslinking protein, filamin[331]. Please refer to the introduction of the nN chapter for further examples of AFM probing of cells.

1.4.4.2 Optical and magnetic tweezers

Optical tweezers create an optical trap by focusing a laser to a diffraction-limited spot with a high numerical aperture (NA) microscope objective[332]. Any dielectric particle that comes into the vicinity of this spot will experience a force directed towards the spot. Optical tweezers can exert forces in excess of 100 pN on nm to μm sized particles, therefore single cells[333] and organelles within cells[334] can be trapped. At the same time, optical tweezers can measure the 3D displacement of the cell/organelle with sub-nanometer accuracy and sub-millisecond time resolution. For example, optical tweezers have been used to assess the force and displacement of kinesin coated beads moving along fixed microtubules[335–337] and to measure the activation state of single fibrinogen-integrin pairs on living cells[338].

Magnetic tweezers are made up of a pair of permanent magnets placed above the sample holder of an inverted microscope[339,340]. They can exert forces > 1 nN (electromagnetic tweezers), and can be used to rotate and manipulate magnetic particles 0.5–5 μm in size.

Magnetic tweezers have the advantage of having a force clamp which is passive with an infinite bandwidth over large displacements. They have mainly been used to study nucleic acid enzymes e.g. DNA topoisomerases[341–343] but could also be used to assess mechanotransductive organelles.

1.4.4.3 Magnetic twisting cytometry and magnetic pulling cytometry

Magnetic twisting cytometry (MTC) and magnetic pulling cytometry (MPC) are techniques which use bound ligand-coated ferromagnetic microbeads to apply controlled shear forces and superparamagnetic beads to apply controlled tensional forces to cell surface receptors respectively[344–347]. Micromagnetic techniques are advantageous since they can apply a larger range of stress (pN-nN) and frequency range of forces (0-1000 Hz). Moreover, they can target specific cell receptors and cells can engulf beads, enabling forces to be applied within cells. Finally, many cells and bound beads can be analysed in parallel, cells can be probed for days without incurring heating problems, and magnetic systems are cheaper, more robust, and easier to set up.

The MTC method has been used to show that forces applied to integrins and non-adhesion receptors produce different cellular responses. For example, integrins show less angular rotation compared to transmembrane receptors such as metabolic and growth factor receptors that are not bound to the cytoskeleton[344,348]. Moreover, the MTC method has shown that different transmembrane adhesion receptors show different levels of cytoskeletal coupling[348–350]. MTC has shown that when shear stress is applied to integrins the cAMP signalling pathway is activated[351], and mRNA and ribosome recruitment to FA is increased, inhibiting cytoskeletal tension[352]. The MPC method has been used to show that cells use a number of mechanisms to respond to both static and dynamic changes in force application at integrin sites[353]. Moreover, MPC has demonstrated that > 1 nN force loads at integrin- bound beads cause a calcium wave within 2-5 seconds and that this can be prevented by treatment of cells with the stress-sensitive ion channel blocker gadolinium chloride[353].

1.4.4.4 Traction force microscopy

Traction force microscopy (TFM) can be used to assess and quantify cell matrix adhesion. Well characterised materials such as polyacrylamide or polydimethylsiloxane are used as synthetic

substrates. Following cell seeding, substrate deformation can be tracked using fluorescent marker beads. Using the elastic theory, the displacement can be converted to an estimated traction-force pattern[354–356] and cellular traction forces can be measured with micrometre resolution[357]. TFM has revealed a relationship between the adhesion structure, the organisation of the actin cytoskeleton, and cellular traction force patterns. TFM has been applied to measure 3D traction forces on 2D substrates[358–360] as well as traction forces in cells seeded in 3D hydrogels[361]. Another technique to study cell traction forces is to study the interactions between cells and microfabricated elastic pillar arrays[362]. Cell adhesions interact with individual pillars and the deflection of the pillar enables cell traction force to be estimated. No computational force reconstruction is required, force from individual adhesions can be measured, and anisotropic mechanical environments can be investigated by designing different shaped pillars[363].

Recently, cellular forces have been assessed in 3D elastic scaffolds[364]. Traction force measurements have shown that cell-generated stresses are of similar magnitude to those found in the surrounding ECM. Physiological environments can vary from 100 Pa in the brain to 10 kPa in connective tissue and 50 kPa in bone[180,365] and the traction forces measured for migrating 3T3 fibroblasts has been shown to be 10 kPa[354].

Measuring intracellular forces has proved much more challenging and the most promising method has been to assess the recoil of cytoskeletal elements following laser ablation. This has been used to show the spatial variation in stress fibre tension[366,367] and to show how zyxin localises to highly stressed regions between stress fibres and the extracellular substrate[368]. This technique is invasive, however, and so an alternative approach has been to use fluorescent biosensors whose fluorescence intensity depends on the level of tension. For example, a vinculin biosensor has been developed which can measure the forces acting at FAs[207].

1.4.4.5 Arrays of one dimensional micro- and nano-structures

Arrays of one dimensional micro- and nano-structures have also been used as methods to assess cell-matrix interactions. Micropost arrays have been used to decouple substrate stiffness from surface properties. This has been achieved by synthesising microposts with the

same surface geometry but different post heights to control substrate stiffness/rigidity, since the post height determines the degree to which a post bends in response to a horizontal traction force[272]. Micropost stiffness was shown to impact cell morphology, FA, cytoskeletal contractility and stem cell differentiation. Moreover, a high density array of elastomeric micropillars has been used to investigate the cellular forces involved in migration[369]. Traction forces induced by cell migration were deduced by measuring pillar bending and a multiple-particle tracking method was used to estimate the mechanical activity of cells in real time down to 2 µm resolution, due to the periodicity of the array.

Nanostructured arrays provide an improved method to monitor cell traction forces compared to microstructured arrays since they are of smaller size and can have higher packing densities, enabling smaller forces to be detected with higher spatial resolution. For example, forces have been mapped across single cells seeded on nanoimprinted polycarbonate pillars, demonstrating larger traction forces at the cell periphery compared to the cell centre[370]. Moreover, GaP nanowires grown by epitaxy on electron-beam lithography defined gold nanodots have been shown to detect cellular forces of 15 pN, with a spatial resolution of 1 µm[371]. Nerve cells were cultured on the arrays and live cellular forces could be calculated by assessing the displacement of the nanowire tips using confocal microscopy.

1.4.4.6 Super resolution microscopy

Resolution in conventional light microscopy is limited by diffraction. The term resolution can be understood by taking two spots and seeing how close these two spots can be such that you can still see them as two spots. Ernst Abbé derived an equation to describe the diffraction limit of microscopy; $D=\lambda/2NA$, where D is the diffraction limit, λ is the wavelength of the light, and NA is the numerical aperture. The resolution limit is described by the point spread function (PSF), which shows the spread of a single point of light as a result of diffraction through a microscope. If two molecules can be contained within this PSF then they cannot be distinguished, and objects that are smaller than the PSF are seen to be the same size as the PSF.

In 2014, the Nobel Prize in Chemistry was jointly awarded to Eric Betzig, Stefan W. Hell and William E. Moerner "for the development of super-resolved fluorescence microscopy". Super-

resolution microscopy (SRM) breaks the diffraction limit of conventional light microscopy[372]. Super-resolution can either be achieved by spatially modulating the fluorescence emission using patterned illumination (e.g. stimulated emission depletion microscopy (STED), ground state depletion (GSD) and structured illumination microscopy (SIM)) or by stochastically switching on and off individual molecules using photoswitchable probes (e.g. stochastic optical reconstruction microscopy (STORM)[373], or photoactivatable/photoconvertible fluorescent proteins (e.g photoactivation localisation microscopy (PALM)[374,375]).

SRM shows great promise in advancing the understanding of cell-matrix interactions. For example, 3D SRM has been used to map nanoscale protein organisation in focal adhesions, and to show that actin and integrins are vertically separated by a ~40-nm FA core region[376]. This core region consists of: a lower, integrin-signalling layer containing integrin cytoplasmic tails, FAK and paxillin; an intermediate force-transduction layer containing talin and vinculin; and then an actin-regulatory layer containing zyxin, vasodilator-stimulated phosphoprotein and α-actinin. Moreover, SIM has been used to visualise the interactions between actin stress fibres, nuclear lamina and LINC complexes at a super-resolution scale[377]. When apical stress fibres experience tension, the nucleus shows deep indentation which deform the nuclear lamina. The indented areas show local enrichment of LINC complexes and induce the formation of segregated domains of condensed chromatin. This process is reversible, and the indented areas are removed when apical actin stress fibres relax. Quantitative SRM has been used to characterise early integrin clusters and has shown that very early adhesions consist of ~100-nm clusters of ~50 β3-activated integrins[378]. These early adhesions form under a wide variety of conditions on RGD surfaces and form similarly on fluid and rigid substrates, however most adhesions are transient on rigid substrates.

1.4.5 Limitations of mechanobiology and cell-matrix interaction studies

For mechanobiology studies, cells are often plated onto coverslips coated with thin gels (e.g. acrylamide) whose material stiffness can be modified by cross linking density and whose structural stiffness can be altered with gel thickness. The stiffness of these gels is not an independent variable, however, since crosslinking density has an effect on substrate porosity, topography and matrix protein anchoring[305]. Moreover, these materials tend to show a linear

relationship between mechanical response and strain, whereas the native matrix shows a nonlinear response in which stiffness increases with extension[379,380]. These gels also fail to mimic the variations in matrix proteins in vivo since they tend to contain uniformly deposited matrix proteins.

Cells are subjected to a range of mechanical forces *in vivo*, including fluid shear stress, tension, and hydrostatic compression. Indeed, it is a challenge to assess the multifactorial and dynamic nature of these mechanical stimuli using materials. Materials have been used to assess individual types of mechanical force (e.g. strain, compression and shear) on cells but these forces can act in unison and can also vary in magnitude, duration, frequency and dimensionality (uniaxial or biaxial). Individual studies on different force types have shown that cyclic strain favours osteogenesis or chondrogenesis[381,382], fluid shear stress favours osteogenesis and vasculogenesis[383], and hydrostatic pressure or uniaxial compression favours chondrogenesis[384,385].

Further materials need to be developed to explore cell mechanobiology. To date, most materials have been treated as purely elastic, wholly described by their Young's modulus. More recently, the role of viscoelasticity on stem cell differentiation has been explored[386], since the ECM is visoelastic and exhibits stress relaxation. Hydrogels have been developed which have a tunable stress relaxation rate, independent of the initial elastic modulus, degradation, and cell-adhesion-ligand density. It has been shown that MSC spreading, proliferation, and osteogenic differentiation are promoted on hydrogels with faster relaxation, and that this is mediated by actomyosin contractility, adhesion-ligand binding, and the mechanical clustering of adhesion ligands. Visoelasticity should therefore be an important design parameter in materials developed for mechanotransduction studies.

There is also the issue of matrix dimensionality. When a cell pulls on a 2D matrix, where a compliant substrate is attached to a rigid surface, there is a localised deformation which decays exponentially and whose range depends on the substrate thickness[4]. However, when a cell pulls on a 3D matrix, the deformations propagate over a longer range, roughly decaying at the inverse-square of the distance from the cell[387]. The ECM allows mechanical information to be carried further *in vivo* since it contains fibres which can propagate tensional force if they

are not cross-linked to other filaments. Non-linear elasticity effects should also be explored, since native tissue can show mechanical anisotropy. Moreover, efforts should be made to dynamically modulate mechanical cues, physically tuning the physical stimuli presented to cells as they advance along their differentiation pathways. Therefore, it is essential that novel biomaterial platforms are developed in order to further understand cellular mechanotransduction and cellular interactions with the ECM. Moreover, further experiments should be conducted *ex vivo* and *in vivo* due to the inherent *in vitro* artefacts.

1.5 Scope of the thesis

This PhD assesses the interactions between cells and their extracellular environment in two different ways. Firstly, in chapter 2, a synthetic system comprising a porous silicon nN array is used as a probe to assess mechanotransduction in primary human cells. Secondly, in chapter 3, a naturally derived protein fragment, generated by matrix metalloproteinase (MMP) processing of the laminin-111 BM protein, is added to normal mouse mammary gland epithelial (NMuMg) cells as a soluble factor and its effect on TGF-β1 signalling and the epithelial-to mesenchymal transition (EMT) is investigated. This thesis therefore studies both mechanical and biochemical cues from the extracellular environment on a range of different cell types, and assesses interactions at cell-material and cell-matrix interfaces. A greater understanding of the diverse functions of the ECM and the cellular response to mechanical cues will contribute to the development of new therapeutics for ECM-related diseases and will enable novel strategies for tissue engineering and regenerative medicine.

2 Microscopy of the interactions at the cell-nanoneedle interface

Porous silicon nanoneedle (nN) arrays have been used for intracellular sensing and the delivery of cargo to the cell cytosol, however the details of the cell-nanoneedle (nN) biointerface remain controversial and an assessment of the cell's mechanotransductive response to the nN arrays is required. This chapter studies the interaction of porous silicon nN arrays with two primary cell types: human umbilical vein endothelial cells (HUVECs), and human mesenchymal stem cells (hMSCs). Cells were seeded on nN arrays and flat silicon control substrates and were assessed six and 48 hours post-interfacing. Confocal, widefield and super-resolution microscopy were employed together with qPCR to assess the cell mechanobiology response to nN arrays.

Nanoneedle interfacing led to alterations in cell mechanobiology without affecting cell viability. Primary cells showed altered morphology on nN arrays compared to flat control substrates and formed protrusions which could interact and/or align along the nN arrays. Cells were unable to form mature FA on nN arrays and showed reduced levels of actomyosin tension and YAP activity. The actin cytoskeleton and nucleus directly responded to sites of nN interfacing; the actin cytoskeleton formed rings around the nN and the nucleus remodelled around the nN, with higher levels of lamin-A, but not lamin-B at the nN locations. Finally, this was shown to be a reversible process since cell phenotype was restored to that on flat control substrates once the nN had degraded at 48 hours.

This chapter characterises the peculiarity of the biophysical interactions that occur between sharp, high-aspect ratio nanomaterials and multiple cellular organelles. Nanoneedles were able to modulate cellular signalling events that resulted in a decoupling of YAP activity and cell area, and a divergent expression of lamin A and lamin B. Further work will involve the identification of the mechanistic factors that underlie the observed phenomena.

2.1 Introduction

The term “nanoneedle" (nN) refers to a range of needle-shaped nanostructures that can interface directly with cells and tissues to generate a desired response or to measure their activities. Nanoneedles are also referred to as nanostraws and nanowires, and can be solid, hollow, or porous in nature. They can be found in a variety of forms for varying applications, such as on the end of an atomic force microscope or as part of an array[388].

Nanoneedles are a useful platform to study cell behaviour since many cells can be assessed simultaneously, and a single cell can be interfaced with many nN, allowing spatial resolution across the entire cell[389,390]. A large number of cell types, including neurons, stem cells and primary immune cells, have shown viability on a variety of nN, suggesting a general biocompatibility of nN[388]. Nanoneedle arrays also show significant potential for a variety of biological applications including cargo delivery[389–394], electrophysiology measures[395,396], and chemical sensing[397–401]. Moreover, nN show the potential to both deliver and collect material from specific subcellular compartments[393,402,403] and to investigate cells which are difficult to assess[404].

In this introduction, nN are introduced: nN fabrication and functionalisation methods are described; the ability of nN to penetrate the cell membrane and gain intracellular access is assessed; the biological applications of nN are presented; and cell properties on nN interfacing are introduced. The porous silicon nN arrays which are employed in the chapter are then described.

2.1.1 Nanoneedle fabrication

Nanoneedle arrays can be fabricated by a number of methods, either by “top-down” or “bottom-up” approaches[405]; the more commonly used top-down techniques involve etching out nN from bulk material whereas bottom-up approaches use catalytic particles to enable the formation of vertical nN (**Figure 2.1**). Both these approaches can fabricate nN of different materials and geometries and nN arrays with different densities and regularity[388]. Silicon is the most common nN material and it is usually made by top-down fabrication. Silicon nN

arrays can be ordered or randomly distributed, can be grown as dense patches or as grass-like carpets of semi-vertical rods[388]. Silicon nanoneedles can be solid, porous or hollow.

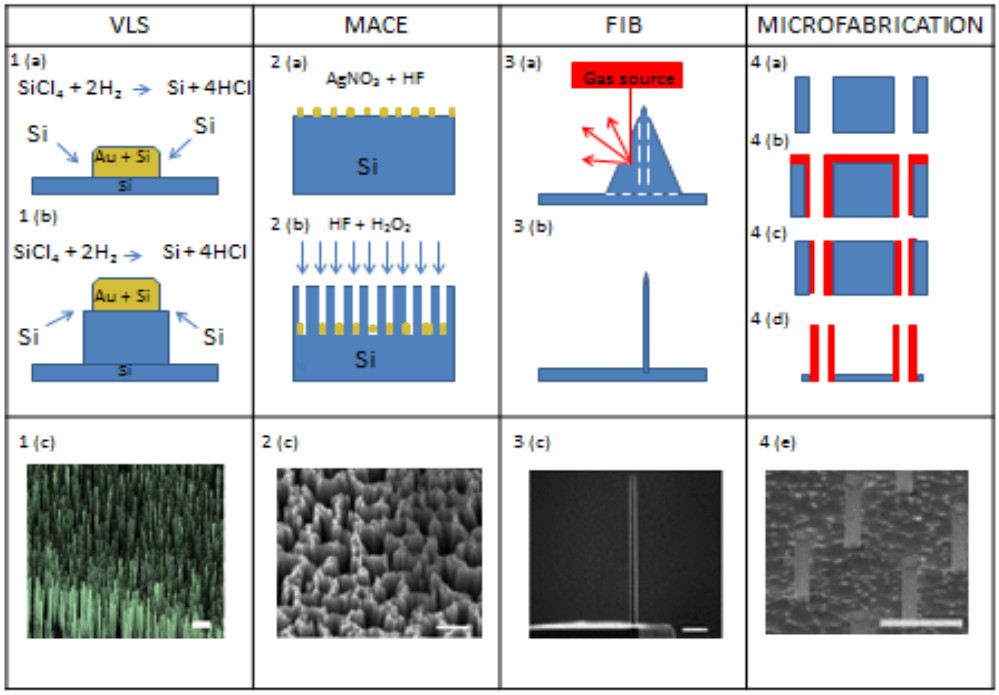


Figure 2.1: Fabrication strategies for nanoneedles, modified from C. Chiapinni and C. Almeida Semiconducting Silicon Nanowires for Biomedical Applications, pp.144-167 2014[406]. Vapour-liquid-solid (VLS): 1(a) liquid eutectic Au-Si alloy droplet formation through Si incorporation in its vapour phase. 1(b) Above saturation point, Si nucleates in the solid phase. 1(c) Scanning electron microscopy (SEM) image of nanoneedles (nN) produced by VLS, scale bar = 1 µm. Metal-assisted chemical etch (MACE): 2(a) patterning of Silicon with noble metal b) etching of Si by noble metal in oxidising hydrogen fluoride (HF)/ hydrogen peroxide (H_2O_2) solution. 2(c) SEM of nN produced by MACE, scale bar = 1 µm. Focused ion beam (FIB): 3(a-b) shaping of nN through gas source (e.g. gallium) milling 3(c) SEM of nN shaped by FIB milling, scale bar = 1 µm. Microfabrication: 4(a) deep pores are etched into a silicon membrane, 4(b) silicon dioxide (SiO_2) addition and 4(c) removal of the top SiO_2 layer 4(d) selective etching of Si to form hollow SiO_2 nanoneedles. 4(e) SEM of hollow nN, scale bar = 3 µm.

Other materials used to make nN include gallium phosphide, gallium nitride, and indium arsenide. These nN can also be grown in random or ordered patterns[388]: platinum nN have been positioned with high precision in a ring[310] or as ordered patches of a few nN[310,407]; dense random arrays of semi-vertical zinc oxide nN have been fabricated[311,408,409]; random arrays of copper oxide nN of varying height have been produced[410]; and ordered arrays of lower-aspect-ratio quartz[411,412], polystyrene[413], and poly-(lactic-co-glycolic-acid)[414] nN have been

created. Hollow nN have also been fabricated from silica[402], aluminum oxide[403,415–417], aluminum indium phosphate[418], or iridium oxide[419].

2.1.1.1 Solid silicon nanoneedles

Solid nN are fabricated by vapour-liquid-solid (VLS) growth and focused ion beam (FIB) etch. These technqiues are able to produce nN with tightly controlled dimensions and geometries. VLS is a highly reproducible and versatile technique and is usually utilised in the production of solid vertically aligned silicon nN[420]. A metal-silicon alloy droplet is formed by heating a metal nanocluster above its eutectic temperature in the presence of a silicon gas source. This droplet is placed on a surface (e.g. Au) where it adsorbs the silicon gas source (e.g. silane, SiH_4) until supersaturation occurs. Supersaturation is followed by nucleation at the liquid/solid interface, enabling a nN to form with the alloy droplet riding at the tip[421]. Elongation occurs when Si is incorporated at the liquid/solid interface and thickening occurs when Si is incorporated at the vapour/solid interface[421]. The conditions for VLS are severe and the synthetic conditions must be tightly controlled, enabling control over the elongation and thickening of the nN[422]. nN diameter, density and arrangement can be further controlled by combining VLS with lithography[423].

Solid nN can also be made by FIB etching. This involves a heavy beam of ions (usually gallium) which can mill the surface of micro-and nano-structures at nanometre precision. nN tips with diameters > 50 nm can be made when combined with scanning electron microscopy (SEM)[424]. A disadvantage of FIB etching is that it is time consuming since each nN must be milled individually. Therefore FIB etching is usually used to produce nN for atomic force microscopy (AFM) probing of cells since only one nN is required[424–427].

2.1.1.2 Porous silicon nanoneedles

Porous silicon is partially dissolved silicon containing an interconnected network of air holes/pores. Vertically aligned porous nN can be produced using metal-assisted chemical etch (MACE)[428–431]. Like VLS, MACE is reliable and versatile but also has the added bonus of being lower in cost. A noble metal is deposited on a photolithographically-patterned silicon substrate immersed in an oxidising solution of hydrogen fluoride (HF)/ hydrogen peroxide (H_2O_2). An electrochemical reaction between the silicon substrate and HF/ H_2O_2 then causes

dissolution of the silicon. The noble metal acts as a catalyst and so etching primarily occurs in its vicinity, allowing the dissolution of silicon below the noble metal to form pores in the silicon substrate. The etching occurs in an isotropic manner, inducing the formation of porous silicon nN[432–434]. The lithographic pattern controls the pitch arrangement and the etching conditions control the shape of the nN. The porosity, pore size and crystalline orientation of the nN is controlled by silicon substrate resistivity, oxidant concentration and etch temperature[435]. nN porosity can be increased by using longer etching times or higher HF/ H_2O_2 concentration since this facilitates the diffusion and nucleation of noble metal ions. It is postulated that pores are formed as a result of surface and charge instabilities at the solid-solution interface[429].

2.1.1.3 Hollow nanoneedles

Hollow nN, also known as "nanostraws" are produced by microfabrication involving deep reactive ion etch (DRIE). Hollow nN microfabrication begins by forming an array of nanopores on a silicon wafer using electron-beam lithography and DRIE. These pores are coated with silicon dioxide via thermal oxidation; this creates the bodies of the hollow nN and determines the thickness of the hollow nN. Directional plasma etching is then used to remove the top layer of silicon dioxide from the silicon wafer. Selective etching of silicon (over silicon dioxide) enables preferential thinning of the silicon wafer to reveal the silicon dioxide nanostraws[402,403]. The DRIE technique is limited since it breaks down at the nanoscale, limiting the depth of pores (the length is restricted to 3 µm), and the diameters of hollow nN are large compared to those created by VLS, FIB, and MACE[406].

2.1.2 Functionalisation of nanoneedles

Functionalisation of nN enables the conjugation of drugs and biomolecules for delivery and sensing (e.g. loading quantum dots, DNA, proteins, and biomolecules)[424–426,436–440]. nN can undergo a variety of functionalisations, either by adsorption (covalent and noncovalent) or by coating them with metals (e.g. Au[436,440,441]). Covalent methods involve chemical bonds whereas non-covalent methods utilise electrostatic and hydrophobic interactions[442]. The most common method of nN functionalisation is the condensation of trialkoxysilanes with the surface silanol group[443]. The silane coupling reaction enables self-assembled alkylsilanes

networks to be formed on nN[426]. For example, nN have also been functionalised with 3-aminopropyltriethoxysilane (APTES) in order to adsorb red-fluorescent protein DsRed2-NES for intracellular delivery to human embryonic kidney (HEK293) cells[426]. APTES provides a positively charged surface which enables negatively charged nucleic acids and proteins to be adsorbed, and detachment of cargo is possible by hydrolysing the silane layer[393,444].

2.1.3 Intracellular access

For many promising nN applications, intracellular access is crucial, and it is therefore important to establish cell membrane penetration by nN **(Figure 2.2)**. When cells are seeded onto nN arrays, gravity causes sedimentation of cells but penetration does not necessarily occur; instead, the membrane can wrap around the nN, forming a tight interface with the nN surface[308,410,412,445,446]. Cell adhesion, limited cell motility[309], and cargo delivery[393] have been used as evidence for nN penetration, however penetration remains to be visually proven. Since cells would need to play an active role for nN internalisation to occur, the seeding method is sensitive to cell type and environmental conditions (e.g. temperature, medium)[393,402], as well as the nN design (e.g. array density, nN functionalisation)[309,388,446,447].

The distinction between membrane penetration and engulfment by nN is under debate[388]. For example, the lack of cytosolic material lost on nN interfacing might imply a failure in membrane penetration however this could also be the result of a rapid resealing mechanism of the cell membrane[412]. Moreover, cargo may not be delivered by nN via membrane penetration[389,390,393,416,417,447,448], instead endocytotic pathways may be upregulated due to the constantly high membrane curvature around the nN[393]. During endocytosis, localised regions of the cell membrane progressively enclose around the cargo, forming endocytotic vesicles containing the cargo. Therefore, the membrane curvature caused by the nN could influence the transport properties of the cell membrane, facilitating cargo delivery into the cell[449]. Indeed, it has been show that phospholipid head groups on the outside of forming vesicles are subject to higher membrane curvatures and show greater exposure to lipid-binding and modifying enzymes[450]. Moreover, phosphoinositide (PI) 3-kinase and PI-specific phospholipase C activity can be enhanced by higher membrane curvature[451,452]. The localised membrane curvature may cause a positive feedback loop that initiates the hydrolysis of

phosphatidylinositol-4,5-biphosphate (PIP_2) which is activated for endocytosis[453,454]. A number of transmission[410,412] and focused ion-beam scanning electron microscopy[407,455,456] studies of the cell-nN interface also support engulfment over penetration by nN since they show the cell membrane wrapping tightly around the nN[407,410,412]. Moreover, theoretical modelling has shown that cells can energetically afford to bend their membrane around the nN, rather than being penetrated[308].

On the other hand, action potential recordings suggest that nN can directly penetrate into the cell and the cell membrane can rapidly reseal around them, forming a tight interaction which results in less leakage of electrolytic fluid compared to the patch clamp technique[395]. Using patch clamp recordings as a control, the voltages and currents of seeded HEK293 cells were monitored simultaneously using a patch pipette and a vertical nanowire electrode array (VNEA) pad[395]. An immediate response was found to current injection by VNEA and this suggested that membrane penetration had occurred. It must be noted that although some nN spontaneously penetrated the membrane, other nN only entered the cells in the presence of applied electric fields through electroporation. Therefore, it appears that the solid silicon nN did not have 100% penetration efficiency and this could hinder the precise recordings of cell action potentials in cell microenvironments.

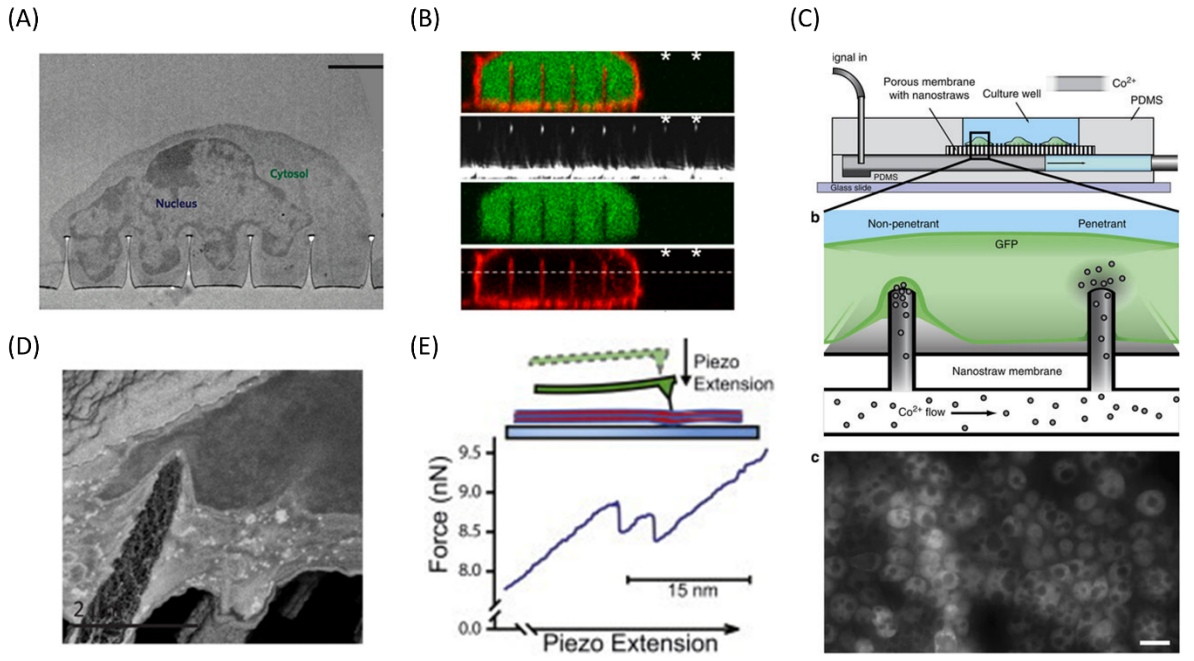


Figure 2.2: The cell–nanoneedle interface. A) Silicon dioxide nanopillar arrays do not penetrate through the cell membrane, instead the cell and nuclear membranes deform around the nanopillars. Scale bar = 2 µm. Reprinted from reference [195] with permission from Macmillan Publishers Ltd., copyright 2015. B) Similar results are shown for Indium Arsenide (InAs) nanoneedle (nN) arrays. InAs nN arrays do not penetrate into the cell cytosol but instead strongly deform the cell membrane (red), (cytosol – green). Reprinted from reference [445] with permission of IOP Publishing, copyright 2012. C) Hollow nN/ nanostraws can deliver the membrane-impermeant ion Co^{2+} to the cell cytosol at an efficiency of approximately 7%, suggesting some cell membrane penetration. In the cell cytosol, the Co^{2+} ion can quench GFP fluorescence: a-b) schematic of the delivery mechanism by hollow nanostraws; c) spots of GFP quenching observed by optical microscopy, enabling membrane penetration to be quantified. Scale bar = 20 µm. Reprinted from reference [417] with permission from Macmillan Publishers Ltd., copyright 2014. D) Porous silicon nanoneedle arrays show tight interfacing with the cell cytosol and they deform the nuclear membrane. Scale bar = 2 µm. Reprinted from reference [389] with permission from the American Chemical Society, copyright 2015. E) Membrane penetration of AFM controlled nN can be detected by a sudden drop in the force–displacement curve. Reprinted from reference [457] with permission from Elsevier, copyright 2014.

2.1.1.4 Techniques to improve intracellular access

Intracellular access is crucial for many of the promising nN applications and is a major focus for the continued development of nN arrays. Since intracellular access by nN is highly debated, techniques have been used to improve intracellular access. It has been shown that in order for cells to be penetrated by gravity alone, the nN diameter should be approximately 10 nm[447], and that penetration efficiency can be enhanced by application of a force **(Table**

1)[448,458–461]. Modification of the nN surface, the addition of detergent solutions, and electroporation have also been shown to improve intracellular access of nN.

Table 2.1: Cell-nanoneedle interfacing strategies, modified from C. Chiappini, *ACS Sensors*, August 2017[401], with permission from the American Chemical Society, copyright 2017.

Interfacing strategy	**Force applied?**	**Tunable parameters**	**Interfacing efficiency (%)**	**Key reference**
Seeding	No	Cell density	> 90	[390]
Hypergravity	Yes	Acceleration Duration	~80	[462]
AFM	Yes	Force speed	70	[392]
Micromanipulation	Yes/No	Position	>90	[463]
Piezo oscillation	Yes	Distance duration	42	[464]

Nanoneedles produced by FIB can be used as atomic force microscope (AFM) tips[392,424–427,437–439,465,466]. The force and insertion depth of an AFM nN can be controlled and monitored down to the pico-Newton using an AFM force-distance curve[394,426], and these force-distance curves can provide evidence for successful AFM membrane penetration[392]. This is because cell indentation causes a repulsive force increase, with a sudden force drop when the cell membrane is penetrated by the nN, which is followed by a steep repulsive force increase due to the friction between the nN and the cell cytoskeleton. AFM studies have shown that a force between 0.5 and 2 nM is required to insert a nN probe with < 200 nm diameter through the cell membrane[392,438].

Other methods of forcible insertion of nN arrays include hypergravity through centrifugation and tapping[448], linear actuation[464] and high-frequency oscillating piezoelectric movements for rapid, repeated interfacing[464]. Centrifugation increases the sedimentation rate of cells through an increase in gravitational force[467] and cells can either be centrifuged onto nN arrays or nN can be centrifuged down onto the cells from above[467]. The centrifugation method has been used to enhance green fluorescence protein (GFP) plasmid delivery into cells: a

centrifugal force of 600 g enabled transfection expressions of < 1 %, whilst gentle pressing of the nN into cells enabled efficiencies of ∼50 % in certain regions[458]. Tapping experiments, in which nN arrays are tapped down onto cells using a sterilised tweezer by hand, also allow force loading rates compared to centrifugation[448,458]. In one study, centrifugation of cells onto carbon nN did not enable intracellular access, however inverting the nN array on top of the cells and pressing or tapping it down with tweezers was sufficient to gain some (variable) penetration[448,458,460,461]. Micromanipulation has been used in a carbon-nanotube-based endoscope to probe the intracellular environment with a spatial resolution of ∼100 nm, showing a > 90 % interfacing efficiency[463]. A custom-built linear actuator has been designed which can tilt a nN array so that it is parallel to the cell culture substrate[464]. This enables controlled interfacing and also maximises the number of interacting cells. The linear actuator can be equipped with a piezoelectric crystal which enables the actuator to oscillate the nN when in contact with cells, and this has been shown to improve cell interfacing whilst minimally impacting cell viability.

As well as loading cargo onto nN, surface functionalisation can be used to aid penetration into the cell cytosol by making the nN more compatible with the lipid bilayer found in the cell membrane. Hydrophobic coatings assist membrane penetration and nN with a phospholipid bilayer have been developed[468]. A branched intracellular nanotube field effect transistor (BIT-FET) developed for cell action potential recordings contains phospholipid modified nN and this has been reported to facilitate cell membrane penetration[396]. A dramatic change in recordings was seen 45 seconds after cell seeding which was claimed to arise from spontaneous cell penetration, moving from an extracellular to an intracellular signal. Moreover, when polyethyleneimine-coated nN are modified with aminosilane the number of nN gaining intracellular access increases from 0–7%[445], and polyorthinone and fibronectin coatings have also shown increased cell penetration efficiencies[417].

Mild detergents can be used in conjunction with nN to destabilise the cell membrane while still maintaining cell viability. A combination of hollow nN and a low concentration of detergents (e.g. saponin) has been shown to be necessary to deliver molecules intracellularly[402]. The cell membrane can also be destabilised by electroporation. Hollow nN of 250 nm diameter are unable to penetrate the cell membrane spontaneously and require

electroporation for nN penetration[416]. It is possible to use nN-based electroporation by turning the nN into nanoelectrodes. These nanoelectrodes are tightly coupled to the cell membrane and can therefore create a strong electric field from a small voltage, increasing the cell membrane permeability transiently and locally.

2.1.4 Biological applications of nanoneedles

Nanoneedles are able to intimately localise within the intracellular space and have therefore been utilised to deliver membrane-impermeant cargo to the cytosol[389,390,393,402,403,410,416,417], sense enzymatic activity[397,400], and stimulate/record electrical activity from within the cell[395,407].

2.1.1.5 Cargo delivery

A range of biological and physical techniques have been designed to enable biomolecule delivery to cells, since many molecules are unable to bypass the cell membrane based on their size, charge and hydrophilicity. Biological delivery techniques often exploit cellular uptake and transport mechanisms[469]; such techniques include viral systems, liposomal encapsulation and cell penetrating peptide carriers. Physical delivery strategies tend to disrupt and permeabilise cell membranes; for example through the use of detergents, electrical pulses, ultra-violet (UV) light and pore-forming toxins[470].

nN can directly deliver cargo into the cell cytosol of a variety of cell types, bypassing endocytosis without affecting cell viability[393]. This is achieved by loading the nN with the cargo and then allowing the nN to interface with the cell membrane. The cargo can diffuse off the nN or dissociate via a chemical reaction[470]. Solid, porous and hollow nN with a variety of different functionalisations have been used to deliver biomolecules intracellularly through a number of different mechanisms[392,394,436,438,465]. Small biological molecules such as siRNA, peptides, proteins, and DNA sequences have been delivered into cells using nN arrays with efficiencies ranging from 40–99%[393,403,404,410,417,471]. DNA expression following nN delivery is often below 1%[410,458,472], and rarely up to 5–10%[403,448]. The highest expression efficiencies to date (70–80%) have been achieved by a combination of hollow nN and electroporation[416]. In some cases, delivery efficiencies on flat controls are equivalent to those on nN arrays[410,471].

However, when delivered by nN, the cargo is directly in the cell cytosol and is not contained in intracellular endo- and lysosomes as it is with flat controls[471]. This is of importance since cargo can be degraded in endosomes and lysosomes.

Control of biological delivery remains a major challenge. For example, physisorbed molecules are rapidly desorbed from nN, thus a large excess of biomolecules must be loaded[392]. Chemisorbed biomolecules are covalently bonded to the nN and cleavage of these bonds enables their delivery [424,438,448]. Biomolecules have been covalently linked to nN via disulphide bonds. The conditions in the cell interior reduce the two thiol groups, enabling detachment of the cargo: (R−SS−R + 2H+ + 2e− → R− SH + SH−R) [394,436]. Hollow nN have the advantage that they do not need to be functionalised with the cargo. They can provide continuous and sustained delivery of cargo since they can be connected to a reservoir containing the cargo to be delivered[473–475]. Recently, hollow nN have been used to deliver the metabolite UDP-*N*-azidoacetylgalactosamine (UDP-GalNAz) into cells[476]. UDP-GalNAz is an intermediate in the glycosylation pathway, and there had previously not been an effective strategy for its delivery into cultured mammalian cells.

2.1.1.6 Electrophysiology measurements

Electrophysiology describes the study of the electrical properties of cells and tissues. A number of recording techniques have been developed to measure the ion flow in biological tissues since this can lead to a greater understanding of cellular signalling processes. The patch clamp technique is the most common electrophysiology method and is used to record cell action potentials[477]. Nanoneedle based electrode arrays provide an alternative method for electrophysiology recordings[395,407]. They are advantageous since they have high temporal resolution (resolving power increases with decreasing electrode size), and they have high spatial resolution since arrays can be fabricated with a pitch of several microns or less between the wires. In addition, the nN arrays can be used to both electroporate and measure the electrophysiological activity of cells. There is minimal signal loss as the cell membrane is able to seal tightly around the nN generating megaohm[395] to gigaohm[478] seal resistances.

A scalable intracellular electrode platform composed of an array of vertical nN (VNEA) has been developed which is able to intracellularly stimulate and record individual neuronal

activity and multiple synaptic connections in rat cortical neurons[479]. Moreover, nN-mediated current injections have been shown to induce action potentials in primary neurons[395], and the activity of this action potential could be followed in the same cells over several days[407]. It has been demonstrated that hollow nN show improved signal compared to solid nN, enabling recordings to be measured at longer time scales[419].

2.1.1.7 Biomolecule sensing

Intracellular protein sensing is highly valuable since certain proteins can be used as a marker for disease in cells. When used to assess intracellular biomolecules, cell membrane penetration is essential. nN arrays have been used as a real-time label free method for multiplexed electrical detection of protein cancer markers[398,401]. Moreover, apoptosis and inflammation has been monitored by analysing the activity of the caspase-3 protease using a nN−cell "sandwich" assay; with the top assay immobilising the cells and the bottom assay presenting the enzymatic substrates[397]. Caspase-3-activity has also been evaluated in a single living cell using an AFM nN and a fluorescent probe, in a method known as MOlecular MEter with NW Technology (MOMENT)[399]. AFM probe tips can penetrate the cell membrane through application of force and have therefore been used to measure intrinsic mRNA[480] and the cell cytoskeleton[481,482]. A nN array functionalised with enzymatic substrates has been used to measure the intracellular activity of three different enzymes. The array was introduced to the cells and then retracted and the enzyme activity was evaluated based on intracellular fluorescence and mass spectrometry of the nN[397]. When configured as field effect transistors, semiconducting nN can electrically detect biological molecules. They detect changes in conductance when charged molecules bind to their surfaces and show high sensitivity to surface species due to their large surface to volume ratio[483–486].

2.1.1.8 Extracellular nanoneedles

Intracellular access is not essential for all nN applications. Nanoneedles can provide physical guidance to cells, forcing them to form networks. For example, artificial neuronal networks have been created through the use of nN arrays[487–489]. Nanoneedles have also been used extracellularly to capture cells. Cell motility is hindered on nN arrays[310,455], and so nN have been used to capture cells for single cell analysis. Flexible nN have been created which can be

deflected by cells, and these can be used as a means to measure forces exerted by cells[371,401,490,491].

2.1.5 Cell properties on nanoneedle interfacing

Since cells are exposed to a 3D extracellular matrix with micro- and nanoscale components *in vivo*, cells *in vitro* are also sensitive to micro-[492–494] and nanoscale[296,495,496] surface topographies. Adherent cells respond to the surface chemistry of a material[497], its deformability[166,498,499], and in the case of nN arrays, nN density[308,500], diameter[472,501,502] and height[312,455,503,504]. Nanoneedles intimately localise with cells and cell properties such as adhesion[300,308,309,445,505], cellular morphology[311,413,500,506,507], nuclear morphology[195,412], cytoskeletal tension[508,509] and migration[310,403] are altered on nN interfacing, with minimal alteration in viability and proliferation **(Figure 2.3)**. nN can be used as a tool to probe and manipulate cells to gain a better understanding of how cells respond to their environment. Indeed, this is necessary since a thorough evaluation of the cell mechanotranductive response to nN is still lacking. Once this has been achieved, nN arrays could be rationally designed for biological applications by correlating these cellular adaptations with the surface topography.

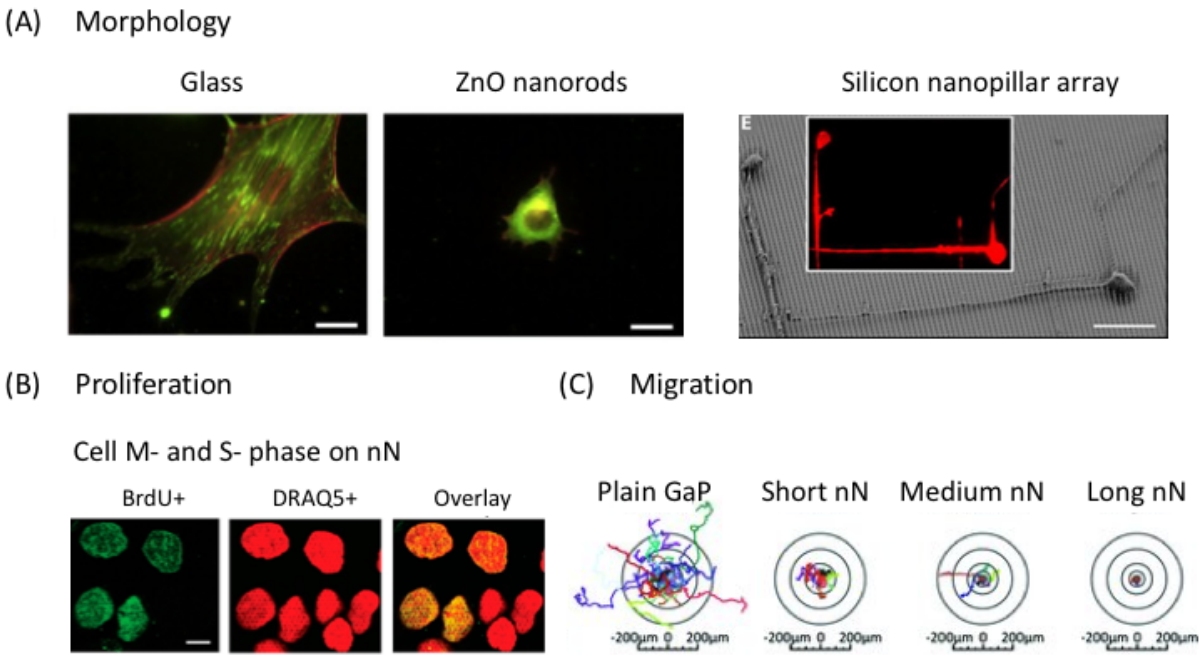


Figure 2.3: Representative images of cell behaviour on nanoneedle arrays. Nanoneedle (nN) arrays affect cell morphology. A) Left: Cells show greatly reduced spreading on zinc(II) oxide (ZnO) nanorods compared to flat glass surfaces, scale bars = 20 μm. Reprinted from reference [311] with permission from Elsevier, copyright 2008. Right: Cells commonly align with the nN array pattern. Reprinted from reference [500] with permission from American Chemical Society, copyright 2012. B) Cells show altered proliferation on nN arrays. Cells have been shown to synthesise more DNA (BrdU+) on nN than on controls. DRAQ5 = all cell counterstain, scale bar = 10 μm Reprinted from reference [308] with permission from American Chemical Society, copyright 2013. C) Cells show reduced migration on nN arrays compared to flat controls. Reprinted from reference [455] with permission from John Wiley and Sons, copyright 2013.

2.1.1.9 Cell viability and proliferation

A variety of different cell types have been seeded on nN arrays with minimal loss in viability[388]. For example, more than 95% of HEK293 and F11 cells have been shown to be viable after 2 days of culture on InAs nN arrays[308]. Moreover, primary immune cells[404] and primary neurons[510] have been shown to survive to the same extent on nN and flat substrate controls. Cell viability on nN has been measured in numerous ways, by looking at cell membrane[511] and nuclear envelope[472,510] integrity, the activity of the cells' enzymes[308,410,445] and mitochondria[309,404], and the measurement of apoptotic cell death[389], cell stress[455] and protein expression[445]. Studies have shown that single nN penetration into the cell membrane by AFM maintains cell viability, however effects of nN insertion into the nucleus remain unknown[466].

The geometry and shape of the nN affects toxicity and how it interfaces with the cell. Cytotoxicity decreases with decreasing nN diameter, irrespective of the interfacing technique[391]. A nN diameter < 200 nm shows little impact on cell metabolism, viability and proliferation; whereas a diameter > 400 nm ultimately leads to cell death following penetration, with cell apoptosis being seen within a day[404,448]. Interestingly, when cells are seeded on a nN array the density of the nN does not affect viability, however it does affect cell attachment[388].

Signs of stress have been observed when cells are seeded on nN[455,512]. An upregulation of the stress marker Hspa8 and the redox activity regulator Cybasc3 have been shown for cortical neural stem cells seeded on 4 μm long GaP nanowire arrays[512]. Moreover, L929 fibroblasts cultured on GaP nanowire arrays have been shown to have greater levels of reactive oxygen species and a higher mitochondrial metabolic activity compared to flat controls[455].

Cell division involves the synthesis of new DNA, mitotic spindle formation, and then division into two daughter cells; this can be subdivided into three key cell cycle phases (S-, M-, and cytokinesis phase)[513]. Cells seeded on nN arrays have been shown to divide[514], and HEK293 cells have been shown to synthesise more DNA (BrdU+) on nN compared to control samples[308]. BrdU is a thymidine analogue which is incorporated into DNA during the S-phase of the cell cycle, and can be detected in cells by immunocytochemical labelling of its bromo-epitope. In contrast, fibroblasts show a lower rate of proliferation on GaP nanowires compared to flat controls, and proliferation was reduced with nanowire length[455]. Moreover, multinuclear cells were more frequently observed on the nanowires, suggesting altered cell division on GaP nanowires.

2.1.1.10 Cell settling

Nanoneedle density appears to affect where cells grow. Cells remain close to the top of nN arrays with 0.5 μm spacing[412], and sink lower to the underlying surface as the nN spacing is increased[308]. A critical threshold pitch of 2–3 μm has been shown to dictate whether the cells reside above or below the nN surface. This has been determined both theoretically and experimentally[308,500]. Timing post seeding[393] and cell type also influence where the cell

chooses to settle e.g. HEK293 cells reach down to the underlying substrate, whereas NIH/3T3 cells remain suspended on top of nN with the same spacing[402].

2.1.1.11 Cell morphology

Cell morphology is often used as a measure of cell health and it can also influence gene expression[515] and cell survival[316]. The majority of studies show a change in cell morphology on nN compared to flat controls[388]. Cell morphology can be quantified using parameters such as cell area, circularity, aspect ratio, and solidity. Cells generally show a smaller projected cell area on nN compared to flat controls[308,311,312,500,506], and an increase in nN height further decreases the projected cell area[312]. It has also been demonstrated that cell area decreases with increasing nN density[308]. nN density also influences cell elongation, with lower nN spacing promoting elongation of cells along the direction of the nN array[308,500]. For example, axons from a mouse superior cervical ganglion have been demonstrated to align along rows of vertical GaP nanowire arrays[489].

2.1.1.12 Cell adhesion

Cells can grow on high-density (≥30 nN/100 μm^2) nN arrays, however in most cases cell adhesion is inhibited. Lower density nN arrays (<30 nN/100 μm^2) consistently support cell adhesion and in some cases even encourage adhesion[388]. For example, in one study it has been shown that 90% of seeded cells adhere to nN arrays whereas only 25% of cells adhere to flat controls[516]. Increased cell adhesion to nN may be attributed to the topographic environment. Cells may form a tighter 3D interaction with the nN involving the actin cytoskeleton[308,310,517], and actin rings have been shown to form around individual nN[195,308,410,455,518]. The nN may therefore act as a physical support to cells, enhancing cell adhesion.

Surface area may be a factor which dictates cell adhesion to nN arrays. Cells are able to form FA points on the surface between lower density nN arrays[308] whereas cells are unable to reach the flat base substrate and are forced to adhere to the nN themselves on dense nN arrays, causing the cell to experience a reduced contact area which has been shown to reduce adhesion[519]. This may also be the reason why an increase in the expression of pFAK and vinculin has been shown on short nanowires (10–15 μm) compared to long nanowires (20–

25 µm), since the cells can reach the base of the array on short nanowires[312]. The surface area of the nN may be too small for proper FA formation, dot-like focal complexes have been seen at nN locations[411], and cells are unable to adhere to nN below a threshold of 70 nm in height, diameter, or spacing[517].

2.1.1.13 Nuclear morphology

Several microscopy studies have demonstrated that the nucleus deforms around nN[195,389,410,455]. The nucleus deforms around blunt-tipped nanopillars and this was shown to be dependent on nuclear stiffness, by varying the levels of lamin-A in the nucleus[195]. Nuclear deformation was also shown to be dependent on the actin cytoskeleton and intermediate filaments; the actin cytoskeleton pulls the nucleus onto the nanopillars and the intermediate filaments resist deformation of the nucleus. In addition, the dimensions and curvature of the nuclear deformation could be varied by altering the geometry of the nN array.

2.1.1.14 Cell migration

Cell motility and migration are reduced on nN arrays. Cells are relatively immobile on solid and hollow nN whereas they migrate longer distances on flat controls[403,455]. For example, primary rat neurons remained stationary over four days on nN positioned in a circle whereas they migrated up to several hundred µm on the flat controls over the same time period[310]. It has been shown that a few nN are enough to immobilise cells, while a high nN spatial density enables a "bed-of-nails" effect, where cells sit on top of the nanowires and are fully motile[520]. It has been hypothesised that migration may depend on surface flexibility since cells have been shown to migrate less on longer nN compared to shorter nN arrays[455,488,506].

2.1.6 Porous silicon nanoneedle arrays

The Stevens group has recently developed high aspect ratio porous silicon nN that physically interact with both the cell membrane and the nucleus[389], and whose properties have been exploited for intracellular sensing and enhanced delivery of biomolecules **(Figure 2.4)**[389,390,400]. The nN are fabricated by combining MACE[428] with standard microfabrication. The conical nanoneedle has 5 µm length, 50 nm apical width and 600 nm base diameter. The tunable tip diameter is less than 50 nm, which is sufficiently below the cutoff diameter

established for nanoneedle cytotoxicity[427]. These nN are arranged in a square lattice with 2 μm pitch[389].

Porous silicon is a highly useful biomaterial since it has a high surface area and is biocompatible. Indeed, the porous silicon nN are biocompatible both *in vitro* and *in vivo*, showing minimal impact on cell viability[389,390,400], and the porous nN have an over 300-fold increase in surface area compared to a solid cylindrical nanowire of equivalent apical diameter (2.4×10^8 versus 7.8×10^5 nm^2). This makes porous silicon nN highly suitable for intracellular delivery; its high surface area enables high concentrations of cargo to be loaded.

The nN keep their structural integrity following *in vitro* and *in vivo* applications and a failure load of 260 nN and a critical buckling load of 264 nN has been estimated for the nN[390]. This is two orders of magnitude higher than the forces experienced during active penetration of a cell (0.5 to 2 nN[427]). Compression testing highlighted the onset of nanoneedle failure at 3.1 μN, with terminal failure occurring at 6.2 μN[390]. Porous silicon is biodegradable, producing non-toxic degradation products[521]. The nN dissolve over time in physiologic conditions, first thinning and increasing in porosity, losing their characteristic after 15 hours, and leaving a solid stump behind at 72 hours[390].

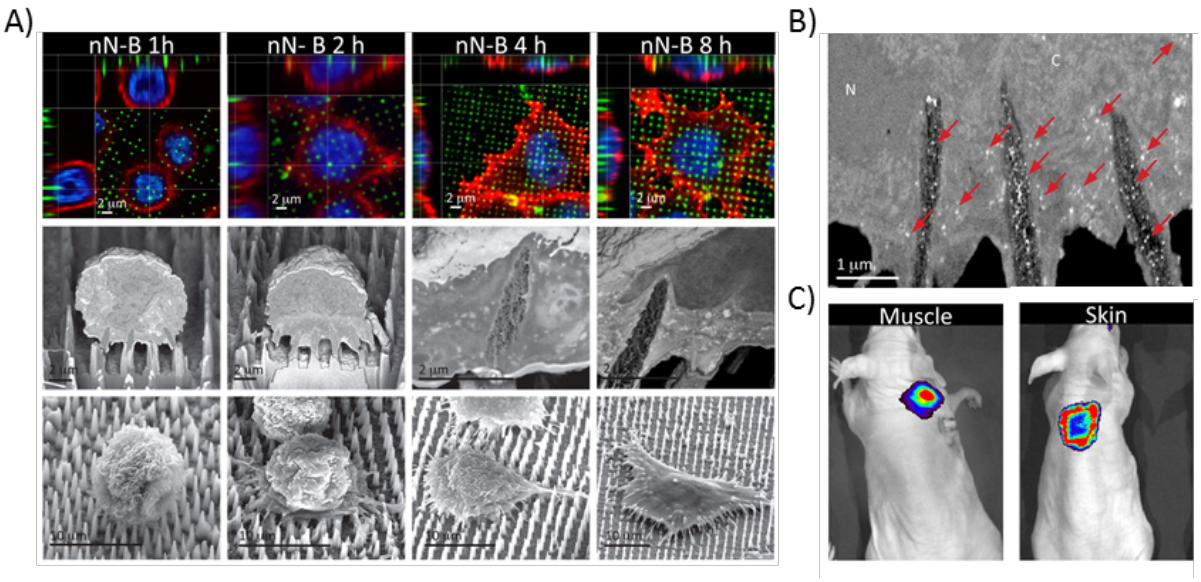


Figure 2.4: Porous silicon nanoneedle arrays strongly interface with the cell and can deliver cargo in vitro and *in vivo*, adapted from Chiappini *et al.*, *ACS Nano*, 9, 5500-5509, 2015[389], with permission from the American Chemical Society, copyright 2015. A) Nanoneedles (nN) show progressive cytosolic interfacing and nuclear exclusion with associated remodeling of the nuclear envelope over the course of eight hours. Top row: Confocal images at the indicated timepoints (cell membrane- red, nuclei - blue, nN – green), scale bars = 2 µm. Middle row: Focussed ion beam- scanning electron microscopy (FIB-SEM) cross sections of cells interfaced with nN, scale bars = 2 µm. Bottom row: 54° tilt SEM impages showing retained cell morphology, scale bars = 50 nm. B) FIB-SEM cross sections of nN-mediated delivery of quantum dots into cells. The loaded nN deliver quantum dots to the cytosol (indicated by red arrows). N = nucleus, and C = cytosol, scale bar = 1 µm. C) *In vivo* delivery of quantum dots by nN. Fluorescent live imaging of the muscle and skin at nN injection sites.

Two methods are used to interface nN with cells *in vitro*: the nN on bottom approach (nN-B) and the nN on top approach (nN-T). The nN-B technique involves seeding cells onto the nN, and nN-T technique relies on the application of a centrifugal force to induce cell membrane penetration; the nN is centrifuged onto a cell monolayer. Cargo is delivered with greater uniformity using the nN-B approach compared to the nN-T approach, especially for shorter time points[389]. However, the nN-T approach can be used for *in vivo* interfacing of cells and is a faster delivery method than the nN-B approach.

Indeed, the nN-T approach has been used to deliver cell-impermeant quantum dots[389] and to transfect the VEGF-165 gene[390] *in vivo.* The nN-B approach has been used to co-deliver of DNA and siRNA *in vitro* with an efficiency greater than 90%[390]. With both interfacing methods, cargo is delivered to the cell cytosol, bypassing the endolysosomal system[389]. The nN have

also been applied to live intracellular pH sensing[389] and cathepsin B activity sensing across normal and tumour human esophageal mucosa[400]. Cathepsin B is a cysteine protease which is a known biomarker in a wide range of solid tumors[522,523]. The nN were functionalised with a peptide-based cathepsin B cleavable sensor and cancer cells could be distinguished from healthy cells in mixed culture. When applied to tissue, it was possible to map cathepsin B activity across the tumour margin of esophageal adenocarcinoma[400].

Regardless of the nanoinjection strategy (nN-B or nN-T), confocal and dual-beam focused ion beam–scanning electron microscopy (FIB-SEM) have revealed that intact nanoneedles tightly interface to the cytosol of cells[389,390]. In some cases, the nN interface with the nucleus and the nuclear envelope remodels to wrap around the nN. The nN do not appear to penetrate through the top side of the cell membrane, and cells wrap the tips of their filopodia around neighbouring nN. Cells therefore exhibit flexible nuclear and cell membrane rearrangements in response to the porous silicon nN arrays.

2.2 Chapter aims

Porous silicon nN arrays have been utilised as a platform to deliver cargo to cells and for intracellular sensing[389,390,400], however it is necessary to assess how the nN interface with the cells in order to carry out these functions. Therefore the interaction between nN and specific organelles is assessed, such as the actin cytoskeleton and the nuclear membrane, as well as cell mechanobiology, since the nN are imposing force onto the cells. The aim of this chapter is to characterise how the nN affect primary human cell behaviour in order to further optimise nN design for future applications.

2.3 Materials and Methods

2.3.1 Nanoneedle preparation

Nanoneedles were fabricated according to our established protocol[390,428], and quality control was carried out using SEM. The nN and flat control substrates were first cleaned using an oxygen plasma cleaner (10 minutes - Plasma Prep 5, Gala Instrument, Germany) and then

functionalised with 3-aminopropyltriethoxysilane (APTES, Sigma Aldrich A3648, St. Louis, Missouri; United States) by liquid phase conjugation in a 2% v:v ethanoic solution of APTES for 2 hours. The nN and flat controls were repeatedly washed in absolute ethanol (Sigma Aldrich 32221, St. Louis, Missouri; United States) and dried under nitrogen. APTES functionalised nN were fluorescently tagged by 2 hour incubation with 0.0005% w/v 5 carboxy-tetramethylrhodamine N-succinimidyl ester (TAMRA, Sigma Aldrich 53048, St. Louis, Missouri; United States) in phosphate-buffered saline (PBS) or 0.05 mg/ml fluorescein isothiocyanate isomer I (Sigma Aldrich F7250, St. Louis, Missouri; United States) in PBS. This was followed by repeated washes with PBS and water. Non-fluorescent nN arrays and flat silicon substrate controls were sterilised under UV light for at least 20 minutes before conducting experiments with cells. Nanoneedles were prepared by Ciro Chiappini and Michele Becce at Kings College, London and Imperial College, London.

2.3.2 Cell culture

Human umbilical vein endothelial cells (HUVECs, Lonza, Basel, Switzerland) were expanded and seeded in Endothelial Growth Medium-2 (EGM-2, Lonza, Basel, Switzerland) according to the manufacturer's instructions. HUVECs were used between passage 5-10 and seeded at a density of 30,000 viable cells / cm^2 for the six hour experiments and for the 48 hours experiments HUVECs were seeded at 3,000 cells / cm^2 and 12,500 cells / cm^2 for flat and nN substrates, respectively.

Human mesenchymal stem cells (hMSCs, Lonza Ltd - Basel, Switzerland) were expanded in serum-free, chemically-defined medium (MSCGM-CD) with supplements (TheraPEAK, Lonza, Basel, Switzerland), according to the manufacturer's instructions. hMSCs were seeded on nN or flat samples in Minimum Essential Medium alpha (αMEM, Gibco ThermoFisher Scientific, Paisley, United Kingdom) with 10% v/v MSC-qualified foetal bovine serum (FBS, Gibco) and 1% v/v penicillin/streptomycin (P/S, Gibco). hMSCs were used between passage 4-6 and seeded at a density of 20,000 viable cells / cm^2 for the six hour experiments. For the 48 hour experiments seeding densities were adjusted on the different substrates to avoid confluent overgrowth. hMSCs were seeded at 2,500 cells / cm^2 and 8,375 cells / cm^2 for flat and nN substrates, respectively.

2.3.3 Latrunculin B treatment

Cells were cultured flat or nN substrates in regular media for five hours and then the media was replaced with media containing either dimethyl sulfoxide control (DMSO, Sigma Aldrich, St. Louis, Missouri; United States, 1:10,000) or latrunculin B (LatB) (Sigma Aldrich, St. Louis, Missouri; United States, 1:10,000 in DMSO, final concentration 100 nM). Cells were then cultured for one hour in the treated condition before fixation for immunofluorescent labelling.

2.3.4 Immunofluorescent labelling and imaging

Cells were fixed in 3.7% w/v paraformaldehyde (PFA, Sigma Aldrich, St. Louis, Missouri; United States) in PBS for 15 minutes at room temperature, and were then washed three times for five minutes in PBS. Cells were permeabilised with 0.25% v/v Triton X (Sigma Aldrich, St. Louis, Missouri; United States) for 10 minutes and blocked with 5% v/v goat serum for 1-2 hours. Primary antibodies diluted in fresh 0.1% w/v bovine serum albumin (BSA, Sigma Aldrich, St. Louis, Missouri; United States) in PBS were added to the cells overnight at 4˚C (see **Table 2.2**). Samples were then washed three times with PBS for five minutes before being incubated with Alexa Fluor secondary antibodies (ThermoFisher Scientific, Paisley, United Kingdom, 1:500) in 0.1% w/v BSA for 60-90 minutes at room temperature, protected from light. Following this, cells were washed three more times with PBS for five minutes. In most cases, samples were incubated with AlexaFluor-conjugated phalloidin (1:400 in PBS) for 30 minutes and were stained with DAPI (1:5,000) for 5 minutes, and stored upside down in Vectashield (Vector Laboratories, Peterborough, United Kingdom) in glass-bottom chamber slides for imaging (Nunc, ThermoFisher Scientific, Paisley, United Kingdom). Confocal imaging was performed on a Leica SP5 microscope (Leica Microsystems, Wetzler, Germany). Widefield imaging was performed with an Axio Observer automated microscope (Carl Zeiss Meditec, Jena, Germany). Structured illumination microscopy (SIM) imaging was performed with an Elyra PS.1 (Carl Zeiss Meditec, Jena, Germany).

Table 2.2: Antibody information for immunofluorescent labelling.

Target	Host	Supplier	Product #	Dilution
YAP	mouse	Santa Cruz Biotech	sc-101199	1:200
Vinculin	mouse	Sigma Aldrich	V9131	1:200
Paxillin	mouse	BD biosciences	610052	1:200
pPax	rabbit	Abcam	ab4833	1:50
pMLC	rabbit	Cell Signalling	CST 3671	1:50
Lamin-A/C	mouse	Santa Cruz Biotech	sc-7292	1:500
Lamin-A/C-C	mouse	Abcam	ab8984	1:200
Lamin-A/C	rabbit	Abcam	ab26300	1:1000
Lamin-B1	goat	Santa Cruz Biotech	sc-6217	1:500
Caspase-3	rabbit	Cell Signalling	CST 9661	1:400
hnRNP	mouse	Santa Cruz Biotech	sc-32301	1:500
Ki67	rabbit	Abcam	ab15580	1:500

2.3.5 Cytoskeleton stabilisation buffer treatment

For treatment with the cytoskeletal stabilisation buffer (CSK, vinculin images), cells were incubated with CSK (10 mM PIPES, 50 mM NaCl, 3 mM $MgCl_2$, 300 mM sucrose, 0.5% v/v Triton-X 100) for 1 minute at 4˚C prior to fixation, following an established protocol[524].

2.3.6 Live cell imaging

HUVECs were seeded in 35mm plates for next day 70% confluency (100k/cm2). A ratio of 3:1 FuGENE® HD Transfection Reagent (Promega, E2311): DNA (Lifeact plasmid) with 1ug DNA was made up in Opti-MEM® I Reduced Serum Medium, GlutaMAX (Lifetechnologies, 51985-026) and 100 uL was added to the cells in EBM-2 basal medium (Lonza CC-3156) with 2% FBS. After six hours the medium was replaced with EGM. 48 hrs after transfection, cells were trypsinised and seeded on the nanoneedles in 24 well plates at a seeding density determined by the transfection efficiency. Following two hours of incubation, to allow adherence of cell to the nN, the nN were inverted and placed down in an 8 well chamber slide containing EGM media, and imaged on a widefield Ti-E Eclipse microscope (Nikon -Minato, Japan). The cells were imaged every 15 minutes for 2 hours and 45 minutes.

2.3.7 Scanning electron microscopy

Cells on nN or flat substrates were fixed in 2.5% v/v glutaraldehyde solution (Sigma Aldrich, St. Louis, Missouri; United States) for one hour in PBS at room temperature, and then washed 3 times in PBS. PBS buffer was substituted with 0.1M sodium cacodylate buffer (Electron Microscopy Sciences, USA) and cells were washed twice for five minutes. Cells were post-fixed in 1% v/v osmium tetroxide for 1 hour in 0.1M sodium cacodylate buffer and subsequently washed with distilled water two times for five minutes. Samples were dehydrated in a series of ethanol dilutions (20, 30, 50, 70, 80, 90% v/v ethanol in water), treated with 100% ethanol four times for five minutes after which they were treated with hexamethyldisilazane (HMDS) for five minutes and air-dried. Samples were mounted and sputtered with 10 nm of chromium (Q150, Quorum, USA) and imaged using Sigma300 (Zeiss Meditec, Jena, Germany) scanning electron microscope with working distance of 10 mm and an accelerating voltage of 5 keV. SEM imaging taken with Sahana Gopal and Michele Becce, Imperial College, London.

2.3.8 Quantitative real-time polymerase chain reaction (qRT-PCR)

Cells on nN or flat substrates were firstly incubated with Trizol reagent (Life Technologies, Carlsbad, California, United States). They were then mixed with chloroform (5:1 Trizol:chloroform), and this mixture was separated by centrifugation (12,000x g, 15 minutes, 4°C). The RNA was contained in the aqueous phase, and this was isolated using RNeasy columns (Qiagen). cDNA was then synthesised using a reverse transcription kit (Applied Biosystems - Life Technologies, Product #4368814), and qRT-PCR was carried out on a SYBR Green master mix (Applied Biosystems – Life Technologies, Product #1179401K) mixed with 2-5 ng cDNA and 250-500 nM of forward and reverse primers, respectively. qRT-PCR was processed using either a StepOne Plus or QuantStudio6 machine (Applied Biosystems). The StepOne Plus protocol involved 95°C for 20 seconds followed by 40 cycles of denaturation at 95°C for 3 seconds and annealing at a temperature between 55-60°C for 30 seconds. The QuantStudio6 protocol involved 95°C for 20 seconds followed by 40 cycles of denaturation at 95°C for 1 second and annealing at a temperature between 55-60°C for 20 seconds. Cycles-to-threshold (Ct) values were generated by the ThermoFisher Scientific Cloud Software for qPCR file processing (https://www.thermofisher.com/uk/en/home/cloud.html). The values

were then manually processed using Excel to generate fold change expression values compared to the geometric mean[525] expression of housekeeping genes. qRT-PCR analysis was performed by Spencer Crowder, Imperial College, London. Custom primers were purchased from Invitrogen, and tested for specificity prior to use. Sequences are listed in **Table 2.3.**

Table 2.3: qRT-PCR primer sequences.

Gene Name	Accession Number	Forward / Reverse Primer 3'-5'	Amplicon (bp)	Total Primer Concentration
ANKRD1	NM_014391.2	AGTAGAGGAACTGGTCACTGG	138	500 nM
		TGGGCTAGAAGTGTCTTCAGAT		
CTGF	NM_001901.2	AGGAGTGGGTGTGTGACGA	117	500 nM
		CCAGGCAGTTGGCTCTAATC		
FAK	NM_153831.3	CAGTGCCTTCTGCAGTTTCC	292	500 nM
		CTTCTGAATGATGCCCCTGACA		
PXN	NM_001080855.2	TGGACAGCCCTACTGTGAAA	125	500 nM
		AGAAGTGTTCAGGGTGCCA		
VCL	NM_003373.3	GAAGAGAGCATTGGCCTCCA	388	500 nM
		AAGCCAGTTCTGAGCAGCAT		
ZYX	NM_001010972.1	TTTCAAAGCCCGGGTGTCAT	81	500 nM
		GCAGGCTTGGTACTGGACTT		
LMNA	NM_170707.3	CGTCGGTGACTCAGTGTTCG	156	250 nM
		GAAGGACAGAGACTGCTCGG		
LMNB1	NM_005573.3	CTCGTCTTGCATTTTCCCGC	170	250 nM
		TGGCGTTTAGAGGAACGGAG		
PPIA	NM_021130	CTTCACACGCCATAATGGC	273	500 nM
		GTGATCTTCTTGCTGGTCTTG		
RPL13A	NM_012423	AAGTACCAGGCAGTGACAG	100	500 nM
		CCTGTTTCCGTAGCCTCATG		
HPRT	XM_011531328.1	TGACACTGGCAAAACAATGCA	94	500 nM
		GGTCCTTTTCACCAGCAAGCT		

2.3.9 Quantification of lamin signal

ImageJ software (National Institutes of Health, Bethesda, MD, USA) was used to quantify the lamin signal in confocal z-stacks of individual cells. A line was drawn along a row of nN

interfacing with the nuclear envelope in the x-y plane. From this line, a reslice image was then created in either the x-z or y-z plane. The width of the line used to assess the reslice image was 25 pixels for Figure 2.20B and 20 pixels for Figure 2.20C.

For Figure 2.20B analysis, a horizontal line of 20 pixel width was drawn in the reslice image, with the base of the line touching the base of the nuclear envelope and the top of the line touching the tip of the nN. The lamin-A and lamin-B signal was then recorded along this line. In another area where the nN were not interacting with the nuclear envelope (i.e. the top nuclear envelope or the space in between nN interfacing), another line of 20 pixel width was drawn, and the lamin-A and lamin-B signal values over this line were averaged and used as a normalisation factor for the specific reslice image in question.

For Figure 2.20C analysis, reslice images were prepared in the same way, and two additional lines were prepared for measurement of signal within the reslice image. Two identical 20 pixel width lines were drawn perpendicular to the nN height in the y-direction. One line was placed in the middle of the nN z-height (*middle line*) and an identical line was z-shifted to the top of the nN z-height (*top line*), and signal for nN, lamin-A, and lamin-B channels were recorded. Similar to above, a normalisation line was also recorded from an area within the reslice along a 20 pixel width line where nN were not interacting. The troughs within the nN signal were detected from the inflexion points around local maxima of the nN signal from the middle line, and lamin-A and/or lamin-B signals were integrated from trough-to-trough distances for the middle and top lines. This analysis was performed because measurement of lamin-A or -B signal at specific points along the nN width did not reveal the accumulation of the protein signal around the nN in the y-direction. Integrated values were subsequently normalised to the respective average values calculated from the *normalisation line*, and the ratio of integrated lamin A:B at the nN middle and top are reported. Figure 2.20C analysis was conducted with Spencer Crowder, Imperial College, London.

2.3.10 Quantitative cell morphology analysis

Quantification of cell and protrusions morphology was performed on tiled widefield microscopy images using the MATLAB image analysis toolbox[526]. Background correction was

performed by negating the image with a widefield gaussian blurred copy of the image itself. Marker controlled watershed segmentation was then performed on the DAPI channel to identify nuclei. Nuclei touching the border, or below a threshold intensity were filtered. To identify the cell cytoplasm, thresholding was performed on the actin channel to identify the image region containing cells. Watershed on the actin channel resulted in extensive mis-segmentation, thus utilising nuclei as markers, and the actin containing image region as the boundary, marker controlled watershed segmentation was performed on the YAP channel. This resulted in effective detection of cell boundaries with the substrate and with other cells. Cells with mean actin intensity similar to background were filtered out, as were those touching the border. Quantitative cell morphology analysis was carried out by Samuel Cooper at the Institute of Cancer Research and Imperial College, London.

2.3.11 Feature extraction

Features describing cell, and protrusion morphology were extracted from cell and nuclei segments. For intensity and texture properties the original images were used, without background correction, however images were log transformed, and subsequently the 10^{th} percentile intensity was deducted, to align background intensity to zero, thus reducing technical intensity variations between replicates. Protrusion regions are defined by applying a large erosion and dilation operation to the whole cell segment. This generated a highly rounded core, region of cytoplasm not in this core are defined as protrusions. A list of the features extracted and in the data tables is given below, for linear discriminant analysis (LDA).

2.3.11.1 Morphology (except actin channel intensity)

1. Cell area
2. Cell major axis length: length of the equivalent ellipse based upon second order moments
3. Cell minor axis length: width of the equivalent ellipse
4. Cell eccentricity: eccentricity of the equivalent ellipse
5. Cell extent: proportion of pixels within the bounding box
6. Cell solidity: proportion of pixels in the convex
7. Cell perimetre: perimetre length of cell segment
8. Cell roundness: defined as $4\pi \frac{Area}{Perimetre^2}$
9. Cell channel intensity: mean actin intensity: not included for LDA
10. Number of protrusions per cell
11. Mean protrusion area per cell
12. Max protrusion area per cell

13. Total protrusion area per cell
14. Mean length of protrusions per cell (major axis length of equivalent ellipse)
15. Max length of protrusion per cell
16. Total length of protrusions per cell
17. Mean width of protrusion per cell (minor axis length of equivalent ellipse)
18. Max width of protrusion per cell
19. Total width of protrusion per cell
20. Mean extent of protrusions per cell, defined as length from nuclei centre of mass to furthest point in protrusion region minus length from nuclei centre of mass to nearest point in protrusion region.
21. Max extent of protrusion per cell
22. Total extent of protrusion per cell

2.3.11.2 Actin texture calculated from Grey Level Co-occurrence Matrix (GLCM)

23. Contrast: variance between neighbouring pixels
24. Correlation: correlation between neighbouring pixels
25: Energy: angular second moment of the image
26: Homogeneity: a measure of how sharp are gradients within the image

2.3.11.3 Additional features

27. Nuclear centroid X position
28. Nuclear centroid Y position
29. Nuclear orientation angle of equivalent ellipse
30. Cell orientation angle of equivalent ellipse
31. Mean intensity of central actin (following erosion of cytoplasmic segment mask)
32. Mean intensity of cortical actin (mask of cytoplasmic ring region that is eroded to form central region)

2.3.11.4 Protrusion features

1. Index of cell protrusion. This links protrusions to the unique cell ID in the corresponding single cell data file.
2. Protrusion area
3. Length of protrusion (major axis length of equivalent ellipse)
4. Width of protrusion (minor axis length of equivalent ellipse)
5. Protrusion orientation angle of equivalent ellipse
6. Extent, defined as length from nuclei centre of mass to furthest point in protrusion region minus length from nuclei centre of mass to nearest point in protrusion region

Feature extraction was carried out by Samuel Cooper at the Institute of Cancer Research and Imperial College, London.

2.3.12 Linear discriminant analysis

Linear discriminant analysis (LDA) between flat and nN substrates was performed on cells pooled over 3 experimental repeats for HUVEC and hMSC cells, with two technical repeats for two experiments, and one technical replicate for one experiment. Each cell type was analysed independently, where cells were labelled as “flat” or “nN” and the features described above were extracted for all cells. R^2 values for HUVEC and hMSC cells were 0.286 and 0.343 respectively; $p < 0.001$ in both cases. Also, LDA applied to data following random permutation of class labels led to insignificant separation. These R^2 values correspond to 75% and 78% correct substrate classification of HUVEC and hMSC cells respectively. The box plot in Figure 2.7A shows a random sample of 900 cells from each group. This analysis was conducted with the Scikit-Learn module for Python. Linear discriminant analysis was carried out by Samuel Cooper at the Institute of Cancer Research and Imperial College, London.

2.3.13 Quantifying actin stress fibres

Actin stress fibres were quantified from confocal images. To highlight stress fibres the actin channel was filtered by performing convolution with a 6 by 10 kernel with the central two columns containing a positive value and the outer four columns containing a negative value. Convolution was performed with orientations of the kernel at 3 degree intervals between 0 and 180 degrees, the maximum value for each pixel over 60 orientations was then selected. Other kernel shapes and orientation regimes were tested, however this choice emphasised stress fibres most effectively, as judged by visual inspection.

Thresholding was then performed on these images, and the subsequent binary mask appeared to match stress fibres well. Regions below 100 pixels in size were removed as these were largely noise.

2.3.14 Focal adhesion quantification

To identify focal adhesions, a similar approach to actin stress fibre identification was employed. Confocal images of cells treated with cytoskeletal stabilisation buffer (CSK) and then stained for vinculin were used for image analysis. Vinculin channel images were filtered

by performing convolution with a 5 by 6 kernel with the central two columns containing a positive value and outer two columns containing a negative value. Convolution was performed with orientations of the kernel at 10 degree intervals between 0 and 90 degrees, the maximum value for each pixel over the 9 orientations was then selected. Following thresholding similar to actin bundle quantification, regions below 10 pixels in size were removed as these were largely noise.

Again, to determine the focal adhesion density, the number of focal adhesion regions in the image, divided by the image area covered by actin (determined by a similar threshold operation) was calculated. Significance was determined by pairwise t-test between 10 analysed fields of view taken over 2 experimental repeats. Focal adhesion quantification was carried out by Samuel Cooper at the Institute of Cancer Research and Imperial College, London.

2.3.15 YAP localisation analysis

YAP intensities and localisation were calculated following cell and nuclei segmentation as described above. Three features on YAP localisation were recorded:

1. Nuclear YAP intensity: taken as the median of the nuclear YAP intensities
2. Cytoplasmic YAP intensity: the cytoplasmic segments was eroded by a fixed width (10px), such that pixels bordering the substrate and other cell were not included, subsequently the median YAP intensity from this region was taken.
3. Log nuclear to cytoplasmic YAP ratio

YAP nuclear to cytoplasmic localisation changes both in wildtype and following drug and DMSO treatment, were recorded from a pooled random sample of 180 cells taken over 2 experimental repeats, with two technical repeats per experiment. Significance of differences was calculated using a pair wise t-test between single cell populations. YAP localisation analysis was carried out by Samuel Cooper at the Institute of Cancer Research and Imperial College, London.

2.3.16 Statistical analysis

Statistics on biochemical data was performed using GraphPad Prism software (La Jolla, California, USA). When comparing two groups, a Student's unpaired t-test was performed and when more than two groups were compared, a one-way analysis of variance (ANOVA) was performed, followed by pairwise comparisons via Bonferroni's Multiple Comparison Test. For the comparison of lamin-A:B ratios in Figure 2.20, a non-linear exponential curve was fit to the data set, and the best-fit values are reported. For image analysis, MatLab (Mathworks, Cambridge, UK) was used to analyse data and prepare charts. Image analysis was conducted by Samuel Cooper at the Institute of Cancer Research and Imperial College, London. Statistical analysis of qPRCR data and the lamin-A:B ratios in Figure 2.20 was carried out by Spencer Crowder at Imperial College, London.

For qPCR analysis, three to four experimental replicates, with at least two biological replicates, were performed. For each experimental replicate, the expression of the gene of interest (GOI) was normalised to the geometric mean of at least two housekeeping genes (HKGs) following previous method, which generated the ΔCt values[525]. For each cell type, the average was calculated for the normalised GOI expression on flat samples, and the expression of all the other groups was then normalised to these values. This resulted in an expression value equal to 1 for HUVEC or hMSC flat samples, but carried a non-zero standard deviation that reflected the intra-experimental heterogeneity of biological replicates. In order to propagate this error, the relative standard deviation (RSD) was calculated for all groups of interest, where:

$$RSD = \sqrt{(SD_ExpRep1^2 + \cdots + SD_ExpRepN^2)} \text{ / N}$$

Where N = number of experimental replicates (N = 3 – 4) and SD_ExpRep represents the standard deviation of the normalised expression for each group within each experimental replicate. This approach allowed for the variability within each experiment to be propagated. Of note, for lamin-A and lamin-B gene expression in Figure 2.18A, the expression of all groups was normalised to HUVEC flat so that cell type-specific differences in lamin signal could be observed.

For all box plots, the 25th and 75th quartiles are shown, the line is the median value, and the whiskers extend to the minimum and maximum data points, unless the point is a statistical outlier (and is therefore shown in red). For all experiments, $p < 0.05$ was considered significant.

2.4 Results

2.4.1 Cell viability

A number of cell types have previously been interfaced with porous silicon nN arrays without a loss in cell viability[389,390,400]. For example, HeLa cells have been shown to retain their physiologic metabolic activity and normal proliferation in nN arrays over the course of five days[390]. However, the viability of primary human cells on nN has not yet been determined. Two different primary human cell types, human umbilical vein endothelial cells (HUVECs) and human mesenchymal stem cells (hMSCs), were therefore seeded on nN arrays for six hours and 24 hours, 48 hours, and 72 hours. On visual inspection, cells appeared viable for up to 72 hours. The six hour timepoint was selected as the timepoint to assess cell-nN interactions, since there is less nN degradation at this timepoint, enabling an assessment of primary human cells with sharp high-aspect ratio structures, as opposed to blunted structures after 24 hours[390].

Next, the viability and proliferation of HUVECs and hMSCs was assessed six hours post nN interfacing. In order to achieve this, cells were immunofluorescently labelled for caspase-3, since caspase-3 is a frequently activated protease in mammalian cell apoptosis[527]. Moreover, cells were also immunofluorescently labelled with Ki67 to assess cell proliferation, since the Ki-67 protein is present during all active phases of the cell cycle but is absent in resting cells[528]. Culture on nN did not stimulate an apoptotic response or abolish cell proliferation in comparison to flat controls, as indicated by negative staining for caspase-3 and positive staining for Ki67, respectively **(Figure 2.5)**.

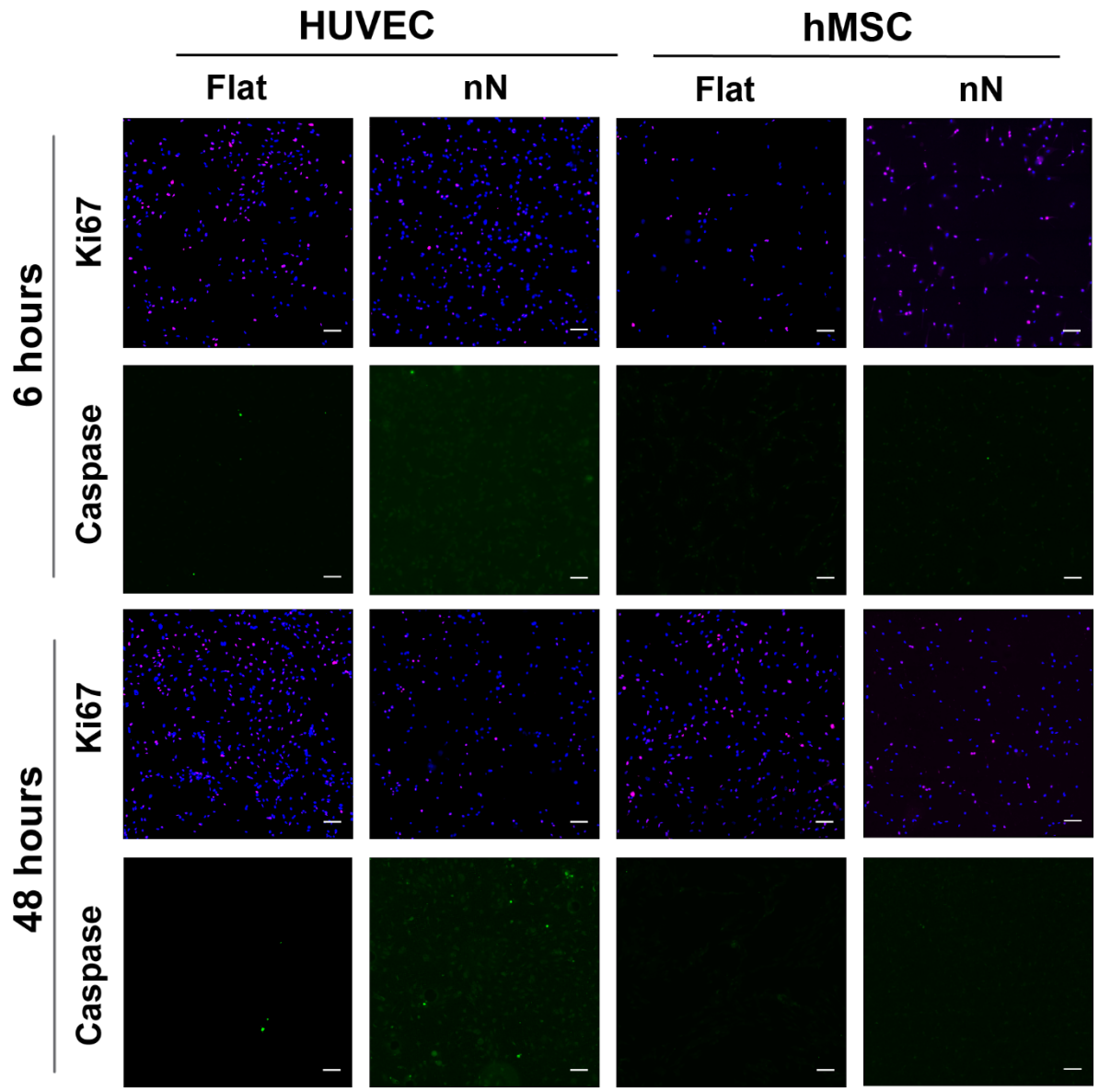


Figure 2.5: Nanoneedle arrays minimally affect cell viability. Proliferation of primary human cells was retained on nanoneedle (nN) arrays, demonstrated by positive staining for Ki67 (magenta), and apoptosis was not activated, since there is an absence of caspase-3-positive cells (green). DAPI – blue. Scale bars = 100 µm.

2.4.2 Cell morphology and the actin cytoskelton

Although cells showed minimal loss of viability on nN arrays, they displayed morphological alterations, as compared to the flat substrate controls **(Figure 2.6A-B)**. Scanning electron microscopy (SEM) demonstrated that cells directly interact with the nN, extending membrane projections which clasp around individual nN (**Figure 2.6A**). Indeed, membrane projections have previously been shown to extend and clasp around these nN arrays[389,390] and other nN

arrays[309] in other cell types, and filopodia membrane extensions have been shown to play a significant role in topography sensing, preferentially interacting with nN over flat controls[490].

HUVECs tended to form multiple membrane projections in all directions on nN arrays, whereas hMSCs often became highly elongated with one or two protrusions extending from the centre **(Figure 2.6A-B)**. Moreover, on closer inspection, the actin cytoskeleton of HUVECs was shown remodel around the nN, whereas linear fibres of actin were demonstrated on flat controls **(Figure 2.6C-D)**. On nN arrays, promintent actin structures at the cell centre showed an absence of immunofluorescence at nN locations, and the cortical actin at the cell periphery was shown to be pinned around the nN **(Figure 2.6D)**. Interesingly, actin has previously been shown to be pinned around nN along cell edges, and it has been suggested that this contributes to increased cell adhesion on nN vs. flat controls, through a physical entrapment of the cells[308].

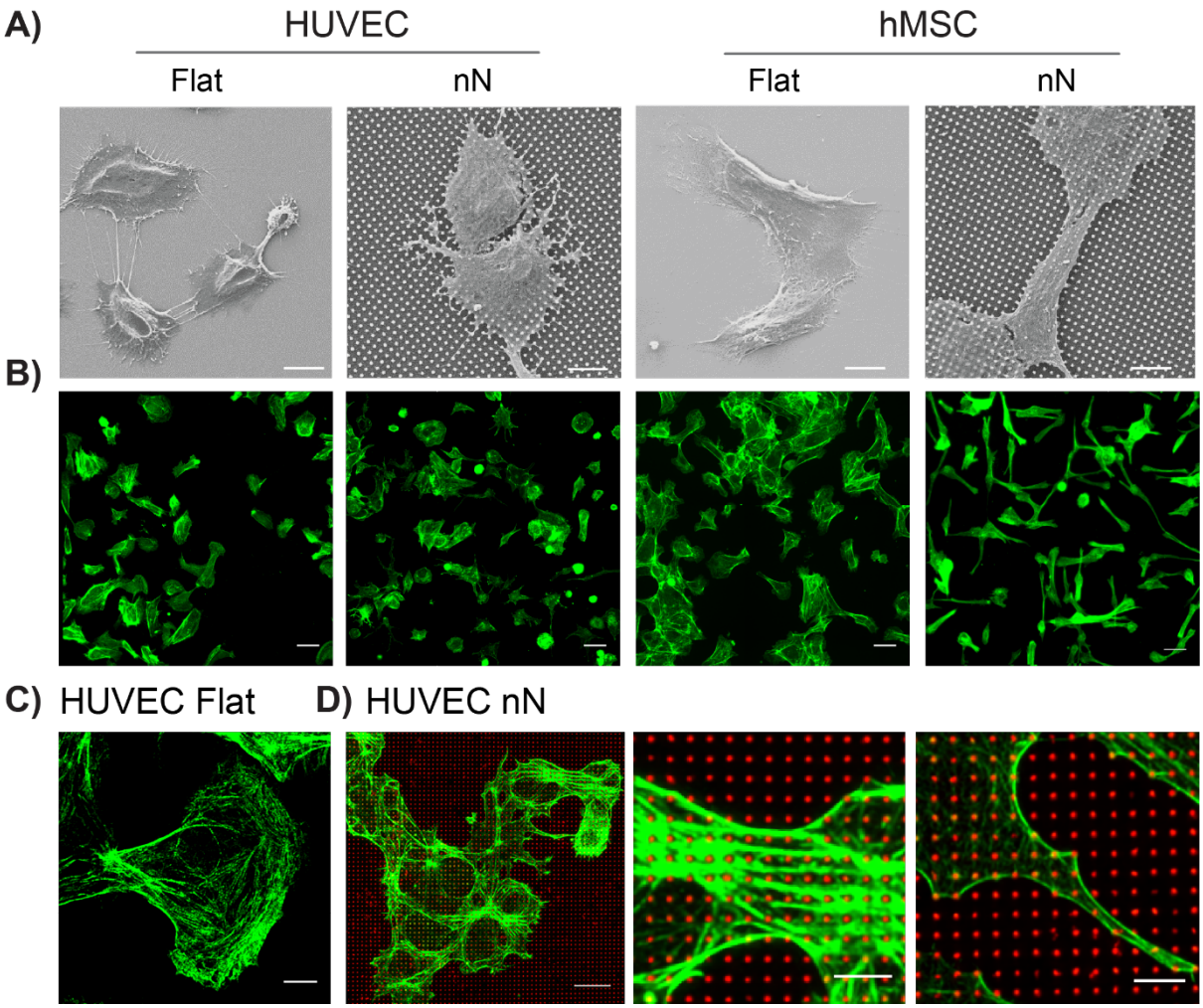


Figure 2.6: Nanoneedle arrays interact with cells and affect cell morphology. A) Scanning electron microscopy (SEM) images show that nanoneedles (nN) interact with primary human cells six hours post seeding. Scale bars = 10 µm. B) Widefield immunofluorescence images of the actin cytoskeleton showed alterations to cell morphology on nN compared to flat controls (green – phalloidin). HUVECs displayed altered membrane protrusions on nN whereas hMSCs aligned with the nN array. Scale bars = 50 µm. C) HUVECs formed linear actin fibres on flat substrate controls, scale bar = 10 µm. D) HUVECs showed actin cytoskeleton remodelling on nN arrays. Left panel: Promintent actin structures at the cell centre showed an absence of immunofluorescence at nN locations whereas the cortical actin at the cell periphery was shown to be pinned around the nN, scale bar = 20 µm. Middle panel: zoom in of promintent actin structures at the cell centre, showing an absence of immunofluorescence at nN locations, scale bar = 5 µm. Right panel: zoom in of cortical actin at the cell periphery, pinning around the nN, scale bar = 5 µm. SEM image taken wih Sahana Gopal, Imperial College, London.

Twenty-five features of cell morphology and actin features were therefore compared by linear discriminate analysis (LDA) for both cell types on nN arrays vs. flat substrates (by Samuel Cooper, Imperial College, London and the Institute of Cancer Research, London) **(Figure 2.7)**. LDA is a statistical technique which classifies a categorical dependent label (the

cell type and substrate) and then compares this to continuous independent variables (the cell shape descriptors). The LDA analysis could indeed distinguish the cell types on the flat and nN substrates using cell shape descriptors and actin features **(Figure 2.7A)**. The best discriminators between nN and flat cultured cells were actin texture, as well as features describing cell protrusions **(Figure 2.7B)**. Moreover, for HUVECs, there was a clear reduction in cell area on nN arrays.

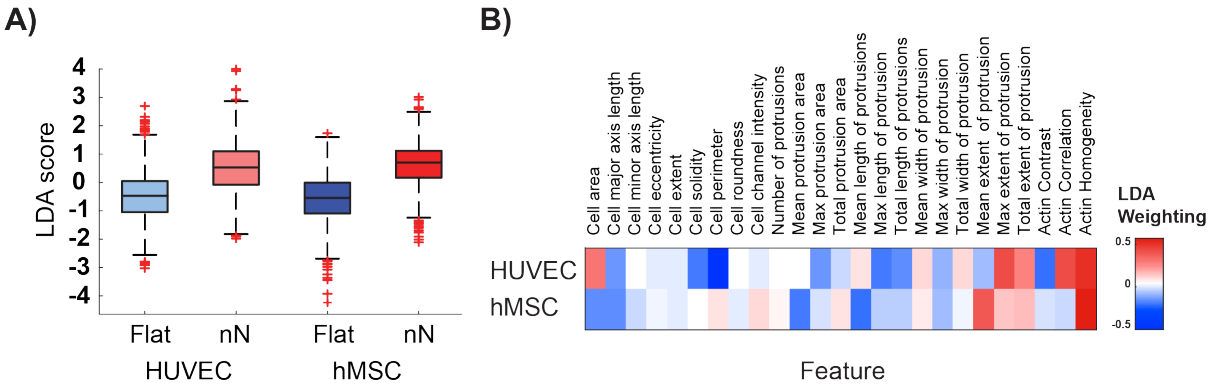


Figure 2.7: Linear discriminant analysis can distinguish cells on flat and nanoneedle substrates. A) Twenty-five shape and actin features were compared by linear discriminant analysis (LDA) for the two cell types on the flat and nN substrates (mean +/- standard deviation (S.D.)), and B) the parameter which was most affected by nN arrays is actin homogeneity. Image analysis was conducted by Samuel Cooper at the Institute of Cancer Research and Imperial College, London.

For both cell types, nN significantly reduced actin stress fibre formation, suggesting a reduction in intracellular tension on nN arrays (**Figure 2.8A**). This is in line with the literature, since a significant decrease in the number of actin filaments has previously been shown for cells seeded on other vertical nN arrays[411]. Moreover, HUVECs and hMSCs both displayed protrusions which were significantly longer (higher length/width ratio) and which extended further from the nucleus on nN **(Figure 2.8B-C)**. HUVECs also displayed a reduced ratio of cortical-to-central actin on nN **(Figure 2.8D)**. Additionally, the protrusions of hMSC aligned along the nN array, indicating that nN can guide protrusion formation **(Figure 2.8E)** (image analysis carried out by Samuel Cooper). Remodelling of the actin cytoskeleton has also been shown in other nN systems. For example, F-actin has been shown to reorganise into characteristic puncta at nN locations on nN arrays[410,417,455], and has also been shown to align along the nN array[500].

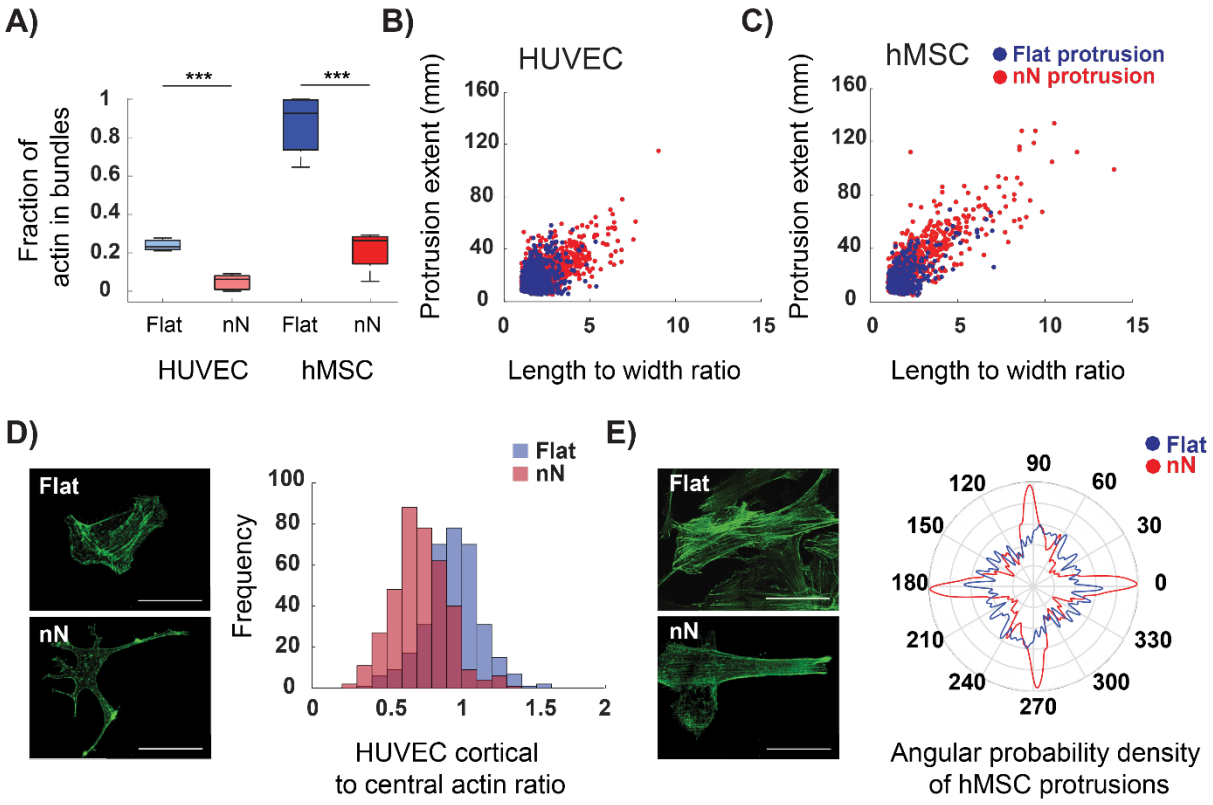


Figure 2.8: Nanoneedle arrays remodel the actin cytoskeleton. A) Image analysis showed reduced stress fibre formation (actin bundling) on nanoneedles (nN) compared to flat substrates for both cell types (box plots, minimum/maximum, mean +/- standard deviation). B-C) Image analysis of the actin cytoskeleton revealed that cells on nN show longer protrusions with higher aspect ratios compared to flat controls. D) HUVECs showed decreased levels of cortical versus central actin on nN (green – phalloidin), as seen in deconvolved maximum projection confocal immunofluorescence images and image analysis data. Scale bars = 50 µm. E) The actin cytoskeleton of hMSCs aligned along the nN array, as seen in deconvolved maximum projection confocal immunofluorescence images and image analysis data. Scale bars = 50 µm.

Nanoneedles were also shown to stimulate a direct physical response by the cytoskeleton at sites of engagement. Dense actin rings formed at sites of nN interaction in both cell types **(Figure 2.9)**, as previously shown on other nN arrays[195,518]. The actin rings formed at various heights along the nN **(Movie 2.1)**, and live cell imaging of the actin cytoskeleton showed that the rings are dynamic and short-lived **(Movie 2.2)**. These actin rings are likely to be located at sites of high membrane curvature and altered membrane tension[28], since actin engagement is required when the cell membrane is under tension, and actin dynamics are essential for membrane invagination[29,30].

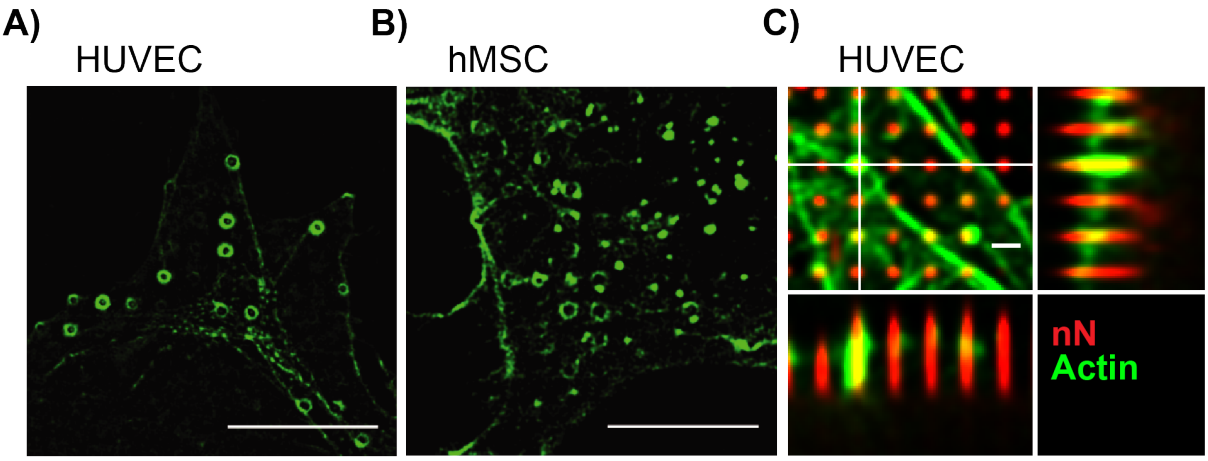


Figure 2.9: Actin rings form at the sites of nN interaction. A) Structured illumination microscopy (SIM) imaging of HUVEC actin rings (single plane). B) Deconvolved confocal microscopy of hMSC actin rings (single plane). Green – phalloidin, scale bars = 10 µm. C) Actin rings were located around the nN (deconvolved confocal z-stack; green – phalloidin, red – nN). Scale bars = 1 µm.

2.4.3 Focal adhesions and phosphorylated myosin light chain

The significant morphological and actin response suggests that nN influence the mechanosensing cell machinery. Since cell spreading and cytoskeletal tension have been shown to correlate with FA maturation[322], FA were assessed on nN arrays, by immunofluorescently labelling vinculin and paxillin FA proteins. Both cell types formed dense focal adhesions (FAs) on flat substrates, and smaller, more diffuse FA staining patterns appeared on nN **(Figure 2.19 & 2.11)**. Indeed, dot-like evenly distributed focal complexes have previously been shown on cells cultured on other nN arrays, compared to strong fibrillar FA on flat substrate controls[411].

Vinculin can be found in an active and inactive form; the active extended form of vinculin is localised to FA sites and is connected to the actin cyctoskeleton, whereas the folded inactive form is located in the cytosol[67]. Since inactive vinculin is not bound to the cell cytoskeleton, vinculin was stained in the presence of cytoskeleton stabilisation bufer (CSK), which removes inactive vinculin which is not bound to the actin cytoskeleton **(Figure 2.10A)**. Indeed very, little active vinculin was present on nN compared to flat controls, as shown by vinculin FA adhesion density image analysis (performed by Samuel Cooper) (**Figure 2.10B)**. Gene-level expression of multiple FA components, including focal adhesion kinase (*FAK*), paxillin (*PAX*), vinculin (*VCL*), and zyxin (*ZYX*), were significantly downregulated on nN in both cell types (all

qPCR data carried out with Spencer Crowder, Imperial College, London) **(Figure 2.10C)**. Zyxin is a hallmark of mature FAs[529] and the downregulation of zyxin suggests that mature FA were unable to form on nN arrays.

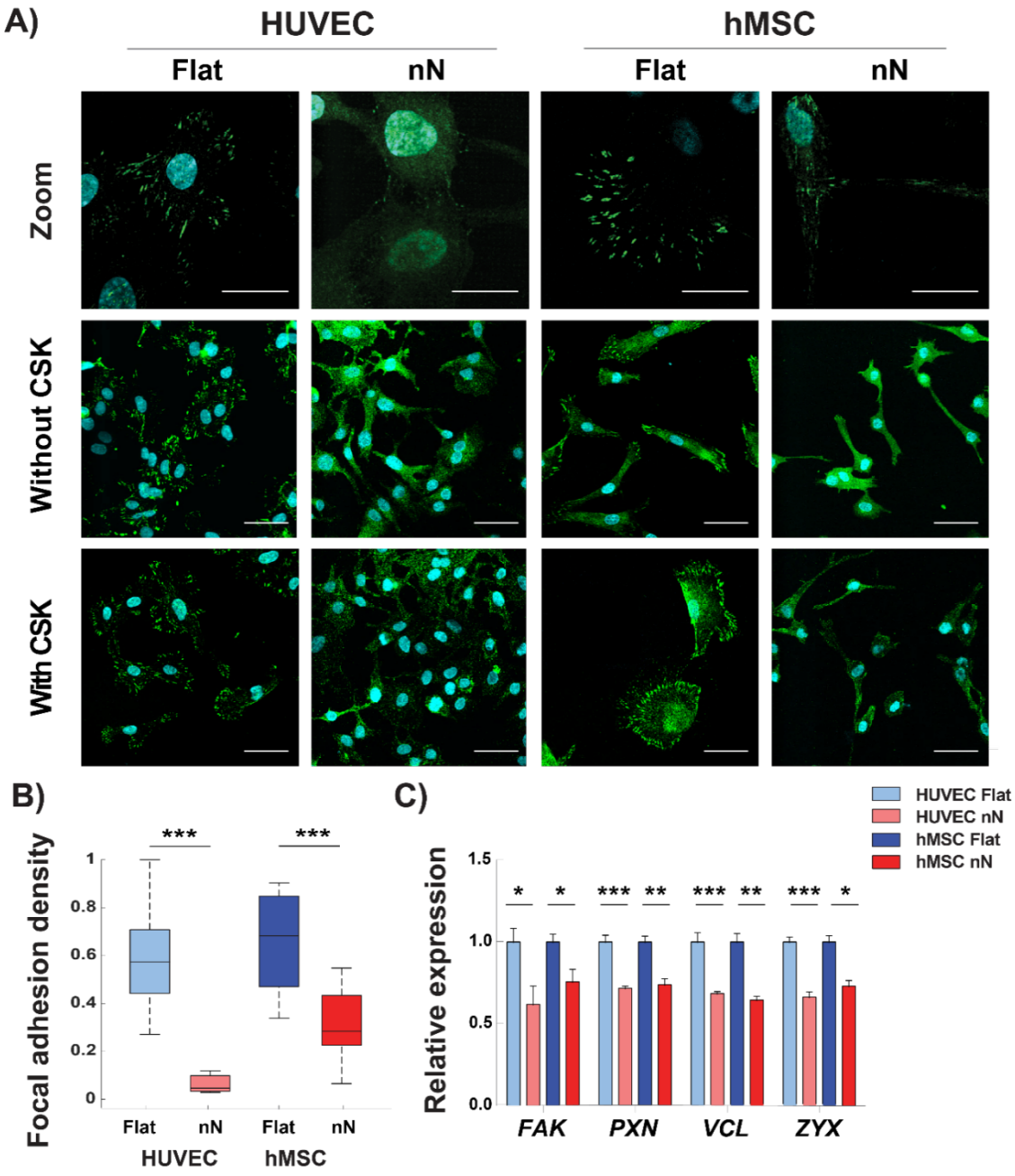


Figure 2.10: Nanoneedle arrays affect vinculin focal adhesion formation. A) Confocal maximum projection images six hours post seeding of vinculin (green) focal adhesions in HUVECs and hMSCs seeded on nanoneedles (nN) and flat controls with and without cytoskeleton stabilisation buffer (CSK). CSK removes inactive vinculin which is not bound to the actin cytoskeleton. All cells counterstained with DAPI (cyan). Clear punctate structures of vinculin were seen on flat substrates whereas smaller and more diffuse vinculin structures were seen on nN arrays. Scale bars: top panel = 25 µm, lower two panels = 50 µm. B) A significant reduction in vinculin FA density on nN was seen (box plots, minimum/maximum; mean +/- S.D.; N = 3). C) PCR analysis showed that a number of FA components were downregulated on nN arrays (focal adhesion kinase (FAK), paxillin (PAX), vinculin (VCL), and zyxin (ZYX); qPCR, N = 3, mean ± S.D.). * $p < 0.05$, ** $p < 0.01$, *** $p < 0.001$ between groups as indicated by the lines. For each experimental replicate, the expression of the gene of interest was normalised to the

geometric mean of at least two housekeeping genes. FA image analysis analysis was conducted by Samuel Cooper at the Institute of Cancer Research and Imperial College, London.

As with the vinculin immunofluorescence staining, HUVECs on flat substrates demonstrated dense paxillin staining located at the end of actin stress fibres. This is expected for a planar substrate upon which cells can readily form FAs and spread. However, HUVECs on nN exhibited unordered and diffuse staining patterns for both actin (green) and paxillin (red) **(Figure 2.11A)**. Phosphorylated paxillin (pPax) is a marker of FA maturation and the reduction in punctate structures of pPax on nN confirmed the limited maturation of FAs on nN **(Figure 2.11B)**.

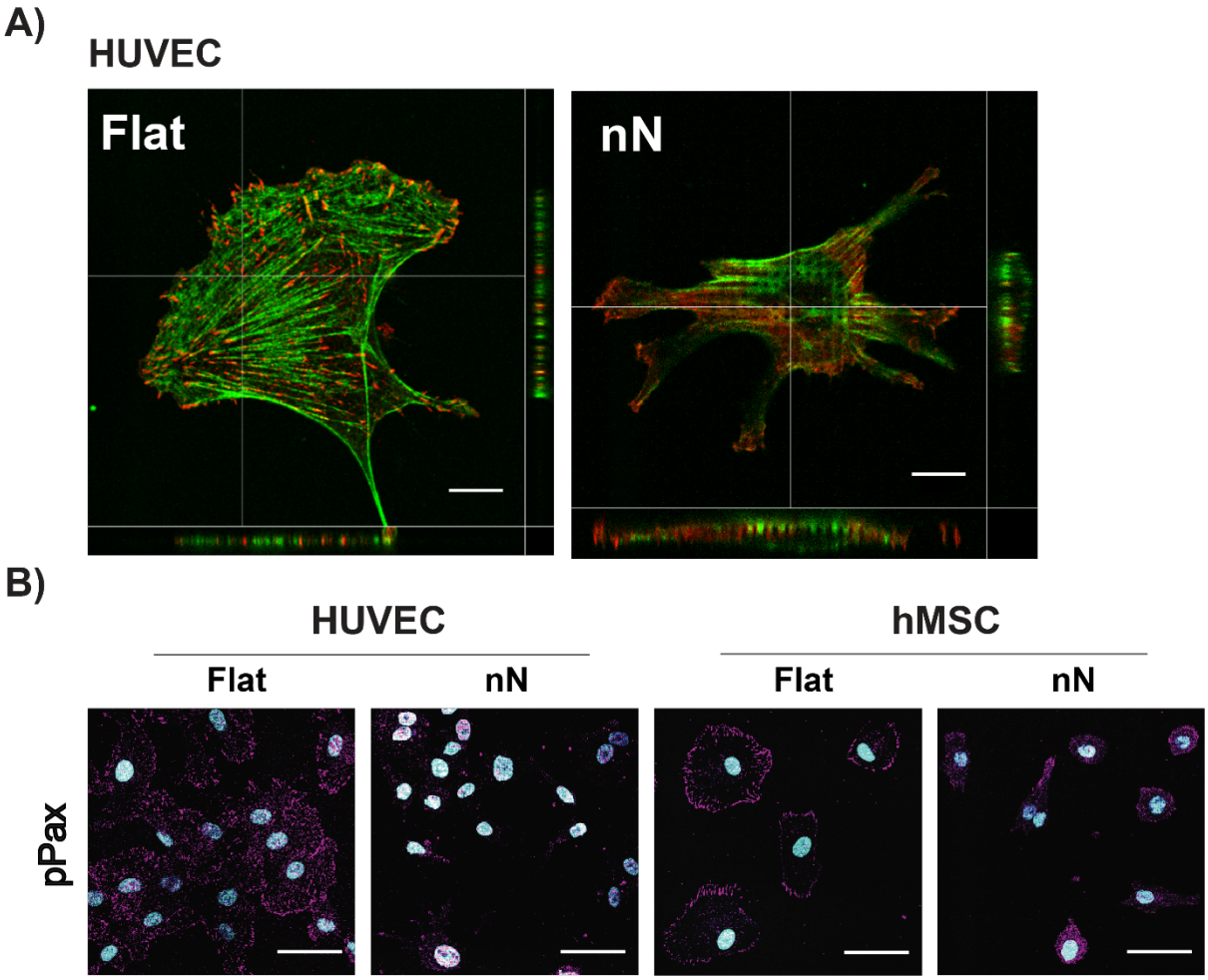


Figure 2.11*:* Nanoneedle arrays affect paxillin focal adhesion formation. A) Deconvolved confocal z-stacks of actin (green) and paxillin (red) of HUVECs on nN arrays and flat controls. Actin and paxillin were diffusely spread throughout the cytosol on nN whereas dense paxillin structures terminated actin stress fibres on flat controls. B) Punctate structures of phosphorylated paxillin (pPax) indicated FA maturation on flat substrates, and reduced and diffuse pPax signal was seen on nN. Scale bars = 50 µm.

Hampered FAs suggests an alteration in actomyosin contractile machinery, since a reduction in FA would prevent the cytoskeleton from binding to the cells ECM effectively. Indeed, a reduction in stress fibres was demonstrated on nN arrays **(Figure 2.8A)** and a visual decrease in active, phosphorylated myosin light chain (pMLC) intensity could be seen at the cell periphery on nN compared to flat controls **(Figure 2.12A)**. The reduction in pMLC intensity on nN was confirmed by immunofluorescent image analysis **(Figure 2.12B)** (image analysis conducted by Samuel Cooper at the Institute of Cancer Research and Imperial College, London).

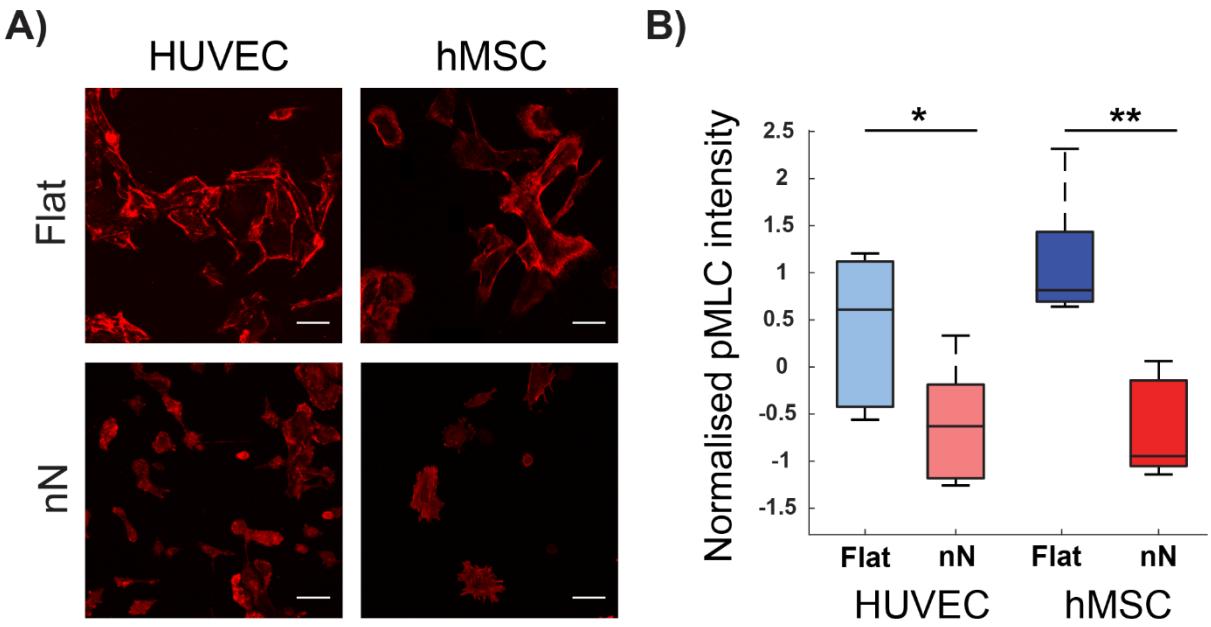


Figure 2.12: Nanoneedle arrays affect phosphorylated myosin light chain levels. A) Confocal maximum projection images of phosphorylated myosin light chain (pMLC) six hours post seeding on nanoneedles (nN) and flat controls. Scale bars = 50 µm. B) Quantification of pMLC signal intensity confirmed a significant reduction for both cell types cultured on nN, as compared to their respective controls (box plots, minimum/maximum, mean +/- S.D. N ≥ 4). The stronger signal on flat substrates indicated more active actomyosin contractile machinery. * $p < 0.05$, ** $p < 0.01$, *** $p < 0.001$ between groups as indicated by the lines. pMLC image analysis analysis was conducted by Samuel Cooper at the Institute of Cancer Research and Imperial College, London.

2.4.4 YAP/TAZ mechanosensors

Biophysical stimuli regulate the functionality of the transcription co-factors yes-associated protein (YAP) and transcriptional coactivator with a PDZ-binding motif (TAZ)[4]. When cytoskeletal tension can be generated, YAP and TAZ localise within the nucleus, activating their transcriptional program. However, when tension is interrupted, the co-factors are localised in the cytosol and their activity is reduced[4]. Indeed, the nuclear/cytosolic YAP ratio decreased on nN for both cell types **(Figure 2.13A-B**) (image analysis carried out by Samuel Cooper), and expression of the YAP target genes ankyrin repeat domain 1 (*ANKRD1*) and connective tissue growth factor (*CTGF*) was significantly decreased **(Figure 2.13C)**, indicating reduced functional YAP activity.

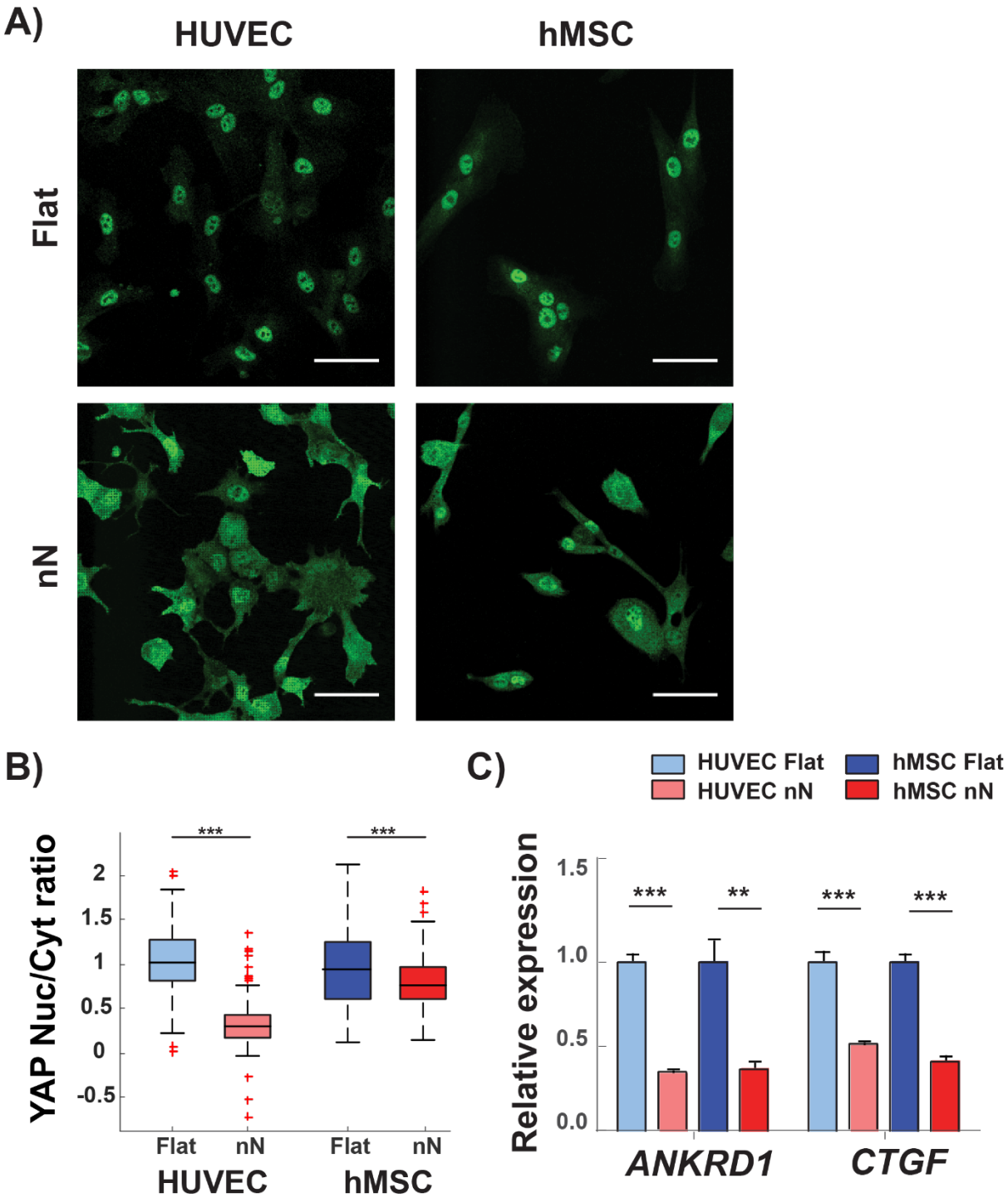


Figure 2.13: Nanoneedle arrays affect yes-associated protein (YAP) localisation and activity. A) Confocal microscopy showed nuclear YAP protein localisation on flat substrates, and cytosolic localisation on nanoneedles (nN). Scale bars = 50 µm. B) Image analysis demonstrated a significant reduction in the nuclear to cytoplasmic ratio of YAP on nN, (minimum/maximum; mean +/- SD; N = 4). C) PCR analysis indicated reduced expression of the YAP target genes ankyrin repeat domain 1 (*ANKRD1*) and connective tissue growth factor (*CTGF*), (N = 4, mean ± S.D.). * $p < 0.05$, ** $p < 0.01$, *** $p < 0.001$ between groups as indicated by the lines. Image analysis analysis was conducted by Samuel Cooper at the Institute of Cancer Research and Imperial College, London.

Cell spreading has been shown to modulate YAP transcriptional activity and nuclear accumulation through Rho/ROCK[9]. Indeed, on flat substrates, cell area correlated highly with YAP nuclear/cytosolic ratio (HUVEC: ρ = 0.592; hMSC: ρ = 0.465). However, on nN this correlation was notably lower (HUVEC: ρ = 0.184; hMSC: ρ = 0.263, **Figure 2.14**) (image analysis carried out by Samuel Cooper). Indeed, the correlations were significantly different (HUVEC: $p < 0.001$; hMSC: $p = 0.0183$, Fischer's z-transformation). Therefore, the nN system causes a loss of correlation between YAP localisation and cell area.

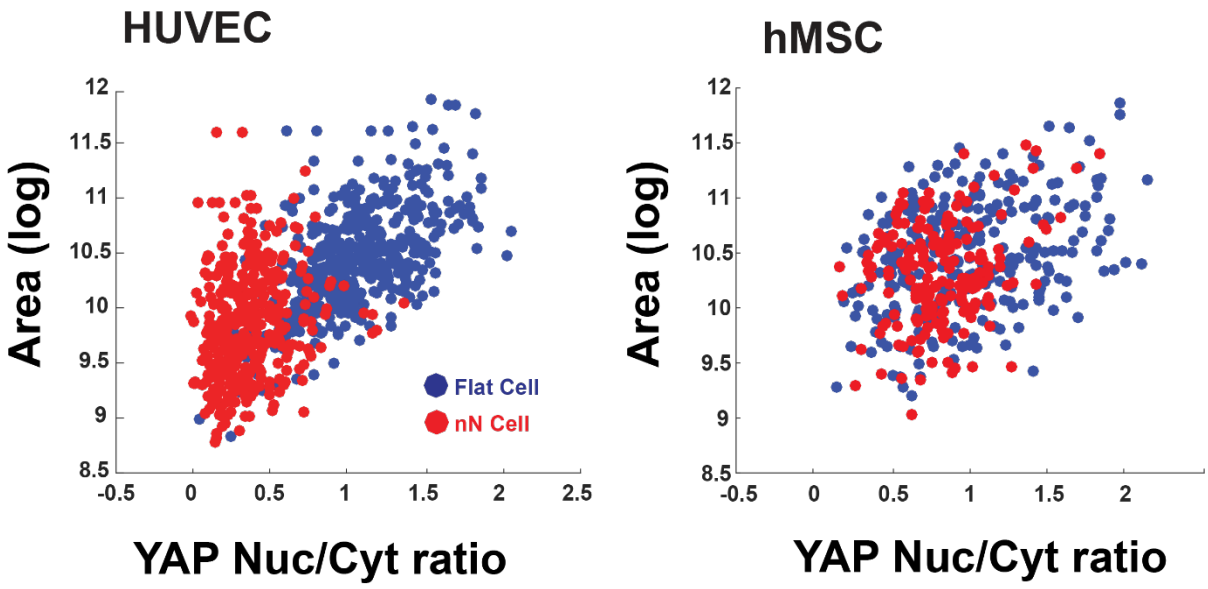


Figure 2.14: Nanoneedle arrays cause a reduction in YAP correlation with cell area. Cell area and nuclear YAP localisation showed greater correlation on flat substrates compared to nN arrays (N = 3). Image analysis analysis was conducted by Samuel Cooper at the Institute of Cancer Research and Imperial College, London.

The actomyosin contractile machinery has been shown to play a role in regulating YAP activation[4,9]. Efforts were therefore made to assess whether the actomyosin contractile machinery played a role in YAP activation on nN arrays. When treated with the actin depolymerising agent latrunculin B (LatB), the YAP ratio on control substrates was significantly reduced to levels comparable to those of nN, while LatB treatment on nN only modestly reduced the YAP ratio **(Figure 2.15)** (image analysis carried out by Samuel Cooper). Therefore, the actomyosin contractile machinery was shown to regulate YAP activation on nN arrays. These data confirm that nN functionally alter the activity of mechanoresponsive

transcription cofactors, and highlight the role of the actomyosin contractile machinery in modulating these events.

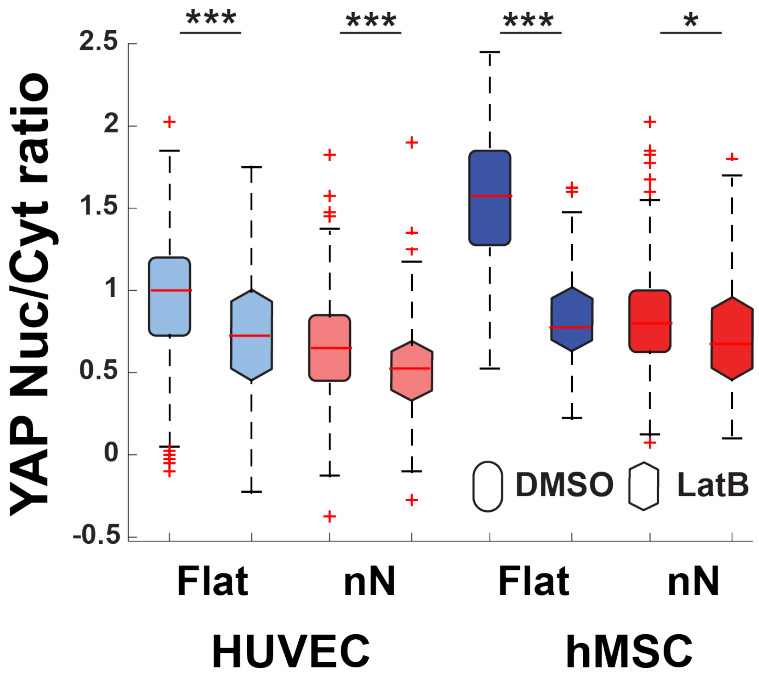


Figure 2.15: YAP localisation is controlled by the actomyosin machinery on nN arrays. YAP localisation following latrunculin B (LatB) actin depolymerisation. LatB treatment of cells on flat substrates reduced nuclear YAP localisation to levels comparable to untreated cells on nN. LatB treatment of cells on nN caused a much smaller reduction in nuclear localisation. (minimum/maximum; mean +/- S.D.; N = 3). * $p < 0.05$, ** $p < 0.01$, *** $p < 0.001$ between groups as indicated by the lines. Image analysis analysis was conducted by Samuel Cooper at the Institute of Cancer Research and Imperial College, London.

2.4.5 The nucleus

The nuclear envelope was also affected at sites of nN engagement. The nucleus was shown to remodel around the nN, and DNA was physically displaced at nN sites, as demonstrated by areas devoid of DAPI signal **(Figure 2.16)**. Nuclear deformation has previously been shown on other nN arrays[195,389,412], however the effects of this nuclear deformation have not been investigated. Therefore, rupture of the nuclear envelope was assessed on nN arrays. nN were shown to maintain an intact nuclear envelope, as evidenced by retention of heterogeneous nuclear ribonucleoprotein (hnRNP) within the nucleus **(Figure 2.17)**.

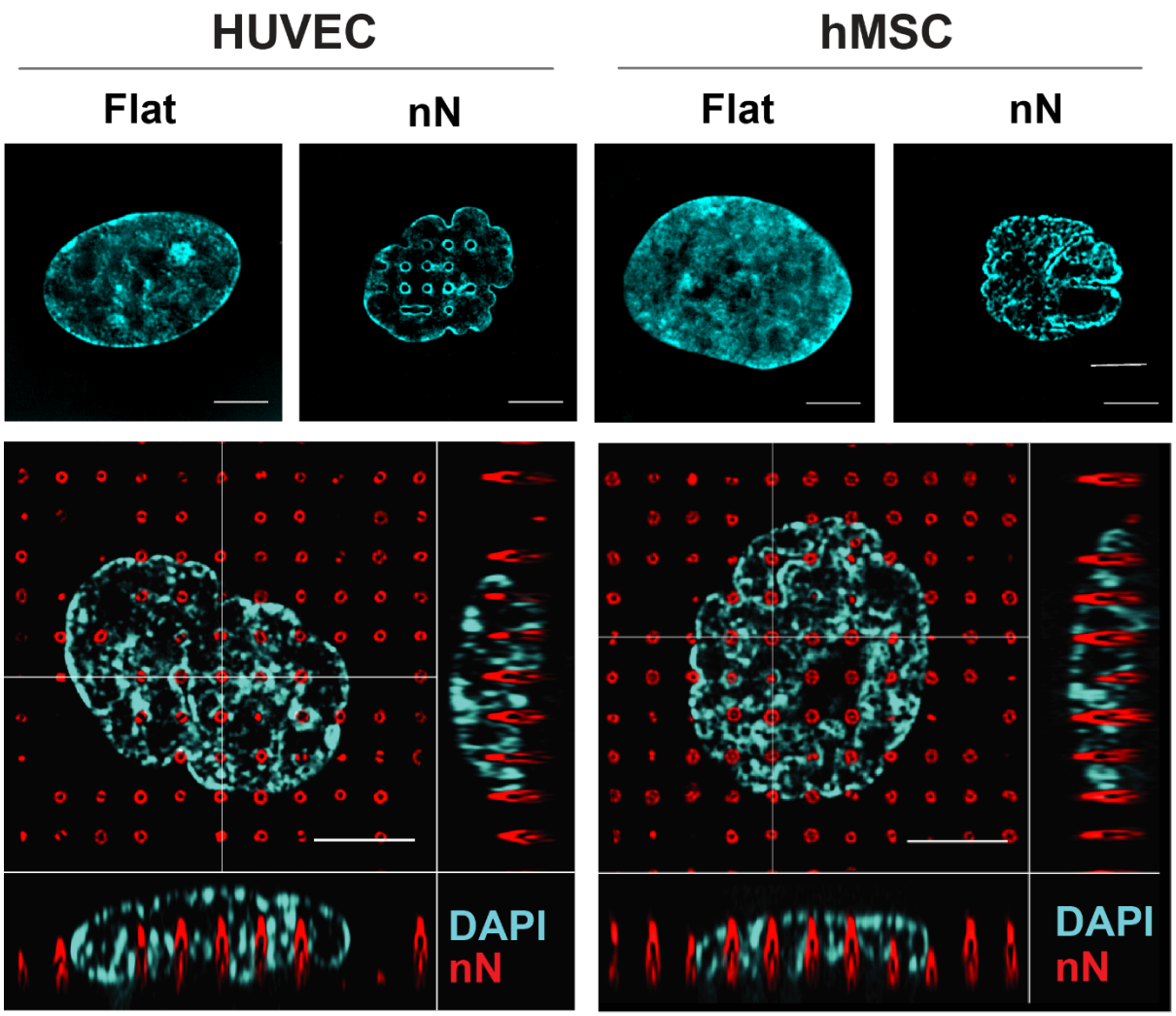


Figure 2.16: Nanoneedle arrays interact with the nucleus. Structured illumination microscopy (SIM) of DAPI-stained nuclei and fluorescent nanoneedles (nN) showed physical displacement of the nucleus at nN sites (single plane; cyan – DAPI, red – nN). Scale bars = 5 µm.

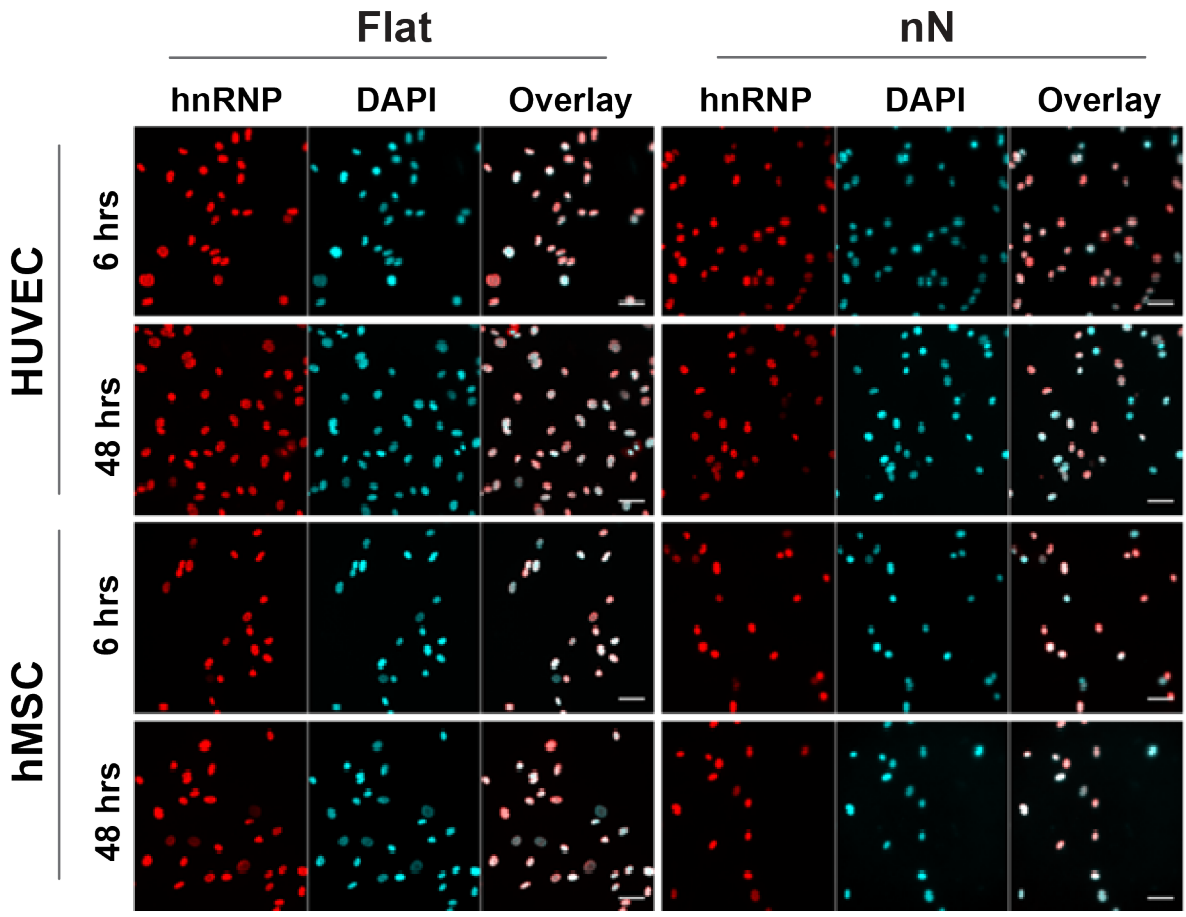


Figure 2.17: Nanoneedle arrays do not cause nuclear leakage. Cells maintained intact nuclei on nN with no nuclear leakage, as shown by nuclear localisation of heterogeneous ribonucleoprotein particle 1 (hnRNP) within DAPI stained nuclei (hnRNP - red, DAPI - cyan). Scale bars = 50 µm.

2.4.6 Nuclear lamins

In order to understand how the nN specifically interact with the nuclear envelope, the localisation and expression of A- and B-type lamins was analysed. Lamins are the intermediate filaments that provide structural integrity to the nuclear envelope[7]. The relative expression of lamin-A (*LMNA*) increased for both cell types on nN, as compared to their respective flat control, while lamin-B (*LMNB*) expression remained unchanged **(Figure 2.18A)**. Interestingly, the gene-level expression of the linker of nucleoskeleton and cytoskeleton (LINC) complex members, Nesprin-2 (*SYNE2*) and SUN2 (*SUN2*), was unchanged **(Figure 2.18B)**.

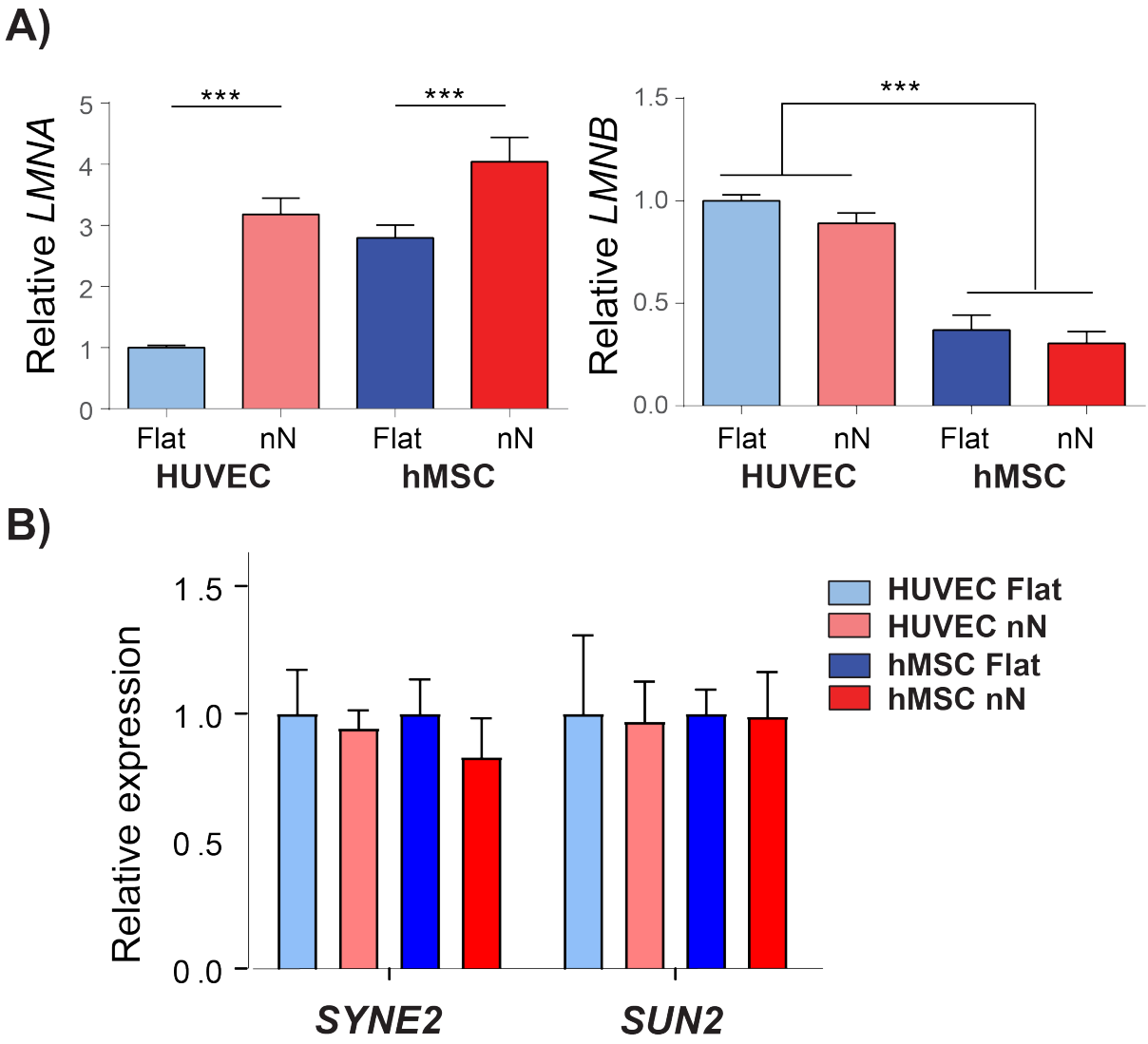


Figure 2.18: Nanoneedle arrays increase levels of *LMNA* but not *LMNB*. A) PCR analysis showed increased *LMNA* but not *LMNB* expression on nanoneedles (nN) whereas B) there was no change in the other linker of nucleoskeleton and cytoskeleton (LINC) complex components *SYNE2* and *SUN2* (N = 4, mean ± S.D.). * $p < 0.05$, ** $p < 0.01$, *** $p < 0.001$ between groups as indicated by the lines.

Since there was an alteration in lamin gene levels on nN arrays, microscopy of the lamin proteins was performed on nN arrays. Structured illumination microscopy (SIM) showed intense lamin-A signal at sites where nN impinged on the nucleus **(Figure 2.19A)**. Of note, lamin remodelling was not observed at all nN sites (24% of hMSCs and 37% of HUVECs demonstrated remodelled nuclei), but where strong impingement was evident, lamin-A was distributed throughout the whole length of the nN interface whereas lamin-B localised mainly around the base of nN **(Figure 2.19B)**.

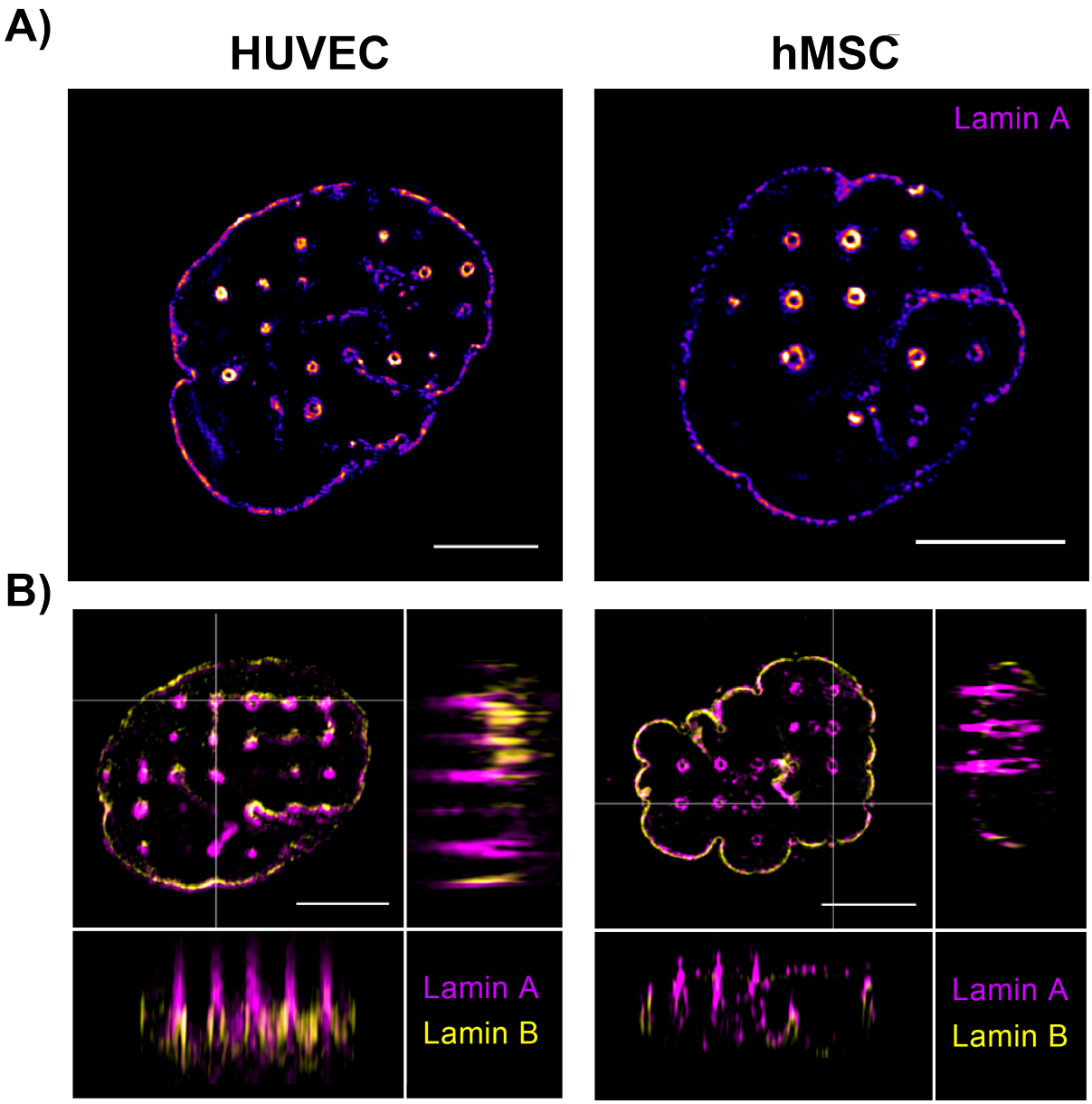


Figure 2.19: Lamin-A protein levels increase at nanoneedle locations, but lamin-B levels do not. A) Structured illumination microscopy (SIM) of lamin-A-stained nuclei (single plane) demonstrated a higher intensity of lamin-A at nN locations compared to the outer nuclear envelope and rings of lamin-A were seen around the individual nN. Scale bars = 5 µm. B) SIM imaging showed that lamin-A localises through the nanoneedle (nN) length whereas lamin-B distributed primarily at the base of the nN (single plane; magenta – lamin-A, yellow – lamin-B). Scale bars = 5 µm.

2.4.7 Lamin quantification

Reslice images of the x-z plane from confocal z-stack images **(Figure 2.20A)** enabled quantification of lamin-A and B signal along the nuclear envelope as it wrapped around the nN, and was normalised to the signal measured at non-nN locations in the nuclear membrane

to generate fold-change values **(Figure 2.20B)**. At sites of remodelling, lamin-A signal more than doubled on average and increased up to four-fold relative to non-nN sites, whereas lamin-B signal was mostly unchanged, indicating that the nN stimulate a dynamic response of lamin-A, but not lamin-B. In order to further illustrate the lamin type-specific response along the nN height, the ratio of lamin-A:B was measured along a straight line in the x-direction of reslice images, one at the middle of the nN and one toward the top. The lamin-A:B ratio at mid-height or at the tip of the nN showed an exponential relationship **(Figure 2.20C)**. For a given increase in A:B ratio at mid-height, a corresponding exponential rise in the A:B ratio at the nN top was observed according to the best-fit relationship: $y = 0.63e^{0.63x}$. The lamin-A:B ratio at the nN tip varied between 0.6 and 7.95. At nN locations that do not stimulate remodelling, the lamin-A:B ratio remained ~1 throughout the entire nN length; however, when remodelling does occur, the observed increase in ratio at the nN middle predicts an exponential increase at the nN top.

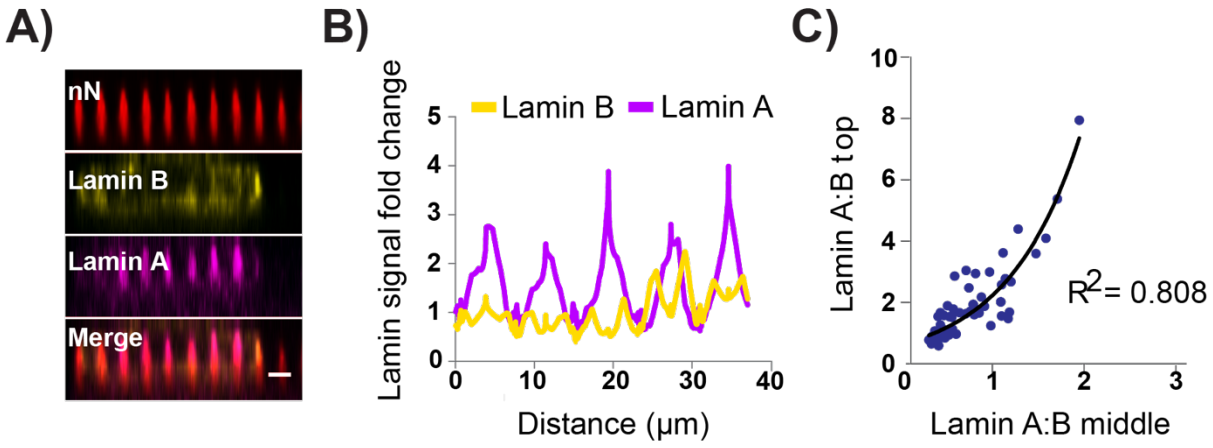


Figure 2.20: Quantification of lamin-A vs. lamin-B localisation. A) Reslice images of the x-z plane from confocal z-stack images; lamin-A signal increased around nN, whereas lamin-B remained constant. (red – nN, yellow – lamin-B, magenta – lamin-A). Scale bar = 2 μm. B) Image analysis of lamin-A and B intensity along the basal nuclear envelope normalised to the signal measured in the nuclear membrane at non-nN locations. C) Normalised intensity values of lamin-A and lamin-B at the middle and top of nN. At sites of nuclear remodelling (i.e. lamin-A / lamin-B > 1) the A:B ratio increased exponentially along the nanoneedle axis (R^2 = 0.808, n = 69 nN sites, n = 14 cells, N = 3). *** $p < 0.001$ between groups as indicated by the lines.

2.4.8 Nanoneedle degradation

After 48 hours in culture at 37 °C, nN were mostly degraded, as demonstrated by SEM imaging of the nN **(Figure 2.21)**. It has previously been shown that nN lose their structural integrity between 8 and 14 hours and that complete degradation occurs at 72 hours. Moreover, inductively coupled plasma atomic emission spectroscopy (ICP-AES) has previously been used to quantify Silicon release into solution by nN arrays, and Silicon release per hour plateaus at 48 hours[390].

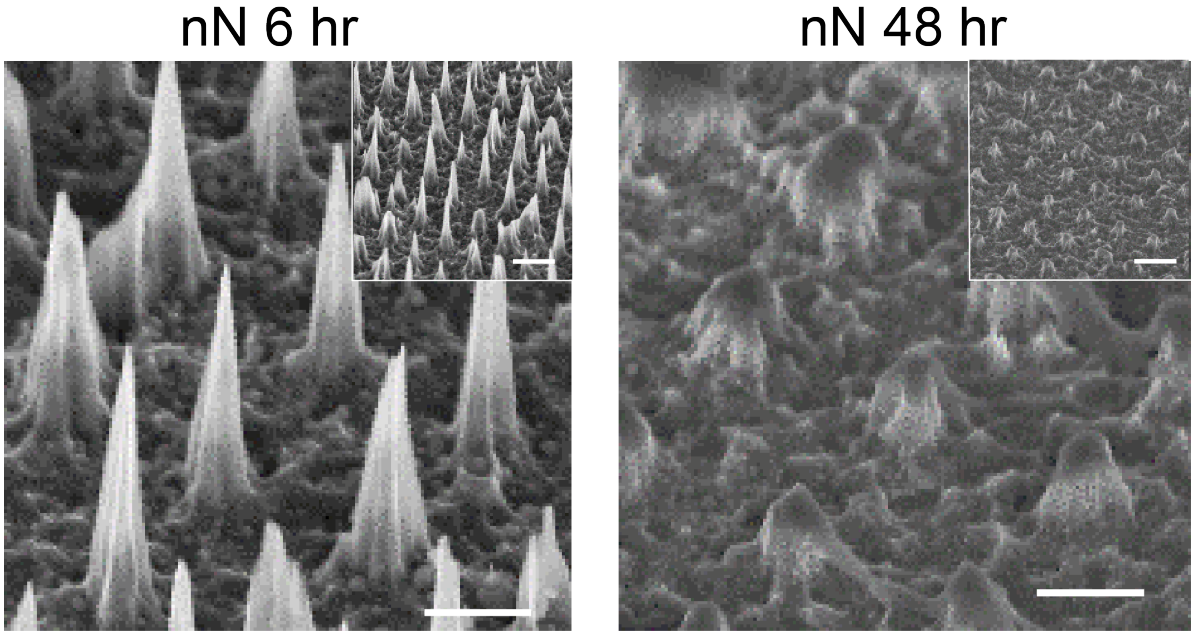


Figure 2.21: Nanoneedles degrade at 48 hours. Scanning electron microscopy (SEM) images shows degradation of nanoneedles (nN) after 48 hours in culture; only stumps remain. Scale bars = 1 µm, 2 µm inset. SEM images taken by Michele Becce, Imperial College, London.

Therefore, cell mechanobiology was tested on nN arrays after 48 hours of culture, to assess if there was any bio-molecular based recovery on the nN arrays once they had degraded to resemble the flat control substrates. Indeed, following 48 hours of culture on nN arrays, the cells recovered the characteristics observed on flat control substrates at six hours **(Figure 2.22)**. Cell morphology and stress fibres were restored to an extent (more notably for HUVECs), and actin rings were not observed at 48 hours. Moreover, punctate vinculin-rich FAs resembling those found on flat contols re-appeared once the nN had degraged after 48 hours and YAP appeared more nuclear on nN at 48 hours vs. six hours of incubation. Finally, DNA was no longer physically displaced at nN sites at 48 hours of culture on nN, since there

were no areas devoid of DAPI signal, and lamin-A remodelling was absent at sites of nN engagement 48 hours post nN interfacing. A-type lamin levels have been shown to respond to changes in stiffness after 24 hours[273], and cells seeded on nN therefore had the required time to restore their A-type lamin levels on nN once they had degraded at 48 hours.

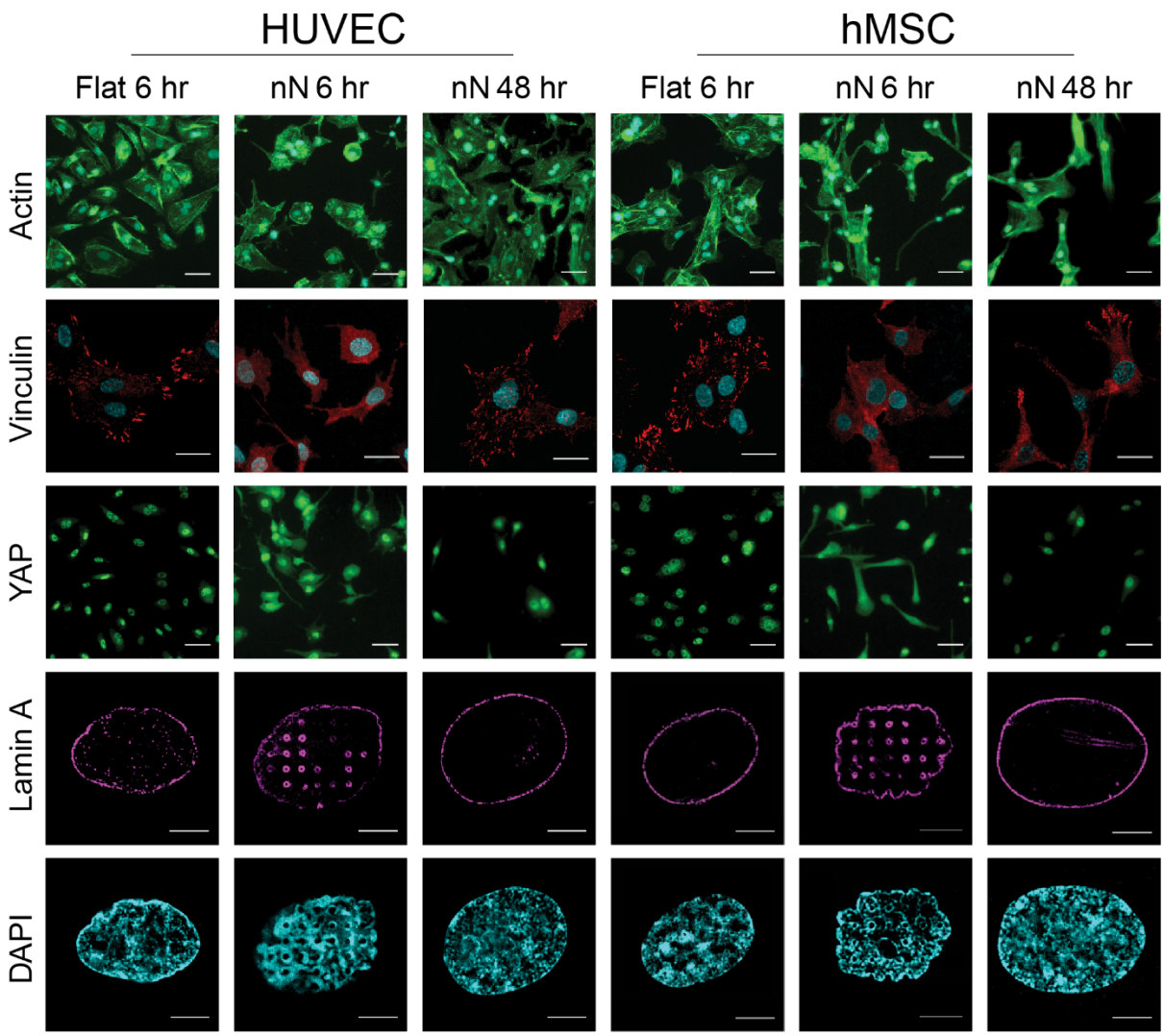


Figure 2.22: Following 48 hours of culture on nN, the flat phenotype is restored. Cells exhibited a spread morphology (green – phalloidin, scale bars = 50 µm), punctate vinculin-rich focal adhesions (red – vinculin, cyan – DAPI, scale bars = 25 µm), nuclear YAP localisation (green, scale bars = 50 µm), and an unimpinged nucleus (magenta – lamin-A, cyan – DAPI, scale bars = 5 µm).

Image analysis showed that the ratio of nuclear/cytosolic YAP was partially recovered to levels on flat controls once the nN had degraded at 48 hours **(Figure 2.23A)** (image analysis carried out by Samuel Cooper). Moreover, the density of FAs on nN at 48 hours, as indicated by

vinculin staining, was similar to what was measured on flat control samples at 6 hours **(Figure 2.23B)** (image analysis carried out by Samuel Cooper). The mechanoresponsive characteristics at 48 hours were therefore similar to culture on a flat substrate: with mature FA, engaged actomyosin machinery and restored nuclear envelope morphology.

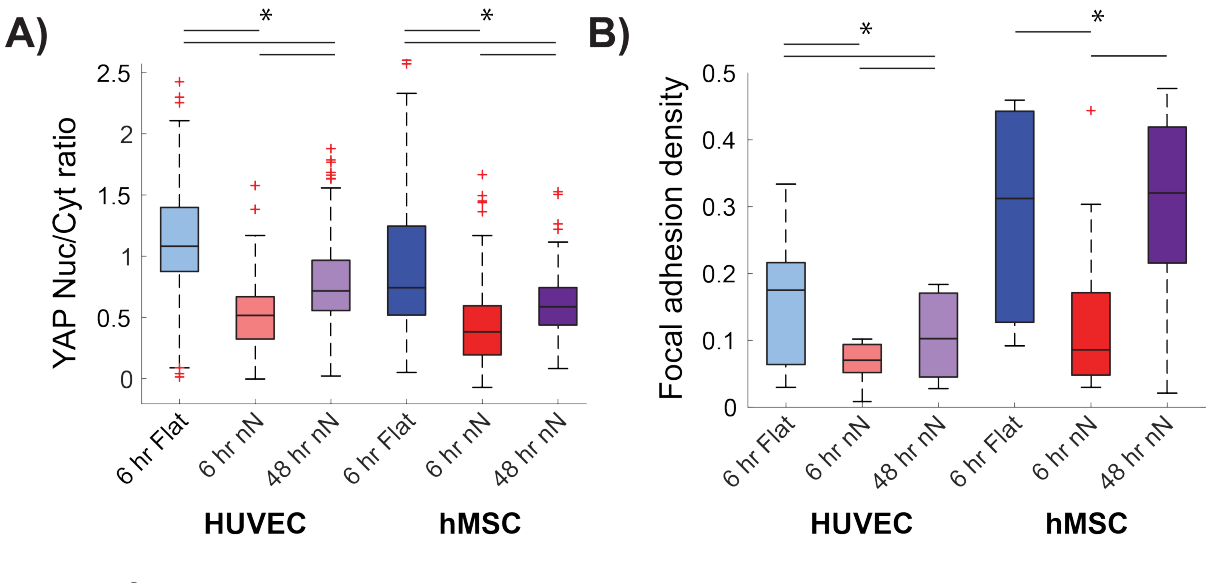


Figure 2.23: Quantification of YAP localisation and focal adhesion density following 48 hours of cell culture on nN. A) Image analysis showed an increase in nuclear YAP levels at 48 hours compared to six hours post seeding on nN arrays and B) increased focal adhesion (vinculin) density (box plots, minimum/maximum, mean +/- S.D.). n = 3, * $p < 0.05$ between groups as indicated by the lines. Image analysis was conducted by Samuel Cooper at the Institute of Cancer Research and Imperial College, London.

2.5 Discussion

Cells dynamically respond to physicochemical cues from the extracellular environment. In most material systems, signals are sensed at the cell membrane and transduced into a range of biological effects; forces are not directly inflicted on organelles. Techniques such as micropipette aspiration[143], optical/magnetic tweezers[530], and atomic force microscopy[531] can achieve direct interaction with organelles; but these approaches require direct application of force, potentially damaging the cells, and the applied forces are short-lived. Microcontact printing[515,532] and micropillar arrays[492,533,534] have been used to alter long-term nuclear shape however these deformations are on a µm scale. Therefore, these techniques do not reveal how organelles respond to physical stimuli in physiologically-relevant conditions.

This chapter demonstrates that nN arrays can be used as a technique to simultaneously stimulate different mechanoresponsive organelles for long periods of time without direct application of force and at a physiologically-relevant nm scale. Direct force was not applied since cells were seeded onto nN by gravity and active cellular processes then enabled tight interfacing between nN and the cell organelles. Indeed, the cell membrane, actin fibres and nucleus of cells were simultaneously stimulated in primary human cells with minimal impact on cell viability. Nanoneedle arrays therefore facilitate the study of intracellular mechanosensory elements and their associated pathways in physiologically relevant conditions, and provide a strategy to modulate their behaviour.

Classical mechanosensing pathways were modulated by nN interfacing. Diminished FA formation, reduced phosphorylation of MLC, inhibited nuclear translocation of YAP, and downregulation of target genes *ANKRD1* and *CTGF* emphasise the mechanosensory nature of this event. This is in line with the literature, since YAP functionality has been shown to be modulated by Rho/ROCK activation, and the nuclear localisation and subsequent transcriptional activity of YAP correlate with increased actomyosin tension and reduced FA formation[4,9].

Nanoneedle arrays have previously been shown to modulate the classical mechanosensing machinery of cells. For example, membrane projections have been shown to interact with nN[309,389,390,490]; the actin cytoskeleton has been demonstrated to remodel around nN[195,308,410,417,455,518], and has been shown to align along the nN arrays[500]; dot-like focal complexes have been described at nN locations[411]; cytosolic YAP has been demonstrated on titanium nanotubes[509]; and nuclear deformation around nN has been described[195,389,412].

A novel finding in this chapter is that YAP cytosolic localisation does not always correlate with cell area. In previous work, limited cell spreading via patterning of adhesive proteins has indicated that intracellular tension can be attenuated on stiff substrates, but this effect has always been a function of cell area[4,9]. Similarly, on flat substrates in our study, cell area correlated strongly with YAP nuclear/cytoplasmic ratio **(Figure 2.14)**; however, the correlation weakened significantly for cells cultured on nN. Cells on nN therefore exhibited a

state of low-tension with a large spread area, a situation which is not observed on planar substrates or micropillars of varying elasticity[4].

Actin fibres directly responded to the presence of nN, forming rings at sites of interfacing **(Figure 2.9, Movie 2.1)**. This is likely to be the reason why the actin network lost the linearity and bundle formation that is typically observed on stiff substrates (**Figure 2.8A)**. Nonetheless, cells on nN retained a degree of cytoskeletal tension, as evidenced by the ability of actin depolymerising agents to reduce the YAP ratio, reaching levels comparable to similarly treated controls **(Figure 2.15)**.

A further novel result was that nN were able to stimulate a dynamic remodelling process of A-type, but not B-type, lamin proteins **(Figure 2.18-2.20)**. In structural models of the nuclear envelope, lamin-A exhibits a viscous response to resist deformation whereas lamin-B is an elastic component that preserves nuclear shape[10]. Indeed, lamin-A is required to prevent nuclear envelope rupture in the presence of external forces both in isolated nuclei[530] and intact cells[143], and lamin-A expression scales with tissue stiffness[10] in order to protect the sensitive nuclear components from external pressures. In this system, lamin-A responded to the mechanical stimulus by accumulating at nN sites, with the lamin-A:B ratio increasing towards the nN tip **(Figure 2.20C)**. Diverging properties in lamin-A versus lamin-B localisation and remodelling was demonstrated in response to direct nuclear stimulus, which provides further evidence for the role of A-type lamins to respond to physical stress in living cells.

Finally, the degradation of nN at 48 hours in culture caused cell phenotype to return to what was observed on flat substrates **(Figure 2.22)**. All the mechanoresponsive elements considered were rescued by nN degradation, resulting in formation of dense FAs and continuous actin fibres, recovery of nuclear YAP localisation, and restoration of nuclear shape and envelope (A-type lamin) composition. This highlights how nN interfacing causes an active cellular response, and the reversal of these behaviours upon nN degradation verifies the role of the physical nano-features in driving changes in mechanoresponsive organelles.

2.6 Conclusion

Porous silicon nN arrays have been shown to mechanically stimulate remodelling of organelles in a reversible manner without loss of cell integrity. nN directly interacted with canonical mechanobiology pathways since they prevented the formation of stable FA complexes at the cell-material interface, modulated cytoskeletal organisation and intracellular tension, and prevented YAP nuclear localisation. Moreover, they induced direct remodelling of the nuclear envelope associated with an alteration in the localisation of nuclear lamins, the intermediate filaments that provide structural integrity to the nuclear envelope. Finally, these behaviours were specifically due to the nNs since the effects were lost upon nN degradation after 48 hours. These findings highlight a novel material to direct cell phenotype through biophysical interaction with mechanoresponsive organelles.

2.7 Future directions

Mechanistic experiments could be carried out to address how the YAP and lamin-A responses are connected. This would involve over-expression and knockdown of YAP and lamin-A, respectively. For example, the overall YAP response to lamin-A over-expression and knockdown could be measured using a YAP luciferase reporter and by image analysis. Since matrix stiffness promotes A-type lamin dephosphorylation at Ser22, which regulates A-type lamin's turnover and physical properties[273], phosphorylated lamin-A could be assessed by immunofluorescence. Moreover, lamin-A, phosphorylated lamin-A and lamin-B Western blots could be performed to assess whether relative protein levels change in the same manner as the gene levels. Nuclear translocation of RARG could be measured since RARG levels scale with matrix elasticity and levels have been shown to be directly affected by lamin-A knockdown or overexpression[10]. Further experiments could be conducted with LatB to assess whether the lamin-A response is due to direct physical interaction with the nN, cytoskeletal tension, or a combination of both.

It would be interesting to see how various lamin mutations alter the nuclear morphology and YAP response to nN, as well as the other mechanosensing organelles. Ideally, 3 – 5

transgenic/mutants would be obtained that represent different disease states (e.g. *LMNA* N195K/N195K to model dilated cardiomyopathy and cells can be transfected with the progerin mutant plasmid from AddGene (#17663)).

Since FA and actin contractility is compromised on nN arrays, cell motility could be investigated on nN arrays. Live cell imaging could be carried out on actin labelled cells and the cells could be imaged over 48 hours. Membrane protrusions could be assessed as well as migration speed and displacement.

Finally, the nN arrays could be fabricated with different porosities, tip diameters, lengths, and densities. Moreover, the surface functionalisation of the nN could also be modified. Cell properties such as settling, morphology, nuclear impingement, YAP localisation, FA density and lamin-A levels could then be assessed on nN arrays with these different geometries and surface chemistries. A model might be created to predict cell behaviour on different nN array types. A proper quality control method should be developed for the nN arrays if these experiments are to be conducted. Nanoneedle dimensions could be thoroughly assessed using SEM, in particular the shape of the nN tips and a certain number of nN tips could be assessed in different areas within the nN array. Following this, the homogeneity of any nN functionalisation could be confirmed using fluorescenct labelling techniques or raman spectroscopy. A bioassay could then be developed to confirm that cells respond similarly to different batches of nN arrays and also to different nN arrays within a batch. For example, the cells actin homogeneity could be assessed, since this phenotype is highly altered when cells are seeden on nN compared to flat controls.

3 Microscopy of the cell-matrix interface

The epithelial-to-mesenchymal transition (EMT) is a critical event in the formation of fibroblast/mesenchymal cells and relates to development of epithelial-derived metastatic cancer cells. The interaction between epithelial cells and the basement membrane (BM), a specialised form of the extracellular matrix, may be pivotal in controlling EMT. The BM contains "cryptic" sites, which can be mechanically or proteolytically cleaved as fragments during EMT, and the role of one such fragment, a fragment of the laminin-111 BM protein (laminin β1-fragment), is assessed during EMT. This laminin β1-fragment is known to interact with α3β1-integrin and has been suggested to interfere with transforming growth factor-beta 1 (TGF-β1) mediated EMT[535,536]. The effect of the laminin β1-fragment on TGF-β1 signalling in EMT is further explored in this chapter.

Normal murine mammary gland epithelial (NMuMg) cells were seeded in well plates for 24 hours and were then replenished with fresh media (control), or treated with TGF-β1 with or without the laminin β1-fragment. 24 hours later, TGF-β1 signalling was assessed using microscopy and Western blotting. The laminin β1-fragment was shown to affect TGF-β1 nuclear factor kappa-light-chain-enhancer of activated B cells (NF-κB) p65 nuclear translocation by Western blotting. However, HCI analysis showed no alterations in NF-κB p65, pSmad3 or YAP nuclear translocation; Smad7, lamin AC or MT1-MMP intensity; or FA number when comparing control cells, cells treated with TGF-β1, and cells treated with TGF-β1 and laminin β1-fragment. Moreover, there was no change in migration with TGF-β1 with or without the laminin β1-fragment.

3.1 Introduction

3.1.1 The epithelial-to-mesenchymal transition

The epithelial-to-mesenchymal transition is a reversible process which allows polarised epithelial cells with tight cell-cell junctions that are attached to the basement membrane (BM) to assume a motile mesenchymal phenotype with front-rear polarity and increased production of fibrillar ECM components, such as collagen type 1 (**Figure 3.1**)[537]. EMT is necessary for a number of processes including gastrulation, embryo formation and organ development[538–543]; wound healing, tissue morphogenesis/regeneration, and tissue fibrosis[544–548]. EMT is also involved in cancer metastasis in which cancer cells are disseminated from the primary tumour[549–554].

EMT involves extensive cross-talk between different signalling pathways. Small mothers against decapentaplegics (Smads), Wnt, protein kinase B (Akt), FAK and mitogen-activated protein kinase (MAPK) signalling results in a switch from E- to N-cadherin, and EMT-transcription factor (snai1, snai2, twist, zeb1, zeb2), vimentin and MMP up-regulation[555–559]. EMT is regulated by ECM receptors (e.g. integrins), hypoxia, and a number of growth factors (e.g. transforming growth factor beta (TGF-β), and tyrosine kinase receptors)[18,536,560]. The underlying BM, which primarily consists of laminin and collagen type IV proteins, is degraded during EMT and the mesenchymal cells are able to migrate away from the original epithelial layer. The molecular mechanisms of BM remodelling during EMT, and the role played by matrix metalloproteinases (MMPs) are still under investigation[18].

EMT has been classified into three different subtypes: type 1 EMT is associated with implantation, embryo formation, and organ development, and it generates mesenchymal cells which do not cause fibrosis or induce an invasive phenotype; type 2 EMT is associated with wound healing, tissue regeneration and organ fibrosis, and it generates fibroblasts as a part of repair-associated events and are associated with trauma and inflammation; type 3 EMT occurs in neoplastic cells which have gone epigenetic and genetic changes to produce invasive cancerous cells[537]. Although there are many similarities in the different forms of EMT,

it must be noted that EMT has mostly been investigated in cancer (type 3 EMT), and the findings in cancerous EMT might not hold true for EMT in fibrosis or gastrulation, for example.

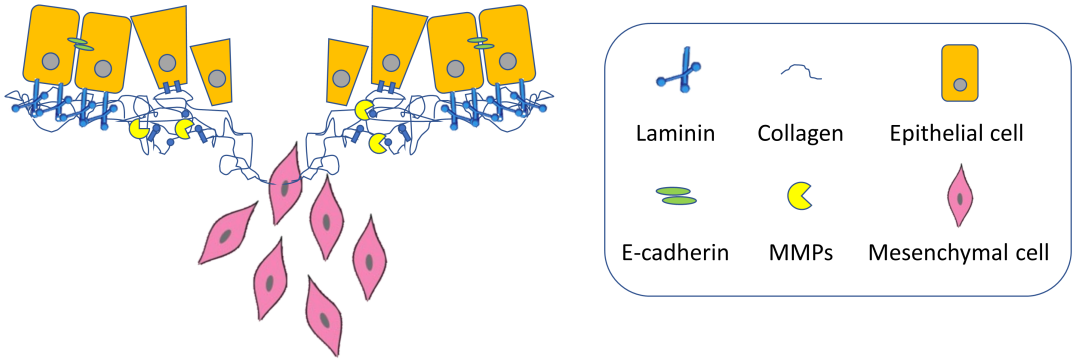


Figure 3.1: The epithelial to mesenchymal transition, modified from C. M. Horejs *et al. Eur. J. Cell Biol.* **95**, 427–440 (2016)[18], with permission from Elsevier, copyright 2016. Epithelial cells lose their adherens junctions and tight junctions and transition to a migratory mesenchymal phenotype. This disrupts the basement membrane via activated membrane-bound matrix metalloproteinases (MT-MMPs) and secreted matrix metalloproteinases (MMPs) and mesenchymal cells can penetrate the basement membrane (BM) using their invadopodia; actin-rich membrane structures which form at the leading edge of migrating cells. MMPs interact with the BM and release fragments of the BM proteins laminin and collagen type IV, exposing integrins which had previously been bound to the BM.

3.1.2 The basement membrane

The ECM forms a thin BM, covering almost all organs and all body cavities[561]. The BM is largely synthesised by the cells that rest on it and its precise composition varies from tissue to tissue and even from region to region in the same BM[562]. The BM primarily consists of laminin and collagen type IV, which are interconnected by nidogen and the heparan sulphate proteoglycan perlecan or agrin (**Figure 3.2**)[16,26,563–566]. These proteins form insoluble networks which provide a structural role and also influence the behaviours of associated cells[16]. The BM has a small pore size, which prevents the pathogenic migration of cells[565,567,568]. For example, the BM beneath an epithelium prevents fibroblast in the underlying connective tissue from making contact with the epithelial cells but enables macrophages, lymphocytes, and nerve processes to pass through. Larger cells are only able to travel through the BM with the help of force and/or enzymes[18,569–574]. The BM is important in tissue regeneration

following an injury since it provides a scaffold along which the regenerating cells can migrate[575]. Finally, the BM comprises cryptic sites, usually hidden within the tertiary structure of the protein or within the BM, that can regulate biological processes such as migration[576]. These cryptic sites can be mechanically or proteolytically revealed by MMPs, exposing new binding sites for cell receptors and initiating a cellular response[577,578].

Basement membrane components are able to self-assemble and form a sheet-like structure[17,579,580]. In tissues, laminins and type IV collagen preferentially polymerise while bound to receptors on the surface of the cells that produce them. Cell-surface receptors such as integrins (especially β1 integrins), dystroglycans and sulphated glycolipids facilitate the initial deposition of laminin polymers via site-specific interactions[581–584]. Type IV collagen polymers then associate with the laminin polymers on the cell surface via nidogen/enactin and perlecan bridging[585,586], forming an independent covalently bound network providing the BM with mechanical strength[587,588]. This scaffold then provides specific interaction sites for other BM constituents[589]. For example, growth factors, such as fibroblast growth factor (FGF), bone morphogenetic proteins (BMPs) and TGF-β are tethered to the basement membrane and accumulated via the heparan sulphate proteoglycans[590,591].

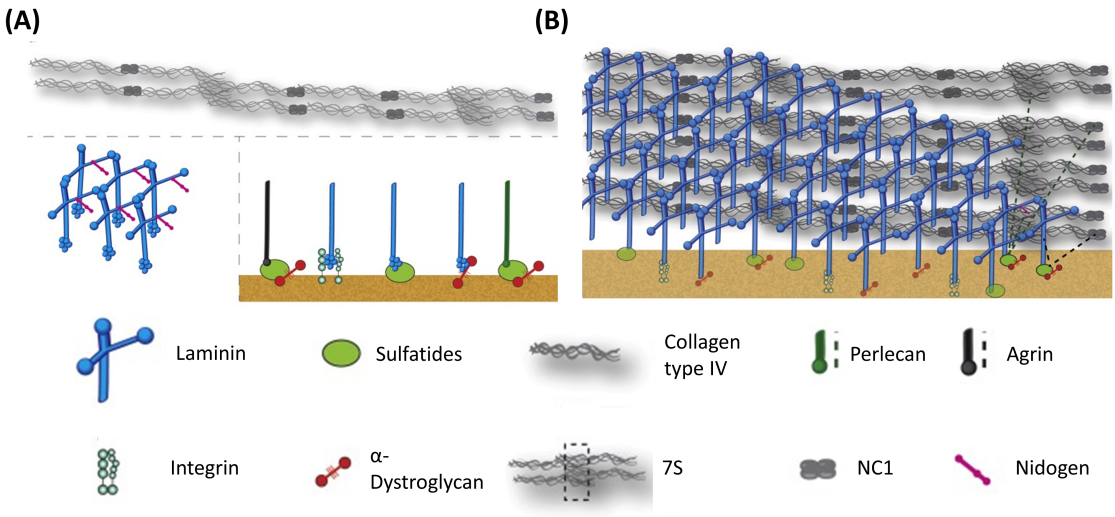


Figure 3.2: The structure of the basement membrane, modified from C. M. Horejs *et al. Eur. J. Cell Biol.* **95**, 427–440 (2016)[18], with permission from Elsevier, copyright 2016. A) Collagen type IV and laminin are the key components of the basement membrane (BM). Secreted collagen heterotrimers form triple helical assemblies containing 7S domains. These assemblies oligomerise into cross-linked tetramers which can form a polymeric collagen scaffold due to interactions between the C-terminal NC1. Laminins consist of an α-, β-, and γ-chain which form a cross-like tertiary structure, containing three short and one long arm. Nidogen interacts with one of the short arms. The BM interacts with the cell membrane through integrins, sulfatides, and α-dystroglycan. These structures can bind to the laminin C-terminal LG domains, perlecan and agrin. B) The BM consists of covalently linked collagen type IV heterotrimers interconnected with pre-assembled laminins via agrin or perlecan and nidogen.

A controlled turnover of ECM macromolecules is essential for many important biological processes. Understanding how cells invade and remodel BM boundaries is of key importance since it is a crucial step in many developmental processes, leukocyte trafficking, and pathogen entry into host tissues, and remains one of the least understood mechanisms in cancer progression[13,592,593]. BM disassembly occurs during EMT[18], and is a critical early step in gastrulation EMT, marking the beginning of mesoderm and endoderm formation[540,594]. It is still unclear as to how BM breakdown during transmigration is regulated due to the difficulty of experimentally examining cell–basement membrane interactions during invasion events *in vivo,* and most of the mechanistic understanding of invasion has been derived from *in vitro* studies[13,564,588,595]. The BM is challenging to assess due to its complexity and insolubility and *in vitro* studies have consisted of artificial matrices and denuded acellular BM which are unable to mimic the dynamic physical and biochemical environment of the BM effectively[564].

A number of general mechanisms for BM breakdown have been proposed, involving mechanical force and physical displacement, localised loss of BM receptors, and proteolysis of BM proteins by MMPs[18,569–574]. Real-time analysis of cell–BM interactions in living model organisms will be essential to understand the mechanisms underlying invasion[564].

Anchor cell invasion in *C. elegans* has been used as a system to assess the molecular mechanisms involved in BM breakdown and cell invasion *in vivo*[592]. When *C. elegans* larvae undergo development, juxtaposed gonadal and epidermal BMs separate the nascent uterine and vulval tissues[596]. The anchor cell is a specialised uterine cell, which invades through these two BMs using invadopodia[597], as a means to initiate attachment between the outer uterine and vulval tissues[596,598]. Shortly following membrane invasion, anchor cells extend their invadopodia into one single protrusion across the structure[597,599] and this has also been seen in other invading cells seeded on a denuded BM[89,600]. BM invasion events tend to cause a loss of the BM at the site of transmigration[594,601–605]. Dissolution of the BM has been suggested based on the increase in type IV collagen degradation products at the sites of invasion *in vitro* and the increase in protease (e.g. MMP) expression in invading cells[606–608]. However, anchor cell imaging experiments have revealed that the BM is moved aside by invasive cell protrusions[597]. This does not make the role of proteases redundant since they increase BM pliancy for displacement and they may be required for initial BM breaching[564]. After the anchor cell breaches the BM, the BM gap widens and this has been shown to be independent of BM deposition or degradation[604]. Instead the BM slides over the invaginating and actively dividing vulval and the vulval cells generate tension forces that shift the BM as they invaginate.

Basement membrane breaching by mechanical force has been also shown in mouse embryos cultured in engineered microcavities[605]. Mechanical forces are exerted between the embryo and the maternal uterine tissue and this induces BM breaching and subsequent epiblast cell transmigration. Moreover, in the chick embryo, RhoA activity and microtubule dynamics play an essential role in BM disassembly; a decrease in RhoA levels leads to a destabilisation of microtubules which causes BM disassembly[594].

It has been hypothesised that MMPs are essential, yet not exclusive, in facilitating BM remodelling. However, the specific interactions between BM proteins and MMPs remains unsolved[13,564,609]. A number of BM protein fragments have been reported to be released by MMPs and this has been demonstrated in various *in vivo* models and patient-derived samples. However, the specific receptor interactions, bioactivities and potential cell-BM-cell feedback mechanisms have been investigated in very few of these fragments[18]. The investigation into these proteolytic mechanisms will be helped by the development of sophisticated mass spectrometry protocols[610] and proteomic analysis will increase our understanding in how the BM can affect EMT signalling[55,611–613] and the mechanisms of BM breakdown *in vivo*.

The Overall laboratory at the University of British Columbia has founded the field of "degradomics" which applies proteomic techniques to assess the range of proteases and protease-substrates found within a cell, tissue or organism. Most importantly, proteomic techniques have been developed to identify proteomic products *in vivo*, and protein substrates and exact cleavage sites can be determined in the same analysis by specifically enriching mature protein N-termini and neo-N-termini of proteins using isotopic labelling[614,615]. This technique, known as Terminal Amine Isotopic Labelling of Substrates (TAILS) has shown that MMPs regulate signalling pathways as well as degrading the ECM[616] and could show promise in revealing the mechanisms in BM breakdown *in vivo*. A next step in deciphering MMP-BM crosstalk will be to generate BM fragments *in vitro* using intact BM and to show release and bioactivities in adequate *in vivo* models[535]. MMP-knockout models need to be developed and the possibility to study live cell migration and capture the action of MT-MMPs using high-resolution imaging techniques will further increase our knowledge of MT-MMP-basement membrane interplay[617,618]. The inhibition of MMPs to prevent EMT has failed in initial clinical trials, and a greater understanding of how BM affect EMT may provide new strategies to target pathological BM turnover and EMT.

3.1.2.1 Basement membrane proteins

3.1.2.1.1 Laminins

Laminins are a family of BM proteins which play a crucial role in cell adhesion, migration, differentiation, phenotype stability and provide resistance to apoptosis[619]. Laminins interact

with cells via cell membrane receptors such as integrins and dystroglycan, initiating a number of signalling pathways[620,621]. 16 different mammalian isoforms of laminin have been described so far, consisting of 12 different laminin chains and these isoforms show differences in chain length and domain architecture but are highly conserved between different species. Laminin isoforms are coiled-coil heterotrimers containing an α-, β-, and γ- chain assembled into a cruciform shape, held together by disulphide bonds. The C-termini of the three chains form an α-helical, coiled-coil domain and the α-chain has a C terminal ending in a G domain consisting of 5 LG sub-domains which is the major site of cell-laminin adhesion. The N-termini of the α-, β-, and γ- chains allow laminin polymerisation and therefore provide a key role in maintaining BM integrity[620].

3.1.2.1.1.1 Laminin-111

Laminin-111 is one of the first ECM proteins expressed during embryonic development which assembles and stabilises the BM[622,623]. The Laminin-111 isoform consists of α1β1γ1 chains[565], and it is able to modulate ECM function when modified by other proteins[624–626]. In particular, laminin-111 can be cleaved by different MMPs, resulting in a loosened BM, facilitating cell migration[624,626–628] and processes such as EMT[536]. The crystal structure of the heterotrimeric integrin-binding region of laminin-111 has recently been revealed at 2.13 Å resolution[629]. Laminin-111 has three short arms coming from the α1-, β1-, and γ1-chains which form the laminin network and MMP-2 cleavage of the β1-chain short arm is believed to disassemble the laminin network and thus the basement membrane[536]. The γ1 tail lies above the LG1 and LG2 domains of the α chain and it has been proposed that is this complex surface that the integrins recognise[629].

3.1.2.1.2 Collagen

Collagen is a glycine and proline-rich protein that is a major component of the ECM and connective tissues. Collagen exists in many forms: 28 different collagen types have been identified, and more than 40 distinct α-chains have been recognised in humans[630,631]. Type I, II, III, V, and XI collagens are fibrillar collagens. Type I is the most common form of collagen and is found in skin, tendon, and bone. Fibril-associated collagens include type IX and XII, these decorate the surface of collagen fibrils, and are thought to link the fibrillar collagens to each other and the ECM. Type IV and VII are network forming collagens. Type IV collagen

molecules assemble into a meshwork that constitutes a major part of mature BM, while type VII molecules form dimers that assemble into specialised anchoring fibrils.

Fibrillar collagen consists of a long, stiff, triple stranded helical structure, in which three polypeptide α-chains, are wound around each other into a rope like superhelix. This structure that is characterised by amino- and carboxy-terminal propeptide sequences, which border a series of Gly-X-Y repeats (where X and Y describe any amino acids but are frequently proline and hydroxyproline)[632]. The C-terminal propeptide initiates triple helix formation in the rough endoplasmic reticulum. Procollagen is then secreted by the cells into the extracellular space, and collagen type-specific metalloproteinase enzymes then cleave the procollagen to form collagen by removing the amino- and carboxy-propeptides[630,631,633,634].

After cleavage of procollagen into collagen, microfibrils begin to form at the cell surface[635.] The process of fibril formation is driven partly by the tendency of the collagen molecules to self-assemble, since they are more than a thousand-fold less soluble than procollagen molecules. The fibrils begin to form close to the cell surface, often in deep infoldings of the cell membrane where secretory vesicles fuse with the cell surface. The underlying cortical cytoskeleton can therefore influence the sites, rates, and orientation of fibril assembly. Indeed, cells help organise the collagen fibrils they secrete by exerting tension on the ECM. The microfibrils mature to fibrils with the help of accessory macromolecules and cell adhesion receptors[635,636]. Lysyl oxidase catalyses the formation of intramolecular and intermolecular covalent crosslinks between collagen molecules, enabling mature fibres to be formed[637–640]. These fibres are bundled together within a connective tissue and form linear structures capable of transmitting tensile forces through stabilising interactions with fibril-associated collagens with interrupted triple helices (FACIT) collagens and small leucine-rich repeat proteoglycans (SLRPs)[20,641].

3.1.2.1.2.1 Type IV collagen

Type IV collagen is a non-fibrillar collagen whose abundance increases with age comprising more than 50% of adult BM[642]. It comprises six genetically distinct α-chains (α1(IV) to α6 (IV)) that assemble into three heterotrimers (α1α1α2, α3α4α5, α5α5α6), with α1 and α2 being

present in every tissue[643]. Type IV collagens exist in several isoforms which have a more flexible structure than the fibrillar collagens since their triple-stranded helix is interrupted in 26 regions, allowing multiple bends. They are not cleaved after secretion, but interact via their uncleaved terminal domains to assemble extracellularly into a flexible, sheet-like, multi-layered network. Secreted protomers form triple helical assemblies with N-terminal 7S domains that oligomerise into cross-linked tetramers covalently stabilised by disulphide bonds and lysine-hydroxylysine crosslinks. Additional interactions between the C-terminal NC1 domains result in a dense polymeric collagen scaffold promoting the significant stability, insolubility and small pore size of basement membranes. Sulphilimine chemical bonds further stabilise the collagen scaffold by covalently linking methionine and hydroxylysine residues at the interface of adjoining triple helical protomers[644].

3.1.2.2 Integrin-basement membrane crosstalk in EMT

Integrins are involved in almost all elements of EMT signalling and the interaction between specific integrins and certain BM domains is constantly changing during EMT[578,645]. MMP mediated degradation of the BM leads to a dynamic switch in integrin-interactions since the BM network is broken, causing a loss of receptor binding sites. Moreover, mesenchymal cells deposit ECM, increasing the abundance of collagen type I, type II, and fibronectin, leading to the expression and re-localisation of collagen and fibronectin binding integrins such as α5β1 and αVβ1. The re-localisation and loss of integrin receptor binding sites causes “cryptic” sites in the BM to be exposed[18].

Over the course of EMT, the loss of epithelial junction causes actin stress fibre formation which results in integrin-clustering at the leading edge of the cell. EMT reorganises cadherin, adheren and tight junctions and these all contain transmembrane proteins linked to the actin cytoskeleton (e.g. Zonula occludens-1 (ZO-1))[646–648]. Integrins directly contribute to EMT *via* integrin-linked kinase (ILK). This initiates remodelling of the cytoskeleton and activates nuclear factor kappa-light-chain-enhancer of activated B cells (NF-κB). Activated NF-κB translocates to the nucleus and activates key EMT transcription factors (EMT-TFs)[18]. Integrins can also signal through the p38 MAPK pathway and PI-3-K[555,649]. Moreover, it has been shown that β1-integrin signalling is required for TGF-β-activation through the MAPK pathway and

epithelial plasticity[650], and that the β1-integrin binding partner disabled-2 (Dab2), is necessary for TGF-β1-induced EMT[651].

Crosstalk between E-cadherin, TGF-β-receptors and integrins is also important in EMT signalling. Endocytosis of E-cadherin causes Ras-related protein 1 (Rap1) activation, which is a GTPase involved in focal adhesion formation and the cytoplasmic activation of integrins[652]. Moreover, ILK causes a down-regulation in E-cadherin expression[653] and adherens junctions are disrupted when RhoA and Ras-related C3 botulinum toxin substrate 1 (Rac1) are activated by β1-integrin[654,655]. It has been further proposed that clustering of α3-integrin with the TGF-β-receptor and E-cadherin is required for the phosphorylation of β-catenin at tyrosine residue 654 and complex formation with p-Smad2. The nuclear translocation of this complex initiates EMT of alveolar epithelial cells to myofibroblasts in a lung fibrosis model[656–658]. Finally, Horejs *et al.* have shown that a cryptic laminin fragment can bind to α3-integrin, triggering changes in MMP-2, MMP-9, E-cadherin and EMT-TF expression[536].

3.1.3 Matrix metalloproteinases

Matrix metalloproteinases (MMPs) are zinc dependent cellular enzymes belonging to the metzincin group of proteases which are responsible for the cleavage of almost all ECM proteins. To date, 25 vertabrate MMPs and 22 human homologues have been described[659–661]. MMPS play an important role in matrix remodelling in embryonic development, angiogenesis, and wound healing. They are also essential in pathological processes such as inflammation and cancer, with fibrosis and cancer showing elevated expression levels of MMPs[662–664]. MMPs recognise and cleave specific sequences of ECM proteins releasing protein fragments[18,665,666] and are involved in regulating extracellular tissue signalling networks[610]. Indeed MMP-1, MMP-2, MMP-3, MMP-7, MMP-9, MMP-10, MMP-12, and MT1-MMP (MMP-14) have been shown to process either purified or recombinant collagen type IV and/or laminin.

MMPs are heavily regulated both intracellularly and extracellularly to ensure that ECM proteins are processed at different cell stages[667]. MMPs can be activated by several cytokines including interleukin-1 (IL-1), tumour necrosis factor-α (TNF-α) or TGF-β, nitric oxide or micro-

RNA[610], which activate intracellular signalling pathways such as extracellular signal-regulated kinase (ERK) 1/2 MAPK. MMP activity is then controlled through transcription, proenzyme activation, non-specific proteinase inhibitors (e.g. α2-macroglobulin), and tissue inhibitors of metalloproteinases (TIMPs)[610]. TIMPs are endogenous protein regulators of MMPs, and of families such as the disintegrin metalloproteinases (ADAM and ADAMTS)[668]. They are therefore critical in influencing the ECM, cell adhesion molecules and many cytokines, chemokines and growth factors.

MMPs can be categorised as either secreted inactive proenzymes or membrane bound membrane type MMPs (MT-MMPs)[669]. Secreted MMPs are inactive until their pro-domain is cleaved; the pro-domain contains a "cysteine switch" sequence motif in which the free cysteine residue interacts with the catalytic zinc ion preventing interaction with the substrate[670]. The MMP is activated when water is able to interact with the zinc ion at the MMP enzyme's active site due to a change in conformation, pulling out the cysteine residue. This activation occurs extracellulary either by protease-mediated activation (by another protease or by auto-activation), oxidant-mediated activation or matrix-mediated activation[670], whilst TIMPs inhibit most of the secreted MMPs[671]. MMPs secreted as latent pro-enzymes include MMP-1, MMP-8, peptidase M9, MMP-3, MMP-7, MMP-2 and MMP-9[672]. MT-MMPs are anchored to the membrane via a transmembrane domain or a glycosylphosphatidylinocitol (GPI)-anchor and play a role in modifying the immediate cellular environment since they act at the cell surface[673,674]. MT1-MMP is the most studied MT-MMP and has been shown to promote cell migration since it has been implicated in BM breakdown and in cell invasion through collagen and laminin degradation[675].

3.1.3.1 MMP involvement in EMT

MMPs are heavily involved in EMT[676–690]. For example, MMP-2, MMP-9, MT1-MMP and MMP-3 have been correlated to EMT processes[92,558,680,685,691–699]. During EMT, there is increased expression of MMP-2 and MMP-9, thus enhancing ECM protein degradation and enabling invasion[685]. MMPs additionally target certain transmembrane proteins, for example MMP-3 can activate EMT in tumour cells by shedding of E-cadherin, causing nuclear localisation of β-catenin[700,701]; and MMP-2 has been shown to activate tubular EMT independently of TGF-β1[702]. Furthermore, MMP-3 can induce EMT through increased expression and activity of

rac1B, which results in increased levels of cellular reactive oxygen species, leading to increased snail1 expression[694]. Snail, a key EMT transcription factor, has been shown to mobilise MT-MMPs[696,703]. MMP-2 and MMP-3 are required for mammary gland branching morphogenesis, a developmental EMT process recapitulated in the adult, which facilitates the invasion of mammary epithelial cells into the stromal mammary fat pad[688]. Moreover, increased expression of MMPs in epiblast cells during gastrulation has been measured in several developmental EMT models[684,704].

EMT-related processes in cancer metastasis and tissue fibrosis can be correlated with elevated MMP levels and thus specific MMP levels could potentially be used as prognostic factors[705]. MMPs have been viewed as promising targets for inhibiting epithelial cell migration and transition. However, clinical trials of MMP suppression in tumour models using synthetic MMP inhibitors have been unsuccessful to date due to their redundancy, tissue specificity and dosage dependence, and because the role of specific MMPs has not yet been fully understood[705,706].

3.1.3.1.1 MT1-MMP

MT1-MMP/ MMP-14 is one of the critical proteinases involved in cell migration and it is found at invadopodia sites. Invadopodia are dynamic actin and cortactin rich protrusions of the plasma membrane which mediate ECM degradation through the local deposition of proteases. Invadopodia are found on cancer cells and are similar to podosomes of normal cells. MT1-MMP accumulates at the edge of invadopodia and has been described as the main invadopodial ECM protease[113,707–709]. During EMT, MT1-MMP becomes concentrated at invadopodia via intracellular trafficking[79]. MT1-MMP is produced as a latent ~72 kDa transmembrane zymogen and is converted into a ~60kDa catalytically active protease via furin-like proprotein convertases during its journey to the cell membrane[710]. There is a constant flow of active MT1-MMP to the cell membrane via endocytosis and exocytosis. Rather than being trafficked through to endoplasmic reticulum, to the Golgi apparatus and then to the cell membrane through the biosynthetic pathway, MT1-MMP is internalised and then redirected to invadopodia in late endosomes along microtubules[711]. Following attachment of MT1-MMP-positive endosomes to the cell membrane for several minutes, the

endosomes detach rather than collapsing into the cell membrane[712]. Docking cycles enable MT1-MMP to adapt to changing ECM microenvironments[711].

MT1-MMP enhances cell migration by degrading the ECM, releasing cell surface molecules to give migratory signals and by activating extracellular signal-regulated protein kinase (ERK) and other secreted MMPs. MT1-MMP degrades the ECM both directly and indirectly. MT1-MMP directly degrades a number of ECM components including collagen type I, II and III, laminin-1 and -5, fibronectin, vitronectin, fibrin and aggrecan[713,714]. MT1-MMP indirectly degrades the ECM by activating proMMP-2[715] and proMMP-13[716] at the cell surface. MT1-MMP knockouts are the only lethal MMP-mutants in which mice develop abnormalities and die at three weeks[717–719]. MT1-MMP-/-/MMP-2-/- double mutant mice cannot survive early postnatal life, and MMP9 cannot compensate for MT1-MMP-/-/MMP-2-/- mutations[720].

3.1.3.1.2 MMP-2 and MMP-9

MMP-2 and MMP-9 can be distinguished from the other secreted MMPs by a collagen-binding domain within their catalytic domain. This collagen-binding domain consists of three fibronectin type II repeats and is involved in the binding of collagenous substrates, elastin, fatty acids and thrombospondins[721]. MMP-2 and MMP-9 are secreted as inactive zymogens (proMMP-2: 72 kDa, proMMP-9: 92 kDa) and are activated by cleavage of a prodomain (MMP-2: 65 kDa; MMP-9: 82 kDa) through a number of mechanisms. The major activation route of proMMP-2 on the cell surface is through the formation of a molecular complex containing proMMP-2 (*via* its PEX domain), MT1-MMP (*via* its catalytic domain) and TIMP-2. This causes clustering of proMMP-2 in the vicinity of a TIMP-free, active MT1-MMP which initiates the activation of proMMP-2. MMP-2 can also be activated by MMP-1, MMP-7, thrombin and activated protein C. MMP-2 expression can be increased by the ERK-MAPK pathway through FAK and by the PI3K/Akt pathways through NF-κB[722–724]. MMP-9 can be activated by plasmin, trypsin-2, MMP-2, MMP-13 (activated by MMP-2) and MMP-3 (activated by plasmin)[659]. NF-κB is involved in MMP9 production[725,726] and activation of AP-1 and NF-κB transcription factors is insufficient but absolutely required for upregulation of MMP9[726].

Once activated, the gelatinases are can degrade various components of the ECM, in particular they can degrade type IV collagen. When epithelial cells undergo EMT they start expressing MMP-2, and MMP-2 has been further linked to EMT due to its involvement in BM

degradation, enabling cell migration[679]. MMP-9 is also involved in BM degradation and can induce the EMT by disrupting the E-cadherin/β-catenin- adhesion complex[727]. Gelatinases have garnered much attention since they are often overexpressed in malignant tumours and this expression is often associated with the aggressiveness of the tumour[728].

3.1.4 α3β1-integrin

The α3β1–integrin is one of the main BM receptors and is involved in maintaining cell-cell junctions, cytoskeleton assembly, cell migration (due to its interactions with tetraspanin proteins), and MMP regulation via the CD147/EMMPRIN protein[657,729–734]. α3β1-integrin is highly expressed in epithelial cells and mediates cell–matrix interactions with its major ligand laminin-332 as well as another ECM ligands[735]. α3β1 is also found along lateral cell borders in association with E-cadherin in adherens junctions[736,737], and this colocalisation is believed to contribute to the assembly and maintenance of cell–cell contacts and normal barrier function[729,738,739]. Interestingly, it is possible to distinguish the α3β1-integrin receptors associated with the cadherin–catenin complex (cell-matrix adhesion) and those involved in binding laminin (cell-cell adhesion)[737]. Mutations in the gene encoding the α3 subunit (*ITGA3*) have been linked to a congenital nephrotic syndrome, interstitial lung disease and a mild form of epidermolysis bullosa[740–742]. α3 knockout mice have a perinatal-lethal phenotype[743] and defects can be seen in the structural organisation of the BM[744]. α3 knockout also produces kidney tubule defects, reduced branching morphogenesis in the lungs, and mild skin blistering[743]. Indeed, α3 knockout mice have demonstrated crucial roles for α3-integrin in skin tumour formation[745], regulation of contractility in mammary myoepithelial cells[746], directional migration and wound re-epithelialisation in the skin[747].

Laminin-332 is a key ligand for α3β1-mediated adhesion[748,749], however, a large number of other extracellular ligands have also been reported for α3β1, including fibronectin, Engelbreth-Holm-Swarm (EHS)-laminin/laminin-111, and collagens[750–753]. The α3A subunit (one of 2 isoforms of the α 3 subunit) has been detected in FAs in several cell types cultured on fibronectin, kalinin/laminin-332, EHS-laminin/laminin-111, type IV collagen, or vitronectin. In contrast, α5 and αV integrins are only seen in FAs when cells are grown on their known ligands. Transfection of α3A into K562 cells (which do not express endogenous α3A) does not

cause adhesion to EHS laminin/laminin-111, collagens, entactin/nidogen, or fibronectin[754–756]; therefore, α3Aβ1 is not sufficient for initial cell adhesion to these matrix proteins. Initial cell adhesion to these ligands most likely requires other integrins and α3β1-integrin is likely to be a secondary receptor with post-cell-adhesion functions. Precedent for post-adhesion integrin function has also been shown for αVβ3 in HUVECs, where it is important for cell adhesion maintenance, but not for initial cell attachment[757].

Laminin-111 and laminin-332 are both ligands for the α6β1-integrin, while α3β1-integrin only shows affinity for laminin-332; these two laminin isoforms can therefore distinguish the roles of α3β1-integrin α6β1-integrin[758]. Similar adhesion of normal skin human fibroblasts has been seen on laminin-111 and -332 however the two laminin isoforms promote different cell shapes; laminin-111 promotes filopodia-like structures, whereas laminin-332 promotes lamellipodia formation. The actin cytoskeleton is similarly ordered however FA proteins such as vinculin, talin and paxillin show different arrangements. They form thick and short aggregates localised at the end of "actin stress fibres" on laminin-111, whereas they formed dots or streaks clustered on a long portion of actin microfilaments on laminin-332. Cross-talk between α6β1-integrin and α3β1-integrin has also been shown; when α3β1-integrin is ligated it is integrated into focal adhesions and can regulate the clustering of α6β1 integrins and can regulate FA proteins[758].

α3β1–integrin has been connected to E-cadherin and cytoskeletal organisation in a number of cell types[729,733]. Association of α-actinin with the cadherin–catenin complex is reduced in cells deficient in α3β1-integrin[729], and it has been suggested that the CD151-α3β1 complex controls the stability of E-cadherin mediated cell–cell adhesion by regulating the expression of the membrane protein tyrosine phosphatase PTPμ and its association with the E-cadherin-catenin complex[737]. Indeed, it has been shown *in vitro* that α3β1-integrin–deficient collecting duct epithelial cells assemble actin stress fibres instead of a subcortical actin cytoskeleton, and show reduced association between α-actinin and the cadherin–catenin complex[729]. A recent study has shown that α3β1–integrin can coordinate cross-talk between the Smad and β-catenin signalling pathways and therefore regulates MMPs and response to TGF-β1 activation[657,734]. After TGF-β1 stimulation, wild-type epithelial cells can internalise complexes of E-cadherin and TGF-β1 receptors, generate phospho-Smad2 (p-Smad2)–pY654–β-catenin

complexes, and up-regulate mesenchymal target genes. This is not possible in cells expressing an H245A mutant preventing α3-integrin from engaging with E-cadherin. Although Smad2 phosphorylation remains unchanged, p-Smad2–pY654–β-catenin complexes do not form in the absence of α3 or when α3β1 is mainly engaged on laminin-332 or E-cadherin in adherens junctions, leading to attenuated EMT. This suggests that α3β1 coordinates cross talk between β-catenin and Smad signalling pathways as a function of extracellular contact cues, regulating responses to TGF-β1 activation[657]. Interestingly, mouse mammary gland epithelial (NMuMG) cells contain nuclear Y654-phosphorylated β-catenin however when they are treated with TGFβ1 nuclear Y654-phosphorylated β-catenin cannot be identified[535].

The ECM metalloproteinase inducer (CD147/EMMPRIN) is a transmembrane protein which shows similar characteristics to the immunoglobulin superfamily[759,760]. It has been argued that CD147/EMMPRIN association with integrins regulates several biological processes, such as BM formation, cell adhesion, signalling and MMP production, by regulating integrin/laminin binding[761]. It has been shown that CD147/EMMPRIN can stimulate MMP secretion in fibroblasts upon interaction with α3β1-integrin, however it does not localise with FAs[732,759,762]. Moreover, CD147/EMMPRIN co-localises with α3β1-integrins in human 7721 hepatoma cells resulting in an increase in FAK, p-FAK, paxillin and p-paxillin expression, and CD147/EMMPRIN has been linked to PI3K via intracellular Ca^{2+} regulation[763]. Finally, blocking of CD147/EMMPRIN has been shown to reverse the inhibitory effects of a laminin β1-fragment which binds to α3β1-integrin and decreases MMP-2, MMP-9, and E-cadherin expression in mouse embryonic stem cells[536]. This suggest that there is an interaction between α3β1-integrin and CD147/EMMPRIN which regulates these processes.

3.1.5 TGF-β1 induced epithelial-to-mesenchymal transition

Transforming growth factor beta (TGF-β) is a family of multifunctional cytokines which includes 3 isoforms (TGF-β1, TGF-β2, and TGF-β3). Each isoform is composed of a signal peptide which directs the isoform to the endoplasmic reticulum, a large N-terminal domain known as the latency-associated peptide (LAP) and a short C-terminal domain[764]. The isoforms are 25 kDa homodimers and each subunit consists of around 112 amino acids. The amino acid sequence identity between the mature human TGF-β1 and TGF-β2, TGF-β1 and

TGF-β3, or TGF-β2 and TGF-β3 is 71%, 76%, or 80%, respectively. In culture, all three isoforms show similar function and behave as inhibitors of normal and transformed epithelial cell growth[765,766]. TGF-β ligands are secreted by many cell types, including macrophages, as inactive precursors which are either directly activated or embedded in the ECM to be activated at a later point[767]. Inactive TGF-β ligands are bound to latency-associated peptides and can be activated by the lytic action of MMPs or through conformational changes induced by integrins[768,769]. When activated, TGF-β can bind to TGF-β-receptors (TGF-βRs). The TGF-β receptor complex consists of a tetrameric structure with two different homodimers, TGF-βRI and TGF-βRII: TGF-β binds to active TGF-βRII, recruiting TGF-βRI to form a complex[770]. Both of the receptors are serine/threonine kinases, and following TGF-β binding, TGF-βRII phosphorylates the cytoplasmic domain of TGF-βRI, which then phosphorylates intracellular proteins such as Smads[771–774].

TGF-β is involved in regulating cell growth, differentiation, and development[775–779]. TGF-β signalling generally involves ligand-induced oligomerisation of serine/threonine receptor kinases and phosphorylation of Smad2 and Smad3 cytoplasmic signalling molecules. The activated Smad molecules then translocate to the nucleus and complex with transcription factors, modulating transcription. TGF-β signalling can also affect Smad-independent pathways such as the ERK 1/2 MAPK pathway, FAK/ Src pathway, phosphatidylinositol-3-kinase (PI3K)/ AKT pathway, Wnt/ β-catenin pathway, NF-κB pathway and pathways involving Rho-like GTPases[780–784]. TGF-β1, TGF-β2, and TGF-β3 are all able to induce EMT, however TGF-β1 is the most commonly used isoform in the context of EMT research[649,732,772,785], and is the most commonly found isoform in human tissues[786].

3.1.5.1 The canonical Smad pathway

In the canonical TGF-β-initiated Smad pathway, TGF-β binds to the TGF-βRII which phosphorylates TGF-βR1 which then phosphorylates Smad2 and Smad3. pSmad2 and pSmad3 then associate with Smad4, forming a trimeric Smad complex which translocates to the nucleus, increasing the expression of EMT-related transcription factors such as snai1 (snail), snai2 (slug) and a downregulation in the expression of epithelial cadherin (E-cadherin). E-cadherin is a calcium-dependent transmembrane cell-cell adhesion glycoprotein involved in epithelial cell behaviours, tissue formation and cancer suppression[787]. E-cadherin's

extracellular domain is involved in cell-cell adhesion[788] and its intracellular domain forms a high affinity interaction with β-catenin and thus α-catenin, F-actin and vinculin[789,790].

The Smad pathway is inhibited by Smad6 and Smad7 (**Figure 3.3**)[649,771,773]. Smad7 is a nuclear protein which can translocate to the cytoplasm and complex with E3 ubiquitin ligase smurf2. Here, it binds to the TGF-β1R complex, inhibiting the Smad pathway by blocking phosphorylation of Smad2 and Smad3[791–793]. Interestingly, Smad7 has also been shown to exert its inhibitory effect on TGF-β1 signalling in the nucleus[794].

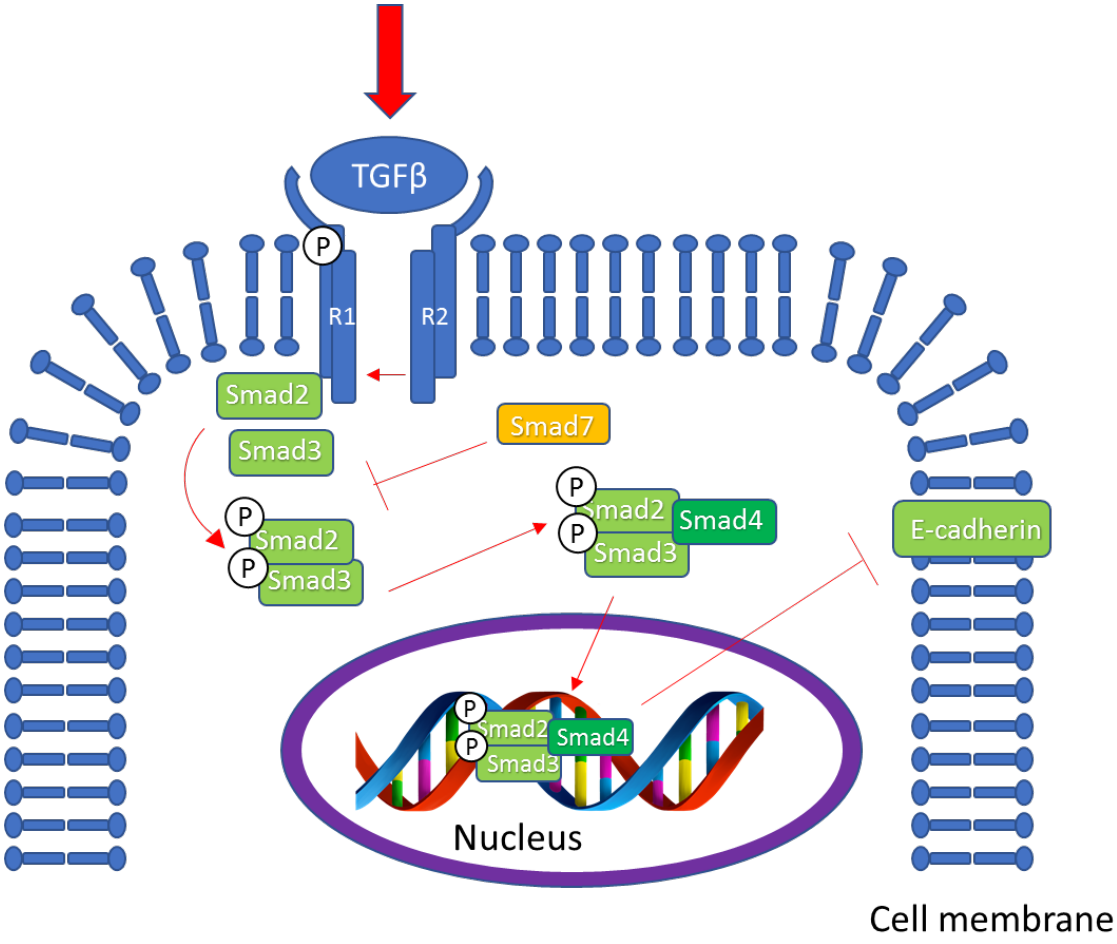


Figure 3.3: Canonical TGF-β Smad signalling. TGF-β binds to the transmembrane TGF-β receptor (TGF-βR) at the cell surface. The TGF-β receptor complex consists of two different serine/threonine kinase homodimers, TGF-βRI and TGF-βRII. TGF-β binds to TGF-βRII, which recruits TGF-βRI to form a complex. TGF-βRII then phosphorylates the cytoplasmic domain of TGF-βRI, which phosphorylates Smad2 and Smad3. Phosphorylated Smad2 and Smad3 (pSmad2 and pSmad3, respectively) establish a trimeric Smad complex with Smad4 which translocates to the nucleus. Here, it regulates the transcription of target genes such as snail1 and snail2, which decrease E-cadherin expression, through physical interaction and functional cooperation with DNA binding transcription factors (X) and cAMP-regulated-enhancer-binding protein (CBP) or p300 co-activators. This pathway can be inhibited by competition from Smad6 or Smad7. Smad7 inhibits the TGF-β/Smad signalling pathway by competing with Smad2 and Smad3 for TGF-βRI binding and has also been shown to exert its inhibitory effect on TGF-β1 signalling in the nucleus.

3.1.5.2 Erk 1/2 MAPK pathway

Mitogen-activated protein kinases (MAPKs) are a family of serine/threonine protein kinases involved in various cellular activities such as proliferation, migration, differentiation, stress response, apoptosis, and survival[795]. Some examples of MAPKs include the extracellular

signal-regulated kinase 1 and 2 (Erk1/2), the c-Jun N-terminal kinases 1-3 (JNK1-3)/ stress activated protein kinases (SAPK1A, 1B, 1C), the p38 isoforms (p38α, β, γ, and δ), and Erk5[796,797]. The Erk1/2 MAPK pathway can be activated by interaction between integrins and growth factors or by TGF-β activation, while JNK and p38 kinases respond to stress stimuli, like osmotic shock[796,797].

When the ERK1/2 MAPK pathway is activated by TGF-β, the Src homology 2 domain-containing-transforming A (SHCA) associates with TGF-β receptor I, and is phosphorylated at tyrosine and serine[798]. This reveals a docking site for growth factor receptor bound protein 2 (GRB2) and Son of Sevenless (SOS) which initiates the pathway. When ERK 1/2 is inhibited, TGF-β-induced EMT is repressed *in vitro*[649,797,799–801]. ERK activation is important in EMT[802,803], since it is required for disassembly of cell adherens junctions and induction of cell motility by TGF-β. Indeed ERK's target genes are involved in cell-matrix interaction, cell motility, and endocytosis[802]. Moreover, ERK can also phosphorylate receptor-activated Smads, including Smad1, Smad2 and Smad3, to regulate their activities[804–807]. For example, phosphorylation of Smads by ERK inhibits Smad activity, which has been invoked to explain how oncogenic Ras overrides TGF-β-mediated growth arrest in cancer cells[805]. Moreover, ERK substrates, such as AP-1 family members, can interact and function in conjunction with Smads to regulate gene expression[803,808,809].

In the p38 and JNK MAPK pathways, ubiquitin ligase TNF receptor associated 6 (TRAF6) associates with the TGF-β receptor complex, leading to TGF- β -activated kinase 1 (TAK1) kinase activation, and then p38 and JNK MAPK pathway activation[649]. The receptor-associated factor 6 (RAF6)-TAK1-JNK/p38 pathway is involved in in TGF-β-induced apoptosis and also plays a role in TGF-β-induced EMT. Inhibition of p38 activity impairs TGF-β-mediated changes in cell shape and reorganisation of the actin cytoskeleton[810,811], and TRAF6 knock-down inhibits TGF-β-mediated EMT[812]. Moreover, global inhibition of β1-integrin matrix binding by blocking antibodies has been shown to abrogate active TGF-β1-mediated p38 MAPK activation and EMT in mammary cells[650]. Thus, activation of the TRAF6-TAK1-p38 pathway is required for TGF-β-induced EMT.

3.1.5.3 Focal adhesion kinase (FAK)/Src pathway

Focal adhesion kinase (FAK) has been shown to be key mediator of TGF-β signalling in fibroblasts[813]. FAK is an intracellular protein-tyrosine kinase which acts as a central mediator of signalling in integrins and other cell surface receptors. It has a role in normal cell migration, since it is important for FA turnover, but also contributes to pathogenesis of cancer and other diseases[814]. For example, FAK is expressed at higher levels in invasive tumours compared to benign pre-neopastic tumours[784,815], and FAK activation has been linked to tissue fibrosis, with FAK inhibition decreasing lung fibrosis[26,816].

FAK acts as a signalling-protein scaffold which enables the assembly and maturation of focal contacts[817], and is also involved in the disassembly of FAs through the activation of intracellular proteases such as calpain[818] and extracellular MMPs[819–821]. Maximal FAK activation occurs when it is associated with the Src nonreceptor tyrosine kinase. Src activation is an early event following integrin activation and clustering and this clustering also causes FAK autophosphorylation at tyrosine residue 397. This creates a binding site for Src which mediates phosphorylation of FAK at tyrosine residue 576, 577 and other residues such as tyrosine 581[64,822,823]. FAK can then work at maximal catalytic activity which results in the activation of several signalling pathways such as the ERK2/MAPK cascade and small GTPases such as Rac and Rho[824].

3.1.5.4 PI3K/AKT pathway

The phosphoinositide 3-kinase/protein kinase B (PI3K/AKT) signalling pathway is involved in proliferation, apoptosis and migration, and is strongly linked to pro-survival[825–827]. During TGF-β-induced EMT, the PI3K/AKT pathway activates the mTOR and S6kinase1 pathway, which collaborates and is essential for the activation of snail1. When the PI3K/AKT pathway is blocked in mammary gland epithelial cells, phosphorylation of Smad2 is inhibited in Smad-dependent TGF-β-induced EMT. This suggests that there is an interaction between the PI3K/Akt and Smad signalling pathways[784,828,829].

PI3K/Akt has also been linked to the FAK signalling pathway. TGF-β stimulation recruits the p85 subunit of PI3K to FAK, and this acts as a scaffold to organise this signalling complex. PI3K acts as a branch point for the activation of p21 activated kinase (PAK2)-Abl (Abelson kinase)

and Akt-mechanistic target of rapamycin-1 (mTOR1) profibrotic pathways[830], without the need for Src and tyrosine kinase activity[831]. RhoA has also been shown to be involved in the PI3K/Akt pathway through TGF-β. Mouse mammary epithelial cells transfected with dominant-negative RhoA mutant (N19RhoA) show a significant reduction in the levels of Akt phosphorylation[832].

3.1.5.5 Wnt/β-catenin pathway

Three Wnt pathways have been characterised: the canonical Wnt pathway, the noncanonical planar cell polarity pathway, and the noncanonical Wnt/calcium pathway[833]. β-catenin is a sub-unit of the cadherin protein complex which acts as a key regulator of the canonical Wnt pathway, as well as regulating cell-cell adhesion. β-catenin is continuously degraded by the axin complex in the cytoplasm until Wnt binds to its receptor Frizzled (Fz) and co-receptor lipoprotein receptor-related protein 5/6 (LRP5/6), causing it to translocate to the nucleus. During TGF-β-induced EMT, β-catenin is phosphorylated and forms a complex with pSmad2, E-cadherin and α3β1-integrin at the cell membrane. Following this, β-catenin and pSmad2 are internalised and transported to the nucleus[657,834]. In the nucleus, β-catenin binds to lymphocyte enhancer factor/T-cell transcription factor (Lef/TCF) and stimulates the transcription of Wnt target genes, such as MMP-7, fibronectin, snail and twist.

3.1.5.6 The NF-κB pathway

The NF-κB family is composed of 5 subunits, RelA/p65, c-Rel, RelB, p50/p105, and p52/p100, which can bind to DNA as hetero- or homodimers, regulating gene expression and a number of biological processes[835–837]. It has been shown to be involved in immune and inflammatory responses as well as cell proliferation, migration, differentiation and apoptosis[838,839]. Nf-κB is also involved in cell and tissue morphogenesis, including proliferation and branching of the mammary gland[840], and is heavily involved in cancer initiation and progression[841].

NF-κB is most commonly found as a heterodimer of p50 and p65/RelA transcriptional activator domain. In the canonical pathway, NF-κB dimers are inhibited by IκB proteins which prevent DNA binding and cause cytoplasmic localisation of NF-κB. Pro-inflammatory cytokines such as TNF-α or IL-1 can phosphorylate and degrade IκB, releasing and enabling nuclear translocation of NF-κB and thus the induction of NF-κB responsive genes[842–844]. In the nucleus,

active NF-κB/Rel complexes induce target expression either alone or in combination with other transcription factors including activator protein 1 (AP-1), Ets, and signal transducer and activator of transcription (Stat) proteins.

NF-κB has been shown to be essential for both the induction and maintenance of EMT and has been shown to promote EMT even in the absence of TGF-β in Ras-transformed mammary epithelial cells[844]. Indeed, several NF-κB binding sites have been identified along the promoters of *snail, slug, sip1* and *twist1* genes[845], and overexpression of the NF-κB p65 in non-transformed mammary epithelial cells results in the loss of epithelial markers, including E-cadherin, a gain of mesenchymal markers such as vimentin and an elevated expression of the transcriptional repressors, ZEB-1/ZFHX1A[846] and ZEB-2/ZFHX1B/Smad-interacting protein (SIP1)[847]. NF-κB p65, p65/RelA is required for Smad7 activation, thus linking the NF-κB and TGF-β-Smad-dependent pathways [843,848]. Moreover, TGF-β has been shown to activate canonical IKK-NF-κB signalling through activation of TGF-β–activated kinase-1 (TAK1)[848] (**Figure 3.4**).

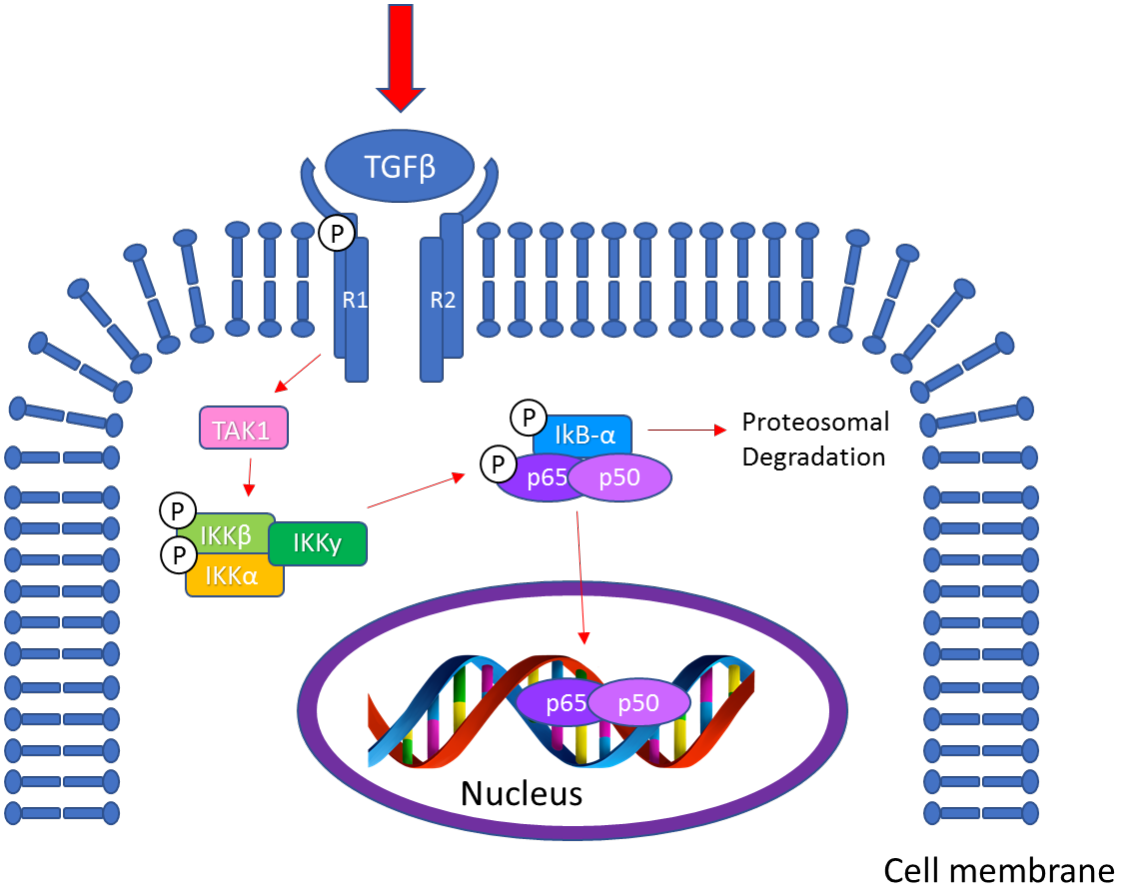


Figure 3.4: TGF-β nuclear factor kappa-light-chain-enhancer of activated B cells (NF-κB) signalling . NF-κB is most commonly found as a heterodimer of p50 and p65/RelA transcriptional activator domain. Inactive NF-κB is present in the cytosol bound to the inhibitory protein IκBα. TGF-β receptor binding causes the inhibitor of IκB kinase (IKK) to be activated either through autophosphorylation or through phosphorylation by a series of mitogen-activated kinases (MAP3K) including TGF-β–activated kinase-1 (TAK1). IKK phosphorylates IκBα which results in proteasome-mediated degradation of IκBα. The active complex of NF-κB is then liberated and can translocate to the nucleus and act as a transcription factor.

3.1.5.7 Rho-like GTPases

The Rho-like GTPases, including RhoA, Rac and Cdc42, play important roles in controlling dynamic cytoskeletal organisation, cell motility, and gene expression through a variety of effectors[849]. TGF-β activates RhoA-dependent signalling pathways via either Smad-dependent or independent routes to induce stress fibre formation and mesenchymal characteristics in epithelial cells[850,851]. TGF-β also induces tight junction dissolution during EMT by recruiting Cdc42 to the receptor complex[852] and by triggering degradation of RhoA at cell protrusions[853].

3.1.6 The laminin β1-fragment

Proteolysis of the BM by MMPs can generate protein fragments with various bioactivities. These protein fragments are hidden within the intact BM and are activated only on release from the BM by certain MMPs or force-induced unfolding[18]. Therefore they are also known as "cryptic" BM fragments or matricryptic sites[576,854–857]. These fragments reveal an additional layer of BM-cell crosstalk involving a shift in integrin-mediated interactions.

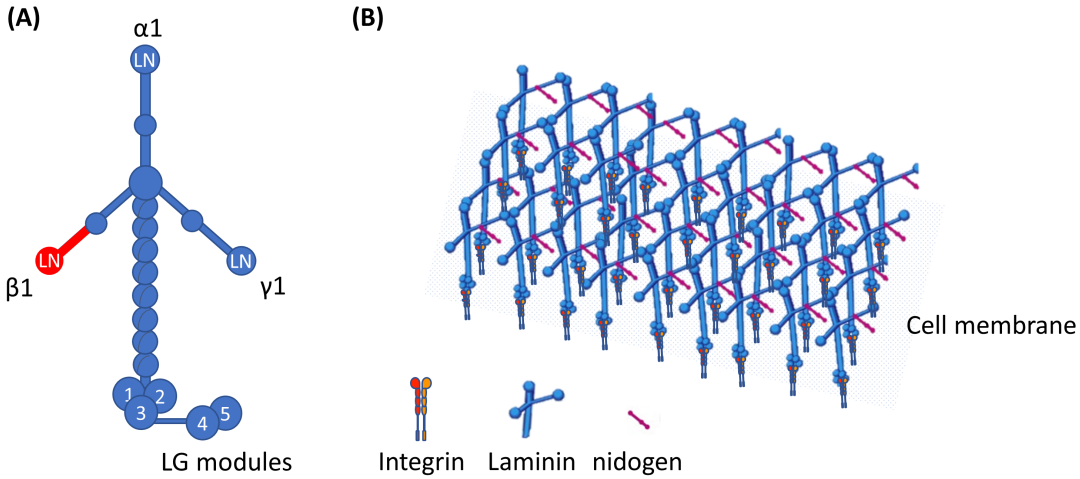


Figure 3.5: The laminin β1-fragment, A) modified from Horejs, C. M. *et al.*, *Proc. Natl. Acad. Sci.* **111**, 5908–5913 (2014), with permission from the National Academy of Sciences, copyright 2014, and B) modified from C. M. Horejs *et al.*, *Eur. J. Cell Biol.* **95**, 427–440 (2016)[18], with permission from Elsevier, copyright 2016. A) A schematic presentation of the cross-shaped laminin-111 heterotrimer. The laminin-111 heterotrimer consists of α1, β1, and γ1 chains. The N-terminal regions of the α1, β1, and γ1 chains form the short arms of the laminin molecule, and their C-terminal regions associate to form a long α-helical coiled coil. The α1 chain continues for another ~1,000 residues after the coiled coil, and its C terminal ends in a G domain consisting of 5 LG sub-domains. The laminin β1-fragment, released by MMP-2, is indicated in red. B) The 5 LG sub-domains are the major site of cell-laminin adhesion whereas the N-termini of the α-, β-, and γ- chains allow laminin polymerisation and therefore provide a key role in maintaining basement membrane integrity.

A biologically-active laminin β1-fragment from the N-terminal region of the β1-chain (β1-LN-LE1-4) can be generated by MMP-2 processing within the BM (**Figure 3.5**)[536]. This laminin β1-fragment can be recombinantly produced as a stable 60 kDa protein which suggests that it could either be released as a soluble factor or remain within the ECM[858]. Horejs *et al.* have demonstrated that the laminin β1-fragment modulates EMT via α3β1–integrin/ECM

metalloproteinase inducer (EMMPRIN) complex in mouse and human embryonic stem cells (ESCs)[536]. When cells are exposed to the laminin β1-fragment with EMT inducing TGF- β1, the laminin β1-fragment causes a down-regulation of MMP-2 compared to TGF-β1 addition alone. During EMT, MMPs are upregulated to allow the cells to escape the dense surrounding BM and to remodel the ECM. Since laminin β1-fragment is a product of MMP-2, and its addition to cells down-regulates MMP-2, it may provide a negative-feedback mechanism on MMP-2 regulation. This could be potentially relevant in tissue homeostasis and might offer a strategy to regulate excess MMP-2 production in pathological EMT. Horejs *et al.* also found that TIMP1 and TIMP2, known inhibitors of MMP, and snai1 and snai1, the transcriptional inhibitors of E-cadherin, were significantly down-regulated upon laminin β1-fragment addition *in vitro*. Blocking of CD147/EMMPRIN reversed the effects of the laminin β1-fragment on E-cadherin, MMP-2 and MMP-9 expression whereas it had no effect on N-cadherin, snai1 and snai2 expression. The laminin β1-fragment can therefore trigger cell responses and is not cleaved for the sole purpose of membrane remodelling. Interestingly, no changes in EMT regulation are seen when cells are exposed to full-length laminin-111 or other full-length laminin isoforms[535,536].

The effects of the laminin β1-fragment have recently been assessed on NMuMG cells. NMuMG cells have extensively been used as a model to study TGF-β1-induced EMT changes in epithelial cells *in vitro*[859], and mammary gland branching is a developmental EMT process during puberty and therefore a valid model system relevant in both development and disease. Immunoprecipitation has demonstrated the specific interaction of the laminin β1-fragment with α3-integrin, but not with α6-integrin, in NMuMG cells. To elucidate the pathways affected by binding of the laminin β1-fragment to α3-integrin, NMuMG cells were cultured in the absence or presence of soluble laminin β1-fragment with TGF-β1. NMuMG cells treated with TGF-β1 alone show an expected upregulation of p-Smad2, p-Smad3, snail, and MT1-MMP protein levels[649]. Treatment with the laminin β1-fragment decreases the upregulation of p-Smad3, snail and MT1-MMP but does not show an effect on p-Smad2. Specific blocking of α3-integrin using a blocking antibody in the presence of the laminin β1-fragment rescues the upregulation of p-Smad3, snail and MT1-MMP. This suggests that the laminin β1-fragment affects TGF-β1 signalling by interfering with α3-integrin functionality. Finally, there is no significant alteration in collagen type I gene expression and collagen deposition in response

to treatment with TGF-β1. Similar results are also shown for primary mouse peritoneal mesothelial cells. Nuclear extracts were used to show that the addition of laminin β1-fragment leads to changes in total protein phosphorylation levels and nuclear localisation of both p-Smad3 and snail, but not p-Smad2. Moreover, nuclear tyrosine 654-phosphorylated β -catenin was not detected in cells treated with the laminin β1-fragment and TGF-β1, while it was detected in control cells that were not treated with TGF- β1[658].

The laminin β1-fragment has been incorporated into a biomaterial in order to prevent tissue fibrosis. Tissue fibrosis is promoted by MMP breakdown of tissue structures such as the BM, and the laminin β1-fragment could provide a successful strategy to inhibit this process since it inhibits MMPs[535]. The laminin β1-fragment has been immobilised on a flexible electrospun poly(e-caprolactone) (PCL) membrane[860] via the deposition of a polydopamine (pDA) coating[861]. This strategy enables the laminin β1-fragment to be interfaced with epithelial tissue in a localised manner, circumventing off-target effects associated with the administration of soluble compounds. The laminin β1-fragment functionalised PCL membrane was directly interfaced with epithelial cells and tissues, resulting in inhibition of MMP-2 expression and activity, and changes in EMT-related molecules and E-cadherin at the gene and protein level both *in vitro* and *in vivo*. When interfaced with peritoneal tissue, the membrane decreased matrix deposition associated with fibrosis. Moreover, it was shown to rescue the peritoneal BM in explanted peritoneal mesothelium and explanted bladder urothelium, as well as in a mouse model of TGF-β1-induced peritoneal fibrosis[535].

3.2 Chapter Aims

It has previously been shown that TGF-β1 treatment causes an increase in pSmad3 and Snail and a decrease in E-cadherin expression in NMuMG cells[535]. Moreover, TGF-β1 treatment causes nuclear translocation of snail, pSmad2 and pSmad3, confirming their activation. Laminin β1-fragment addition with TGF-β1 lowered these effects (except for pSmad2) and it was shown that these effects occurred downstream of α3β1–integrin[535]. The laminin β1-fragment has been shown to specifically interact with α3β1–integrin[535,536] and similar results are seen on TGF-β1 addition with α3-integrin blocking and TGF-β1 addition with laminin β1-

fragment[535]. This suggests that the laminin β1-fragment affects TGF-β1 signalling by affecting α3-integrin functionality. It has also been shown that MT1-MMP and MMP-2 expression is decreased when the laminin β1-fragment is added with TGF-β1 compared to TGF-β1 alone[535].

This chapter uses advanced microscopy techniques to assess how the laminin β1-fragment affects TGF-β1 signalling pathways in NMuMG cells *in vitro*, and how this might change cell phenotype. Since previous studies have shown that the laminin β1-fragment interacts with α3β1–integrin[535,536], the aim was to assess the localisation of α3β1–integrin and the laminin β1-fragment using super-resolution microscopy. Following this, high content image (HCI) analysis was used in an attempt to verify previous pSmad3, E-cadherin, and MMP (MT1-MMP and MMP-2) western blot results[535]. The level and localisation of the NF-κB p65 transcription factor was assessed by western blot and HCI, and its impact on cell migration was also measured (Western blot conducted by Patrícia Barros da Silva). The number and area of vinculin, paxillin and phosphorylated FAK FA proteins was calculated by HCI analysis following TGF-β1 +/- laminin β1-fragment addition. MT1-MMP, cortactin and BM proteins were also imaged. Finally, YAP and A-type lamin nuclear localisation and intensity were assessed to investigate whether the laminin β1-fragment altered the cell's mechanotransductive response.

3.3 Materials and Methods

3.3.1 TGF-β1 reporter cells

140, 000 HEK-Blue™ TGF-β cells were seeded in a 96 well plate (Starsted, Nümbrecht, Germany) in DMEM, 4.5 g / l glucose, 2-4 mM L-glutamine, 10% (v/v) fetal bovine serum, 50 µg / ml penicillin, 50 µg / ml streptomycin, 100 µg / ml Normocin™. Following 24 hours of incubation at 37°C with 5% CO_2, two different batches of TGF-β1 (T7039, Sigma Aldrich, St. Louis, Missouri; United States) or media alone (control) was added and the cells were incubated for another 24 hours under the same conditions. A further condition was conducted where media was added to a well containing no cells (media). 20 µl of the supernatant was then removed and added to 80 µl paranitrile phosphate on ice. This was incubated at 37°C with 5% CO_2 for 10 minutes, until a colour change was visible. 100 µl NaOH

(1 M-3 M) was added to stop the reaction and the absorbance of the solution was read at 405 nm on a Varioskan™ LUX multimode microplate reader (Thermo Scientific, Paisley, United Kingdom).

3.3.2 TGF-β1 reconsitution

400 µl ddH_2O was added to the TGF-β1 stock solution (T7039, Sigma Aldrich, St. Louis, Missouri; United States) and was vortexed to make a solution of 5 µg / ml. Working aliquots were prepared by adding 400 µl stock of the stock solution and 2 mg / ml BSA (sterile filter 0.2 microfilter (Starsted, Nümbrecht, Germany) first) to 1500 µl PBS to make up a working solution of 1 µg / ml.

3.3.3 Cell culture

Normal Murine Mammary gland epithelial cells (NMuMG; ATCC® CRL1636™) were maintained in Dulbecco's modified Eagle Medium with high glucose (DMEM; Life Technologies, Carlsbad, California, United States) with 10% (v/v) FBS (Life Technologies, Carlsbad, California, United States), 10 µg / ml insulin (Sigma Aldrich, St. Louis, Missouri; United States), and 100 µg / ml penicillin-streptomycin (Life Technologies, , Carlsbad, California, United States) at 37°C with 5% CO_2. Cells were harvested with 0.05% (v/v) 1X trypsin-EDTA (Life Technologies, Carlsbad, California, United States) and passaged at 80-90% confluence.

The epithelial-to-mesenchymal transition was initiated 24 hours after cell seeding by complementing the medium with 10 ng / ml TGF-β1 (Sigma Aldrich, St. Louis, Missouri; United States). Laminin β1-fragment was added 24 hours after cell seeding at a concentration of 1 µg / ml. Cells were incubated for 24 hours at 37°C and 5% CO_2.

3.3.4 Recombinant laminin β1-fragment production

The recombinant laminin β1-fragment was produced as described in the literature[535,536,858]. Human embryonic kidney HEK293 c18 cells (American Type Culture Collection) were used for protein production. The HEK293 cells were cultured at 37 °C with 5% CO_2 in Dulbecco's

modified Eagle's medium (DMEM)/nutrient mixture F-12 (Invitrogen) containing 10% (v/v) fetal bovine serum (FBS; Life Technologies), 2 mM glutamine (Gibco), 10 units/ml penicillin (Gibco), 100 μg/ml streptomycin (Gibco) and 250 μg/ml Geneticin (Gibco). The HEK293 cells were then transfected with the C-His p-CEP-P_0 plasmid expressing the 60kDa laminin β1-fragment using FuGENE 6 (Roche Diagnostics) and selected with 1 μg/ml puromycin (Sigma). The transfected cells were grown to confluence in HYPERFlask vessels (Corning). Once confluent, the cells were washed twice with PBS and incubated with serum-free medium for 3 weeks with weekly medium changes. The laminin β1-fragment was purified from serum-free conditioned medium by nickel affinity chromatography using 5 ml HisTrap FF columns (GE Healthcare) and an ÄKTA FPLC System (GE Healthcare). The purified laminin β1-fragment was concentrated to 1 mg/ml using Amicon ultracentrifugal 10 K molecular weight cutoff (MWCO) units (Fisher Scientific UK), analysed by SDS–PAGE and stored at −20 °C. The laminin β1-fragment was produced by Christine-Maria Horejs and Patrícia Barros da Silva at the Karolinska Institutet, Stockholm.

3.3.5 Confocal and high content imaging

For each experiment, 5,000 cells were seeded 96-well plate (Greiner Sensoplate™ glass bottom multiwell plates, Sigma Aldrich, St. Louis, Missouri; United States) for immunofluorescence analysis. Cells were fixed in 3.7% w/v paraformaldehyde (PFA, Sigma Aldrich, St. Louis, Missouri; United States) in PBS for 15 minutes at room temperature, and were then washed three times for five minutes in PBS. Cells were permeabilised with 0.25% v/v Triton X (Sigma Aldrich, St. Louis, Missouri; United States) for 10 minutes and blocked with 5% v/v goat serum for 1-2 hours. Primary antibodies diluted in fresh 0.1% w/v bovine serum albumin (BSA, Sigma Aldrich, St. Louis, Missouri; United States) in PBS were added to the cells overnight at 4˚C (see **Table 3.1**). Samples were then washed three times with PBS for five minutes before being incubated with Goat anti Rabbit/ Mouse IgG (H+L) Secondary Antibody, Alexa Fluor 488 (ThermoFisher Scientific, Paisley, United Kingdom, 1:500) in 0.1% w/v BSA for 60-90 minutes at room temperature, protected from light. Following this, cells were washed three more times with PBS for five minutes. In most cases, samples were incubated with AlexaFluor 594-conjugated phalloidin (1:400 in PBS) for 30 minutes and were stained with DAPI (1:5,000) for 5 minutes, and stored

in Vectashield (Vector Laboratories, Peterborough, United Kingdom). Confocal imaging was performed on a Zeiss LSM800 microscope (Carl Zeiss Meditec, Jena, Germany) with a 20x objective lens. Widefield and live imaging was performed with a Zeiss Cell Observer microscope (Carl Zeiss Meditec, Jena, Germany) with a 10x objective lens. Structured illumination microscopy (SIM) imaging was performed with an Elyra PS.1 (Carl Zeiss Meditec, Jena, Germany).

High content image analysis was performed using CellProfiler software[862,863] and protocols for focal adhesion analysis and nuclear, perinuclear and cytosolic intensity analysis were developed with the help of Petter Ranefall, Uppsala University and Science For Life Laboratory, Sweden. Whole 96 wells were imaged using the tiling function on a Zeiss Cell Observer microscope (Carl Zeiss Meditec, Jena, Germany) with a 10x objective lens. Channel 1 was the protein of interest, channel 2 was a nuclear stain (DAPI) and channel 3 was an actin stain (phalloidin) which enabled the cell body to be located. Three biological replicates were imaged and then each separate tile within the 96 well plate image was assessed using CellProfiler software. For subcellular intensity analysis, the cell nuclei were segmented using an adaptive thresholding method computing the optimal ellipse fit for each, based on the DAPI channel, the cell body/ cytosol was segmented from the actin channel, and then a perinuclear ring was drawn 10 pixels around the identified nucleus. The intensity of the protein of interest channel was assessed in the nucleus, cytosol and in the perinuclear ring regions. For the focal adhesion analysis, the same ellipse fit based segmentation method was used where the typical diameter of a focal adhesion was set to 3-6 pixels. The logarithmic mean was calculated for each experimental replicate when assessing nuclear/perinuclear intensity and the mean was calculated for each experimental replicate when assessing FA number and cytosolic intensity. Values were compared on GraphPad Prism software (La Jolla, California, USA) using a replicate paired one-way analysis of variance (ANOVA) or t-test, followed by pairwise comparisons via Tukey's multiple comparison test.

Table 3.1: Antibody information for immunofluorescent labelling.

Antibody (AF 568)	Manufacturer	Code	Dilution
pFAK tyr 397	Fisher	S36967	1:200
pFAK (tyr 576/7)	Invitrogen	700013	1:200
α3-integrin	Novus	NBP1-19724	1:200
α3-integrin	BD biosciences	611045	1:200
pSmad3 (S423/5)	Fisher	44-246G	1:500
Laminin β1-fragment	n/a	n/a	1:1000
Collagen type IV	Abcam	ab6586	1:1000
Laminin	Abcam	ab11575	1:1000
NFkB p65	Abcam	ab16502	1:500
E-cadherin	CST	3195	1:200
Vinculin	Sigma Aldrich	V9131	1:200
Paxillin	BD biosciences	BD610052	1:200
Yap	Santa Cruz	sc-101199	1:200
Lamin A/C	Abcam	ab8984	1:500
Cortactin (p80/85)	Merck Millipore	05-180	1:500
α3β1-integrin	Bioussa	1057R-Cy7	1:200

3.3.6 Laminin β1-fragment labelling

10µl laminin β1-fragment (1mg / ml), 90 µl ammonium bicarbonate (0.1M, pH 9), and 5 equivalents and 10 equivalents of Alexa fluor 647/488 NHS ester (succinimidyl ester, Life Technologies, Carlsbad, California, United States) were mixed in anhydrous DMSO (Sigma Aldrich, St. Louis, Missouri; United States) and left on a shaker at 300 rpm at 4°C overnight. The solution was then made up to 1 ml with PBS. This solution was filtered using PD minitrap G-25 columns (GE Healthcare, Little Chalfont, United Kingdom), by the gravity protocol. Fluorescence intensity was measured using a Varioskan™ LUX multimode microplate reader (Thermo Scientific, Paisley, United Kingdom) and the solution had a final concentration of ~6 µg / ml. The fragment was sterilised using a 0.2 microfilter (Starsted, Nümbrecht, Germany).

3.3.7 Live cell imaging

60,000 NMuMG cells were seeded in 12 well costar plate in Dulbecco's modified Eagle Medium with high glucose (DMEM; Life Technologies, Carlsbad, California, United States)

with 10% (v/v) FBS (Life Technologies, Carlsbad, California, United States), and 10 µg / ml insulin (Sigma Aldrich, St. Louis, Missouri; United States) at 37°C with 5% CO_2. Respective treatments were added and the cells were then imaged live for 24 hours at 37°C with 5% CO_2 on a Zeiss Cell Observer Microscope (Carl Zeiss Meditec, Jena, Germany). Live cell imaging was carried out by Christine-Maria Horejs and Hermes Taylor Weiner at the Karolinska Institutet, Stockholm.

3.3.8 Immunoblotting

NMuMG cells were lysed in radioimmunoprecipitation assay (RIPA) Lysis Buffer (Santa Cruz Biotechnology, Dallas, Texas, United States) with protease and phosphatase inhibitors (200mM PMSF in DMSO, protease inhibitor cocktail in DMSO and 100mM sodium orthovanadate in water, Santa Cruz Biotechnology, Dallas, Texas, United States), on ice. After scraping the cells, lysates were incubated in pre-cooled Eppendorf tubes at 300 rpm at 4°C for 30 minutes and then centrifuged at 16,000 g at 4°C for 20 minutes. Supernatants were transferred to new tubes and pellets were stored at -20°C. Samples were mixed with 2x Laemmli-buffer (Invitrogen, Carlsbad, California, United States), loaded on SDS-PAGE gels (4-12% gradient gels, Invitrogen, Carlsbad, California, United States) and separated at 200V for 35 minutes. Proteins were then transferred to a nitrocellulose membrane (Invitrogen, Carlsbad, California, United States) at 20V for 40 minutes.

Membranes were blocked for 1 hour in 5% (w/v) bovine serum albumin (BSA; Sigma Aldrich, St. Louis, Missouri; United States) in PBST (PBS + 0.1% Tween-20, Sigma Aldrich, St. Louis, Missouri; United States) on a rocking shaker. After blocking, membranes were incubated in primary antibody solution in 5% (w/v) BSA overnight at 4°C for all Cell Signalling antibodies and for 2 hours at room temperature for Santa Cruz and Abcam antibodies, followed by three washes with PBS. Membranes were then incubated in secondary antibody solution in 5% (w/v) BSA for 1 hour. After washing with PBS, samples were developed using Western blotting Substrate solution (Pierce™ ECL solution, Thermo Scientific, Paisley, United Kingdom) for 5 minutes at room temperature and chemiluminescence was detected using the ImageQuant LAS 4000 system (General Electrics). Immunoblotting and western blotting were carried out by Christine-Maria Horejs and Patrícia Barros da Silva at the Karolinska Institutet, Stockholm.

3.3.9 Nuclear and cytoplasmic extraction

For nuclear and cytoplasmic protein extraction, a NE-PER kit was used with modifications described below (NE-PER Nuclear and Cytoplasmic Extraction kit, Thermo Scientific). Cells were harvested with trypsin, and centrifuged for 5 min at 500g and 4ºC. The cell pellet was washed with PBS and transferred to a 1.5 mL microcentrifuge tube and centrifuged again. 100 µL of ice-cold cytoplasmic extraction reagent I (CER I) was added to the cell pellet. The pellet was resuspended by vortexing and was then incubated on ice for 5 min. Following this, 5.5 mL ice-cold CER II was added to the tube and vortexed followed by incubation on ice for 5 min. This step was repeated two more times. After centrifuging at 16.000g for 15 min, the supernatant (cytoplasmatic extract) was transferred to a clean pre-chilled tube and stored at -80ºC. Before adding the nuclear extraction reagent (NER), the pellet was washed with cytoplasmic reagent (10mM of HEPES, 60mM of KCL, 1mM of EDTA, 1mM of DTT, all from Sigma, with protease inhibitors from Santa Cruz). The process was continued for the nuclear extraction by adding 50 µL of ice-cold NER to the pellet. After repeated vortexing for 15 secs and incubation on ice every 10 min for 40 min, samples were centrifuged for 15 min at 16000g. The supernatant (nuclear extract) was transferred to a clean pre-chilled tube and stored at -80°C.

3.3.10 Statistical analysis

Statistics on biochemical data was performed using GraphPad Prism software (La Jolla, California, USA). A replicate-paired one way ANOVA with a Tukey's multiple comparison test (3 conditions) or replicate-paired t-test (2 conditions) was performed on the mean values for each experimental replicate.

3.4 Results

3.4.1 System verification and optimisation

A first step was to verify the experimental setup for laminin β1-fragment interactions with NMuMg cells in the presence of TGF-β1 (**Figure 3.6**). Two different batches of TGF-β1 reagent (Sigma Aldrich, T7039, assigned names TGF-β1 A and TGF-β1 B) were assessed using HEK-Blue™ TGF-β cells (Invivogen). Control conditions included HEK-Blue™ TGF-β cells treated with media alone (control) and a well containing no cells treated with media alone (media). HEK-Blue™ TGF-β cells can detect bioactive TGF-β by monitoring the activation of the TGF-β/Smad pathway[864]. The cells express a Smad3/4-binding elements (SBE)-inducible SEAP reporter gene. Stimulation with TGF-β activates the TGF-β/Smad pathway which causes the formation and nuclear translocation of a Smad3/Smad4 complex which binds SBE sites inducing the production of SEAP. The quantity of SEAP secreted in the supernatant was assessed using a paranitrile phosphate assay. Results favoured TGF-β1 B (fluorescence intensity of 5.66) over TGF-β1 A (fluorescence intensity of 2.19) and TGF-β1 B was therefore used in experiments (**Figure 3.6A**).

Actin and vinculin FA immunofluorescence labelling was carried out to verify if TGF-β1 addition caused a visual morphological change in cells as well as a more migratory phenotype, since FA are involved in migration[64] (**Figure 3.6B**). Cells were seeded onto glass well plates and 24 hours later media (control) or media with TGF-β1 was added. The cells were incubated for 24 hours with the treatments and then fixed for immunofluorescent labelling. On visual inspection, the actin cytoskeleton was remodelled, moving from cortical actin in the control cells, to more linear, central structures in the cells which had undergone TGF-β1 treatment. Moreover, rounder cells with cell-cell connections could be seen in the control sample, whereas cells were separated and more elongated in the TGF-β1 samples. TGF-β1 treatment was shown to induce vinculin FAs. Finally, cell proliferation was assessed, since TGF-β1 is known to inhibit proliferation[865], however there was no significant change in proliferation for the TGF-β1 treated samples compared to the control (**Figure 3.6C**).

A)

Media	Control
0.36	2.49
TGF-β1 A	**TGF-β1 B**
2.19	5.66

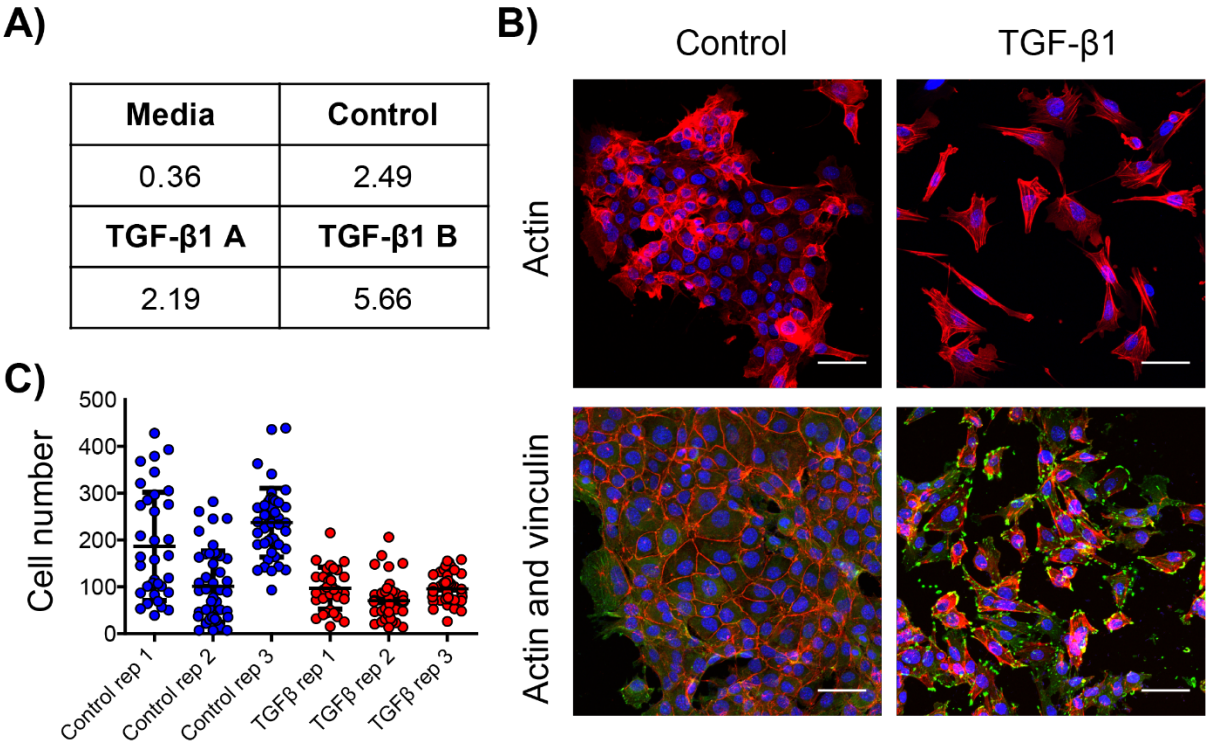


Figure 3.6: TGF-β1 and NMuMg cell proliferation and phenotype. A) Fluorescence intensity measurements were used to assess the HEK-Blue™ TGF-β reporter cell SEAP signal in media alone, the media from control cells and the media from cells with two different batches of TGF-β1 reagents (TGF-β1 A and TGF-β1 B, Sigma Aldrich, T7039). TGF-β1 B worked whereas TGF-β1 A did not. B) Confocal immunofluorescence imaging of actin (red), vinculin (green) and DAPI (blue) in control NMuMg cells and cells treated with TGF-β1. There was a clear change from clustered cells with cell-cell contacts, cortical actin and minimal vinculin focal adhesions in the control sample to individual cells, with linear actin at the centre of the cell body and focal adhesions in the cells treated with TGF-β1. C) High content image (HCI) analysis showed no significant change in cell number with TGF-β1 treatment. Mean +/- S.D., n=3, *p < 0.05, **p < 0.01, ***p < 0.001, scale bar = 50 µm.

3.4.2 α3β1–integrin and laminin β1-fragment interactions

Previous work has demonstrated an interaction between the laminin β1-fragment and α3β1–integrin[535,536]. Therefore, the aim was to image α3β1–integrin and the laminin β1-fragment using super-resolution microscopy to assess their co-localisation and to see how the laminin β1-fragment affects α3β1–integrin clustering. Indeed, integrin binding often results in integrin activation and clustering, initiating a number of signalling cascades[201,866]. A number of different α3-integrin antibodies were tested: BD biosciences (611045); EMD Millipore

(AB1920); Novus Biologicals (NBP1-19724); and Santa Cruz (sc-6587). Moreover, a cy7 conjugated α3β1–integrin antibody was purchased from Bioussa (1057R-Cy7).

The integrin antibodies were imaged using confocal microscopy (**Figure 3.7A**). The Santa Cruz and Millipore antibodies showed unspecific binding and so results were discarded. For the other α3/α3β1–integrin antibodies, labellings were mostly diffusely spread in the cytosol and this was confirmed by structured illumination microscopy (SIM) of the Novus Biologicals α3-integrin antibody (**Figure 3.7B**). However, the BD and Bioussa antibodies showed some localisation of α3/α3β1–integrin at cell-cell junctions.

The α3/α3β1–integrin antibodies therefore showed no clear trend in labelling patterns and results should be treated with caution. Indeed, integrin antibodies are notoriously difficult to label and the adhesive and signalling properties of integrin heterodimers have recently been shown to be dependent on whether the α- or β-subunit of the heterodimer is labelled, since the integrin is partially activated when the β-subunit is tagged[867].

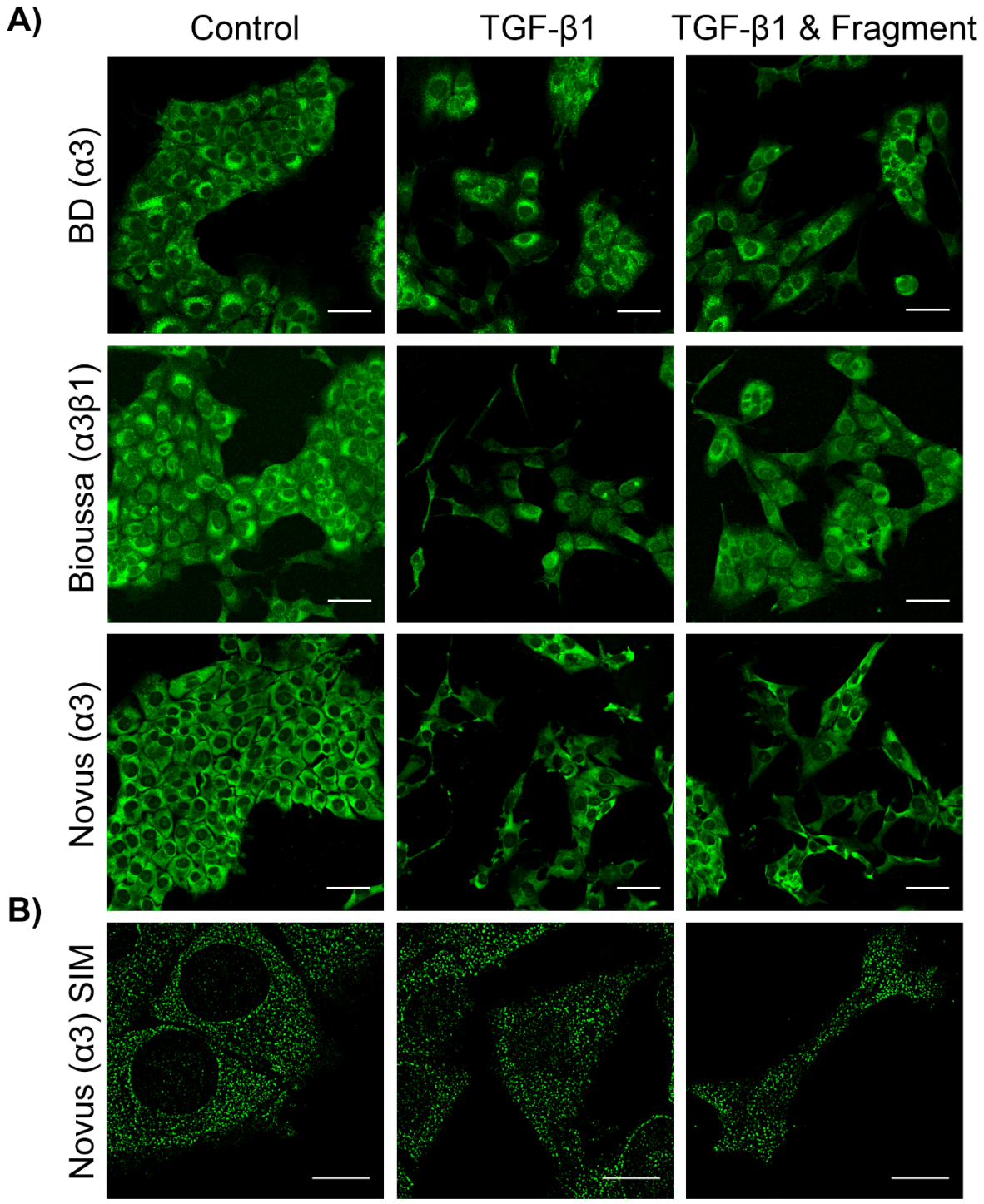


Figure 3.7: α3-integrin immunofluorescence labelling optimisation. A) Confocal immunofluorescence imaging of (from top to bottom): a BD biosciences (611045) α3-integrin antibody, a bioussa α3β1-antibody (1057R-Cy7), and a Novus Biologicals (NBP1-19724) α3-integrin antibody in control NMuMg cells, cells treated with TGF-β1, and cells treated with TGF-β1 and the laminin β1-fragment. The BD biosciences and Bioussa antibodies showed some α3/ α3 β1- integrin staining at cell-cell contacts in the control cells. B) Structured illumination microscopy (SIM) imaging of the Novus Biologicals (NBP1-19724) α3-integrin antibody in NMuMg cells. The α3-integrin antibodies diffusely stained the cell cytosol. n = 3 for confocal images, scale bar 50 µm, n=1 for SIM images, scale bar = 20 µm.

The aim was to image these α3-integrin antibodies with labelled laminin β1-fragment in order to assess colocalisation since this may validate which antibody was working. Laminin β1-fragment was labelled using a fluorescently tagged succinimidyl ester. Although an assessment of fluorescence intensity suggested that the laminin β1-fragment had been fluorescently tagged (**Figure 3.8A)**, no fluorescent fragment was seen using confocal microscopy (**Figure 3.8B**). Different concentrations of starting material succinimidyl ester were tested and the "labelled laminin β1-fragment" was also added in excess, however no signal was seen.

A)

Condition	Blank	5 -equiv	40 -equiv
Intensity	0.1	3,542	17,340

B)

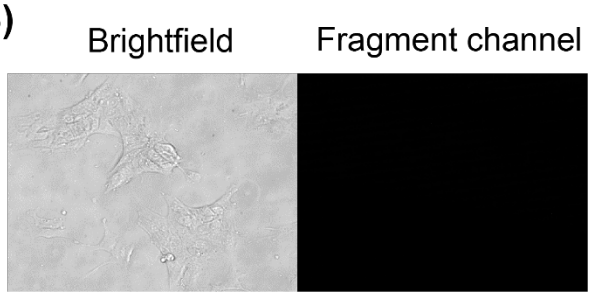


Figure 3.8: Laminin β1-fragment labelling. A) Fluorescence intensity analysis of the laminin β1-fragment suggested successful labelling of the laminin β1-fragment since there was an increase in fluorescence intensity based on the number of equivalents of fluorescently tagged succinimidyl ester molecules added to the laminin β1-fragment. B) Widefield image of brightfield and fragment channel labelling showed no fluorescently labelled laminin β1-fragment.

3.4.3 TGF-β1/Smad canonical signalling

Western blot data has shown a downregulation of nuclear pSmad3 and upregulation of E-cadherin when the laminin β1-fragment is added with TGF-β1 compared to TGF-β1 alone[535]. However, HCI analysis showed no significant change in pSmad3 nuclear translocation between the different conditions (**Figure 3.9**).

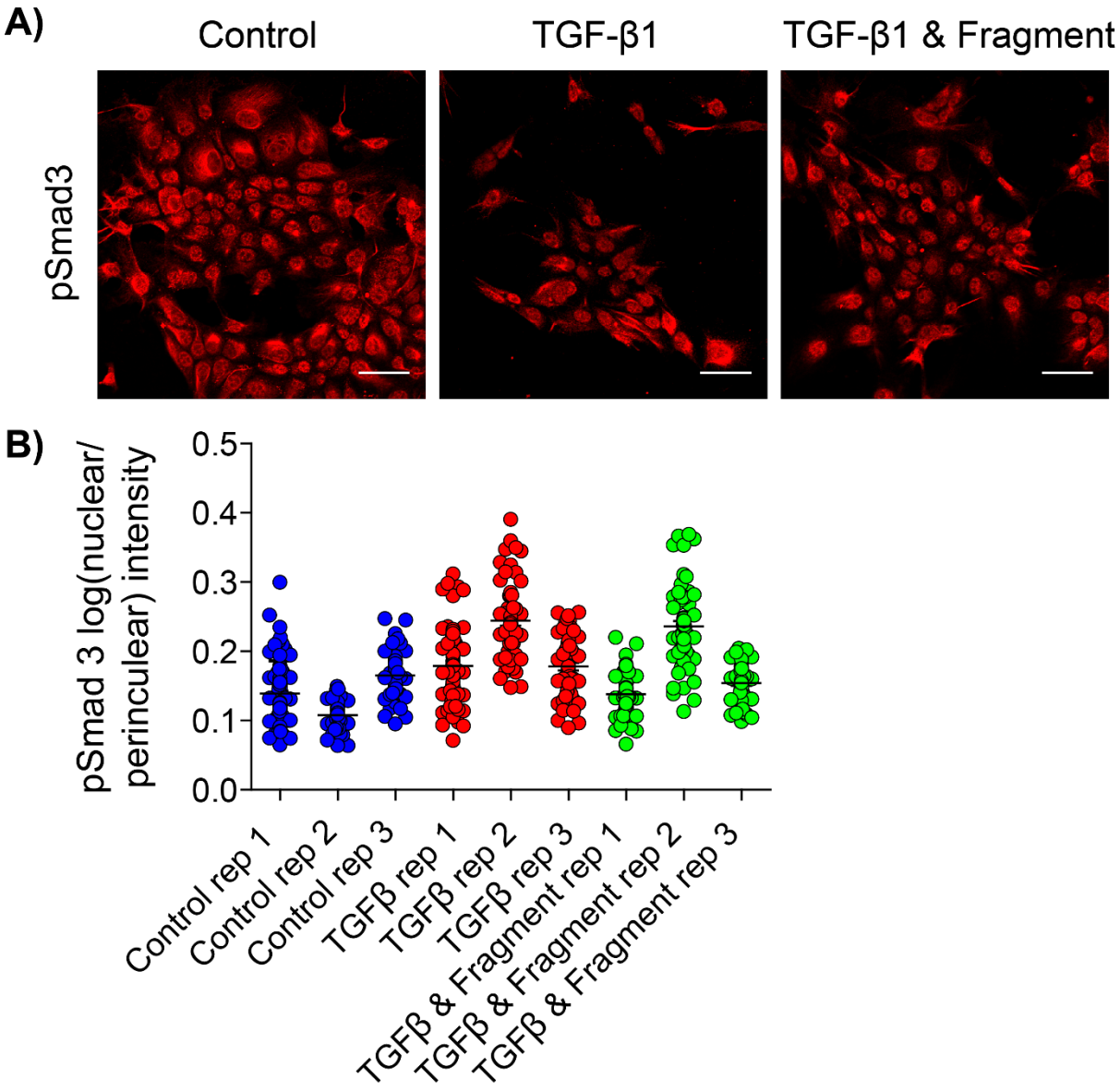


Figure 3.9: pSmad3 localisation in response to the laminin β1-fragment. A) Confocal imaging of pSmad3 in control NMuMg cells, cells treated with TGF-β1, and cells treated with TGF-β1 and laminin β1-fragment. B) High content image (HCI) analysis of pSmad3 under the different conditions showed no significant change. Mean +/- S.D n=3, *p < 0.05, **p < 0.01, ***p < 0.001, scale bars = 50 μm.

Nuclear translocation of pSmad3 causes an increase in the expression of EMT-related transcription factors, such as snail1 and snail2, repressing genes encoding epithelial proteins, such as E-cadherin[649,776]. Since previous western blot results showed a reduction in pSmad3 translocation on laminin β1-fragment addition[535], E-cadherin was likely to be upregulated on laminin β1-fragment addition as a result. Indeed, E-cadherin immunofluorescence labelling visually showed a fine membrane lattice in the control samples, was barely present following TGF-β1 treatment, and could be seen as a coarser, granular membrane labelling when laminin

β1-fragment was added in the presence of TGF-β1 (**Figure 3.10**). Image analysis methods are being investigated to assess E-cadherin fluorescence intensity at the cell periphery.

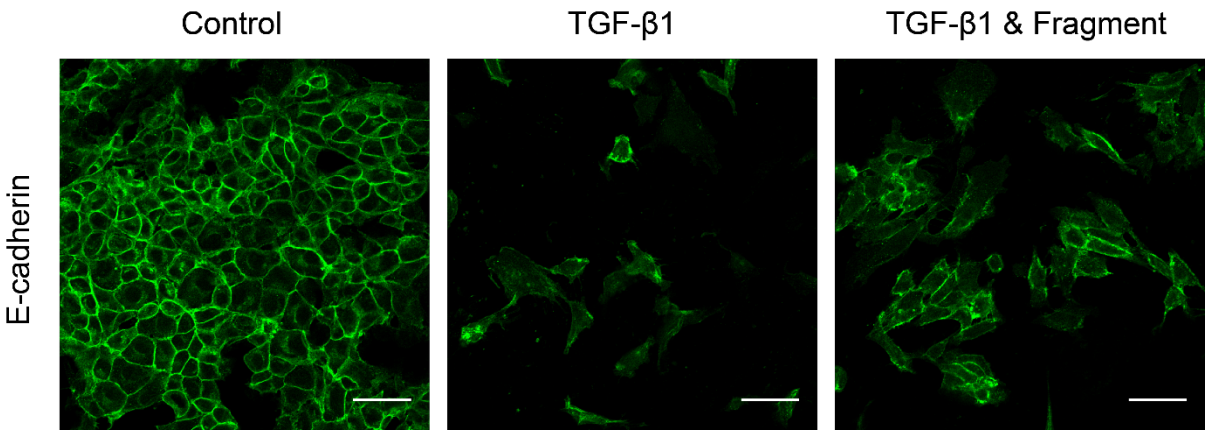


Figure 3.10: E-cadherin response to the laminin β1-fragment. Confocal imaging of E-cadherin (single plane images) in control cells, cells treated with TGF-β1, and cells treated with TGF-β1 and laminin β1-fragment. There was a visual loss in E-cadherin signal following TGF-β1 treatment and this was partially restored when laminin β1-fragment was added. n=3, scale bars = 50 μm.

Smad7 is an inhibitor of the TGF-β1 induced Smad pathway, since it binds to the ligand-activated TGF-β1R complex and blocks phosphorylation of Smad2 and Smad3, preventing the interaction of Smad2/Smad3 with Smad4 and the consequent translocation of this complex to the nucleus[791,792]. Immunofluorescent staining visually demonstrated that Smad7 was mostly located in the nucleus of NMuMG cells under all conditions and minimal fluorescence intensity with no significant change following treatment was shown in the cytosol (**Figure 3.11 A-B**). Smad7 has been shown to be predominantly located in the nuclei of Hep3B cells and a number of other cell types, regardless of TGF-β1 treatment[794]. Moreover, as well as interfering with receptor regulated-Smad activation and targeting receptors for degradation in the cytoplasm, Smad7 has been shown to exert its inhibitory effect on TGF-β1 signalling in the nucleus[794]. The Smad7 results were not clear and further experiments, such as Western blots, should be conducted in order to fully understand these results. Moreover, Smad7 antibodies for immunfluorescent imaging should be tested with Smad7 knockdown.

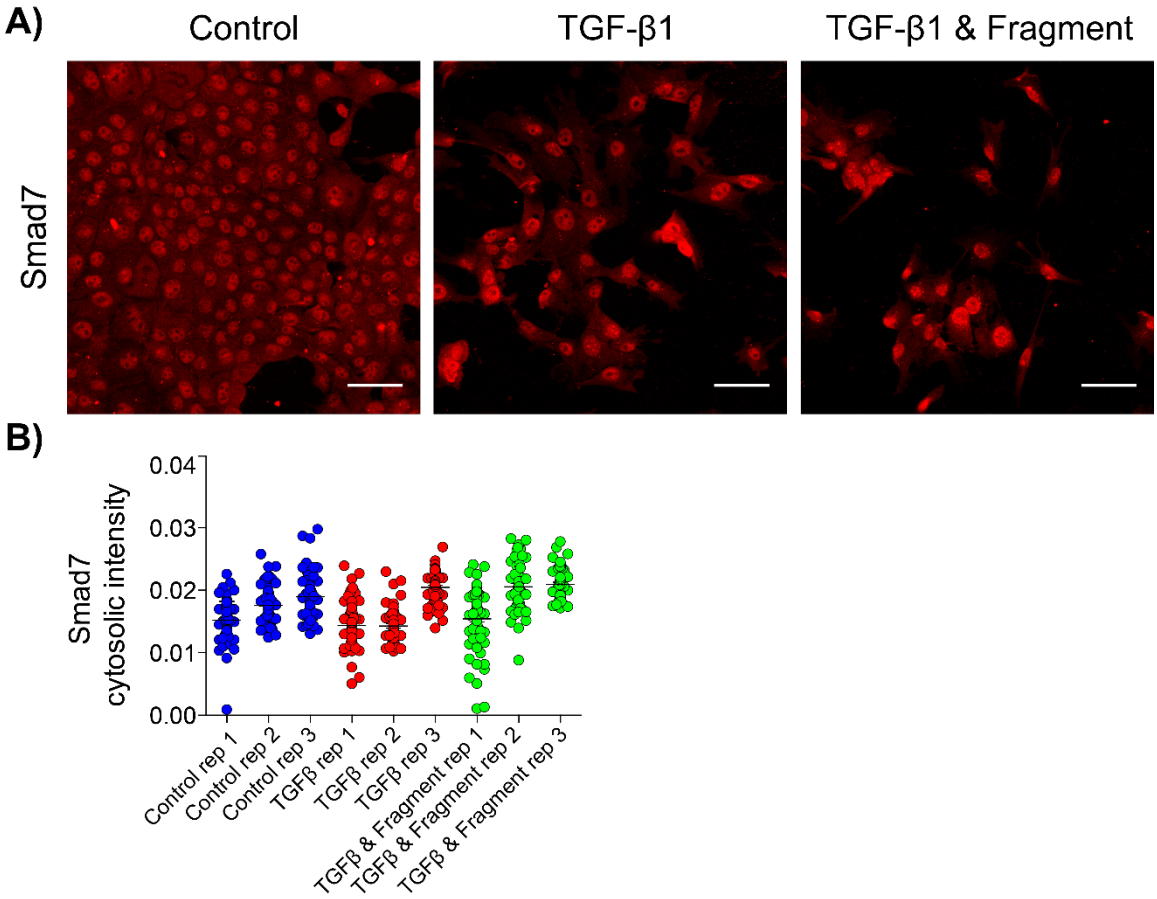


Figure 3.11: Smad7 localisation and intensity in response to the laminin β1-fragment. A) Confocal imaging of Smad7 in control cells, cells treated with TGF-β1, and cells treated with TGF-β1 and laminin β1-fragment. B) High content image (HCI) analysis of Smad7 cytosolic localisation under the same conditions. HCI analysis showed no significant change with TGF-β1 +/- laminin β1-fragment treatment. Mean +/- S.D, n=3, *p < 0.05, **p < 0.01, ***p < 0.001, scale bars = 50 μm.

3.4.4 NF-κB p65 signalling

The NF-κB p65 transcription factor is required for the transcriptional activation of Smad7, and a relationship has therefore been described between NF-κB and TGFβ-smad-dependent pathways[843,848]. NF-κB p65 levels were therefore assessed by Western blot (Christine-Maria Horejs and Patrícia Barros da Silva, Karolinska Institutet, Stockholm), and translocation of NF-κB p65 to the nucleus was shown to increase on TGF-β1 treatment, with a decrease in nuclear translocation on laminin β1-fragment addition (**Figure 3.12A**). Confocal imaging visually matched the western blot results for NF-κB p65 (**Figure 3.12B**), whilst HCI analysis showed no significant change in NF-κB p65 nuclear translocation **(Figure 3.12C**).

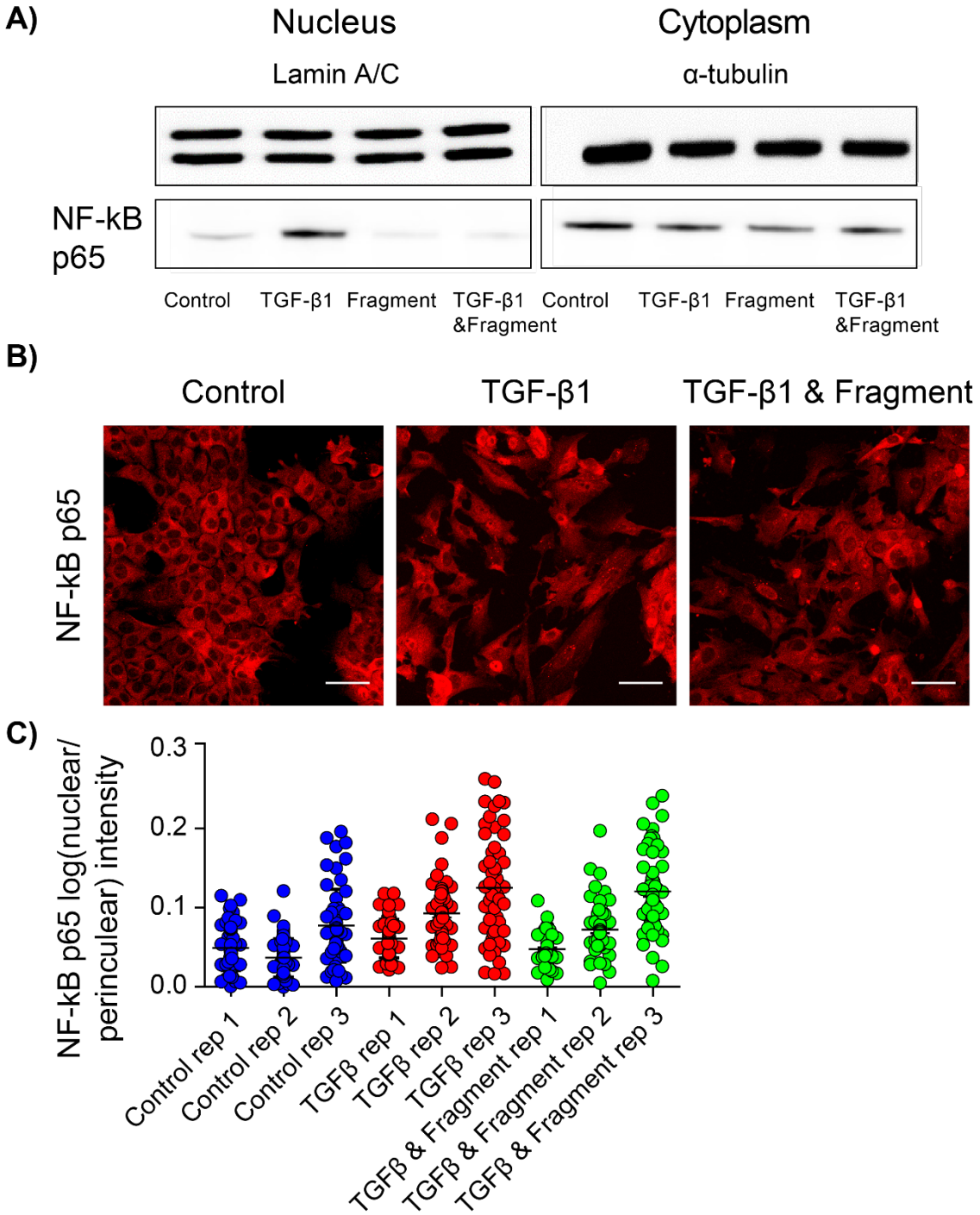


Figure 3.12: NF-κB p65 localisation in response to the laminin β1-fragment. A) Western blot analysis of NF-κB p65 levels in the cell cytosol and the cell nucleus in control NMuMg cells, cells treated with TGF-β1, and cells treated with TGF-β1 and laminin β1-fragment showed that nuclear NF-κB p65 levels were reduced when TGF-β1 was added with laminin β1-fragment compared to TGF-β1 treatment alone. B) Confocal imaging visually matched these results, however C) high content image (HCI) analysis of NF-κB p65 nuclear vs. perinuclear localisation under the same conditions showed no significant difference. Mean +/- S.D, n=3, *p < 0.05, **p < 0.01, ***p < 0.001, scale bars = 50 µm. Western blot analysis was carried out by Christine-Maria Horejs and Patrícia Barros da Silva at the Karolinska Institutet, Stockholm.

3.4.5 Cell migration

Since NF-κB p65 has been shown to affect cell migration[868], cell migration was assessed in the presence of the different treatments. Cells were imaged live every 20 minutes for 24 hours following TGF-β1 with and without laminin β1-fragment treatment on a ZEN cell-observer widefield microscope. Migration speed and persistancy showed no significant change on TGF-β1 and TGF-β1 with laminin β1-fragment (Christine-Maria Horejs and Hermes Taylor-Weiner, Karolinska Institutet, Stockholm) (**Figure 3.13A-B**).

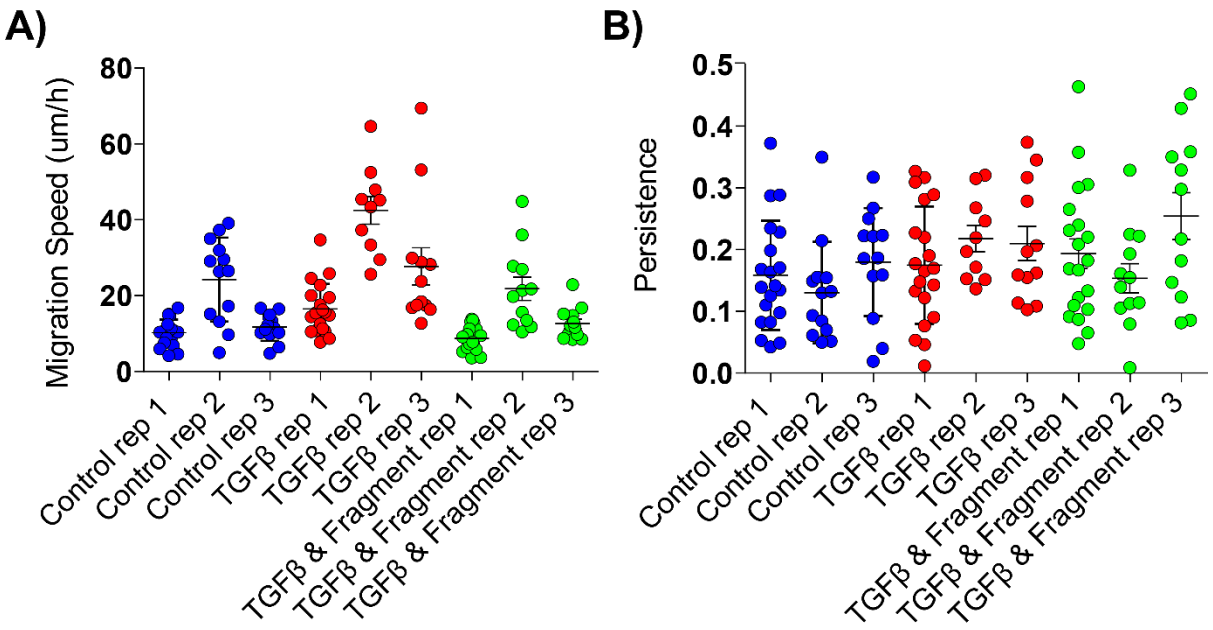


Figure 3.13: Cell migration in response to the laminin β1-fragment. TGF-β1 +/- laminin β1-fragment treatment showed no change in A) migration speed or B) persistence. Mean +/- S.D, n=3, *p < 0.05, **p < 0.01, ***p < 0.001. Migration studies were carried out by Christine-Maria Horejs and Hermes Taylor-Weiner, at the Karolinska Institutet, Stockholm.

Interestingly, cells undergoing TGF-β1 treatment migrated away from each other and preferred to exist as single cells. When laminin β1-fragment was added with TGF-β1, the cells initially migrated away from each other but when they came in contact with each other they appeared to re-form cell-cell contacts and migrate collectively as a unit (**Movie 3.1**).

3.4.6 Focal adhesions

Focal adhesions are key for cell motility[64] and are critical for matrix-informed cell signalling events. Vinculin, paxillin, phosphorylated focal adhesion kinase at tyrosine 397 (pFAKtyr397) and phosphorylated focal adhesion kinase at tyrosine 576 and 577 (pFAKtyr576/7) FA proteins were assessed (**Figure 3.14-3.15**). TGF-β1 +/- laminin β1-fragment treatment caused an increase in the number of vinculin and paxillin containing FA compared to control cells, but showed no change in levels when comparing TGF-β1 +/- laminin β1-fragment (**Figure 3.14A, 3.14B & 3.15B**). Vinculin FA proteins were visibly seen to colocalise with pFAKtyr397 and pFAKtyr576/7 FA proteins respectively (**Figure 3.15A**), and whilst there was no change in pFAKtyr397 FA protein number on TGF-β1 +/- laminin β1-fragment treatment, pFAKtyr576/7 containing FA showed similar trends in number as vinculin and paxillin (**Figure 3.15B**).

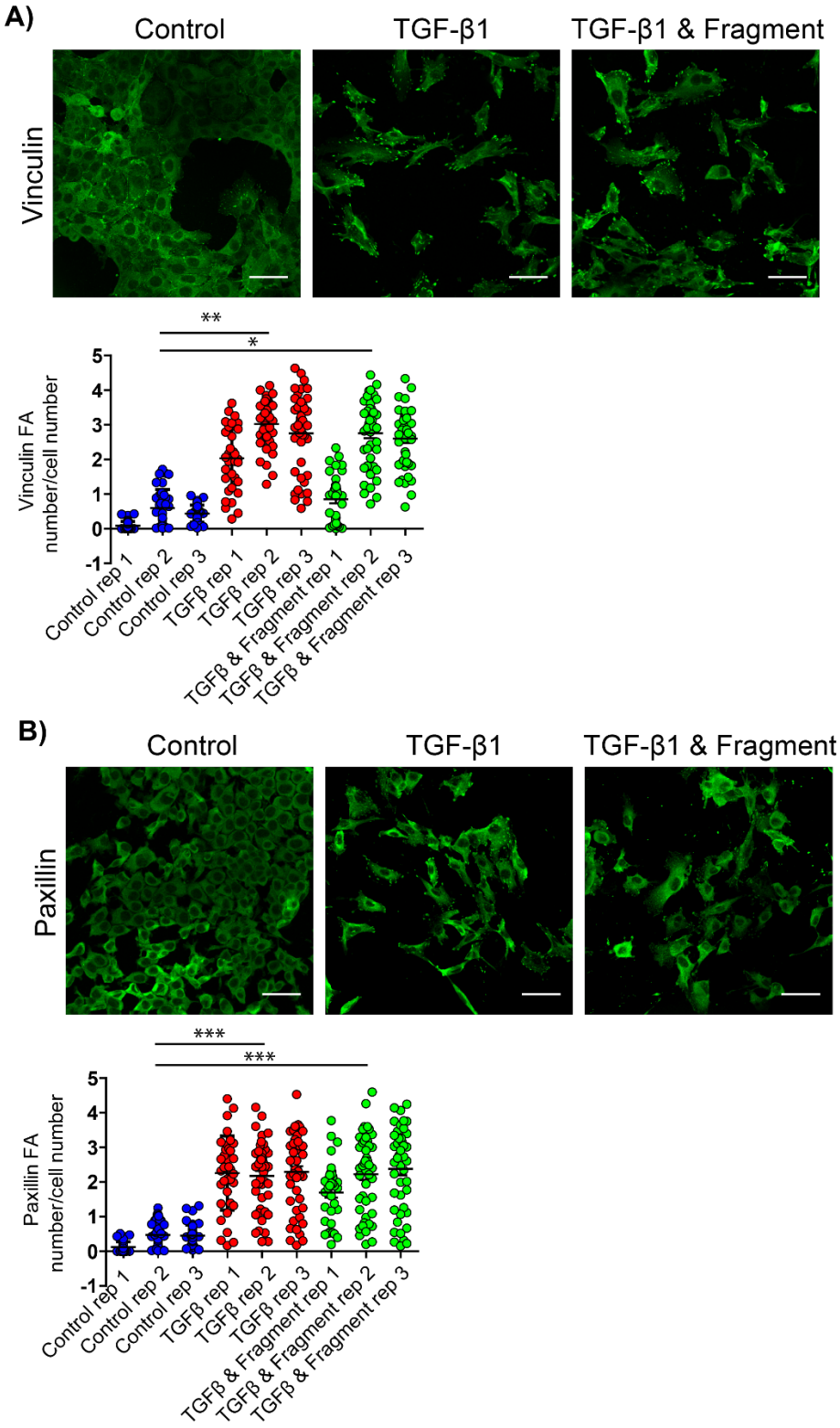


Figure 3.14: Focal adhesion number on laminin β1-fragment addition. A) Confocal imaging and high content image (HCI) analysis of vinculin focal adhesion (FA) protein in control NMuMg cells, cells treated with TGF-β1, and cells treated with TGF-β1 and laminin β1-fragment. B) Confocal imaging and HCI analysis of paxillin FA protein under the same conditions. TGF-β1 +/- laminin β1-fragment treatment increased vinculin and paxillin FA number compared to control cells but there was no change when comparing TGF-β1 +/- laminin β1-fragment. Mean +/- S.D, n=3, *$p < 0.05$, **$p < 0.01$, ***$p < 0.001$, scale bar = 50 µm.

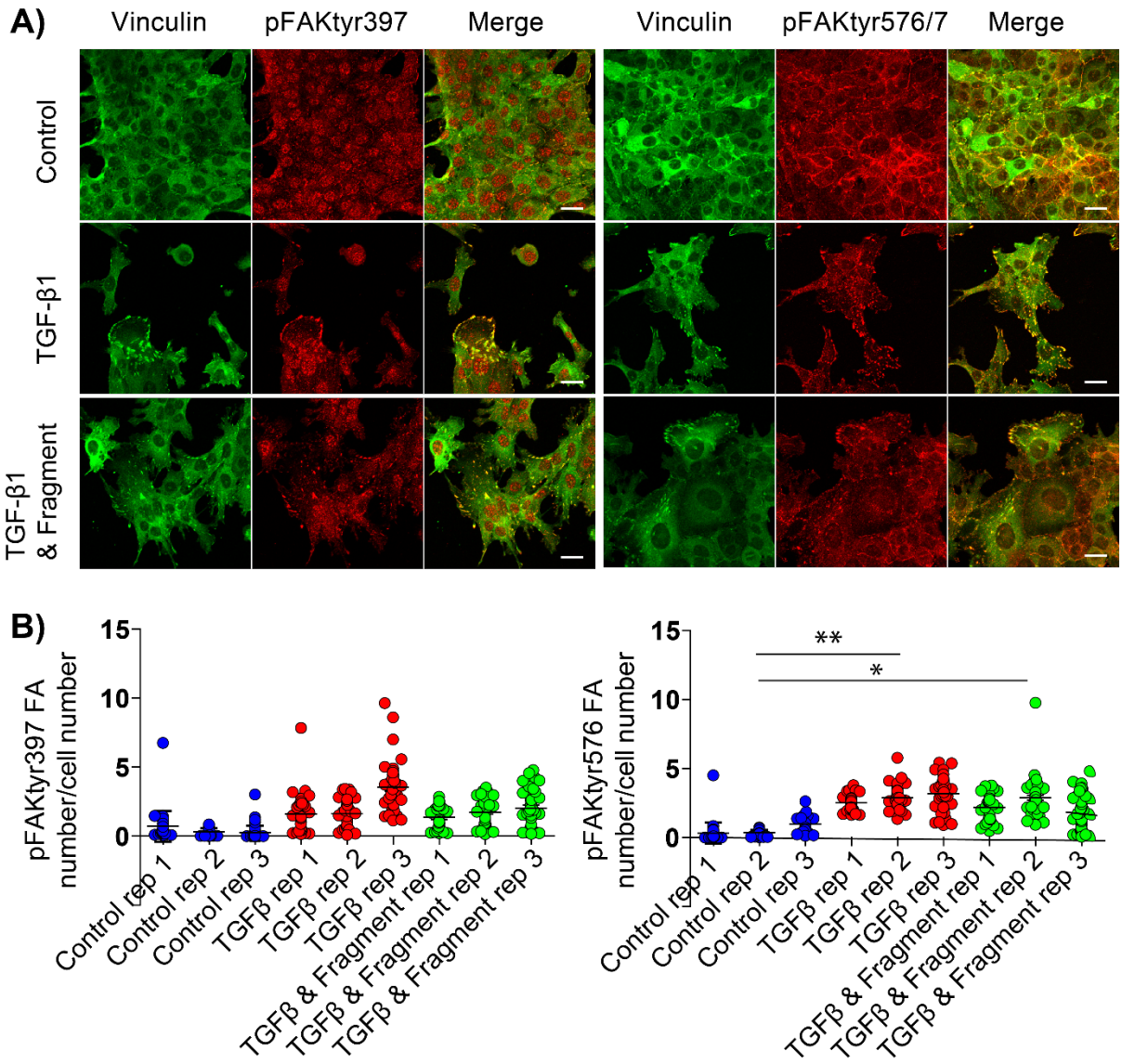


Figure 3.15: Focal adhesion kinase and its interaction with vinculin and the laminin β1-fragment. A) Confocal imaging of vinculin and 397 tyrosine phosphorylated focal adhesion kinase (pFAKtyr397) and vinculin and 576/7 tyrosine phosphorylated focal adhesion kinase (pFAKtyr576/7) in control NMuMg cells, cells treated with TGF-β1, and cells treated with TGF-β1 and laminin β1-fragment. The pFAKs and vinculin were shown to be colocalised. B) High content image (HCI) analysis of pFAKtyr397 and pFAKtyr576/7 number vs. cell number with the different treatments showed no change for pFAKtyr397 but ther was an increase in pFAKtyr576/7 FA number with TGF-β1 +/- laminin β1-fragment addition compared to control, and no change when comparing TGF-β1 +/- laminin β1-fragment. Mean +/- S.D, n=3, *$p < 0.05$, **$p < 0.01$, ***$p < 0.001$, scale bar = 50 µm.

3.4.7 Matrix metalloproteinases and basement membrane breakdown

MT1-MMP and MMP-2 levels have been shown to decrease when laminin β1-fragment is added with TGF-β1 compared to TGF-β1 alone[535]. Two MT1-MMP antibodies were tested (CST 13130 and Sigma AB8345), however MT1-MMP was not visibly located at the cell membrane of membrane protrusions on TGF-β treatment (**Figure 3.16A**). Following TGF-β1 treatment, one would expect MT1-MMP to accumulate at the edge of membrane projections critical for cell migration since it has been described as a key membrane-protease for BM degradation[113,707–709,869,870]. Indeed, HCI analysis of the cyotosolic intensity of the brighter Sigma antibody showed no significant change on TGF-β1 addition (**Figure 3.16B**).

A next step could be to conduct immunofluorescence labelling with these MT1-MMP antibodies in MT1-MMP knockdown NMuMg cells. If labelling were still to occur in the knockdown cells with these antibodies, other antibodies could be tested and validated using this method.

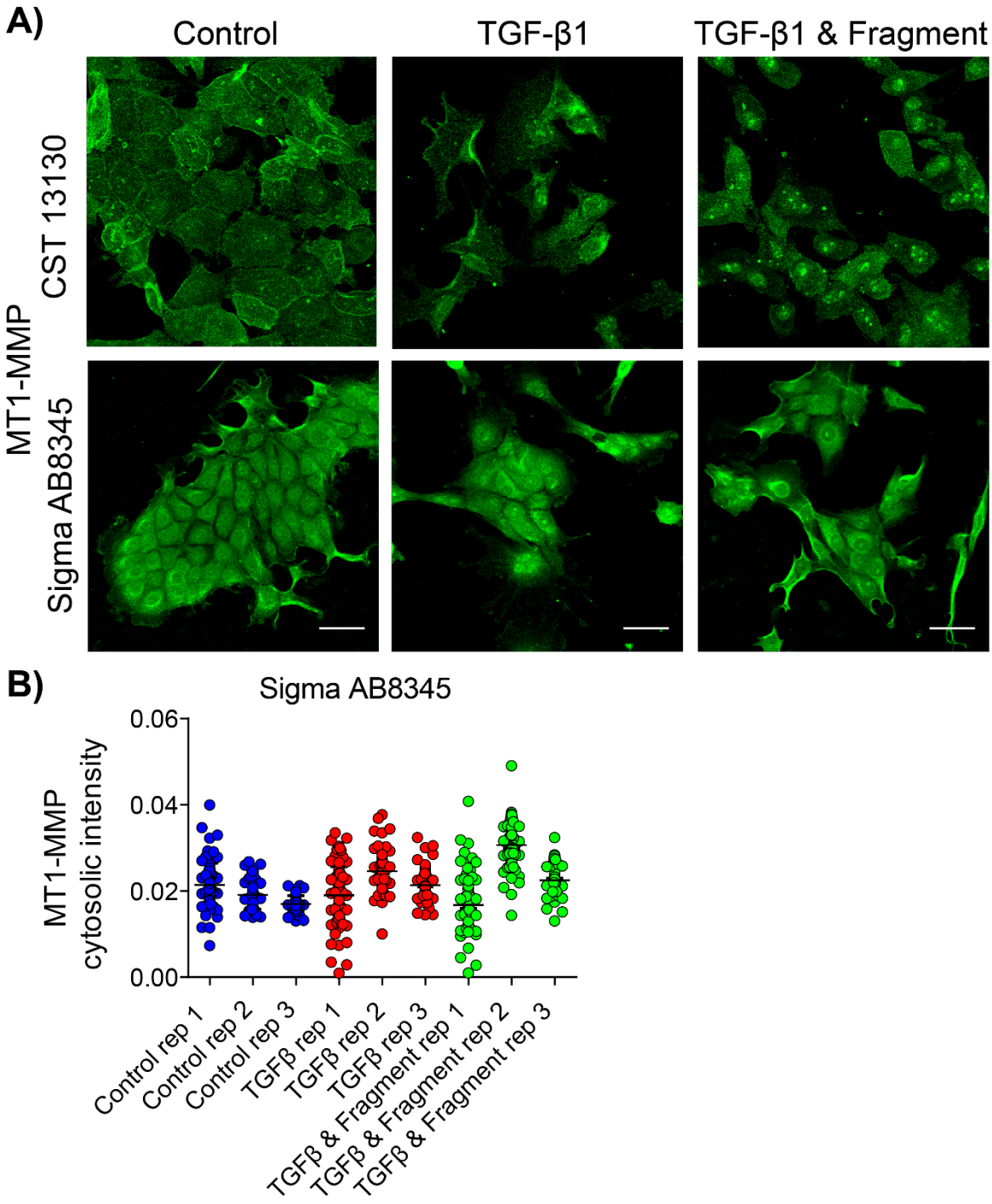


Figure 3.16: Membrane type 1 matrix metalloproteinase immunofluorescence optimisation. A) Confocal imaging of Cell Signalling Technology (CST 13130) and Sigma (AB8345) membrane type 1 matrix metalloproteinase (MT1-MMP) antibodies in control NMuMg cells, cells treated with TGF-β1, and cells treated with TGF-β1 and laminin β1-fragment. B) High content image (HCI) analysis of Sigma (AB8345) MT1-MMP cytoplasmic intensity with the different treatments showed no significant change. Mean +/- S.D, n=3, *p < 0.05, **p < 0.01, ***p < 0.001, scale bar = 50 µm.

The actin-nucleation-promoting factor cortactin plays a key role in the development and maturation of these membrane projections[107,871]. Cortactin could visibly be seen at the edge of membrane projections following TGF-β1 treatment (**Figure 3.17**).

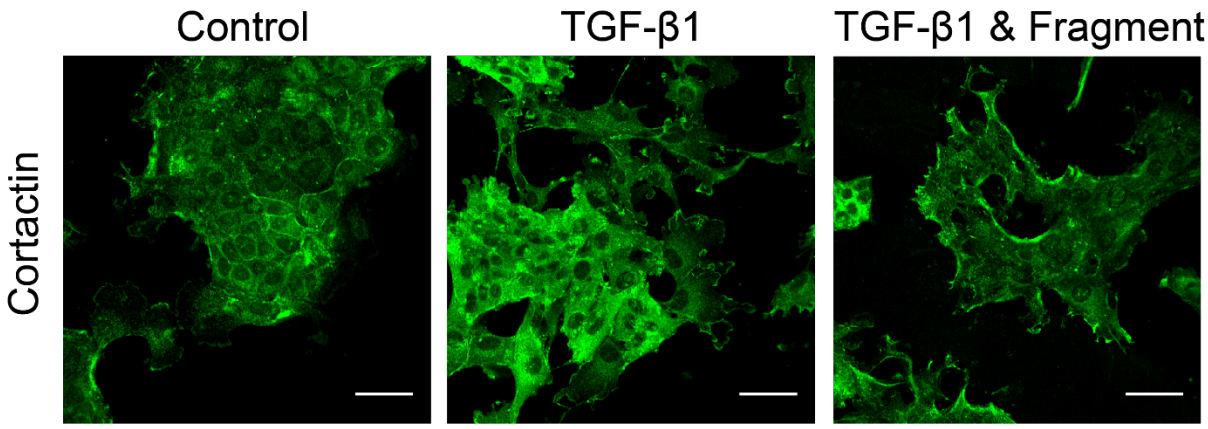


Figure 3.17: Cortactin response to the laminin β1-fragment. Confocal imaging of cortactin in control NMuMg cells, cells treated with TGF-β1, and cells treated with TGF-β1 and laminin β1-fragment. Cortactin was located at the tips of cytoplasmic protrusions in the samples treated with TGF-β1. n=3, scale bars = 50 µm.

MMPs are involved in BM breakdown[872], and collagen IV and laminin were therefore imaged by confocal microscopy (**Figure 3.18**). A visual change could be seen for control vs. TGF-β1 +/- laminin β1-fragment cells; small equally dispersed dot like structures were seen in the control samples whereas fewer longer aggregates were seen for the TGF-β1 treatments.

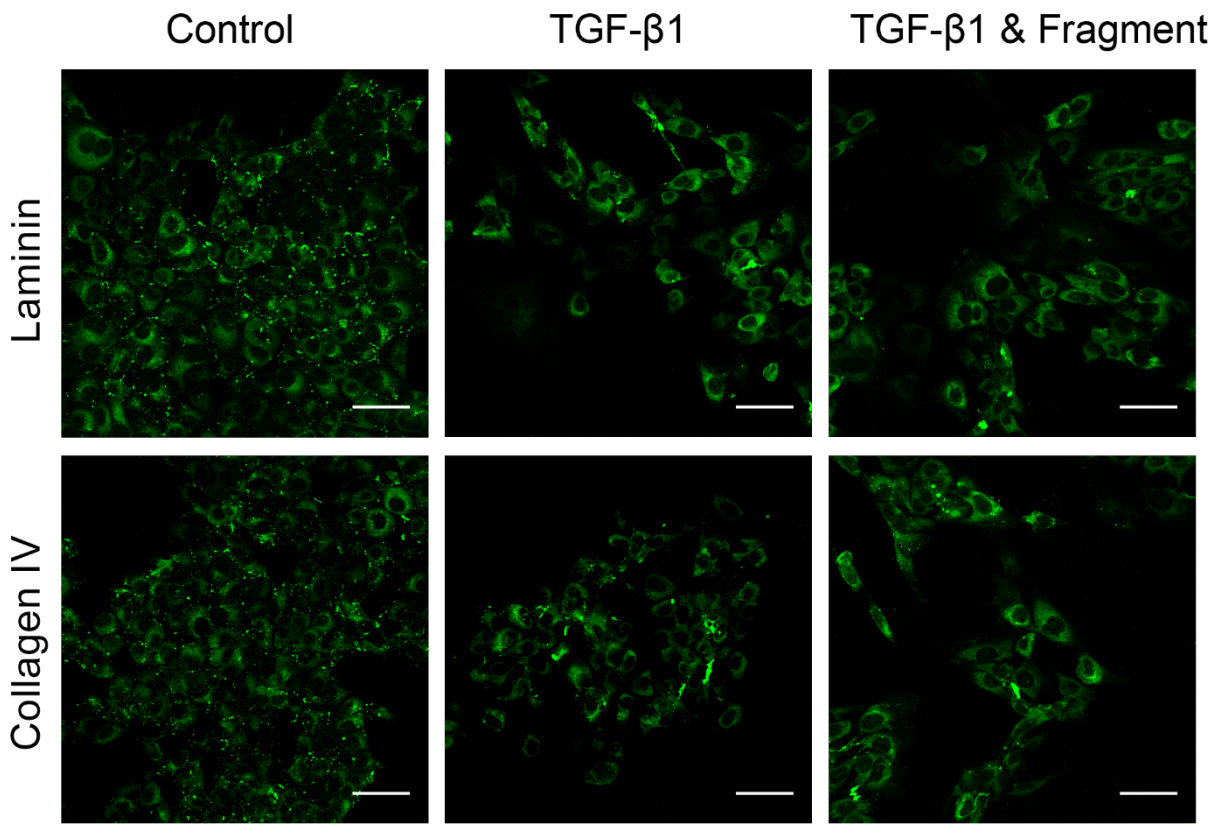


Figure 3.18: Basement membrane breakdown in response to TGF-β1 treatment. Confocal imaging of laminin and collagen type IV basement membrane (BM) proteins in control NMuMg cells, cells treated with TGF-β1, and cells treated with TGF-β1 and laminin β1-fragment. Small equally dispersed dot like structures were seen in the control samples whereas fewer longer aggregates were seen for the TGF-β1 treatments. Scale bars = 50 µm.

3.4.8 YAP and lamin-A

There was no change in YAP nuclear translocation when TGF-β1 +/- laminin β1-fragment was added to the NMuMG cells (**Figure 3.19A-B**). Moreover Lamin-A levels were unaltered by the treatments (**Figure 3.20A-B**).

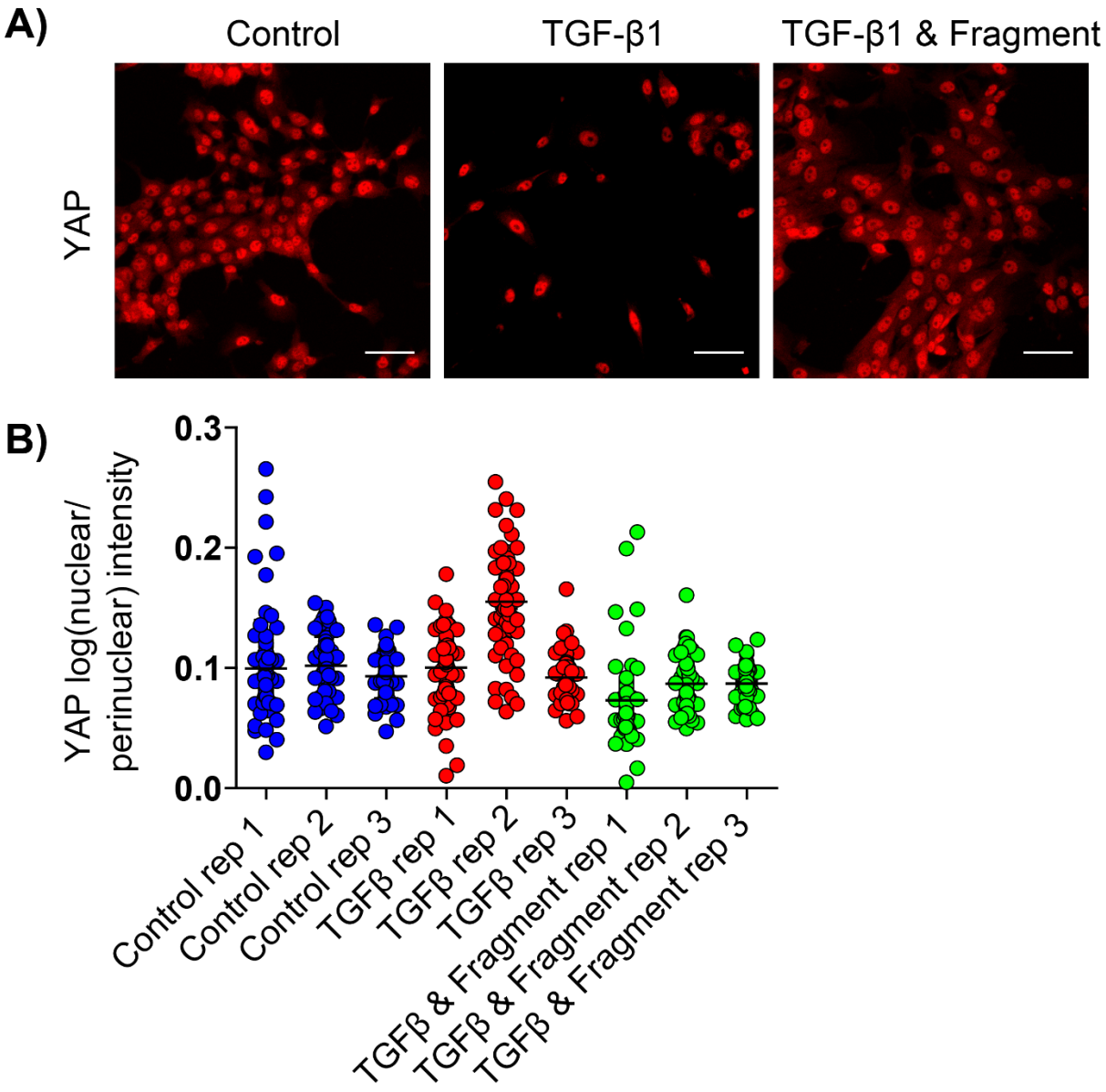


Figure 3.19: Yes associated protein (YAP) response to the laminin β1-fragment. A) Confocal imaging of YAP in control NMuMg cells, cells treated with TGF-β1, and cells treated with TGF-β1 and laminin β1-fragment. B) High content image (HCI) analysis demonstrated no change in YAP localisation following TGF-β1 +/- laminin β1-fragment treatment. Mean +/- S.D, n=3, *p < 0.05, **p < 0.01, ***p < 0.001, scale bars = 50 µm.

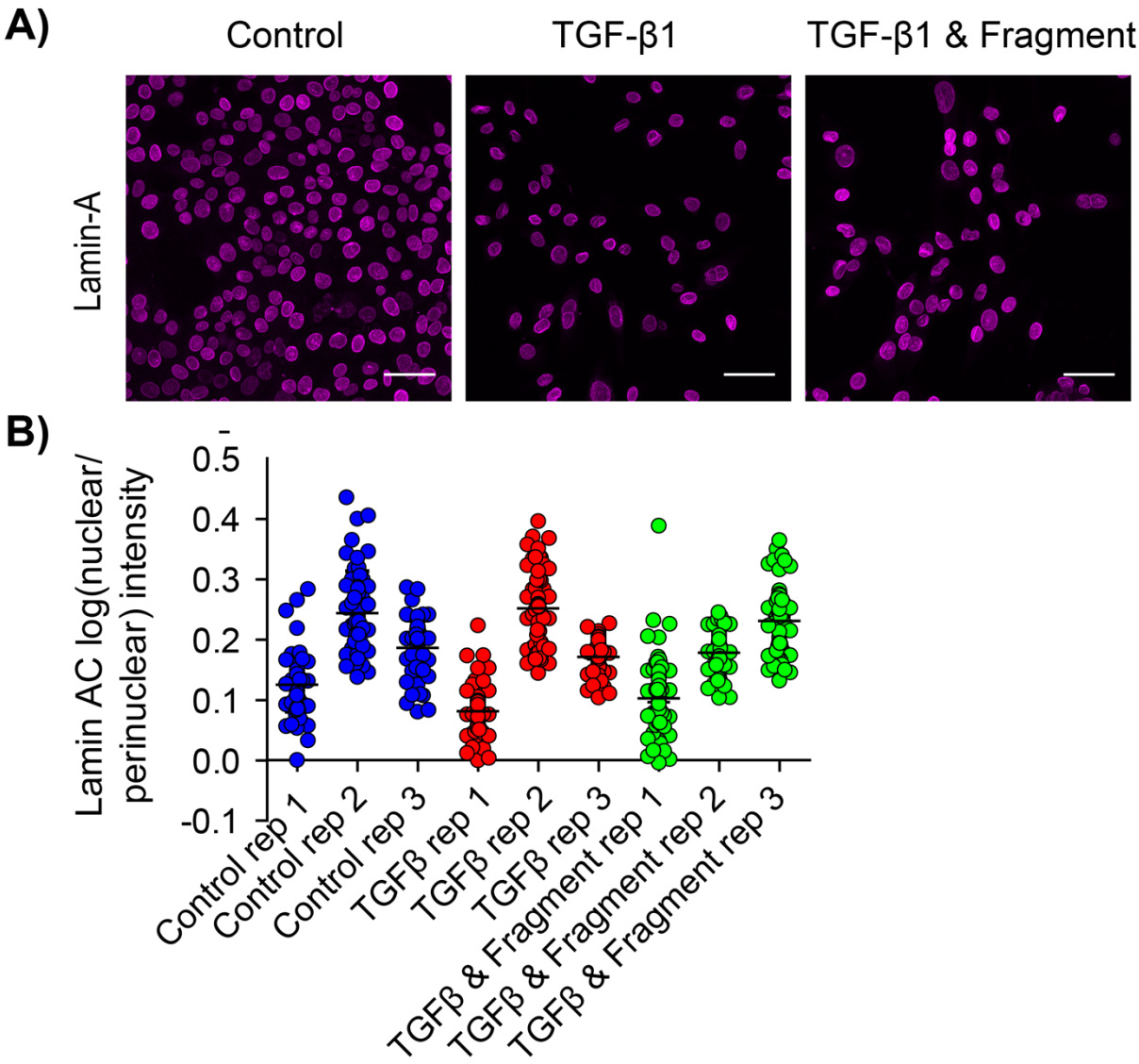


Figure 3.20: Lamin-A response to the laminin β1-fragment. A) Confocal imaging of lamin-A in control NMuMg cells, cells treated with TGF-β1, and cells treated with TGF-β1 and laminin β1-fragment. B) High content image (HCI) analysis demonstrated that lamin-A levels were unaltered following TGF-β1 +/- laminin β1-fragment treatment. Mean +/- S.D, n=3, *p < 0.05, **p < 0.01, ***p < 0.001, scale bars = 50 µm.

3.5 Discussion

TGF-β1 induces different cellular responses by binding to the TGF-β receptor complex; a tetrameric structure consisting of two different serine/threonine kinase homodimers, TGF-βRI and TGF-βRII. TGF-β1 binds to TGF-βRII, which recruits TGF-βRI to form a complex. TGF-βRII then phosphorylates the cytoplasmic domain of TGF-βRI, which phosphorylates intracellular proteins, such as Smads[771,772]. Smad2 and Smad3 are phosphorylated and

establish a trimeric Smad complex with Smad4 which translocates to the nucleus. Here, it enhances the expression of transcription factors, such as snail1 and snail2, which repress genes encoding epithelial proteins, such as E-cadherin. This pathway can be inhibited by competition from Smad6 or Smad7[649,771,776]. Smad7 inhibits the TGF-β/Smad signalling pathway by competing with Smad2 and Smad3 for TGF-βRI binding[873] and has also been shown to exert its inhibitory effect on TGF-β1 signalling in the nucleus[794].

As well as the canonical Smad pathway, TGF-β1 also impacts other proteins and transcription factors, such as NF-κB, FAK and MMPs. The TGF-β activated kinase 1 (TAK1) has been shown to directly phosphorylate the inhibitor-kappaB kinase (IKK) complex which is involved in NF-κB activation[874–876]. Moreover, both NF-κB and Smad2/3 have been shown to upregulate Smad7, which acts as a negative feedback inhibitor of TGF-β activated TAK1 and TGF-β activation of the canonical Smad pathway[843,848]. TGF-β can induce FAK autophosphorylation at Tyr397[877], which mediates phosphorylation of FAK tyr576/7, thus promoting maximal FAK catalytic activity and FA formation[64]. TGF-β1 also regulates MMP expression[878–881] which is known to cleave BM components, releasing proteolytic laminin and collagen type IV fragments which can modulate cell adhesion and migration[576,882–890]. However, MMP-basement membrane crosstalk during cell breaching of the BM *in vivo* is poorly understood, and it is unknown how the BM contributes to the regulation of these signalling events[18].

In this chapter, HCI analysis showed no significant change in pSmad3 and NF-κB p65 levels on TGF-β1 +/- laminin β1-fragment treatment, whereas significant changes were seen in western blot levels[535]. Although this data showed no significant change following 3 experimental replicates, there was a trend that matched the western blot results, and further experiments could be undertaken to clarify this relationship. Moreover, trends for FAK activation and migration suggested an increase with TGF-β1 which was lowered when the laminin β1-fragment was added with TGF-β1. Again, further experimental replicates could be undertaken for these analyses in order to assess whether there is a significant relationship.

α3β1-integrin has been shown to be involved in TGF-β1 signalling and EMT. Indeed, it has been suggested that when α3β1-integrin engages with laminin in the BM or with cell-cell contacts, its role in promoting TGF-β1-induced EMT is supressed[658]. Indeed, alveolar epithelial

cells (AECs) which are cultured on laminin/collagen IV have been shown to be resistant to TGF-β1-induced EMT, whereas AECs cultured on fibronectin, which is not an α3β1 ligand, do undergo TGF-β1-induced EMT[656]. Collagen type IV has been reported as a ligand for α3β1-integrin[891], and kidney epithelial cells growing on collagen IV have also shown resistance to EMT[892]. It has been shown that the the laminin β1-fragment binds to α3β1-integrin[535,536]. Thus, the laminin β1-fragment may trick α3β1-integrin into thinking that it is binding to laminin in the BM, suppressing TGF-β1-induced signalling. A mechanism has been proposed in which TGF-β1 stimulation causes a tripartite α3β1-integrin-E-cadherin–TGF-βR1 complex to form, enabling EMT to occur[657]. α3β1-integrin-laminin β1-fragment binding may therefore also inhibit the tripartite α3β1-integrin-E-cadherin–TGF-βR1 complex formation, altering TGF-β1-induced EMT signalling. Further experiments could be conducted to assess such interactions.

YAP and TAZ can act as mechanotransducers[4] but they also promote TGF-β1 signalling by retaining activated Smad2/3 in the nucleus[893–895]. Cytosolic inactive YAP on soft matrices and YAP knockdown result in impaired TGF-β1–induced Smad2/3 nuclear accumulation and transcriptional activity[896]. A number of signalling pathways are likely to affect pSmad3 levels however YAP activity was assessed since it may be related to the decrease in nuclear pSmad3 levels shown by western blot when TGF-β1 is added to cells with the laminin β1-fragment compared to TGF-β1 alone[535]. Although YAP HCI analysis showed no response to the treatments, which suggests that it does not mediate pSmad3 levels in this case, the relationship between YAP and pSmad3 could be confirmed in YAP knockdown cells by western blot.

Lamin-A also shows a mechanosensitive response[10], and is involved in mediating effective cell migration through narrow confinements[165]. Cell migration is important during development, and the nucleus is often the limiting factor in cell migration through a 3D-ECM since it is generally the largest and stiffest organelle. Migration through narrow pores requires nuclear deformation, and this shows a dependence on lamin composition; over-expression of lamin-A leads to limited migration and slower recovery from nuclear deformation[165]. TGF-β1 treatment initiates cell breaching of the BM by upregulating MMP levels[881]. Indeed TGF-β1 treatment might result in lowered lamin-A levels and this may be to facilitate transmigration

through the pores created in the BM by TGF-β1 signalling. Unfortunately, this cannot be assessed in this system, since it is a 2D system, and so experiments could be conducted on a 3D gel to verify if this is the case.

3.6 Conclusion

This chapter has investigated how the BM influences TGF-β1 signalling, and vice versa, and therefore enables a greater understanding of cell-matrix interactions. The process of BM transmigration is highly regulated and is challenging to assess both *in vitro* and *in vivo*[13,18,564]: the BM is a very thin, insoluble matrix and so is difficult to decellularise; BM crossing events are rapid and rare and are therefore hard to track *in vivo*; and it is not yet possible to recreate a BM *in vitro*. Moreover, the biochemical and biophysical mechanisms by which BM breakdown is regulated are still unclear[13,564,588]. In this chapter, the effect of a "cryptic" BM fragment on TGF-β1 signalling was described. TGF-β1 signalling pathways (Smad, NF-κB and FAK) was assessed as well as TGF-β1-induced phenotypic changes (E-cadherin and MMP levels, FA number and cell migration). Although no changes were shown in TGF-β1 +/- fragment conditions using HCI analysis, this chapter has provided further investigation into how BM breakdown can affect cell function and this is of high importance since any cell that migrates through tissue interacts first with a BM, a critical event in development and tissue remodelling. Moreover, cells breach the BM during cancer metastasis and tissue fibrosis, and a greater understanding of the mechanisms involved (or not involved) in cell-BM crosstalk may provide new strategies to prevent pathological BM turnover.

3.7 Future directions

As reported in this chapter, antibodies specific for α3A (one of 2 isoforms of the α 3 subunit) have been shown to stain in a diffuse pattern using standard fixation and permeabilisation methods in most cell types[749,752,897]. However, it has been demonstrated that if integrins are chemically cross-linked to the ECM and the cytoskeleton is extracted before immunofluorescent labelling, α3A is located in the FAs of many cells e.g. chicken embryo fibroblasts, human foreskin fibroblasts, MG63 human osteosarcoma cells and Chinese hamster ovary cells[737,756]. Interestingly, not all cell types show α3A located at FAs following

this protocol (e.g. chicken muscle cells, HeLa or NIH 3T3) and in some cell types such as keratinocytes[756,897,898] and kidney mesangial cells[899] α3β1 is localised to FAs with the standard immunofluorescence protocols. This suggests that the cytoplasmic domain of α3A is concealed by cytoskeletal proteins, and different cell types on different ECMs show different localisations of α3β1-integrin since they have different cytoskeletal interactions. A next step could be to image α3-integrin following ECM cross-linking and cytoskeletal extraction method. α3-integrin is likely to be located at FA sites since FAK has been pulled down together with α3-integrin, and pFAK is colocalised with the FA protein vinculin.

Although previous laminin β1-fragment tagging with succinimidyl ester worked[536], the labelled laminin β1-fragment was imaged with embryonic stem cells which cluster together in spheres expressing a significant amount of α3-integrin and are therefore much more likely to interact with larger amounts of laminin β1-fragment, thus providing a greater signal. The labelling protocol could next be attempted with wheat germ agglutinin (WGA). WGA binds to sialic acid and *N*-acetylglucosaminyl residues and is used as a cell membrane stain. The NMuMG cells could be treated with the tagged WGA as well as purchased Alexa Fluor® 488 conjugate of WGA (ThermoFisher Scientific). The membrane labelling could then be compared to ensure that the labelling protocol works.

Super-resolution microscopy (SRM) shows great promise in advancing the understanding of cell-matrix interactions. For example, 3D SRM has been used to map nanoscale protein organisation in focal adhesions, and to show that actin and integrins are vertically separated by a ~40-nm FA core region[376]. Moreover, quantitative SRM has been used to characterise early integrin clusters and has shown that very early adhesions consist of ~100-nm clusters of ~50 β3-activated integrins[378]. The localisation of α3-integrin and labelled laminin-β1 fragment could be imaged using stimulated depletion (STED) microscopy, to see if they are indeed colocalised. STED microscopy breaks the diffraction limit of conventional light by exciting the fluorophore with a doughnut shaped depletion beam immediately after excitation. This induces a downward transition by the excited electron (stimulated emission) to a higher vibrational state in the ground state than would be reached by fluorescence[900]. Total internal reflection (TIRF) live super-resolution microscopy could also be used to image α3-integrin's response to the laminin β1-fragment. NMuMg cells could be temporarily

transfected with α3-integrin GFP and the dynamics, localisation and internalisation of α3-integrin will be assessed following laminin β1-fragment addition.

NF- κB could be knocked down in NMuMG cells using siRNA and Western blot analysis of FAK, MT1-MMP, MMP-2, Smad3 and pSmad3 could be conducted to see if there is a link between these TGF-β1 signalling components. Moreover, cell migration studies could be repeated using the NF- κB knockdown cells, to confirm whether NF-κB signalling pathways are affecting migration. The cells could be fluorescently labelled (e.g. with WGA alexa 488 membrane stain) in order to conduct live image analysis of cell clustering in control and NF- κB knockdown cells.

A lentiviral-based, dual fluorescent reporter system, known as the "Z-cad dual sensor" has been developed to detect dynamic changes between the epithelial and mesenchymal cellular states[901] and to capture partial EMT and intermediate phenotypes. This sensor consists of a destabilised green fluorescent protein containing the ZEB1 3' UTR and red fluorescent protein driven by the E-cadherin (CDH1) promoter. This sensor has been shown to detect both EMT and MET in breast cancer cells by flow cytometry and fluorescence microscopy, with dynamic changes being observed. In this chapter, there is a clear need to assess whether the entire population of cells are undergoing "partial EMT" on TGF-β1 and laminin β1-fragment addition, or whether a subpopulation of cells is failing to undergo EMT, causing there to be a population of epithelial-like cells and a population of mesenchymal-like cells. The "Z-cad dual sensor" could enable this to be elucidated by live cell imaging and flow cytometry[901]. The reporter cell line could also enable the optimisation of timings and the concentration of laminin β1-fragment; could enable properties such as cell shape to be correlated to EMT phenotype; and it could be used to assess whether the fragment can reverse EMT.

The minimal quantified change observed in laminin and collagen IV with TGF-β1 +/- laminin β1-fragment treatment might be because the NMuMG cells only had 24 hours to deposit their ECM and so levels of BM proteins are likely to be low. For example, corneal epithelial cells cultured on collagen gels only show deposition of perlecan at one week and it takes two weeks for all the BM components to be detectable[902]. Moreover, at 1 day of SV40-T2 cell culture on TCP, only small deposits of laminin-1 and entactin can be seen, whilst after 10 days a mesh structure of BM components can be seen[903]. A next step could be to deposit

fluorescent BM components (laminin and collagen IV) into well plates prior to cell seeding and to see how they are affected by cells with TGF-β1 +/- laminin β1-fragment treatment.

The effects of the laminin -β1 fragment on TGF-β1 signalling and EMT could be tested on other epithelial cell types, for example cancer epithelial cell lines and bronchial epithelial cells from patients with pulmonary fibrosis, patients with epithelial cancers and normal volunteers. Moreover, EMT could also be induced by other means, such as hypoxia, and the effects of laminin -β1 fragment on hypoxia-induced EMT could be assessed. Finally, the effect of the of laminin -β1 fragment on EMT could be recorded in NMuMg cells seeded on decellularised mouse peritoneum samples.

4 Final conclusions and future directions

The ECM is composed of a variety of structural and functional macromolecules and is crucial for tissue and organ morphogenesis, the maintenance of tissue structure and function, and for cell signalling[13,14]. An understanding of the interactions between cells and the ECM is important, especially in the context of biomaterials which can provide extracellular signals to promote proliferation and differentiation. Biomaterials can provide extracellular signals in the form of growth factors and ligands, cell-ECM and cell-cell interactions, and also through chemical and mechanical stimuli[904]. This thesis concentrates on two of these external signalling mechanisms; mechanical stimuli and cell-ECM interactions. Firstly, porous silicon nN arrays were used as a tool to mechanically stimulate cells, and then a laminin β1 fragment from the BM, a specialised form of ECM, was used to assess cell-ECM interactions. Microscopy was used as a key tool to evaluate these cell-material and cell-matrix interfaces. This PhD provides novel insight into how cells can respond to their extracellular environment and highlight novel materials which could be used to direct cell phenotype.

4.1 Porous silicon nanoneedle arrays as a novel tool to manipulate cell mechanobiology

Mechanobiology is a fast-developing field, significantly impacting studies in biology and biomaterial designs, and novel tools to dissect mechanotransduction in live cells are required. Silicon nN arrays were introduced as a novel tool which can directly interact with several mechanoresponsive organelles (e.g. FAs and the actin cytoskeleton). Nanoneedle arrays were shown to modulate cellular signalling events that resulted in a decoupling of YAP activity from cell area, and a divergent expression of lamin A and lamin B **(Figure 4.1)**.

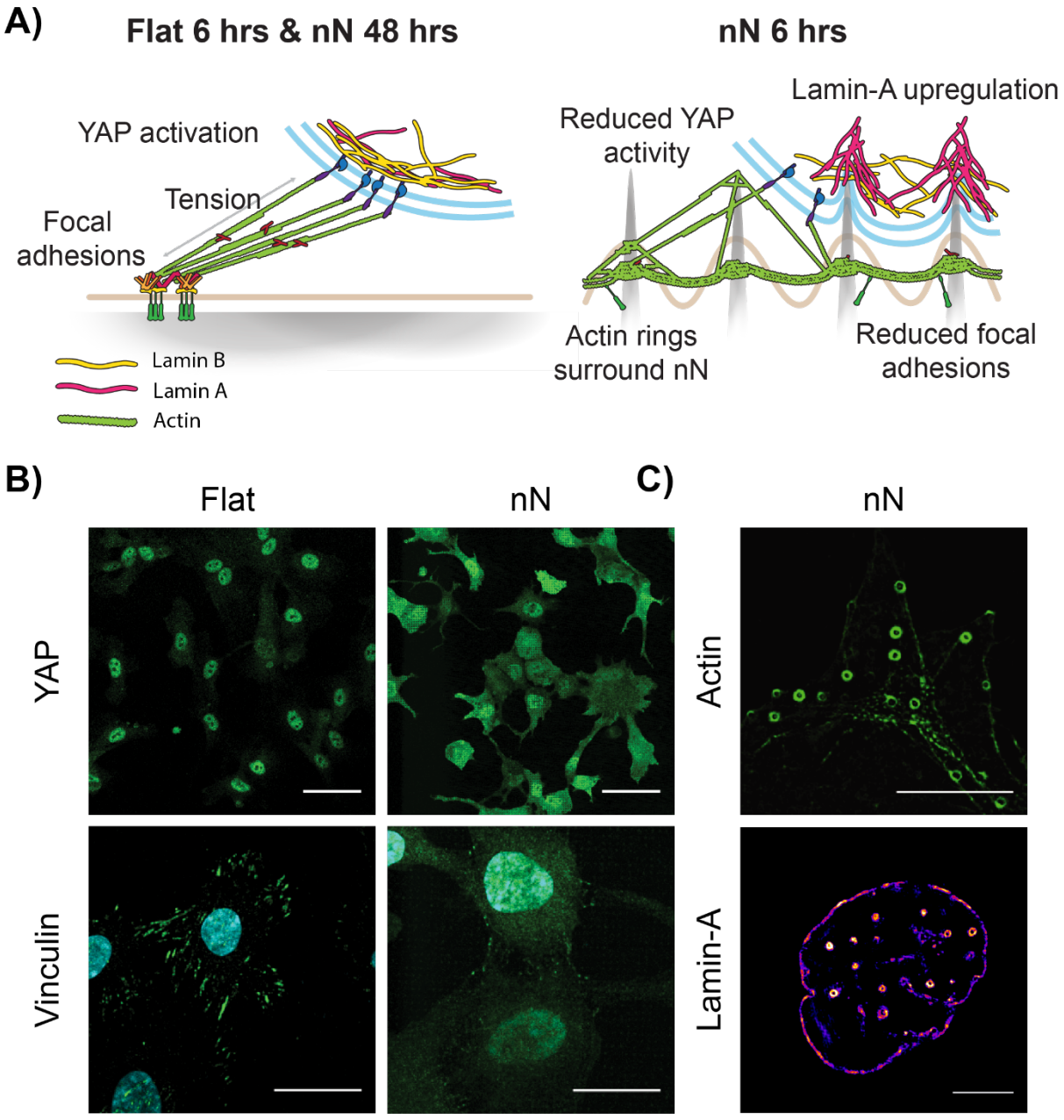


Figure 4.1: Summary of chapter 2 results: nN arrays alter primary human cell mechanobiology. (A) Schematic representation of how nN reversibly cause reduced YAP activity, lamin-A upregulation at nN locations, actin rings around nN, and reduced focal adhesion (FA) formation. (B) Confocal imaging of YAP (top panel) and vinculin (bottom panel) in human umbilical vein endothelial cells (HUVECs) on flat and nN substrates six hours post seeding. YAP is more nuclear on flat substrates whereas it is more cytosolic on nN. There are clear punctate vinculin FAs on flat substrates and these are not as prominent on nN. YAP – green, Vinculin – green, nucleus – cyan, scale bars for YAP and vinculin = 50 µm. (C) Structured illumination microscopy (SIM) imaging of the actin cytoskeleton (top panel) and lamin-A (bottom panel) in HUVECs on nN substrates six hours post seeding. Rings of actin and lamin-A form at the nN locations. Scale bar for actin = 10 µm, scale bar for lamin-A = 5 µm.

The novel findings in this chapter were the YAP and lamin responses, since the alterations in canonical mechanotransduction pathways on nN arrays have previously been recorded in the literature. For example, fewer adhesive structures[300,308,309,445,505] and reduced cytoskeletal tension[300,508,509] have been observed on vertically aligned nanostructures and changes in cellular[311,413,500,506,507] and nuclear morphology[195,412] have also been identified. In this thesis, these finding were a necessary pre-requisite to highlight the importance and novelty of the other observed changes, such as the YAP and lamin responses, and were required to isolate the contribution of each individual interaction, as well as its contribution to the overall observed phenomena.

Previous papers have also reported YAP expression on nanostructures[508,509]. However, Ankam *et al.* merely investigated YAP in undifferentiated versus differentiated cells, and did not assess the relationship between YAP and changes in the substrate[508]. Moreover, although Zhang *et al.* demonstrated that cells with smaller spread areas had more cytosolic YAP, there was no investigation into YAP activity and this was investigated in an entirely different system[509]. When cells were seeded on porous silicon nN arrays, a loss of correlation between YAP localisation and cell area was quantified, which has yet to be shown in the literature (a recent manuscript observed that cells could spread and have cytosolic YAP, but this was in an entirely different biomaterial system[905]).

Hanson *et al.* have shown that micropillars deform the nuclear envelope, and that such deformation can be prevented by externally regulating lamin A or actomyosin contractility. Cell interfacing with porous silicon nN arrays also demonstrates nuclear deformation in response to nN, but additionally shows a lamin type-specific response. The lamin type-specific remodelling observed at the cell-nN interface has not been described in the literature, and represents an entirely new observation of how nN can actively alter the physical properties of organelles. Swift *et al.* have shown that an increase in lamin A protein expression is observed for hMSCs on matrices of increasing stiffness. YAP nuclear localisation was also shown to increase with matrix stiffness, however this effect was reduced when lamin A was overexpressed[10]. This suggests that lamin A and YAP localisation tend to correlate with matrix rigidity *in vitro*, but that an overabundance of lamin A might block nuclear entry of YAP. This is in accordance with the results on nN arrays since an increase in *LMNA* levels but a decrease

in nuclear levels and activity of YAP was demonstrated. Interestingly, Swift *et al.* also demonstrated that *LMNA* knockdown had little to no effect on the expression of YAP target genes, and these two pathways were therefore considered uncorrelated[10]. This suggests that our system offers insight into how material-derived cues can simultaneously influence multiple pathways, such as pathways involving YAP and pathways involving lamin-A.

A divergent response in lamin-A and lamin-B has previously been shown in outward nuclear protrusions and in response to stress[165]. In the former case, rupture of lamin B was suggested with cell death in serum gradients. In contrast, our nN arrays show changes in lamin-A and lamin-B in inward nuclear protrusions and do not rupture the nuclear envelope, as demonstrated by retention of heterogeneous nuclear ribonucleoprotein (hnRNP) within the nucleus **(Figure 2.16)**.

Finally, a recovery of the cellular behaviours observed in cells on flat substrates following nN degradation was demonstrated. This is unique to the porous silicon system that has been developed and adds to the limited investigation of biomolecular-based recovery on nN systems.

In this chapter, the peculiarity of the biophysical interactions that occur between sharp, high-aspect ratio nN and multiple cellular organelles was identified, described, and characterised. The next step will be to identify the mechanistic factors that underlie these phenomena, and this will constitute a significant molecular and cellular biology investigation. However, before this is carried out the nN system must be further optimised so that observations such as nuclear deformation and rings of actin can be seen in the majority of cells. A common problem throughout the nN array studies described in this thesis, was a lack of consistency between different production batches of nN arrays, and this may have been due to insufficiently regulated production conditions and inadequate quality control steps during the manufacture of nN.

Further methods of validation should be implemented to ensure homogeneity of manufacture and nN arrays. This should also be carried out for nN functionalisation, and a number of different APTES functionalisation techniques could be tested and explored. Cells

could then be seeded on commercial nN arrays vs. nN arrays produced in the laboratory and results could be compared to ensure that a robust material system has been developed. Once a controlled material system has been produced, an attempt should be made to obtain maximal heterogeneity for changes induced in the cells. For example, cells could be synchronised using methods such as: chemical/pharmacological inhibition of DNA replication/synthesis or mitotic spindle formation; mitogen or growth factor withdrawal; or density arrest by contact inhibition[906]. The question of why only some cells show nuclear deformation might then be answered. Moreover, more decisive results would be obtained if tighter cell homogeneity was ensured.

The Stevens group is currently carrying out further studies. To begin with, the pathways affected by culture on nN are being investigated by global-scale "omics-level" analysis. Secondly, since nN arrays have been shown to interact with the nucleus, the effect of nN on cellular gene expression and epigenetic state is being investigated. Finally, intricate analysis of the cell membrane-nN interface is being conducted using state-of-the-art electron microscopy. Once the mechanistic pathways affected by nN are better understood, nN could be utilised as a tool to direct cell phenotype. For example, the major changes induced by the nN may improve stem cell differentiation. Moreover, a full assessment of the cell-nN interface, along with the effects of the nN on cellular endocytosis will enable nN to be further developed for applications such as cargo delivery and intracellular sensing.

4.2 The laminin β1-fragment and its effect on TGF- β1 signalling and EMT pathways

In chapter 3, the effect of a laminin β1-fragment on TGF-β1 signalling pathways in NMuMG cells was investigated **(Figure 4.2)**. The laminin β1-fragment visually showed altered morphology compared to control cells and cells treated with TGF-β1 **(Figure 4.2A)** and visually minimised TGF-β1 induced E-cadherin down-regulation **(Figure 4.2B)**. However it showed no effect on TGF-β1 induced pSmad3 nuclear translocation **(Figure 4.2C)**; TGF-β1 induced NF-κB signalling **(Figure 4.2D)**; the number of FA formed by TGF-β1 treatment **(Figure 4.2E)**; and no effect on TGF-β1 induced migration **(Figure 4.2F)**.

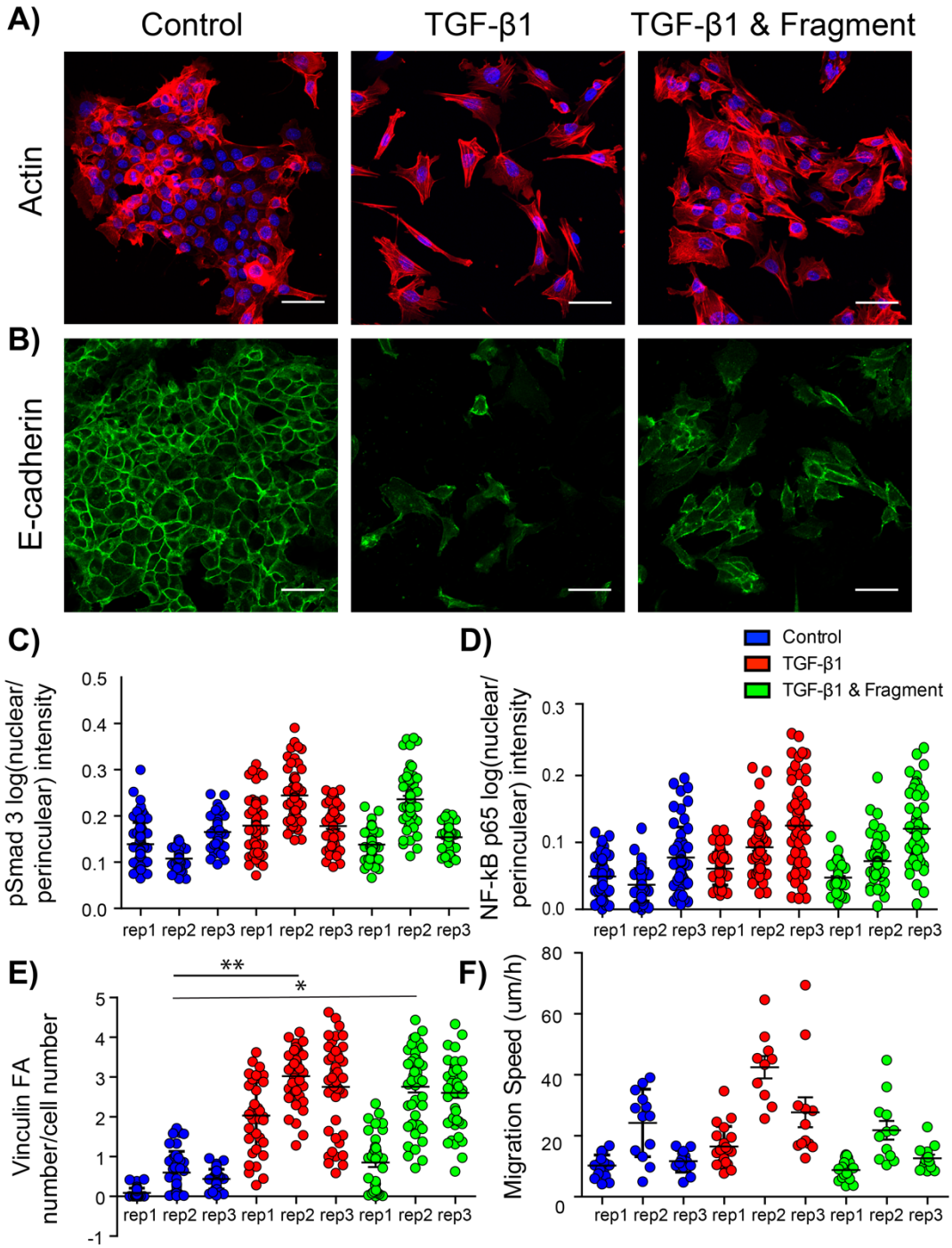


Figure 4.2: Summary of chapter 3 results: The laminin β1-fragment and its effect on TGF-β1 signalling. A-B) TGF-β1 treatment visually showed NMuMg epithelial cells with cell-cell contacts and cortical actin and E-cadherin cell-cell contacts to lose their cell-cell contacts and form more prominent fibrous actin. When the laminin β1-fragment was added with TGF-β1, the phenotypes associated with TGF-β1 treatment were only partially observed. However, HCI analysis showed that the laminin β1-fragment caused no significant change in nuclear translocation of C) pSmad3 and D) NF-κB p65 compared to TGF-β1 and control treatments. E) Moreover, although TGF-β1 +/- laminin β1-fragment increased the number of vinculin containing FA, there was no significant difference between TGF-β1 +/- laminin β1-fragment, and F) there was no significant change in motility on TGF-β1 treatment. Mean +/- S.D, n=3, *p < 0.05, **p < 0.01, ***p < 0.001, scale bars = 50 µm.

The laminin β1-fragment has also been used to treat tissue fibrosis in mouse models[535]. Tissue fibrosis describes the formation of excess fibrous connective tissue as a result of acute or chronic inflammation and is a major cause of organ dysfunction[907]. Indeed, ~45% of deaths in the western world can be accredited to organ or tissue fibrosis[908]. Therapeutic treatment of tissue fibrosis is limited due to its heterogeneity in different tissues, and the lack of understanding of the complex signalling pathways involved. It has been debated as to whether EMT pathways are involved in tissue fibrosis, however it is known that MMP levels are increased in fibrotic tissues[548]. Evidence which supports EMT involvement in tissue fibrosis includes: EMT-TF deletion has been shown to hinder renal fibrosis in a mouse model[544,545]; and the transition of mesothelial cells has been shown to contribute to the build-up of myofibroblasts in the tissue interstitium during peritoneal fibrosis[909–911].

It has been suggested that reducing MMP activity may prevent BM breakdown and EMT, thus inhibiting fibrosis. The Stevens group recently immobilised the laminin β1-fragment onto a flexible electrospun poly(ε-caprolactone) (PCL) membrane, which can directly interface with epithelial cells and tissues *in vitro* and *in vivo* to inhibit MMP-2 expression and activity. This functionalised membrane was shown to decrease fibrosis-associated matrix deposition in peritoneal tissue and to rescue the peritoneal BM in a mouse model of TGF-β1-induced peritoneal fibrosis[535]. A next step could be to assess the therapeutic properties of the laminin β1-fragment functionalised scaffold in a range of different tissues, given the broad range of tissue types in which the laminin β1-chain is found, with the eventual aim of developing a human therapeutic agent. However, the mechanistic pathways that the laminin β1-fragment affects should first be fully confirmed.

The complex signalling involved in tissue fibrosis remains to be elucidated, and an understanding of these processes will help develop new tissue fibrosis therapies. It has been shown that the laminin β1-fragment interferes with TGF- β1 induced tissues fibrosis[535], and this chapter has further investigated the signalling pathways involved, as well as how the laminin-β1 affects/does not affect these signalling pathways.

In addition, the work carried out in this chapter has provided a system to assess TGF-β1 and EMT signalling pathways. The HCI analysis carried out in this chapter could be applied to

rapidly study EMT in multiple modified systems, for example in cultured bronchial epithelial cells from patients with pulmonary fibrosis vs. normal volunteers, and patients with epithelial cancers vs. normal volunteers. TGF-β exerts dual and opposing roles in cancer progression, from cytostatic and apoptotic tumour-suppressive roles in early stage tumours, to proliferative, invasive, angiogenic, and oncogenic roles in advanced cancer[912]. It has been argued that TGF-β not only enables primary carcinoma cell metastasis but also facilitates the generation of cells with both a mesenchymal and a stem-cell-like phenotype (cancer stem cells (CSC)) which then leads to the formation of secondary tumours with epithelial characteristics[649,913–915]. A detailed understanding of TGF-β signalling in cancer is therefore required to design successful therapeutic approaches. Indeed, a Smad inhibitor was recently used to induce liver CSC differentiation, resulting in significant chemosensitisation, which could be an effective strategy to target CSCs via TGF-β pathways[916]. The HCI system could be used to screen a variety of Smad inhibitors to assess their effect on TGF-β signalling pathways and thus their potential in CSC treatment.

The HCI system could also be used to assess the effects of other "cryptic" protein fragments on TGF-β1 and EMT signalling pathways. As well as the laminin β1-fragment, other "cryptic" protein fragments generated by MMP proteolysis of the BM have been identified. These fragments are also "cryptic" in the sense that they only become bioactive once they have been cleaved from the intact BM[576,854–857]. These fragments have been shown to have effects on cell migration[624,917,918], MMP expression and tumour angiogenesis[919], tissue fibrosis[535,890,920], and vascularisation[921,922]. Cryptic protein fragments have mainly been made *in vitro*, incubating recombinant collagen type IV and laminin isoforms with specific MMPs. It is difficult to use this technique when it comes to soluble collagen type IV α-chains, however. These chains are sensitive to thermal denaturation, and they are more easily degraded by proteolysis than when they are part of a collagen network[923]. Interestingly, several collagen type IV fragments have been shown to be proteolytically released *in vivo*[890,920]; as well as HUIV26 collagen fragments[922], arresten[924], canstatin[885] and tumstatin[884,886]; and laminin-332 fragments[925] and laminin-511 fragments[918]. The HCI and Western blots described in this chapter could be used to assess the effect of these BM fragments on TGF-β1 signalling and EMT in NMuMG cells and other epithelial cell types. The BM fragments which produce

interesting results could then be incorporated into a synthetic PCL matrix and their ability to rescue peritoneal tissue from the effects of TGF-β1 could be assessed.

4.3 Concluding remarks

This thesis has provided new perspectives into how cells can respond to their extracellular environment. Porous silicon nN arrays have been used as a tool to manipulate cell mechanobiology, demonstrating an increase in lamin-A, but not lamin-B levels at sites of inward nuclear impingement as well as a decoupling of cell spread area and YAP activity and localisation. Moreover, a laminin β1-fragment produced by MMP processing of the BM has been shown to not interfere with TFβ-1 signalling pathways and EMT progression when assessed by HCI analysis. These findings have provided insight into the complex signalling pathways of a cell with its extracellular surroundings and could be used to design novel materials with a therapeutic function.

5 References

1. Bissell, M. J. & Aggeler, J. Dynamic reciprocity: how do extracellular matrix and hormones direct gene expression? *Prog Clin Biol Res* **249,** 251–262 (1987).
2. Humphrey, J. D., Dufresne, E. R. & Schwartz, M. A. Mechanotransduction and extracellular matrix homeostasis. *Nat. Rev. Mol. Cell Biol.* **15,** 802–812 (2014).
3. Lu, P., Takai, K., Weaver, V. M. & Werb, Z. Extracellular matrix degradation and remodeling in development and disease. *Cold Spring Harb. Perspect. Biol.* **3,** a005058–a005058 (2011).
4. Dupont, S. *et al.* Role of YAP/TAZ in mechanotransduction. *Nature* **474,** 179–83 (2011).
5. Schwartz, M. A., Schaller, M. D. & Ginsberg, M. H. Integrins: Emerging paradigms of signal transduction. *Annu Rev Cell Dev Biol* **11,** 549–599 (1995).
6. Ciobanasu, C., Faivre, B. & Le Clainche, C. Integrating actin dynamics, mechanotransduction and integrin activation: The multiple functions of actin binding proteins in focal adhesions. *Eur. J. Cell Biol.* **92,** 339–348 (2013).
7. Muschler, J. & Streuli, C. H. Cell-matrix interactions in mammary gland development and breast cancer. *Cold Spring Harb. Perspect. Biol.* **2,** a003202 (2010).
8. Schwartz, M. A. Integrins and extracellular matrix in mechanotransduction. *Cold Spring Harb. Perspect. Biol.* **2,** a005066–a005066 (2010).
9. Nardone, G. *et al.* YAP regulates cell mechanics by controlling focal adhesion assembly. *Nat. Commun.* **8,** 15321 (2017).
10. Swift, J. *et al.* Nuclear lamin-A scales with tissue stiffness and enhances matrix-directed differentiation. *Science (80-.).* **341,** 1240104–1240104 (2013).
11. Mecham, R. P. in *Current Protocols in Cell Biology* **Chapter 10,** Unit 10.1 (John Wiley & Sons, Inc., 2012).
12. Naba, A. *et al.* The matrisome: In silico definition and in vivo characterization by proteomics of normal and tumor extracellular matrices. *Mol. Cell. Proteomics* **11,** M111.014647 (2012).
13. Rowe, R. G. & Weiss, S. J. Breaching the basement membrane: who, when and how? *Trends Cell Biol.* **18,** 560–574 (2008).
14. Schaefer, L. & Schaefer, R. M. Proteoglycans: From structural compounds to signaling molecules. *Cell Tissue Res.* **339,** 237–246 (2010).
15. Rozario, T. & DeSimone, D. W. The extracellular matrix in development and morphogenesis: A dynamic view. *Dev. Biol.* **341,** 126–140 (2010).
16. Paulsson, M. Basement membrane proteins: Structure, assembly, and cellular interactions. *Crit. Rev. Biochem. Mol. Biol.* **27,** 93–127 (1992).
17. Yurchenco, P. D. & Ruben, G. C. Basement membrane structure in situ: Evidence for lateral associations in the type IV collagen network. *J. Cell Biol.* **105,** 2559–2568 (1987).
18. Horejs, C. M. Basement membrane fragments in the context of the epithelial-to-mesenchymal transition. *Eur. J. Cell Biol.* **95,** 427–440 (2016).
19. Hynes, R. O. & Naba, A. Overview of the matrisome: An inventory of extracellular matrix constituents and functions. *Cold Spring Harb. Perspect. Biol.* **4,** a004903–a004903 (2012).
20. Mouw, J. K., Ou, G. & Weaver, V. M. Extracellular matrix assembly: A multiscale deconstruction. *Nat. Rev. Mol. Cell Biol.* **15,** 771–785 (2014).
21. Arribas, S. M., Hinek, A. & González, M. C. Elastic fibres and vascular structure in hypertension. *Pharmacol. Ther.* **111,** 771–791 (2006).

22. Kielty, C. M. Elastic fibres in health and disease. *Expert Rev. Mol. Med.* **8,** 1–23 (2006).
23. Uzer, G. *et al.* Cell mechanosensitivity to extremely low-magnitude signals is enabled by a LINCed nucleus. *Stem Cells* **33,** 2063–2076 (2015).
24. Ramovs, V., te Molder, L. & Sonnenberg, A. The opposing roles of laminin-binding integrins in cancer. *Matrix Biol.* **57–58,** 213–243 (2017).
25. Hohenester, E. Signalling complexes at the cell-matrix interface. *Curr. Opin. Struct. Biol.* **29,** 10–16 (2014).
26. Hood, J. D. & Cheresh, D. A. Role of integrins in cell invasion and migration. *Nat. Rev. Cancer* **2,** 91–100 (2002).
27. Xiong, J.-P. Crystal structure of the extracellular segment of integrin alpha V beta 3. *Science (80-.).* **294,** 339–345 (2001).
28. Partridge, A. W., Liu, S., Kim, S., Bowie, J. U. & Ginsberg, M. H. Transmembrane domain helix packing stabilizes integrin αIIbβ3 in the low affinity state. *J. Biol. Chem.* **280,** 7294–7300 (2005).
29. Shimaoka, M., Takagi, J. & Springer, T. A. Conformational regulation of integrin structure and function. *Annu Rev Biophys Biomol Struct* **31,** 485–516 (2002).
30. Calderwood, D. A. Integrin activation. *J. Cell Sci.* **117,** 657–666 (2004).
31. Banno, A. & Ginsberg, M. H. Integrin activation. *Biochem Soc Trans* **36,** 229–234 (2008).
32. Takagi, J., Petre, B. M., Walz, T. & Springer, T. A. Global conformational rearrangements in integrin extracellular domains in outside-in and inside-out signaling. *Cell* **110,** 599–611 (2002).
33. Puklin-Faucher, E., Gao, M., Schulten, K. & Vogel, V. How the headpiece hinge angle is opened: New insights into the dynamics of integrin activation. *J. Cell Biol.* **175,** 349–360 (2006).
34. Hynes, R. O. Integrins: Bidirectional, allosteric signaling machines. *Cell* **110,** 673–687 (2002).
35. Kim, C., Ye, F. & Ginsberg, M. H. Regulation of integrin activation. *Annu. Rev. Cell Dev. Biol.* **27,** 321–345 (2011).
36. Ye, F., Snider, A. K. & Ginsberg, M. H. Talin and kindlin: The one-two punch in integrin activation. *Front. Med. China* **8,** 6–16 (2014).
37. Legate, K. R., Wickström, S. A. & Fässler, R. Genetic and cell biological analysis of integrin outside-in signaling. *Genes Dev.* **23,** 397–418 (2009).
38. Calderwood, D. A. *et al.* The talin head domain binds to integrin β subunit cytoplasmic tails and regulates integrin activation. *J. Biol. Chem.* **274,** 28071–28074 (1999).
39. Wegener, K. L. *et al.* Structural basis of integrin activation by talin. *Cell* **128,** 171–182 (2007).
40. Wegener, K. L. & Campbell, I. D. Transmembrane and cytoplasmic domains in integrin activation and protein-protein interactions (review). *Mol. Membr. Biol.* **25,** 376–387 (2008).
41. Giancotti, F. & Ruoslahti, E. Integrin signaling. *Science (80-.).* **285,** 1028–1032 (1999).
42. Shattil, S. J. & Newman, P. J. Integrins: Dynamic scaffolds for adhesion and signaling in platelets. *Blood* **104,** 1606–1615 (2004).
43. Berrier, A. L., Mastrangelo, A. M., Downward, J., Ginsberg, M. & LaFlamme, S. E. Activated R-Ras, Rac1, PI 3-kinase and PKCε can each restore cell spreading inhibited by isolated integrin β1 cytoplasmic domains. *J. Cell Biol.* **151,** 1549–1560 (2000).
44. Bodeau, A. L., Berrier, A. L., Mastrangelo, A. M., Martinez, R. & LaFlamme, S. E. A functional comparison of mutations in integrin beta cytoplasmic domains: Effects on

the regulation of tyrosine phosphorylation, cell spreading, cell attachment and beta1 integrin conformation. *J. Cell Sci.* **114,** 2795–2807 (2001).
45. Díaz-González, F., Forsyth, J., Steiner, B. & Ginsberg, M. H. Trans-dominant inhibition of integrin function. *Mol. Biol. Cell* **7,** 1939–1951 (1996).
46. Kim, M., Carman, C. V & Springer, T. A. Bidirectional transmembrane signaling by cytoplasmic domain separation in integrins. *Science (80-.).* **301,** 1720–1725 (2003).
47. LaFlamme, S. E., Akiyama, S. K. & Yamada, K. M. Regulation of fibronectin receptor distribution. *J. Cell Biol.* **117,** 437–447 (1992).
48. LaFlamme, S. E., Thomas, L. A., Yamada, S. S. & Yamada, K. M. Single subunit chimeric integrins as mimics and inhibitors of endogenous integrin functions in receptor localization, cell spreading and migration, and matrix assembly. *J. Cell Biol.* **126,** 1287–1298 (1994).
49. Ylänne, J. *et al.* Distinct functions of integrin alpha and beta subunit cytoplasmic domains in cell spreading and formation of focal adhesions. *J. Cell Biol.* **122,** 223–233 (1993).
50. Zhu, J. *et al.* Requirement of α and β subunit transmembrane helix separation for integrin outside-in signaling. *Blood* **110,** 2475–2483 (2007).
51. Miyamoto, S., Akiyama, S. K. & Yamada, K. M. Synergistic roles for receptor occupancy and aggregation in integrin transmembrane function. *Science* **267,** 883–5 (1995).
52. Shattil, S. J., Kim, C. & Ginsberg, M. H. The final steps of integrin activation: the end game. *Nat. Rev. Mol. Cell Biol.* **11,** 288–300 (2010).
53. Zaidel-Bar, R., Itzkovitz, S., Ma'ayan, A., Iyengar, R. & Geiger, B. Functional atlas of the integrin adhesome. *Nat. Cell Biol.* **9,** 858–867 (2007).
54. Deakin, N. O. & Turner, C. E. Paxillin comes of age. *J. Cell Sci.* **121,** 2435–2444 (2008).
55. Horton, E. R. *et al.* Definition of a consensus integrin adhesome and its dynamics during adhesion complex assembly and disassembly. *Nat. Cell Biol.* **17,** 1577–1587 (2015).
56. Webb, D. J., Parsons, J. T. & Horwitz, A. F. Adhesion assembly, disassembly and turnover in migrating cells – over and over and over again. *Nat. Cell Biol.* **4,** E97–E100 (2002).
57. Zaidel-Bar, R., Cohen, M., Addadi, L. & Geiger, B. Hierarchical assembly of cell-matrix adhesion complexes. *Biochem. Soc. Trans.* **32,** 416–20 (2004).
58. Choi, C. K. *et al.* Actin and alpha-actinin orchestrate the assembly and maturation of nascent adhesions in a myosin II motor-independent manner. *Nat. Cell Biol.* **10,** 1039–50 (2008).
59. Geiger, B., Bershadsky, A., Pankov, R. & Yamada, K. M. Transmembrane crosstalk between the extracellular matrix--cytoskeleton crosstalk. *Nat. Rev. Mol. Cell Biol.* **2,** 793–805 (2001).
60. Chen, H. C. *et al.* Interaction of focal adhesion kinase with cytoskeletal protein talin. *J. Biol. Chem.* **270,** 16995–16999 (1995).
61. Zhang, X. *et al.* Talin depletion reveals independence of initial cell spreading from integrin activation and traction. *Nat. Cell Biol.* **10,** 1062–1068 (2008).
62. Frame, M. C., Patel, H., Serrels, B., Lietha, D. & Eck, M. J. The FERM domain: organizing the structure and function of FAK. *Nat. Rev. Mol. Cell Biol.* **11,** 802–814 (2010).
63. Lawson, C. *et al.* FAK promotes recruitment of talin to nascent adhesions to control cell motility. *J. Cell Biol.* **196,** 223–232 (2012).
64. Mitra, S. K., Hanson, D. A. & Schlaepher, D. D. Focal adhesion kinase: In command and control of cell motility. *Mol Cell Bio* **6,** 56–68 (2005).

65. Jiang, G., Giannone, G., Critchley, D. R., Fukumoto, E. & Sheetz, M. P. Two-piconewton slip bond between fibronectin and the cytoskeleton depends on talin. *Nature* **424,** 334–337 (2003).
66. Izard, T. *et al.* Vinculin activation by talin through helical bundle conversion. *Nature* **427,** 171–175 (2004).
67. Chen, H., Cohen, D. M., Choudhury, D. M., Kioka, N. & Craig, S. W. Spatial distribution and functional significance of activated vinculin in living cells. *J. Cell Biol.* **169,** 459–470 (2005).
68. Giannone, G., Jiang, G., Sutton, D. H., Critchley, D. R. & Sheetz, M. P. Talin1 is critical for force-dependent reinforcement of initial integrin-cytoskeleton bonds but not tyrosine kinase activation. *J. Cell Biol.* **163,** 409–419 (2003).
69. Carisey, A. & Ballestrem, C. Vinculin, an adapter protein in control of cell adhesion signalling. *Eur. J. Cell Biol.* **90,** 157–63 (2011).
70. Turner, C. E., Glenney, J. R. & Burridge, K. Paxillin: a new vinculin-binding protein present in focal adhesions. *J. Cell Biol.* **111,** 1059–68 (1990).
71. Ridley, A. J. Cell migration: integrating signals from front to back. *Science (80-.).* **302,** 1704–1709 (2003).
72. Lauffenburger, D. A. & Horwitz, A. F. Cell migration: A physically integrated molecular process. *Cell* **84,** 359–369 (1996).
73. Om Alblazi, K. M. & Siar, C. H. Cellular protrusions - Lamellipodia, filopodia, invadopodia and podosomes - and their roles in progression of orofacial tumours: Current understanding. *Asian Pacific J. Cancer Prev.* **16,** 2187–2191 (2015).
74. Dosremedios, C. G. *et al.* Actin binding proteins: Regulation of cytoskeletal microfilaments. *Physiol Rev* **83,** 433–473 (2003).
75. Puius, Y. A., Mahoney, N. M. & Almo, S. C. The modular structure of actin-regulatory proteins. *Curr. Opin. Cell Biol.* **10,** 23–34 (1998).
76. Raftopoulou, M. & Hall, A. Cell migration: Rho GTPases lead the way. *Dev. Biol.* **265,** 23–32 (2004).
77. Ridley, A. J. Rho GTPases and actin dynamics in membrane protrusions and vesicle trafficking. *Trends Cell Biol.* **16,** 522–529 (2006).
78. Nobes, C. D. & Hall, A. Rho, Rac, and Cdc42 GTPases regulate the assembly of multimolecular focal complexes associated with actin stress fibers, lamellipodia, and filopodia. *Cell* **81,** 53–62 (1995).
79. Murphy, D. A. & Courtneidge, S. A. The 'ins' and 'outs' of podosomes and invadopodia: characteristics, formation and function. *Nat. Rev. Mol. Cell Biol.* **12,** 413–26 (2011).
80. Mattila, P. K. & Lappalainen, P. Filopodia: Molecular architecture and cellular functions. *Nat. Rev. Mol. Cell Biol.* **9,** 446–454 (2008).
81. Chhabra, E. S. & Higgs, H. N. The many faces of actin: Matching assembly factors with cellular structures. *Nat. Cell Biol.* **9,** 1110–1121 (2007).
82. Dikovsky, D., Bianco-Peled, H. & Seliktar, D. Defining the role of matrix compliance and proteolysis in three-dimensional cell spreading and remodeling. *Biophys. J.* **94,** 2914–25 (2008).
83. Raucher, D. & Sheetz, M. P. Cell spreading and lamellipodial extension rate is regulated by membrane tension. *J. Cell Biol.* **148,** 127–136 (2000).
84. Gimona, M., Buccione, R., Courtneidge, S. A. & Linder, S. Assembly and biological role of podosomes and invadopodia. *Curr. Opin. Cell Biol.* **20,** 235–241 (2008).
85. Luxenburg, C. *et al.* The architecture of the adhesive apparatus of cultured osteoclasts:

From podosome formation to sealing zone assembly. *PLoS One* **2,** e179 (2007).
86. Gawden-Bone, C. *et al.* Dendritic cell podosomes are protrusive and invade the extracellular matrix using metalloproteinase MMP-14. *J. Cell Sci.* **123,** 1427–1437 (2010).
87. Furlan, F. *et al.* Urokinase plasminogen activator receptor affects bone homeostasis by regulating osteoblast and osteoclast function. *J. Bone Miner. Res.* **22,** 1387–1396 (2007).
88. Weaver, A. M. Invadopodia. *Curr. Biol.* **18,** R362–R364 (2008).
89. Schoumacher, M., Goldman, R. D., Louvard, D. & Vignjevic, D. M. Actin, microtubules, and vimentin intermediate filaments cooperate for elongation of invadopodia. *J. Cell Biol.* **189,** 541–556 (2010).
90. Buccione, R., Caldieri, G. & Ayala, I. Invadopodia: Specialized tumor cell structures for the focal degradation of the extracellular matrix. *Cancer Metastasis Rev.* **28,** 137–149 (2009).
91. Stylli, S. S., Kaye, A. H. & Lock, P. Invadopodia: At the cutting edge of tumour invasion. *J. Clin. Neurosci.* **15,** 725–737 (2008).
92. Clark, E. S. & Weaver, A. M. A new role for cortactin in invadopodia: Regulation of protease secretion. *Eur. J. Cell Biol.* **87,** 581–590 (2008).
93. Krause, M. & Gautreau, A. Steering cell migration: Lamellipodium dynamics and the regulation of directional persistence. *Nat. Rev. Mol. Cell Biol.* **15,** 577–590 (2014).
94. Gupton, S. L. & Gertler, F. B. Filopodia: The Fingers That Do the Walking. *Sci. STKE* **2007,** re5-re5 (2007).
95. Goh, W. I. *et al.* Rif-mDia1 interaction is involved in filopodium formation independent of Cdc42 and rac effectors. *J. Biol. Chem.* **286,** 13681–13694 (2011).
96. Pellegrin, S. & Mellor, H. The Rho family GTPase Rif induces filopodia through mDia2. *Curr. Biol.* **15,** 129–133 (2005).
97. Carlier, M. F., Ducruix, A. & Pantaloni, D. Signalling to actin: The Cdc42-N-WASP-Arp2/3 connection. *Chem. Biol.* **6,** R235–R240 (1999).
98. Partridge, M. A. & Marcantonio, E. E. Initiation of attachment and generation of mature focal adhesions by integrin-containing filopodia in cell spreading. *Mol. Biol. Cell* **17,** 4237–48 (2006).
99. Galbraith, C. G., Yamada, K. M. & Galbraith, J. A. Polymerizing actin fibers position integrins primed to probe for adhesion sites. *Science* **315,** 992–5 (2007).
100. Steketee, M. B. & Tosney, K. W. Three functionally distinct adhesions in filopodia: Shaft adhesions control lamellar extension. *J. Neurosci.* **22,** 8071–83 (2002).
101. Vasioukhin, V., Bauer, C., Yin, M. & Fuchs, E. Directed actin polymerization is the driving force for epithelial cell-cell adhesion. *Cell* **100,** 209–219 (2000).
102. Campa, C. C., Ciraolo, E., Ghigo, A., Germena, G. & Hirsch, E. Crossroads of PI3K and Rac pathways. *Small GTPases* **6,** 71–80 (2015).
103. Amaro, H., Russo, N. F. & Johnson, J. Family and work predictors of psychological well-being among hispanic women professionals. *Psychol. Women Q.* **11,** 505–521 (1987).
104. Quintavalle, M., Elia, L., Condorelli, G. & Courtneidge, S. A. MicroRNA control of podosome formation in vascular smooth muscle cells in vivo and in vitro. *J. Cell Biol.* **189,** 13–22 (2010).
105. Varon, C. *et al.* Transforming growth factor beta induces rosettes of podosomes in primary aortic endothelial cells. *Society* **26,** 3582–3594 (2006).
106. Gatesman, A., Walker, V. G., Baisden, J. M., Weed, S. a & Flynn, D. C. Protein Kinase C

α Activates c-Src and Induces Podosome Formation via Protein Kinase C ␣ Activates c-Src and Induces Podosome Formation via AFAP-110. *Mol. Cell. Biol.* **24,** 7578–7597 (2004).
107. Yamaguchi, H. & Condeelis, J. Regulation of the actin cytoskeleton in cancer cell migration and invasion. *Biochim. Biophys. Acta - Mol. Cell Res.* **1773,** 642–652 (2007).
108. Tatin, F., Varon, C., Génot, E. & Moreau, V. A signalling cascade involving PKC, Src and Cdc42 regulates podosome assembly in cultured endothelial cells in response to phorbol ester. *J. Cell Sci.* **119,** 769–781 (2006).
109. Diaz, B. *et al.* Tks5-dependent, Nox-mediated generation of reactive oxygen species is necessary for invadopodia formation. *Sci. Signal.* **2,** ra53-ra53 (2009).
110. Destaing, O. *et al.* β1A integrin is a master regulator of invadosome organization and function. *Mol. Biol. Cell* **21,** 4108–4119 (2010).
111. Xin, M. *et al.* MicroRNAs miR-143 and miR-145 modulate cytoskeletal dynamics and responsiveness of smooth muscle cells to injury. *Genes Dev.* **23,** 2166–2178 (2009).
112. Cordes, K. R. *et al.* miR-145 and miR-143 regulate smooth muscle cell fate and plasticity. *Nature* **460,** 705–710 (2009).
113. Artym, V. V., Zhang, Y., Seillier-Moiseiwitsch, F., Yamada, K. M. & Mueller, S. C. Dynamic interactions of cortactin and membrane type 1 matrix metalloproteinase at invadopodia: Defining the stages of invadopodia formation and function. *Cancer Res.* **66,** 3034–3043 (2006).
114. Linder, S. The matrix corroded: podosomes and invadopodia in extracellular matrix degradation. *Trends Cell Biol.* **17,** 107–117 (2007).
115. Chrzanowska-Wodnicka, M. & Burridge, K. Rho-stimulated contractility drives the formation of stress fibers and focal adhesions. *J. Cell Biol.* **133,** 1403–1415 (1996).
116. Tojkander, S., Gateva, G. & Lappalainen, P. Actin stress fibers - assembly, dynamics and biological roles. *J. Cell Sci.* **125,** 1855–1864 (2012).
117. Gabbiani, G., Hirschel, B. J., Ryan, G. B., Statkov, P. R. & Majno, G. Granulation tissue as a contractile organ. A study of structure and function. *J. Exp. Med.* **135,** 719–34 (1972).
118. Tomasek, J. J., Gabbiani, G., Hinz, B., Chaponnier, C. & Brown, R. a. Myofibroblasts and mechano-regulation of connective tissue remodelling. *Nat. Rev. Mol. Cell Biol.* **3,** 349–63 (2002).
119. Wong, a J., Pollard, T. D. & Herman, I. M. Actin filament stress fibers in vascular endothelial cells in vivo. *Science (80-.).* **219,** 867–869 (1983).
120. White, G. E., Gimbrone Jr., M. A. & Fujiwara, K. Factors influencing the expression of stress fibers in vascular endothelial cells in situ. *J. Cell Biol.* **97,** 416–24. (1983).
121. Richards, T. A. & Cavalier-Smith, T. Myosin domain evolution and the primary divergence of eukaryotes. *Nature* **436,** 1113–8 (2005).
122. Goodson, H. V & Spudich, J. A. Molecular evolution of the myosin family: Relationships derived from comparisons of amino acid sequences. *Proc. Natl. Acad. Sci.* **90,** 659–663 (1993).
123. Tuxworth, R. I. & Titus, M. a. Unconventional myosins: Anchors in the membrane traffic relay. *Traffic* **1,** 11–18 (2000).
124. Krendel, M. Myosins: Tails (and heads) of functional diversity. *Physiology* **20,** 239–251 (2005).
125. De Lozanne, A. & Spudich, J. A. Disruption of the Dictyostelium myosin heavy chain gene by homologous recombination. *Science (80-.).* **236,** 1086–1091 (1987).

126. Knecht, D. A. & Loomis, W. F. Antisense RNA inactivation of myosin heavy chain gene expression in Dictyostelium discoideum. *Science* **236,** 1081–6 (1987).
127. Syamaladevi, D. P., Spudich, J. A. & Sowdhamini, R. Structural and functional insights on the myosin superfamily. *Bioinform. Biol. Insights* **6,** 11–21 (2012).
128. Lodish, H., Berk, A. & Zipursky, S. Myosin: The actin motor protein. (2000).
129. Stewart, C. L., Roux, K. J. & Burke, B. Blurring the boundary: The nuclear envelope extends its reach. *Science (80-.).* **318,** 1408–1412 (2007).
130. Crisp, M. *et al.* Coupling of the nucleus and cytoplasm. *J. Cell Biol.* **172,** 41–53 (2006).
131. Khatau, S. B. *et al.* A perinuclear actin cap regulates nuclear shape. *Proc. Natl. Acad. Sci. U. S. A.* **106,** 19017–19022 (2009).
132. Luxton, G. G. & Starr, D. A. KASHing up with the nucleus: Novel functional roles of KASH proteins at the cytoplasmic surface of the nucleus. *Curr. Opin. Cell Biol.* **28,** 69–75 (2014).
133. Dahl, K. N. & Kalinowski, A. Nucleoskeleton mechanics at a glance. *J. Cell Sci.* **124,** 675–678 (2011).
134. Starr, D. a & Han, M. Role of ANC-1 in tethering nuclei to the actin cytoskeleton. *Science (80-.).* **298,** 406–409 (2002).
135. Morris, N. R. Nuclear positioning: The means is at the ends. *Curr. Opin. Cell Biol.* **15,** 54–59 (2002).
136. Gundersen, G. G. & Worman, H. J. Nuclear positioning. *Cell* **152,** 1376–1389 (2013).
137. Tapley, E. C. & Starr, D. A. Connecting the nucleus to the cytoskeleton by SUN-KASH bridges across the nuclear envelope. *Curr. Opin. Cell Biol.* **25,** 57–62 (2013).
138. Worman, H. J. & Gundersen, G. G. Here come the SUNs: A nucleocytoskeletal missing link. *Trends Cell Biol.* **16,** 67–69 (2006).
139. Ketema, M. *et al.* Requirements for the localization of nesprin-3 at the nuclear envelope and its interaction with plectin. *J. Cell Sci.* **120,** 3384–3394 (2007).
140. Wilhelmsen, K. *et al.* Nesprin-3, a novel outer nuclear membrane protein, associates with the cytoskeletal linker protein plectin. *J. Cell Biol.* **171,** 799–810 (2005).
141. Burke, B. & Stewart, C. L. The nuclear lamins: flexibility in function. *Nat Rev Mol Cell Biol* **14,** 13–24 (2013).
142. Dahl, K. N., Kahn, S. M., Wilson, K. L. & Discher, D. E. The nuclear envelope lamina network has elasticity and a compressibility limit suggestive of a molecular shock absorber. *J Cell Sci* **117,** 4779–4786 (2004).
143. Pajerowski, J. D., Dahl, K. N., Zhong, F. L., Sammak, P. J. & Discher, D. E. Physical plasticity of the nucleus in stem cell differentiation. *Proc. Natl. Acad. Sci. U. S. A.* **104,** 15619–15624 (2007).
144. Lammerding, J. *et al.* Lamins A and C but not lamin B1 regulate nuclear mechanics. *J. Biol. Chem.* **281,** 25768–25780 (2006).
145. De vos, W. H. *et al.* Repetitive disruptions of the nuclear envelope invoke temporary loss of cellular compartmentalization in laminopathies. *Hum. Mol. Genet.* **20,** 4175–4186 (2011).
146. Gant, T. M. & Wilson, K. L. Nuclear assembly. *Annu. Rev. Cell Dev. Biol* **13,** 669–95 (1997).
147. Lopez-Soler, R. I., Moir, R. D., Spann, T. P., Stick, R. & Goldman, R. D. A role for nuclear lamins in nuclear envelope assembly. *J. Cell Biol.* **154,** 61–70 (2001).
148. Gerace, L. & Blobel, G. The nuclear envelope lamina is reversibly depolymerized during mitosis. *Cell* **19,** 277–287 (1980).

149. Shimi, T. *et al.* The A- and B-type nuclear lamin networks: Microdomains involved in chromatin organization and transcription. *Genes Dev.* **22,** 3409–3421 (2008).
150. Okumura, K., Hosoe, Y. & Nakajima, N. Zic1 is a transcriptional repressor through the lamin A / C promoter and has an intrinsic repressive domain. *J. Heal. Sci.* **50,** 423–427 (2004).
151. Okumura, K., Hosoe, Y. & Nakajima, N. c-Jun and Sp1 family are critical for retinoic acid induction of the lamin A/C retinoic acid-responsive element. *Biochem. Biophys. Res. Commun.* **320,** 487–492 (2004).
152. Olins, A. L. *et al.* Nuclear envelope and chromatin compositional differences comparing undifferentiated and retinoic acid- and phorbol ester-treated HL-60 cells. *Exp. Cell Res.* **268,** 115–127 (2001).
153. Shin, J. *et al.* Lamins regulate cell trafficking and lineage maturation of adult human hematopoietic cells. *Proc. Natl. Acad. Sci. U. S. A.* **110,** 18892–18897 (2013).
154. Sullivan, T. *et al.* Loss of A-type lamin expression compromises nuclear envelope integrity leading to muscular dystrophy. *J. Cell Biol.* **147,** 913–919 (1999).
155. Kubben, N. *et al.* Post-natal myogenic and adipogenic developmental: Defects and metabolic impairment upon loss of A-type lamins. *Nucleus* **2,** 195–207 (2011).
156. Jahn, D. *et al.* A truncated lamin A in the Lmna -/- mouse line: Implications for the understanding of laminopathies. *Nucleus* **3,** 463–74 (2012).
157. Worman, H. J. Nuclear lamins and laminopathies. *J. Pathol.* **226,** 316–325 (2012).
158. Schreiber, K. H. & Kennedy, B. K. When lamins go bad: Nuclear structure and disease. *Cell* **152,** 1365–1375 (2013).
159. Kim, Y. *et al.* Mouse B-type lamins are required for proper organogenesis but not by embryonic stem cells. *Science (80-.).* **334,** 1706–1710 (2011).
160. Kim, Y., Zheng, X. & Zheng, Y. Proliferation and differentiation of mouse embryonic stem cells lacking all lamins. *Cell Res.* **23,** 1420–1423 (2013).
161. Dittmer, T. & Misteli, T. The lamin protein family. *Genome Biol.* **12,** 222 (2011).
162. Dechat, T., Adam, S. A., Taimen, P., Shimi, T. & Goldman, R. D. Nuclear lamins. *Cold Spring Harb. Perspect. Biol.* **2,** a000547–a000547 (2010).
163. Ho, C. Y. & Lammerding, J. Lamins at a glance. *J. Cell Sci.* **125,** 2087–2093 (2012).
164. Dechat, T. *et al.* Nuclear lamins: Major factors in the structural organization and function of the nucleus and chromatin. *Genes Dev.* **22,** 832–853 (2008).
165. Harada, T. *et al.* Nuclear lamin stiffness is a barrier to 3D migration, but softness can limit survival. *J. Cell Biol.* **204,** 669–682 (2014).
166. Engler, A. J., Sen, S., Sweeney, H. L. & Discher, D. E. Matrix elasticity directs stem cell lineage specification. *Cell* **126,** 677–689 (2006).
167. Dahl, K. N., Engler, A. J., Pajerowski, J. D. & Discher, D. E. Power-law rheology of isolated nuclei with deformation mapping of nuclear substructures. *Biophys J* **89,** 2855–64 (2005).
168. Friedl, P., Wolf, K. & Lammerding, J. Nuclear mechanics during cell migration. *Curr. Opin. Cell Biol.* **23,** 55–64 (2011).
169. Davidson, P. M., Denais, C., Bakshi, M. C. & Lammerding, J. Nuclear deformability constitutes a rate-limiting step during cell migration in 3-D environments. *Cell. Mol. Bioeng.* **7,** 293–306 (2014).
170. Lammerding, J. *et al.* Lamin A / C deficiency causes Tema Grupo defective nuclear mechanics and mechanotransduction. *J. Clin. Invest.* **113,** 370–378 (2004).
171. Ho, C. Y., Jaalouk, D. E., Vartiainen, M. K. & Lammerding, J. Lamin A/C and emerin

regulate MKL1-SRF activity by modulating actin dynamics. *Nature* **497,** 507–11 (2013).
172. Belt, E. J. T. *et al.* Loss of lamin A/C expression in stage II and III colon cancer is associated with disease recurrence. *Eur. J. Cancer* **47,** 1837–1845 (2011).
173. Stecklein, S. R. *et al.* BRCA1 and HSP90 cooperate in homologous and non-homologous DNA double-strand-break repair and G2/M checkpoint activation. *Proc. Natl. Acad. Sci.* **109,** 13650–13655 (2012).
174. Wang, N., Tytell, J. D. & Ingber, D. E. Mechanotransduction at a distance: Mechanically coupling the extracellular matrix with the nucleus. *Nat. Rev. Mol. Cell Biol.* **10,** 75–82 (2009).
175. Fedorchak, G. R., Kaminski, A. & Lammerding, J. Cellular mechanosensing: Getting to the nucleus of it all. *Prog. Biophys. Mol. Biol.* **115,** 76–92 (2014).
176. Ingber, D. E. Mechanobiology and diseases of mechanotransduction. *Ann. Med.* **35,** 564–577 (2003).
177. Ingber, D. E. Tensegrity and mechanotransduction. *J. Bodyw. Mov. Ther.* **12,** 198–200 (2008).
178. Guilluy, C. & Burridge, K. Nuclear mechanotransduction: Forcing the nucleus to respond. *Nucleus* **6,** 19–22 (2015).
179. Peyton, S. R. & Putnam, A. J. Extracellular matrix rigidity governs smooth muscle cell motility in a biphasic fashion. *J. Cell. Physiol.* **204,** 198–209 (2005).
180. Discher, D. E. Tissue cells feel and respond to the stiffness of their substrate. *Science (80-.).* **310,** 1139–1143 (2005).
181. Klein, E. A. *et al.* Cell-cycle control by physiological matrix elasticity and in vivo tissue stiffening. *Curr. Biol.* **19,** 1511–1518 (2009).
182. Pelham, R. J. & Wang, Y. L. Cell locomotion and focal adhesions are regulated by the mechanical properties of the substrate. *Biol. Bull.* **194,** 348–350 (1998).
183. Plotnikov, S. V., Pasapera, A. M., Sabass, B. & Waterman, C. M. Force fluctuations within focal adhesions mediate ECM-rigidity sensing to guide directed cell migration. *Cell* **151,** 1513–1527 (2012).
184. Lo, C. M., Wang, H. B., Dembo, M. & Wang, Y. L. Cell movement is guided by the rigidity of the substrate. *Biophys. J.* **79,** 144–152 (2000).
185. Ingber, D. E. Cellular tensegrity: defining new rules of biological design that govern the cytoskeleton. *J. Cell Sci.* **104 (Pt 3,** 613–627 (1993).
186. Ingber, D. E. Tensegrity II. How structural networks influence cellular information processing networks. *J. Cell Sci.* **116,** 1397–408 (2003).
187. Maniotis, A. J., Chen, C. S. & Ingber, D. E. Demonstration of mechanical connections between integrins, cytoskeletal filaments, and nucleoplasm that stabilize nuclear structure. *Proc. Natl. Acad. Sci. U. S. A.* **94,** 849–54 (1997).
188. Ingber, D. E. Tensegrity I. Cell structure and hierarchical systems biology. *J. Cell Sci.* **116,** 1157–1173 (2003).
189. Guilak, F. Compression-induced changes in the shape and volume of the chondrocyte nucleus. *J. Biomech.* **28,** 1529–1541 (1995).
190. McBeath, R., Pirone, D. M., Nelson, C. M., Bhadriraju, K. & Chen, C. S. Cell shape, cytoskeletal tension, and RhoA regulate stem cell lineage commitment. *Dev. Cell* **6,** 483–495 (2004).
191. Lovett, D. B., Shekhar, N., Nickerson, J. A., Roux, K. J. & Lele, T. P. Modulation of Nuclear Shape by Substrate Rigidity. *Cell. Mol. Bioeng.* **6,** 230–238 (2013).
192. Ihalainen, T. O. *et al.* Differential basal-to-apical accessibility of lamin A/C epitopes in

the nuclear lamina regulated by changes in cytoskeletal tension. *Nat. Mater.* **14,** 1252–1261 (2015).
193. Kim, D. H. & Wirtz, D. Cytoskeletal tension induces the polarized architecture of the nucleus. *Biomaterials* **48,** 161–172 (2015).
194. Makhija, E., Jokhun, D. S. & Shivashankar, G. V. Nuclear deformability and telomere dynamics are regulated by cell geometric constraints. *Proc. Natl. Acad. Sci. U. S. A.* **113,** E32-40 (2015).
195. Hanson, L. *et al.* Vertical nanopillars for in situ probing of nuclear mechanics in adherent cells. *Nat. Nanotechnol.* **10,** 554–562 (2015).
196. Wang, N. *et al.* Mechanical behavior in living cells consistent with the tensegrity model. *Proc. Natl. Acad. Sci. U. S. A.* **98,** 7765–70 (2001).
197. Zhong, C. *et al.* Rho-mediated contractility exposes a cryptic site in fibronectin and induces fibronectin matrix assembly. *J. Cell Biol.* **141,** 539–551 (1998).
198. Baneyx, G., Baugh, L. & Vogel, V. Fibronectin extension and unfolding within cell matrix fibrils controlled by cytoskeletal tension. *Proc. Natl. Acad. Sci. U. S. A.* **99,** 5139–5143 (2002).
199. Smith, M. L. *et al.* Force-induced unfolding of fibronectin in the extracellular matrix of living cells. *PLoS Biol.* **5,** 2243–2254 (2007).
200. Chen, W., Lou, J., Evans, E. A. & Zhu, C. Observing force-regulated conformational changes and ligand dissociation from a single integrin on cells. *J. Cell Biol.* **199,** 497–512 (2012).
201. Katsumi, A., Naoe, T., Matsushita, T., Kaibuchi, K. & Schwartz, M. A. Integrin activation and matrix binding mediate cellular responses to mechanical stretch. *J. Biol. Chem.* **280,** 16546–16549 (2005).
202. Thodeti, C. K. *et al.* TRPV4 channels mediate cyclic strain-induced endothelial cell reorientation through integrin-to-integrin signaling. *Circ. Res.* **104,** 1123–1130 (2009).
203. Kong, F. *et al.* Cyclic mechanical reinforcement of integrin-ligand interactions. *Mol. Cell* **49,** 1060–1068 (2013).
204. Alexandrova, A. Y. *et al.* Comparative dynamics of retrograde actin flow and focal adhesions: Formation of nascent adhesions triggers transition from fast to slow flow. *PLoS One* **3,** e3234 (2008).
205. Rio, A. *et al.* Stretching single talin rod molecules activates vinculin binding. *Science (80-.).* **323,** 638–641 (2009).
206. Patel, B. *et al.* The activity of the vinculin binding sites in talin is influenced by the stability of the helical bundles that make up the talin rod. *J. Biol. Chem.* **281,** 7458–7467 (2006).
207. Grashoff, C. *et al.* Measuring mechanical tension across vinculin reveals regulation of focal adhesion dynamics. *Nature* **466,** 263–6 (2010).
208. Dumbauld, D. W. *et al.* Contractility modulates cell adhesion strengthening through focal adhesion kinase and assembly of vinculin-containing focal adhesions. *J. Cell. Physiol.* **223,** 746–756 (2010).
209. Lee, C. *et al.* Actin depolymerization under force is governed by lysine 113: Glutamic acid 195-mediated catch-slip bonds. *Proc. Natl. Acad. Sci. U. S. A.* **110,** 5022–7 (2013).
210. Hayakawa, K., Tatsumi, H. & Sokabe, M. Actin filaments function as a tension sensor by tension-dependent binding of cofilin to the filament. *J. Cell Biol.* **195,** 721–727 (2011).
211. Marshall, T. W., Aloor, H. L. & Bear, J. E. Coronin 2A regulates a subset of focal-adhesion-turnover events through the cofilin pathway. *J. Cell Sci.* **122,** 3061–3069

(2009).
212. Nicolas, A., Geiger, B. & Safran, S. A. Cell mechanosensitivity controls the anisotropy of focal adhesions. *Proc. Natl. Acad. Sci. U. S. A.* **101,** 12520–5 (2004).
213. Shemesh, T., Geiger, B., Bershadsky, A. D. & Kozlov, M. M. Focal adhesions as mechanosensors: A physical mechanism. *Proc. Natl. Acad. Sci. U. S. A.* **102,** 12383–8 (2005).
214. Besser, A. & Safran, S. A. Force-induced adsorption and anisotropic growth of focal adhesions. *Biophys. J.* **90,** 3469–84 (2006).
215. Walcott, S., Kim, D. H., Wirz, D. & Sun, S. X. Nucleation and decay initiation are the stiffness-sensitive phases of focal adhesion maturation. *Biophys. J.* **101,** 2919–2928 (2011).
216. Balaban, N. Q. *et al.* Force and focal adhesion assembly: A close relationship studied using elastic micropatterned substrates. *Nat. Cell Biol.* **3,** 466–472 (2001).
217. Riveline, D. *et al.* Focal contacts as mechanosensors: Externally applied local mechanical force induces growth of focal contacts by an mDia1-dependent and ROCK-independent mechanism. *J. Cell Biol.* **153,** 1175–1185 (2001).
218. Galbraith, C. G., Yamada, K. M. & Sheetz, M. P. The relationship between force and focal complex development. *J. Cell Biol.* **159,** 695–705 (2002).
219. Paul, R., Heil, P., Spatz, J. P. & Schwarz, U. S. Propagation of mechanical stress through the actin cytoskeleton toward focal adhesions: model and experiment. *Biophys. J.* **94,** 1470–82 (2008).
220. Beningo, K. A., Dembo, M., Kaverina, I., Small, J. V. & Wang, Y. L. Nascent focal adhesions are responsible for the generation of strong propulsive forces in migrating fibroblasts. *J. Cell Biol.* **153,** 881–887 (2001).
221. Stricker, J., Aratyn-Schaus, Y., Oakes, P. W. & Gardel, M. L. Spatiotemporal constraints on the force-dependent growth of focal adhesions. *Biophys. J.* **100,** 2883–2893 (2011).
222. Iyer, K. V., Pulford, S., Mogilner, A. & Shivashankar, G. V. Mechanical activation of cells induces chromatin remodeling preceding MKL nuclear transport. *Biophys. J.* **103,** 1416–1428 (2012).
223. Miralles, F., Posern, G., Zaromytidou, A. I. & Treisman, R. Actin dynamics control SRF activity by regulation of its coactivator MAL. *Cell* **113,** 329–342 (2003).
224. Small, E. M. *et al.* Myocardin-related transcription factor-a controls myofibroblast activation and fibrosis in response to myocardial infarction. *Circ. Res.* **107,** 294–304 (2010).
225. Mizuno, D., Tardin, C., Schmidt, C. F. & Mackintosh, F. C. Nonequilibrium mechanics of active cytoskeletal networks. *Science* **315,** 370–3 (2007).
226. Wachsstock, D. H., Schwarz, W. H. & Pollard, T. D. Cross-linker dynamics determine the mechanical properties of actin gels. *Biophys. J.* **66,** 801–809 (1994).
227. Trepat, X. *et al.* Viscoelasticity of human alveolar epithelial cells subjected to stretch. *Am. J. Physiol.* **287,** L1025–L1034 (2004).
228. Jungbauer, S., Gao, H., Spatz, J. P. & Kemkemer, R. Two characteristic regimes in frequency-dependent dynamic reorientation of fibroblasts on cyclically stretched substrates. *Biophys. J.* **95,** 3470–3478 (2008).
229. Faust, U. *et al.* Cyclic stress at mHz frequencies aligns fibroblasts in direction of zero strain. *PLoS One* **6,** e28963 (2011).
230. Caille, N., Thoumine, O., Tardy, Y. & Meister, J. J. Contribution of the nucleus to the mechanical properties of endothelial cells. *J. Biomech.* **35,** 177–187 (2002).

231. Guilak, F., Tedrow, J. R. & Burgkart, R. Viscoelastic properties of the cell nucleus. *Biochem. Biophys. Res. Commun.* **269,** 781–786 (2000).
232. Kha, H. N., Chen, B. K., Clark, G. M. & Jones, R. Stiffness properties for nucleus standard straight and contour electrode arrays. *Med. Eng. Phys.* **26,** 677–685 (2004).
233. Vaziri, A. & Mofrad, M. R. K. Mechanics and deformation of the nucleus in micropipette aspiration experiment. *J. Biomech.* **40,** 2053–2062 (2007).
234. Thomas, C. H., Collier, J. H., Sfeir, C. S. & Healy, K. E. Engineering gene expression and protein synthesis by modulation of nuclear shape. *Proc. Natl. Acad. Sci. U. S. A.* **99,** 1972–1977 (2002).
235. Dahl, K. N., Ribeiro, A. J. S. & Lammerding, J. Nuclear shape, mechanics, and mechanotransduction. *Circ. Res.* **102,** 1307–1318 (2008).
236. Meshorer, E. *et al.* Hyperdynamic plasticity of chromatin proteins in pluripotent embryonic stem cells. *Dev. Cell* **10,** 105–116 (2006).
237. Constantinescu, D., Gray, H. L., Sammak, P. J., Schatten, G. P. & Csoka, A. B. Lamin A/C expression is a marker of mouse and human embryonic stem cell differentiation. *Stem Cells* **24,** 177–185 (2006).
238. Zink, D., Fischer, A. H. & Nickerson, J. A. Nuclear structure in cancer cells. *Nat. Rev. Cancer* **4,** 677–87 (2004).
239. Bissell, M. J. *et al.* Tissue structure, nuclear organization, and gene expression in normal and malignant breast. *Cancer Res* **59,** 1757–1763s; discussion 1763s–1764s (1999).
240. Hudson, M. E., Pozdnyakova, I., Haines, K., Mor, G. & Snyder, M. Identification of differentially expressed proteins in ovarian cancer using high-density protein microarrays. *Proc. Natl. Acad. Sci. U. S. A.* **104,** 17494–9 (2007).
241. Coradeghini, R. *et al.* Differential expression of nuclear lamins in normal and cancerous prostate tissues. *Oncol. Rep.* **15,** 609–613 (2006).
242. Wolf, K. & Friedl, P. Molecular mechanisms of cancer cell invasion and plasticity. *Br. J. Dermatol.* **154 Suppl,** 11–15 (2006).
243. Wolf, K. *et al.* Multi-step pericellular proteolysis controls the transition from individual to collective cancer cell invasion. *Nat. Cell Biol.* **9,** 893–904 (2007).
244. Zlatanova, J. & Leuba, S. H. Stretching and imaging single DNA molecules and chromatin. *J. Muscle Res. Cell Motil.* **23,** 377–395 (2002).
245. Marko, J. F. & Poirier, M. G. Micromechanics of chromatin and chromosomes. *Biochem. Cell Biol.* **81,** 209–20 (2003).
246. Deguchi, S., Maeda, K., Ohashi, T. & Sato, M. Flow-induced hardening of endothelial nucleus as an intracellular stress-bearing organelle. *J. Biomech.* **38,** 1751–1759 (2005).
247. Mathur, A. B., Reichert, W. M. & Truskey, G. A. Flow and high affinity binding affect the elastic modulus of the nucleus, cell body and the stress fibers of endothelial cells. *Ann. Biomed. Eng.* **35,** 1120–1130 (2007).
248. Wilson, K. L. & Berk, J. M. The nuclear envelope at a glance. *J. Cell Sci.* **123,** 1973–1978 (2010).
249. Wilson, K. L. & Foisner, R. Lamin-binding proteins. *Cold Spring Harb. Perspect. Biol.* **2,** a000554 (2010).
250. Guelen, L. *et al.* Domain organization of human chromosomes revealed by mapping of nuclear lamina interactions. *Nature* **453,** 948–51 (2008).
251. Kind, J. *et al.* Single-cell dynamics of genome-nuclear lamina interactions. *Cell* **153,** 178–192 (2013).
252. Lund, E. *et al.* Lamin A/C-promoter interactions specify chromatin state-dependent

transcription outcomes. *Genome Res.* **23,** 1580–1589 (2013).
253. Meuleman, W. *et al.* Constitutive nuclear lamina-genome interactions are highly conserved and associated with A/T-rich sequence. *Genome Res.* **23,** 270–280 (2013).
254. Zullo, J. M. *et al.* DNA sequence-dependent compartmentalization and silencing of chromatin at the nuclear lamina. *Cell* **149,** 1474–1487 (2012).
255. Stuurman, N., Heins, S. & Aebi, U. Nuclear lamins: Their structure, assembly, and interactions. *J. Struct. Biol.* **122,** 42–66 (1998).
256. Mattout-Drubezki, A. & Gruenbaum, Y. Dynamic interactions of nuclear lamina proteins with chromatin and transcriptional machinery. *Cell. Mol. Life Sci.* **60,** 2053–2063 (2003).
257. Shumaker, D. K. *et al.* Mutant nuclear lamin A leads to progressive alterations of epigenetic control in premature aging. *Proc. Natl. Acad. Sci. U. S. A.* **103,** 8703–8 (2006).
258. Malhas, A., Lee, C. F., Sanders, R., Saunders, N. J. & Vaux, D. J. Defects in lamin B1 expression or processing affect interphase chromosome position and gene expression. *J. Cell Biol.* **176,** 593–603 (2007).
259. Tang, C. W. *et al.* The integrity of a lamin-B1-dependent nucleoskeleton is a fundamental determinant of RNA synthesis in human cells. *J. Cell Sci.* **121,** 1014–1024 (2008).
260. Bertrand, A. T. *et al.* Cellular micro-environments reveal defective mechanosensing responses and elevated YAP signaling in LMNA-mutated muscle precursors. *J. Cell Sci.* **127,** 2873–2884 (2014).
261. Ozaki, T. *et al.* Complex formation between lamin A and the retinoblastoma gene product: identification of the domain on lamin A required for its interaction. *Oncogene* **9,** 2649–53 (1994).
262. Markiewicz, E., Dechat, T., Foisner, R., Quinlan, R. A. & Hutchison, C. J. Lamin A/C binding protein LAP2alpha is required for nuclear anchorage of retinoblastoma protein. *Mol. Biol. Cell* **13,** 4401–4413 (2002).
263. Ivorra, C. *et al.* A mechanism of AP-1 suppression through interaction of c-Fos with lamin A/C. *Genes Dev.* **20,** 307–320 (2006).
264. Georges, P. C., Miller, W. J., Meaney, D. F., Sawyer, E. S. & Janmey, P. a. Matrices with compliance comparable to that of brain tissue select neuronal over glial growth in mixed cortical cultures. *Biophys. J.* **90,** 3012–3018 (2006).
265. Ulrich, T. A., De Juan Pardo, E. M. & Kumar, S. The mechanical rigidity of the extracellular matrix regulates the structure, motility, and proliferation of glioma cells. *Cancer Res.* **69,** 4167–4174 (2009).
266. Engler, A. J. *et al.* Myotubes differentiate optimally on substrates with tissue-like stiffness: Pathological implications for soft or stiff microenvironments. *J. Cell Biol.* **166,** 877–887 (2004).
267. Engler, A. J. *et al.* Embryonic cardiomyocytes beat best on a matrix with heart-like elasticity: scar-like rigidity inhibits beating. *J. Cell Sci.* **121,** 3794–802 (2008).
268. Gilbert, P. M. *et al.* Substrate elasticity regulates skeletal muscle stem cell self-renewal in culture. *Science (80-.).* **1078,** 1078–1081 (2010).
269. Kong, H. J., Polte, T. R., Alsberg, E. & Mooney, D. J. FRET measurements of cell-traction forces and nano-scale clustering of adhesion ligands varied by substrate stiffness. *Proc. Natl. Acad. Sci. U. S. A.* **102,** 4300–4305 (2005).
270. Huebsch, N. *et al.* Harnessing traction-mediated manipulation of the cell/matrix interface to control stem-cell fate. *Nat. Mater.* **9,** 518–26 (2010).

271. Connelly, J. T. *et al.* Actin and serum response factor transduce physical cues from the microenvironment to regulate epidermal stem cell fate decisions. *Nat. Cell Biol.* **12,** 711–718 (2010).
272. Fu, J. *et al.* Mechanical regulation of cell function with geometrically modulated elastomeric substrates. *Nat. Methods* **7,** 733–736 (2010).
273. Buxboim, A. *et al.* Matrix elasticity regulates lamin-A,C phosphorylation and turnover with feedback to actomyosin. *Curr. Biol.* **24,** 1909–1917 (2014).
274. Raab, M. *et al.* Crawling from sort to stiff matrix polarizes the cytoskeleton and phsphoregulates myosin-II heavy chain. *J.Cell Biol.* **199,** 669–683 (2012).
275. Pan, D. The Hippo signaling pathway in development and cancer. *Dev. Cell* **19,** 491–505 (2010).
276. Badouel, C. & McNeill, H. Snapshot: The Hippo signaling pathway. *Cell* **145,** 484–484.e1 (2011).
277. Zhao, B. *et al.* Inactivation of YAP oncoprotein by the Hippo pathway is involved in cell contact inhibition and tissue growth control. *Genes Dev.* **21,** 2747–2761 (2007).
278. Jaalouk, D. E. & Lammerding, J. Mechanotransduction gone awry. *Nat. Rev. Mol. Cell Biol.* **10,** 63–73 (2009).
279. Mo, J. S., Yu, F. X., Gong, R., Brown, J. H. & Guan, K. L. Regulation of the Hippo-YAP pathway by protease-activated receptors (PARs). *Genes Dev.* **26,** 2138–2143 (2012).
280. Kim, N. G. & Gumbiner, B. M. Adhesion to fibronectin regulates Hippo signaling via the FAK-Src-PI3K pathway. *J. Cell Biol.* **210,** 503–515 (2015).
281. Broers, J. L. V *et al.* A- and B-type lamins are differentially expressed in normal human tissues. *Histochem. Cell Biol.* **107,** 505–517 (1997).
282. Omary, M. B., Ku, N. O., Tao, G. Z., Toivola, D. M. & Liao, J. 'Heads and tails' of intermediate filament phosphorylation: Multiple sites and functional insights. *Trends Biochem. Sci.* **31,** 383–394 (2006).
283. Heald, R. & McKeon, F. Mutations of phosphorylation sites in lamin A that prevent nuclear lamina disassembly in mitosis. *Cell* **61,** 579–589 (1990).
284. Goldman, R. D., Gruenbaum, Y., Moir, R. D., Shumaker, D. K. & Spann, T. P. Nuclear lamins: Building blocks of nuclear architecture. *Genes Dev.* **16,** 533–547 (2002).
285. Bertacchini, J. *et al.* The protein kinase Akt/PKB regulates both prelamin A degradation and Lmna gene expression. *FASEB J.* **27,** 2145–2155 (2013).
286. Solovei, I. *et al.* LBR and lamin A/C sequentially tether peripheral heterochromatin and inversely regulate differentiation. *Cell* **152,** 584–598 (2013).
287. Towbin, B. D. *et al.* Step-wise methylation of histone H3K9 positions heterochromatin at the nuclear periphery. *Cell* **150,** 934–947 (2012).
288. Talwar, S., Jain, N. & Shivashankar, G. V. The regulation of gene expression during onset of differentiation by nuclear mechanical heterogeneity. *Biomaterials* **35,** 2411–2419 (2014).
289. Mata, A., Azevedo, H. S., Botto, L., Gavara, N. & Su, L. New bioengineering breakthroughs and enabling tools in regenerative medicine. *Curr. Stem Cell Reports* **3,** 83–97 (2017).
290. Lele, T. P. *et al.* in *Methods in Cell Biology* **83,** 441–472 (2007).
291. Curran, J. M., Chen, R. & Hunt, J. A. Controlling the phenotype and function of mesenchymal stem cells in vitro by adhesion to silane-modified clean glass surfaces. *Biomaterials* **26,** 7057–7067 (2005).
292. Curran, J. M., Chen, R. & Hunt, J. A. The guidance of human mesenchymal stem cell

differentiation in vitro by controlled modifications to the cell substrate. *Biomaterials* **27,** 4783–4793 (2006).
293. Benoit, D. S. W., Schwartz, M. P., Durney, A. R. & Anseth, K. S. Small functional groups for controlled differentiation of hydrogel-encapsulated human mesenchymal stem cells. *Nat. Mater.* **7,** 816–823 (2008).
294. Tourniaire, G. *et al.* Polymer microarrays for cellular adhesion. *Chem. Commun.* 2118 (2006). doi:10.1039/b602009g
295. Mei, Y. *et al.* Combinatorial development of biomaterials for clonal growth of human pluripotent stem cells. *Nat. Mater.* **9,** 768–778 (2010).
296. Dalby, M. J., Riehle, M. O., Johnstone, H. J. H., Affrossman, S. & Curtis, A. S. G. Polymer-demixed nanotopography: Control of fibroblast spreading and proliferation. *Tissue Eng.* **8,** 1099–1108 (2002).
297. Curtis, A. S. *et al.* Substratum nanotopography and the adhesion of biological cells. Are symmetry or regularity of nanotopography important? *Biophys. Chem.* **94,** 275–83 (2001).
298. Gallagher, J. O., McGhee, K. F., Wilkinson, C. D. W. & Riehle, M. O. Interaction of animal cells with ordered nanotopography. *IEEE Trans. Nanobioscience* **1,** 24–8 (2002).
299. Leven, R. M., Virdi, A. S. & Sumner, D. R. Patterns of gene expression in rat bone marrow stromal cells cultured on titanium alloy discs of different roughness. *J. Biomed. Mater. Res.* **70A,** 391–401 (2004).
300. Dalby, M. J. *et al.* Nanotopographical stimulation of mechanotransduction and changes in interphase centromere positioning. *J. Cell. Biochem.* **100,** 326–338 (2007).
301. McMurray, R. J. *et al.* Nanoscale surfaces for the long-term maintenance of mesenchymal stem cell phenotype and multipotency. *Nat Mater* **10,** 637–644 (2011).
302. Tsimbouri, P. M. *et al.* Using Nanotopography and Metabolomics to Identify Biochemical Effectors of Multipotency. *ACS Nano* **6,** 10239–10249 (2012).
303. Yim, E. K. F., Pang, S. W. & Leong, K. W. Synthetic nanostructures inducing differentiation of human mesenchymal stem cells into neuronal lineage. *Exp. Cell Res.* **313,** 1820–1829 (2007).
304. Morez, C. *et al.* Enhanced efficiency of genetic programming toward cardiomyocyte creation through topographical cues. *Biomaterials* **70,** 94–104 (2015).
305. Trappmann, B. *et al.* Extracellular-matrix tethering regulates stem-cell fate. *Nat. Mater.* **11,** 742–742 (2012).
306. Wen, J. H. *et al.* Interplay of matrix stiffness and protein tethering in stem cell differentiation. *Nat. Mater.* **13,** 979–987 (2014).
307. Khetan, S. *et al.* Degradation-mediated cellular traction directs stem cell fate in covalently crosslinked three-dimensional hydrogels. *Nat. Mater.* **12,** 458–465 (2013).
308. Bonde, S. *et al.* Tuning InAs nanowire density for HEK293 cell viability, adhesion, and morphology: Perspectives for nanowire-based biosensors. *ACS Appl. Mater. Interfaces* **5,** 10510–10519 (2013).
309. Qi, S., Yi, C., Ji, S., Fong, C. C. & Yang, M. Cell adhesion and spreading behavior on vertically aligned silicon nanowire arrays. *ACS Appl. Mater. Interfaces* **1,** 30–34 (2009).
310. Xie, C. *et al.* Noninvasive neuron pinning with nanopillar arrays. *Nano Lett.* **10,** 4020–4024 (2010).
311. Lee, J. *et al.* The control of cell adhesion and viability by zinc oxide nanorods. *Biomaterials* **29,** 3743–3749 (2008).
312. Kuo, S. W. *et al.* Regulation of the fate of human mesenchymal stem cells by mechanical

and stereo-topographical cues provided by silicon nanowires. *Biomaterials* **33,** 5013–5022 (2012).
313. Liu, D. *et al.* Reorganization of cytoskeleton and transient activation of Ca2+ channels in mesenchymal stem cells cultured on silicon nanowire arrays. *ACS Appl. Mater. Interfaces* **5,** 13295–13304 (2013).
314. Xia, Younan; Whitesides, G. M. Soft lithography. *Angew. Chemie - Int. Ed.* **28,** 153–184 (1998).
315. Whitesides, G. M., Technology …, M. & Xia, Y. Soft lithography. *Annu. Rev. Mater. Sci.* **28,** 153–184 (1997).
316. Chen, C. S., Mrksich, M., Huang, S., Whitesides, G. M. & Ingber, D. E. Geometric control of cell life and death. *Science (80-.).* **276,** 1425–8 (1997).
317. Dike, L. E. *et al.* Geometric control of switching between growth, apoptosis, and differentiation during angiogenesis using micropatterned substrates. *In Vitro Cell. Dev. Biol. Anim.* **35,** 441–448 (1999).
318. Singhvi, R. *et al.* Engineering cell shape and function. *Science* **264,** 696–8 (1994).
319. Kilian, K. A., Bugarija, B., Lahn, B. T. & Mrksich, M. Geometric cues for directing the differentiation of mesenchymal stem cells. *Proc. Natl. Acad. Sci.* **107,** 4872–4877 (2010).
320. Arnsdorf, E. J., Tummala, P., Kwon, R. Y. & Jacobs, C. R. Mechanically induced osteogenic differentiation - the role of RhoA, ROCKII and cytoskeletal dynamics. *J. Cell Sci.* **122,** 546–553 (2009).
321. Peng, R., Yao, X. & Ding, J. Effect of cell anisotropy on differentiation of stem cells on micropatterned surfaces through the controlled single cell adhesion. *Biomaterials* **32,** 8048–8057 (2011).
322. Chen, C. S., Alonso, J. L., Ostuni, E., Whitesides, G. M. & Ingber, D. E. Cell shape provides global control of focal adhesion assembly. *Biochem. Biophys. Res. Commun.* **307,** 355–361 (2003).
323. Brock, A. *et al.* Geometric determinants of directional cell motility revealed using microcontact printing. *Langmuir* **19,** 1611–1617 (2003).
324. Parker, K. K. *et al.* Directional control of lamellipodia extension by constraining cell shape and orienting cell tractional forces. *FASEB J.* **16,** 1195–1204 (2002).
325. Wrobel, L. K. *et al.* Micropatterning tractional forces in living cells. *Cell Motil. Cytoskeleton* **52,** 97–106 (2002).
326. Radmacher, M., Tillamnn, R. W., Fritz, M. & Gaub, H. E. From molecules to cells: imaging soft samples with the atomic force microscope. *Science* **257,** 1900–5 (1992).
327. Hoh, J. H. & Schoenenberger, C. a. Surface morphology and mechanical properties of MDCK monolayers by atomic force microscopy. *J. Cell Sci.* **107 (Pt 5,** 1105–1114 (1994).
328. Grandbois, M., Beyer, M., Rief, M., Clausen-Schaumann, H. & Gaub, H. E. How strong is a covalent bond? *Science (80-.).* **283,** 1727–1730 (1999).
329. Fernandez, J. M. & Li, H. Force-clamp spectroscopy monitors the folding trajectory of a single protein. *Sciene* **303,** 1674–1678 (2009).
330. Lee, G. U., Chrisey, L. A. & Colton, R. J. Direct measurement of the forces between complementary strands of DNA. *Science* **266,** 771–3 (1994).
331. Schwaiger, I., Kardinal, A., Schleicher, M., Noegel, A. A. & Rief, M. A mechanical unfolding intermediate in an actin-crosslinking protein. *Nat. Struct. Mol. Biol.* **11,** 81–85 (2004).
332. Valdivia-Valero, F. J. & Nieto-Vesperinas, M. Optical forces on cylinders near

subwavelength slits illuminated by a photonic nanojet. *Opt. Commun.* **294,** 351–360 (2013).
333. Neuman, K. C., Chadd, E. H., Liou, G. F., Bergman, K. & Block, S. M. Characterization of photodamage to Escherichia coli in optical traps. *Biophys. J.* **77,** 2856–63 (1999).
334. Sacconi, L., Tolić-Nørrelykke, I. M., Stringari, C., Antolini, R. & Pavone, F. S. Optical micromanipulations inside yeast cells. *Appl. Opt.* **44,** 2001–7 (2005).
335. Block, S. M., Goldstein, L. S. & Schnapp, B. J. Bead movement by single kinesin molecules studied with optical tweezers. *Nature* **348,** 348–52 (1990).
336. Svoboda, K., Schmidt, C. F., Schnapp, B. J. & Block, S. M. Direct observation of kinesin stepping by optical trapping interferometry. *NatureNature* **365,** 721–727 (1993).
337. Svoboda, K. & Block, S. M. Force and velocity measured for single kinesin molecules. *Cell* **77,** 773–784 (1994).
338. Litvinov, R. I., Shuman, H., Bennett, J. S. & Weisel, J. W. Binding strength and activation state of single fibrinogen-integrin pairs on living cells. *Proc. Natl. Acad. Sci. U. S. A.* **99,** 7426–7431 (2002).
339. Strick, T., Allemand, J. F., Croquette, V. & Bensimon, D. Twisting and stretching single DNA molecules. *Prog. Biophys. Mol. Biol.* **74,** 115–140 (2000).
340. Strick, T. R., Allemand, J. F., Bensimon, D., Bensimon, A. & Croquette, V. The elasticity of a single supercoiled DNA molecule. *Science* **271,** 1835–1837 (1996).
341. Charvin, G., Strick, T. R., Bensimon, D. & Croquette, V. Tracking topoisomerase activity at the single-molecule level. *Annu. Rev. Biophys. Biomol. Struct.* **34,** 201–219 (2005).
342. Strick, T. R., Croquette, V. & Bensimon, D. Single-molecule analysis of DNA uncoiling by a type II topoisomerase. *Nature* **404,** 901–904 (2000).
343. Gore, J. *et al.* Mechanochemical analysis of DNA gyrase using rotor bead tracking. *Nature* **439,** 100–104 (2006).
344. Wang, N., Butler, J. P. P. & Ingber, D. E. E. Mechanotransduction across the cell surface and through the cytoskeleton. *Science (80-.).* **260,** 1124–1127 (1993).
345. Alenghat, F. J., Fabry, B., Tsai, K. Y., Goldmann, W. H. & Ingber, D. E. Analysis of cell mechanics in single vinculin-deficient cells using a magnetic tweezer. *Biochem. Biophys. Res. Commun.* **277,** 93–9 (2000).
346. Matthews, B. D. *et al.* Mechanical properties of individual focal adhesions probed with a magnetic microneedle. *Biochem. Biophys. Res. Commun.* **313,** 758–764 (2004).
347. Overby, D. R., Matthews, B. D., Alsberg, E. & Ingber, D. E. Novel dynamic rheological behavior of individual focal adhesions measured within single cells using electromagnetic pulling cytometry. *Acta Biomater.* **1,** 295–303 (2005).
348. Yoshida, M. *et al.* Leukocyte adhesion to vascular endothelium induces E-selectin linkage to the actin cytoskeleton. *J. Cell Biol.* **133,** 445–455 (1996).
349. Potard, U. S., Butler, J. P. & Wang, N. Cytoskeletal mechanics in confluent epithelial cells probed through integrins and E-cadherins. *Am. J. Physiol.* **272,** C1654-63 (1997).
350. Wang, N. & Ingber, D. E. Probing transmembrane mechanical coupling and cytomechanics using magnetic twisting cytometry. *Biochem. Cell Biol.* **73,** 327–335 (1995).
351. Meyer, C. J. *et al.* Mechanical control of cyclic AMP signalling and gene transcription through integrins. *Nat. Cell Biol.* **2,** 666–668 (2000).
352. Chicurel, M. E., Singer, R. H., Meyer, C. J. & Ingber, D. E. Integrin binding and mechanical tension induce movement of mRNA and ribosomes to focal adhesions. *Nature* **392,** 730–733 (1998).

353. Matthews, B. D., Overby, D. R., Mannix, R. & Ingber, D. E. Cellular adaptation to mechanical stress: role of integrins, Rho, cytoskeletal tension and mechanosensitive ion channels. *J. Cell Sci.* **119,** 508–18 (2006).
354. Dembo, M. & Wang, Y.-L. Stresses at the cell-to-substrate interface during locomotion of fibroblasts. *Biophys. J.* **76,** 2307–2316 (1999).
355. Schwarz, U. S. *et al.* Calculation of Forces at Focal Adhesions from Elastic Substrate Data : The Effect of Localized Force and the Need for Regularization. *Biophys. J.* **83,** 1380–1394 (2002).
356. Butler, J. P., Tolić-Nørrelykke, I. M., Fabry, B. & Fredberg, J. J. Traction fields, moments, and strain energy that cells exert on their surroundings. *Am. J. Physiol. Cell Physiol.* **282,** C595-605 (2002).
357. Sabass, B., Gardel, M. L. M. L., Waterman, C. M. C. M. & Schwarz, U. S. U. S. High resolution traction force microscopy based on experimental and computational advances. *Biophys. J.* **94,** 207–220 (2008).
358. Hur, S. S., Zhao, Y., Li, Y. S., Botvinick, E. & Chien, S. Live Cells Exert 3-Dimensional Traction Forces on Their Substrata. *Cell. Mol. Bioeng.* **2,** 425–436 (2009).
359. Maskarinec, S. A., Franck, C., Tirrell, D. A. & Ravichandran, G. Quantifying cellular traction forces in three dimensions. *Proc. Natl. Acad. Sci. U. S. A.* **106,** 22108–22113 (2009).
360. Delano??-Ayari, H., Rieu, J. P. & Sano, M. 4D traction force microscopy reveals asymmetric cortical forces in migrating dictyostelium cells. *Phys. Rev. Lett.* **105,** 248103 (2010).
361. Legant, W. R. *et al.* Measurement of mechanical tractions exerted by cells in three-dimensional matrices. *Nat. Methods* **7,** 969–71 (2010).
362. Tan, J. L. *et al.* Cells lying on a bed of microneedles: An approach to isolate mechanical force. *Proc. Natl. Acad. Sci. U. S. A.* **100,** 1484–9 (2003).
363. Saez, A., Ghibaudo, M., Buguin, A., Silberzan, P. & Ladoux, B. Rigidity-driven growth and migration of epithelial cells on microstructured anisotropic substrates. *Proc. Natl. Acad. Sci. U. S. A.* **104,** 8281–6 (2007).
364. Klein, F. *et al.* Elastic fully three-dimensional microstructure scaffolds for cell force measurements. *Adv. Mater.* **22,** 868–871 (2010).
365. Janmey, P. A., Winer, J. P., Murray, M. E. & Wen, Q. The hard life of soft cells. *Cell Motil. Cytoskeleton* **66,** 597–605 (2009).
366. Kumar, S. *et al.* Viscoelastic retraction of single living stress fibers and its impact on cell shape, cytoskeletal organization, and extracellular matrix mechanics. *Biophys. J.* **90,** 3762–3773 (2006).
367. Tanner, K., Boudreau, A., Bissell, M. J. & Kumar, S. Dissecting regional variations in stress fiber mechanics in living cells with laser nanosurgery. *Biophys. J.* **99,** 2775–2783 (2010).
368. Colombelli, J. *et al.* Mechanosensing in actin stress fibers revealed by a close correlation between force and protein localization. *J. Cell Sci.* **122,** 1665–1679 (2009).
369. du Roure, O. *et al.* Force mapping in epithelial cell migration. *Proc. Natl. Acad. Sci.* **102,** 2390–2395 (2005).
370. Viela, F., Granados, D., Ayuso-Sacido, A. & Rodríguez, I. Biomechanical cell regulation by high aspect ratio nanoimprinted pillars. *Adv. Funct. Mater.* **26,** 5599–5609 (2016).
371. Hallstrom, W. *et al.* Fifteen-piconewton force detection from neural growth cones using nanowire arrays. *Nano Lett.* **10,** 782–787 (2010).

372. Galbraith, C. G. & Galbraith, J. A. Super-resolution microscopy at a glance. *J Cell Sci* **124,** 1607–1611 (2011).
373. Bates, M., Jones, S. A. & Zhuang, X. Stochastic optical reconstruction microscopy (STORM): a method for superresolution fluorescence imaging. *Cold Spring Harb. Protoc.* **2013,** 498–520 (2013).
374. Betzig, E. *et al.* Imaging Intracellular Fluorescent Proteins at Nanometer Resolution. *Science (80-.).* **313,** 1642–1645 (2006).
375. Subach, F. V., Patterson, G. H., Renz, M., Lippincott-Schwartz, J. & Verkhusha, V. V. Bright Monomeric Photoactivatable Red Fluorescent Protein for Two-Color Super-Resolution sptPALM of Live Cells. *J. Am. Chem. Soc.* **132,** 6481–6491 (2010).
376. Kanchanawong, P. *et al.* Nanoscale architecture of integrin-based cell adhesions. *Nature* **468,** 580–584 (2010).
377. Versaevel, M. *et al.* Super-resolution microscopy reveals LINC complex recruitment at nuclear indentation sites. *Sci. Rep.* **4,** 7362 (2014).
378. Changede, R., Xu, X., Margadant, F. & Sheetz, M. P. Nascent integrin adhesions form on all matrix rigidities after integrin activation. *Dev. Cell* **35,** 614–621 (2015).
379. Storm, C., Pastore, J. J., MacKintosh, F., Lubensky, T. & Jamney, P. A. Nonlinear elasticity in biological gels. *Nature* **435,** 191–194 (2005).
380. Fung, Y. C. *Mechanical Properties of Living Tissues*. *Biomechanics* (Springer New York, 1993).
381. Lohberger, B. *et al.* Effect of cyclic mechanical stimulation on the expression of osteogenesis genes in human intraoral mesenchymal stromal and progenitor cells. *Biomed Res. Int.* **2014,** 189516 (2014).
382. Choi, S., Cho, T.-J., Kwon, S.-K., Lee, G. & Cho, J. Chondrogenesis of periodontal ligament stem cells by transforming growth factor-β3 and bone morphogenetic protein-6 in a normal healthy impacted third molar. *Int. J. Oral Sci.* **5,** 7–13 (2013).
383. Adamo, L. & García-Cardeña, G. Directed stem cell differentiation by fluid mechanical forces. *Antioxid. Redox Signal.* **15,** 1463–1473 (2011).
384. Kisiday, J. D., Frisbie, D. D., McIlwraith, C. W. & Grodzinsky, A. J. Dynamic compression stimulates proteoglycan synthesis by mesenchymal stem cells in the absence of chondrogenic cytokines. *Tissue Eng. Part A* **15,** 2817–24 (2009).
385. Ogawa, R., Orgill, D. P., Murphy, G. F. & Mizuno, S. Hydrostatic pressure-driven three-dimensional cartilage induction using human adipose-derived stem cells and collagen gels. *Tissue Eng. Part A* **0,** 1–10 (2014).
386. Chaudhuri, O. *et al.* Hydrogels with tunable stress relaxation regulate stem cell fate and activity. *Nat. Mater.* **15,** 326–334 (2015).
387. Schwarz, U. S. & Safran, S. A. Physics of adherent cells. *Rev. Mod. Phys.* **85,** 1327–1381 (2013).
388. Bonde, S. *et al.* Exploring arrays of vertical one-dimensional nanostructures for cellular investigations. *Nanotechnology* **25,** 362001 (2014).
389. Chiappini, C. *et al.* Biodegradable nanoneedles for localized delivery of nanoparticles in vivo: Exploring the biointerface. *ACS Nano* **9,** 5500–5509 (2015).
390. Chiappini, C. *et al.* Biodegradable silicon nanoneedles delivering nucleic acids intracellularly induce localized in vivo neovascularization. *Nat. Mater.* **14,** 6–13 (2015).
391. Yum, K., Wang, N. & Yu, M.-F. Nanoneedle: a multifunctional tool for biological studies in living cells. *Nanoscale* **2,** 363–72 (2010).
392. Han, S.-W. *et al.* High-efficiency DNA injection into a single human mesenchymal stem

cell using a nanoneedle and atomic force microscopy. *Nanomedicine* **4,** 215–225 (2008).
393. Shalek, A. K. *et al.* Vertical silicon nanowires as a universal platform for delivering biomolecules into living cells. *Proc. Natl. Acad. Sci. U. S. A.* **107,** 1870–5 (2010).
394. Chen, X., Kis, A., Zettl, A. & Bertozzi, C. R. A cell nanoinjector based on carbon nanotubes. *Proc. Natl. Acad. Sci. U. S. A.* **104,** 8218–22 (2007).
395. Robinson, J. T. *et al.* Vertical nanowire electrode arrays as a scalable platform for intracellular interfacing to neuronal circuits. *Nat. Nanotechnol.* **7,** 180–184 (2012).
396. Duan, X. *et al.* Intracellular recordings of action potentials by an extracellular nanoscale field-effect transistor. *Nat. Nanotechnol.* **7,** 174–179 (2011).
397. Na, Y.-R. *et al.* Probing enzymatic activity inside living cells using a nanowire–cell 'sandwich' assay. *Nano Lett.* **13,** 153–158 (2013).
398. Zheng, G., Patolsky, F., Cui, Y., Wang, W. U. & Lieber, C. M. Multiplexed electrical detection of cancer markers with nanowire sensor arrays. *Nat. Biotechnol.* **23,** 1294–1301 (2005).
399. Kihara, T. *et al.* Development of a method to evaluate caspase-3 activity in a single cell using a nanoneedle and a fluorescent probe. *Biosens. Bioelectron.* **25,** 22–27 (2009).
400. Chiappini, C. *et al.* Mapping local cytosolic enzymatic activity in human esophageal mucosa with porous silicon nanoneedles. *Adv. Mater.* **27,** 5147–5152 (2015).
401. Chiappini, C. Nanoneedle-based sensing in biological systems. *ACS Sensors* acssensors.7b00350 (2017). doi:10.1021/acssensors.7b00350
402. Peer, E., Artzy-Schnirman, A., Gepstein, L. & Sivan, U. Hollow nanoneedle array and its utilization for repeated administration of biomolecules to the same cells. *ACS Nano* **6,** 4940–4946 (2012).
403. VanDersarl, J. J., Xu, A. M. & Melosh, N. A. Nanostraws for direct fluidic intracellular access. *Nano Lett* **12,** 3881–3886 (2012).
404. Shalek, A. K. *et al.* Nanowire-mediated delivery enables functional interrogation of primary immune cells: application to the analysis of chronic lymphocytic leukemia. *Nano Lett* **12,** 6498–6504 (2012).
405. Hobbs, R. G., Petkov, N. & Holmes, J. D. Semiconductor nanowire fabrication by bottom-up and top-down paradigms. *Chem. Mater.* **24,** 1975–1991 (2012).
406. Chiappini, C. & Almeida, C. Silicon nanoneedles for drug delivery. *Semicond. Silicon Nanowires Biomed. Appl.* 144–167 (2014). doi:10.1533/9780857097712.2.144
407. Xie, C., Lin, Z., Hanson, L., Cui, Y. & Cui, B. Intracellular recording of action potentials by nanopillar electroporation. *Nat. Nanotechnol.* **7,** 185–90 (2012).
408. Ciofani, G., Genchi, G. G. & Mattoli, V. ZnO nanowire arrays as substrates for cell proliferation and differentiation. *Mater. Sci. Eng. C* **32,** 341–347 (2012).
409. Zaveri, T. D. *et al.* Contributions of surface topography and cytotoxicity to the macrophage response to zinc oxide nanorods. *Biomaterials* **31,** 2999–3007 (2010).
410. Mumm, F., Beckwith, K. M., Bonde, S., Martinez, K. L. & Sikorski, P. A transparent nanowire-based cell impalement device suitable for detailed cell-nanowire interaction studies. *Small* **9,** 263–272 (2013).
411. Kim, S. Y. & Yang, E. G. Collective behaviors of mammalian cells on amine-coated silicon nanowires. *Nanotechnology* **24,** 455704 (2013).
412. Hanson, L., Lin, Z. C., Xie, C., Cui, Y. & Cui, B. Characterization of the cell–nanopillar interface by transmission electron microscopy. *Nano Lett.* **12,** 5815–5820 (2012).
413. Cha, K. J., Hong, J. M., Cho, D.-W. & Kim, D. S. Enhanced osteogenic fate and function

of MC3T3-E1 cells on nanoengineered polystyrene surfaces with nanopillar and nanopore arrays. *Biofabrication* **5,** 25007 (2013).
414. Koh, L. B., Rodriguez, I. & Venkatraman, S. S. The effect of topography of polymer surfaces on platelet adhesion. *Biomaterials* **31,** 1533–1545 (2010).
415. Persson, H. *et al.* Vertical oxide nanotubes connected by subsurface microchannels. *Nano Res.* **5,** 190–198 (2012).
416. Xie, X. *et al.* Nanostraw–electroporation system for highly efficient intracellular delivery and transfection. *ACS Nano* **7,** 4351–4358 (2013).
417. Xu, A. M. *et al.* Quantification of nanowire penetration into living cells. *Nat. Commun.* **5,** 8 (2014).
418. Sköld, N. *et al.* Nanofluidics in hollow nanowires. *Nanotechnology* **21,** 155301 (2010).
419. Lin, Z. C., Xie, C., Osakada, Y., Cui, Y. & Cui, B. Iridium oxide nanotube electrodes for sensitive and prolonged intracellular measurement of action potentials. *Nat. Commun.* **5,** 2676–2688 (2014).
420. Levitt, A. P. *Whisker technology*. (Wiley-Interscience, 1970).
421. Lu, W. & Lieber, C. M. Semiconductor nanowires. *J. Phys. D. Appl. Phys.* **39,** R387 (2006).
422. Kolasinski, K. W. Catalytic growth of nanowires: Vapor–liquid–solid, vapor–solid–solid, solution–liquid–solid and solid–liquid–solid growth. *Curr. Opin. Solid State Mater. Sci.* **10,** 182–191 (2006).
423. Fan, H. J., Werner, P. & Zacharias, M. Semiconductor nanowires: from self-organization to patterned growth. *Small* **2,** 700–717 (2006).
424. Han, S. W., Nakamura, C., Obataya, I., Nakamura, N. & Miyake, J. A molecular delivery system by using AFM and nanoneedle. *Biosens. Bioelectron.* **20,** 2120–2125 (2005).
425. Han, S.-W. *et al.* Evaluation of the insertion efficiencies of tapered silicon nanoneedles and invasiveness of diamond nanoneedles in manipulations of living single cells. *Arch. Histol. Cytol.* **72,** 261–270
426. Obataya, I., Nakamura, C., Han, S., Nakamura, N. & Miyake, J. Nanoscale operation of a living cell using an atomic force microscope with a nanoneedle. *Nano Lett.* **5,** 27–30 (2005).
427. Obataya, I., Nakamura, C., Han, S., Nakamura, N. & Miyake, J. Mechanical sensing of the penetration of various nanoneedles into a living cell using atomic force microscopy. *Biosens. Bioelectron.* **20,** 1652–1655 (2005).
428. Chiappini, C., Liu, X., Fakhoury, J. R. & Ferrari, M. Biodegradable porous silicon barcode nanowires with defined geometry. *Adv. Funct. Mater.* **20,** 2231–2239 (2010).
429. Hochbaum, A. I., Gargas, D., Hwang, Y. J. & Yang, P. Single crystalline mesoporous silicon nanowires. *Nano Lett.* **9,** 3550–3554 (2009).
430. Huang, Z., Fang, H. & Zhu, J. Fabrication of silicon nanowire arrays with controlled diameter, length, and density. *Adv. Mater.* **19,** 744–748 (2007).
431. Peng, K. *et al.* Fabrication of single-crystalline silicon nanowires by scratching a silicon surface with catalytic metal particles. *Adv. Funct. Mater.* **16,** 387–394 (2006).
432. Huang, Z., Geyer, N., Werner, P., de Boor, J. & Gösele, U. Metal-Assisted Chemical Etching of Silicon: A Review. *Adv. Mater.* **23,** 285–308 (2011).
433. Chartier, C., Bastide, S. & Lévy-Clément, C. Metal-assisted chemical etching of silicon in HF–H2O2. *Electrochim. Acta* **53,** 5509–5516 (2008).
434. Li, X. & Bohn, P. W. Metal-assisted chemical etching in HF/H2O2 produces porous silicon. *Appl. Phys. Lett.* **77,** 2572 (2000).
435. Chiappini, C. *et al.* Tailored porous silicon microparticles: Fabrication and properties.

ChemPhysChem **11,** 1029–1035 (2010).
436. Yum, K., Na, S., Xiang, Y., Wang, N. & Yu, M. F. Mechanochemical delivery and dynamic tracking of fluorescent quantum dots in the cytoplasm and nucleus of living cells. *Nano Lett* **9,** 2193–2198 (2009).
437. Han, S.-W., Nakamura, C., Imai, Y., Nakamura, N. & Miyake, J. Monitoring of hormonal drug effect in a single breast cancer cell using an estrogen responsive GFP reporter vector delivered by a nanoneedle. *Biosens. Bioelectron.* **24,** 1219–1222 (2009).
438. Obataya, I., Nakamura, C., Han, S., Nakamura, N. & Miyake, J. Direct insertion of proteins into a living cell using an atomic force microscope with a nanoneedle. *NanoBiotechnology* **1,** 347–352 (2005).
439. Kihara, T. *et al.* Nanoneedle surface modification with 2-methacryloyloxyethyl phosphorylcholine polymer to reduce nonspecific protein adsorption in a living cell. *Nanobiotechnology* **3,** 127–134 (2007).
440. Vakarelski, I. U., Brown, S. C., Higashitani, K. & Moudgil, B. M. Penetration of living cell membranes with fortified carbon nanotube tips. *Langmuir* **23,** 10893–10896 (2007).
441. Love, J. C., Estroff, L. A., Kriebel, J. K., Nuzzo, R. G. & Whitesides, G. M. Self-assembled monolayers of thiolates on metals as a form of nanotechnology. *Chem. Rev.* **105,** 1103–1169 (2005).
442. Coffer, J. L. *Semiconducting silicon nanowires for biomedical applications*. *Semiconducting Silicon Nanowires for Biomedical Applications* (Woodhead Publishing, 2014). doi:10.1533/9780857097712.1.3
443. Biju, V. Chemical modifications and bioconjugate reactions of nanomaterials for sensing, imaging, drug delivery and therapy. *Chem. Soc. Rev.* (2014). doi:10.1039/c3cs60273g
444. Tasciotti, E. *et al.* Mesoporous silicon particles as a multistage delivery system for imaging and therapeutic applications. *Nat Nanotechnol* **3,** 151–157 (2008).
445. Berthing, T. *et al.* Cell membrane conformation at vertical nanowire array interface revealed by fluorescence imaging. *Nanotechnology* **23,** 8 (2012).
446. Bonde, S., Bolinsson, J., Berthing, T. & Martinez, K. L. Towards a better prediction of cell settling on nanostructure arrays - Simple means to complicated ends. *Adv. Funct. Mater.* **25,** 3246–3255 (2015).
447. Xie, X. *et al.* Mechanical model of vertical nanowire cell penetration. *Nano Lett* **13,** 6002–6008 (2013).
448. McKnight, T. E. *et al.* Tracking gene expression after DNA delivery using spatially indexed nanofiber arrays. *Nano Lett.* **4,** 1213–1219 (2004).
449. Zhou, X., Moran-Mirabal, J. M., Craighead, H. G. & McEuen, P. L. Supported lipid bilayer/carbon nanotube hybrids. *Nat. Nanotechnol.* **2,** 185–190 (2007).
450. Liu, J., Sun, Y., Oster, G. F. & Drubin, D. G. Mechanochemical crosstalk during endocytic vesicle formation. *Curr Opin Cell Biol* **22,** 36–43 (2010).
451. Ahyayauch, H., Villar, A. V, Alonso, A. & Goni, F. M. Modulation of PI-specific phospholipase C by membrane curvature and molecular order. *Biochemistry* **44,** 11592–11600 (2005).
452. Hubner, S. *et al.* Enhancement of phosphoinositide 3-kinase (PI 3-kinase) activity by membrane curvature and inositol-phospholipid-binding peptides. *Eur J Biochem* **258,** 846–853 (1998).
453. Liu, J., Sun, Y., Drubin, D. G. & Oster, G. F. The mechanochemistry of endocytosis. *PLoS Biol.* **7,** e1000204 (2009).

454. Antonescu, C. N., Aguet, F., Danuser, G. & Schmid, S. L. Phosphatidylinositol-(4,5)-bisphosphate regulates clathrin-coated pit initiation, stabilization, and size. *Mol. Biol. Cell* **22,** 2588–2600 (2011).
455. Persson, H. *et al.* Fibroblasts cultured on nanowires exhibit low motility, impaired cell division, and DNA damage. *Small* **9,** 4006–4016 (2013).
456. Wierzbicki, R. *et al.* Mapping the complex morphology of cell interactions with nanowire substrates using FIB-SEM. *PLoS One* **8,** e53307 (2013).
457. Angle, M. R., Wang, A., Thomas, A., Schaefer, A. T. & Melosh, N. A. Penetration of cell membranes and synthetic lipid bilayers by nanoprobes. *Biophys. J.* **107,** 2091–2100 (2014).
458. McKnight, T. E. *et al.* Intracellular integration of synthetic nanostructures with viable cells for controlled biochemical manipulation. *Nanotechnology* **14,** 551 (2003).
459. Mann, D. G. J. *et al.* Inducible RNA interference-mediated gene silencing using nanostructured gene delivery arrays. *ACS Nano* **2,** 69–76 (2008).
460. Peckys, D. B., Melechko, A. V, Simpson, M. L. & McKnight, T. E. Immobilization and release strategies for DNA delivery using carbon nanofiber arrays and self-assembled monolayers. *Nanotechnology* **20,** 145304 (2009).
461. Peckys, D. B., de Jonge, N., Simpson, M. L. & McKnight, T. E. End-specific strategies of attachment of long double stranded DNA onto gold-coated nanofiber arrays. *Nanotechnology* **19,** 435301 (9pp) (2008).
462. Wang, Y. *et al.* Poking cells for efficient vector-free intracellular delivery. *Nat. Commun.* **5,** 4466 (2014).
463. Singhal, R. *et al.* Multifunctional carbon-nanotube cellular endoscopes. *Nat. Nanotechnol.* **6,** 57–64 (2011).
464. Matsumoto, D. *et al.* Oscillating high-aspect-ratio monolithic silicon nanoneedle array enables efficient delivery of functional bio-macromolecules into living cells. *Nat. Publ. Gr.* **5,** 15325 (2015).
465. Han, S., Nakamura, C., Obataya, I., Nakamura, N. & Miyake, J. Gene expression using an ultrathin needle enabling accurate displacement and low invasiveness. *Biochem. Biophys. Res. Commun.* **332,** 633–639 (2005).
466. Ryu, S. *et al.* Nanoneedle insertion into the cell nucleus does not induce double-strand breaks in chromosomal DNA. *J Biosci Bioeng* **116,** 391–396 (2013).
467. Flobak, Å. Investigation of transfection using silica-coated cupric oxide nanowires. (Institutt for fysikk, 2013).
468. Tian, B. *et al.* Three-dimensional, flexible nanoscale field-effect transistors as localized bioprobes. *Science (80-.).* **329,** 830–834 (2010).
469. Chou, L. Y. T., Ming, K. & Chan, W. C. W. Strategies for the intracellular delivery of nanoparticles. *Chem. Soc. Rev.* **40,** 233–245 (2010).
470. Stephens, D. J. & Pepperkok, R. The many ways to cross the plasma membrane. *Proc. Natl. Acad. Sci.* **98,** 4295–4298 (2001).
471. Chan, M. S. & Lo, P. K. Nanoneedle-assisted delivery of site-selective peptide-functionalized DNA nanocages for targeting mitochondria and nuclei. *Small* **10,** 1255–1260 (2014).
472. Kim, W., Ng, J. K., Kunitake, M. E., Conklin, B. R. & Yang, P. Interfacing silicon nanowires with mammalian cells. *J. Am. Chem. Soc.* **129,** 7228–7229 (2007).
473. Schrlau, M. G., Dun, N. J. & Bau, H. H. Cell electrophysiology with carbon nanopipettes. *ACS Nano* **3,** 563–568 (2009).

474. Laforge, F. O., Carpino, J., Rotenberg, S. A. & Mirkin, M. V. Electrochemical attosyringe. *Proc. Natl. Acad. Sci. U. S. A.* **104,** 11895–11900 (2007).
475. Schrlau, M. G. *et al.* Carbon nanopipettes characterize calcium release pathways in breast cancer cells. *Nanotechnology* **19,** 325102 (2008).
476. Xu, A. M., Wang, D. S., Shieh, P., Cao, Y. & Melosh, N. Direct intracellular delivery of cell impermeable probes of protein glycosylation using nanostraws. *ChemBioChem* (2017). doi:10.1002/cbic.201600689
477. Brüggemann, A. *et al.* in *Potassium Channels* (ed. Lippiat, J. D.) **491,** 165–176 (Humana Press, 2009).
478. Verma, P. & Melosh, N. A. Gigaohm resistance membrane seals with stealth probe electrodes. *Appl. Phys. Lett.* **97,** 33704 (2010).
479. Molleman, A. *Patch clamping*. *Wiley* (Wiley, 2002). doi:10.1002/0470856521
480. Kihara, T. *et al.* Development of a novel method to detect intrinsic mRNA in a living cell by using a molecular beacon-immobilized nanoneedle. *Biosens Bioelectron* **26,** 1449–1454 (2010).
481. Silberberg, Y. R. *et al.* Evaluation of the actin cytoskeleton state using an antibody-functionalized nanoneedle and an AFM. *Biosens. Bioelectron.* **40,** 3–9 (2013).
482. Silberberg, Y. R. *et al.* Detection of microtubules in vivo using antibody-immobilized nanoneedles. *J. Biosci. Bioeng.* **117,** 107–112 (2014).
483. Cui, Y., Wei, Q., Park, H. & Lieber, C. M. Nanowire nanosensors for highly sensitive and selective detection of biological and chemical species. *Science (80-.).* **293,** 1289–1292 (2001).
484. Lieber, J. H. and, Charles, M., Hahm, J. & Lieber, C. M. Direct ultrasensitive electrical detection of DNA and DNA sequence variations using nanowire nanosensors. (2003). doi:S1530-6984(03)04853-7
485. Chen, R. J. *et al.* Noncovalent functionalization of carbon nanotubes for highly specific electronic biosensors. *Proc. Natl. Acad. Sci.* **100,** 4984–4989 (2003).
486. Chen, R. J. *et al.* An investigation of the mechanisms of electronic sensing of protein adsorption on carbon nanotube devices. *J. Am. Chem. Soc.* **126,** 1563–1568 (2004).
487. Hällström, W. *et al.* Rectifying and sorting of regenerating axons by free-standing nanowire patterns: A highway for nerve fibers. *Langmuir* **25,** 4343–4346 (2009).
488. Kwiat, M. *et al.* Highly ordered large-scale neuronal networks of individual cells - Toward single cell to 3D nanowire intracellular interfaces. *ACS Appl. Mater. Interfaces* **4,** 3542–3549 (2012).
489. Prinz, C. *et al.* Axonal guidance on patterned free-standing nanowire surfaces. *Nanotechnology* **19,** 345101 (2008).
490. Albuschies, J. & Vogel, V. The role of filopodia in the recognition of nanotopographies. *Sci. Rep.* **1658,** 1–9 (2013).
491. Li, Z. *et al.* Quantifying the traction force of a single cell by aligned silicon nanowire array. *Nano Lett.* **9,** 3575–3580 (2009).
492. Badique, F. *et al.* Directing nuclear deformation on micropillared surfaces by substrate geometry and cytoskeleton organization. *Biomaterials* **34,** 2991–3001 (2013).
493. Cheng, S. L. *et al.* Activation of vascular smooth muscle parathyroid hormone receptor inhibits Wnt/beta-catenin signaling and aortic fibrosis in diabetic arteriosclerosis. *Circ. Res.* **107,** 271–282 (2010).
494. Fozdar, D. Y., Lee, J. Y., Schmidt, C. E. & Chen, S. Hippocampal neurons respond uniquely to topographies of various sizes and shapes. *Biofabrication* **2,** 35005 (2010).

495. Abdul Kafi, M., El-Said, W. A., Kim, T. H. & Choi, J. W. Cell adhesion, spreading, and proliferation on surface functionalized with RGD nanopillar arrays. *Biomaterials* **33,** 731–739 (2012).
496. Brunetti, V. *et al.* Neurons sense nanoscale roughness with nanometer sensitivity. *Proc. Natl. Acad. Sci. U. S. A.* **107,** 6264–6269 (2010).
497. Ross, A. M., Jiang, Z., Bastmeyer, M. & Lahann, J. Physical aspects of cell culture substrates: Topography, roughness, and elasticity. *Small* **8,** 336–355 (2012).
498. Bacharouche, J. *et al.* Biomimetic cryptic site surfaces for reversible chemo- and cyto-mechanoresponsive substrates. *ACS Nano* **7,** 3457–3465 (2013).
499. Saha, K. *et al.* Substrate modulus directs neural stem cell behavior. *Biophys. J.* **95,** 4426–4438 (2008).
500. Bucaro, M. A., Vasquez, Y., Hatton, B. D. & Aizenberg, J. Fine-tuning the degree of stem cell polarization and alignment on ordered arrays of high-aspect-ratio nanopillars. *ACS Nano* **6,** 6222–6230 (2012).
501. von der Mark, K., Bauer, S., Park, J. & Schmuki, P. Another look at 'Stem cell fate dictated solely by altered nanotube dimension'. *Proc. Natl. Acad. Sci.* **106,** E60–E60 (2009).
502. Park, J., Bauer, S., Von Der Mark, K. & Schmuki, P. Nanosize and vitality: TiO2 nanotube diameter directs cell fate. *Nano Lett.* **7,** 1686–1691 (2007).
503. Choi, C. H. *et al.* Cell interaction with three-dimensional sharp-tip nanotopography. *Biomaterials* **28,** 1672–1679 (2007).
504. Sjöström, T. *et al.* Fabrication of pillar-like titania nanostructures on titanium and their interactions with human skeletal stem cells. *Acta Biomater.* **5,** 1433–1441 (2009).
505. Park, Y.-S., Yoon, S. Y., Park, J. S. & Lee, J. S. Deflection induced cellular focal adhesion and anisotropic growth on vertically aligned silicon nanowires with differing elasticity. *NPG Asia Mater.* **8,** e249 (2016).
506. Kim, D.-J., Lee, G., Kim, G.-S. & Lee, S.-K. Statistical analysis of immuno-functionalized tumor-cell behaviors on nanopatterned substrates. *Nanoscale Res. Lett.* **7,** 637 (2012).
507. Jahed, Z. *et al.* Differential collective- and single-cell behaviors on Silicon micropillar arrays. *ACS Appl. Mater. Interfaces* **8,** 23604–23613 (2016).
508. Ankam, S., Lim, C. K. & Yim, E. K. F. Actomyosin contractility plays a role in MAP2 expression during nanotopography-directed neuronal differentiation of human embryonic stem cells. *Biomaterials* **47,** 20–28 (2015).
509. Zhang, H. *et al.* Titanium nanotubes induce osteogenic differentiation through the FAK/RhoA/YAP cascade. *RSC Adv.* **6,** 44062–44069 (2016).
510. Hällström, W. *et al.* Gallium phosphide nanowires as a substrate for cultured neurons. *Nano Lett.* **7,** 2960–2965 (2007).
511. Low, S. P., Williams, K. A., Canham, L. T. & Voelcker, N. H. Evaluation of mammalian cell adhesion on surface-modified porous silicon. *Biomaterials* **27,** 4538–4546 (2006).
512. SanMartin, A., Johansson, F., Samuelson, L. & Prinz, C. N. Microarray analysis reveals moderate gene expression changes in cortical neural stem cells cultured on nanowire arrays. *J. Nanosci. Nanotechnol.* **14,** 4880–4885 (2014).
513. Golias, C. H., Charalabopoulos, A. & Charalabopoulos, K. Cell proliferation and cell cycle control: a mini review. *Int. J. Clin. Pract.* **58,** 1134–1141 (2004).
514. Piret, G., Perez, M.-T. T. & Prinz, C. N. Neurite outgrowth and synaptophysin expression of postnatal CNS neurons on GaP nanowire arrays in long-term retinal cell culture. *Biomaterials* **34,** 875–887 (2013).

515. Jain, N., Iyer, K. V., Kumar, A. & Shivashankar, G. V. Cell geometric constraints induce modular gene-expression patterns via redistribution of HDAC3 regulated by actomyosin contractility. *Proc. Natl. Acad. Sci.* **110,** 11349–11354 (2013).
516. Kim, K. M., Han, S. & Hwang, C. S. Electronic bipolar resistance switching in an anti-serially connected Pt/TiO2/Pt structure for improved reliability. *Nanotechnology* **23,** 35201 (2012).
517. Biggs, M. J. P., Richards, R. G. & Dalby, M. J. Nanotopographical modification: A regulator of cellular function through focal adhesions. *Nanomedicine Nanotechnology, Biol. Med.* **6,** 619–633 (2010).
518. Beckwith, K. S., Cooil, S. P., Wells, J. W. & Sikorski, P. Tunable high aspect ratio polymer nanostructures for cell interfaces. *Nanoscale* **7,** 8438–8450 (2015).
519. Luong-Van, E. *et al.* Review: Micro- and nanostructured surface engineering for biomedical applications. *J. Mater. Res.* **28,** 165–174 (2013).
520. Persson, H., Li, Z., Tegenfeldt, J. O., Oredsson, S. & Prinz, C. N. From immobilized cells to motile cells on a bed-of-nails: effects of vertical nanowire array density on cell behaviour. *Sci. Rep.* **5,** 18535 (2015).
521. Gu, L. *et al.* Multivalent porous silicon nanoparticles enhance the immune activation potency of agonistic CD40 antibody. *Adv. Mater.* **24,** 3981–3987 (2012).
522. Berquin, I. M. & Sloane, B. F. in *Advances in Experimental Medicine and Biology* **389,** 281–294 (Springer US, 1996).
523. Szpaderska, A. M. & Frankfater, A. An intracellular form of cathepsin b contributes to invasiveness in cancer. *Cancer Res.* **61,** 3493–3500 (2001).
524. Yamashita, H. *et al.* The role of the interaction of the vinculin proline-rich linker region with vinexin α in sensing the stiffness of the extracellular matrix. *J. Cell Sci.* **127,** 1875–1886 (2014).
525. Aerts, J. L., Gonzales, M. I. & Topalian, S. L. Selection of appropriate control genes to assess expression of tumor antigens using real-time RT-PCR. *Biotechniques* **36,** 84–91 (2004).
526. Caicedo, J. C. *et al.* Data-analysis strategies for image-based cell profiling. *Nat. Methods* **14,** 849–863 (2017).
527. Porter, A. G., Ja, R. U. & Nicke, È. Emerging roles of caspase-3 in apoptosis.
528. Scholzen, T. & Gerdes, J. The Ki-67 protein: From the known and the unknown. *J. Cell. Physiol.* **182,** 311–22 (2000).
529. Zaidel-Bar, R., Ballestrem, C., Kam, Z. & Geiger, B. Early molecular events in the assembly of matrix adhesions at the leading edge of migrating cells. *J. Cell Sci.* **116,** 4605–4613 (2003).
530. Guilluy, C. *et al.* Isolated nuclei adapt to force and reveal a mechanotransduction pathway in the nucleus. *Nat.Cell Biol.* **16,** 376–381 (2014).
531. Liu, H. *et al.* In situ mechanical characterization of the cell nucleus by atomic force microscopy. *ACS Nano* **8,** 3821–3828 (2014).
532. Versaevel, M., Grevesse, T. & Gabriele, S. Spatial coordination between cell and nuclear shape within micropatterned endothelial cells. *Nat. Commun.* **3,** 671 (2012).
533. Pan, Z. *et al.* Control of cell nucleus shapes via micropillar patterns. *Biomaterials* **33,** 1730–1735 (2012).
534. Davidson, P. M., Özçelik, H., Hasirci, V., Reiter, G. & Anselme, K. Microstructured surfaces cause severe but non-detrimental deformation of the cell nucleus. *Adv. Mater.* **21,** 3586–3590 (2009).

535. Horejs, C. *et al.* Preventing tissue fibrosis by local biomaterials interfacing of specific cryptic extracellular matrix information. *Nat. Commun.* **8,** 15509 (2017).
536. Horejs, C.-M. C.-M. *et al.* Biologically-active laminin-111 fragment that modulates the epithelial-to-mesenchymal transition in embryonic stem cells. *Proc. Natl. Acad. Sci. U. S. A.* **111,** 5908–5913 (2014).
537. Kalluri, R. & Weinberg, R. A. The basics of epithelial-mesenchymal transition. *J. Clin. Invest.* **119,** 1420–1428 (2009).
538. Hay, E. D. & Zuk, A. Transformations between epithelium and mesenchyme: Normal, pathological, and experimentally induced. *Am. J. Kidney Dis.* **26,** 678–690 (1995).
539. Lim, J. & Thiery, J. P. Epithelial-mesenchymal transitions: insights from development. *Development* **139,** 3471–3486 (2012).
540. Nakaya, Y. & Sheng, G. EMT in developmental morphogenesis. *Cancer Lett.* **341,** 9–15 (2013).
541. Nakaya, Y. & Sheng, G. An amicable separation: Chick's way of doing EMT. *Cell Adh. Migr.* **3,** 160–163 (2009).
542. Nakaya, Y. & Sheng, G. Epithelial to mesenchymal transition during gastrulation: An embryological view. *Dev. Growth Differ.* **50,** 755–766 (2008).
543. Theveneau, E. & Mayor, R. Neural crest delamination and migration: From epithelium-to-mesenchyme transition to collective cell migration. *Dev. Biol.* **366,** 34–54 (2012).
544. Grande, M. T. *et al.* Snail1-induced partial epithelial-to-mesenchymal transition drives renal fibrosis in mice and can be targeted to reverse established disease. *Nat. Med.* **21,** 989–997 (2015).
545. Lovisa, S. *et al.* Epithelial-to-mesenchymal transition induces cell cycle arrest and parenchymal damage in renal fibrosis. *Nat. Med.* **21,** 998–1009 (2015).
546. Masszi, A. & Kapus, A. Organ fibrosis: When epithelia are muscled to change. *Cell Cycle* **9,** 2263–2264 (2010).
547. Quaggin, S. E. & Kapus, A. Scar wars: mapping the fate of epithelial-mesenchymal-myofibroblast transition. *Kidney Int.* **80,** 41–50 (2011).
548. Zeisberg, M. & Duffield, J. S. Resolved: EMT produces fibroblasts in the kidney. *J. Am. Soc. Nephrol.* **21,** 1247–1253 (2010).
549. Acloque, H., Adams, M. S., Fishwick, K., Bronner-Fraser, M. & Nieto, M. A. Epithelial-mesenchymal transitions: The importance of changing cell state in development and disease. *J. Clin. Invest.* **119,** 1438–1449 (2009).
550. Ginnebaugh, K. R., Ahmad, A. & Sarkar, F. H. The therapeutic potential of targeting the epithelial–mesenchymal transition in cancer. *Expert Opin. Ther. Targets* **18,** 731–745 (2014).
551. Puisieux, A., Brabletz, T. & Caramel, J. Oncogenic roles of EMT-inducing transcription factors. *Nat. Cell Biol.* **16,** 488–494 (2014).
552. Steinestel, K., Eder, S., Schrader, A. & Steinestel, J. Clinical significance of epithelial-mesenchymal transition. *Clin. Transl. Med.* **3,** 17 (2014).
553. Thiery, J. P. Epithelial–mesenchymal transitions in tumour progression. *Nat. Rev. Cancer* **2,** 442–454 (2002).
554. Pang, M.-F. *et al.* TGF-β1-induced EMT promotes targeted migration of breast cancer cells through the lymphatic system by the activation of CCR7/CCL21-mediated chemotaxis. *Oncogene* **35,** 748–760 (2016).
555. Thiery, J. P. & Sleeman, J. P. Complex networks orchestrate epithelial–mesenchymal transitions. *Nat. Rev. Mol. Cell Biol.* **7,** 131–142 (2006).

556. Eastham, A. M. *et al.* Epithelial-mesenchymal transition events during human embryonic stem cell differentiation. *Cancer Res.* **67,** 11254–11262 (2007).
557. Wheelock, M. J., Shintani, Y., Maeda, M., Fukumoto, Y. & Johnson, K. R. Cadherin switching. *J. Cell Sci.* **121,** 727–735 (2008).
558. Liu, G. *et al.* Effects of E-cadherin on mouse embryo implantation and expression of matrix metalloproteinase-2 and -9. *Biochem. Biophys. Res. Commun.* **343,** 832–838 (2006).
559. Ullmann, U. *et al.* Epithelial-mesenchymal transition process in human embryonic stem cells cultured in feeder-free conditions. *Mol. Hum. Reprod.* **13,** 21–32 (2006).
560. Brown, A. C., Fiore, V. F., Sulchek, T. A. & Barker, T. H. Physical and chemical microenvironmental cues orthogonally control the degree and duration of fibrosis-associated epithelial-to-mesenchymal transitions. *J. Pathol.* **229,** 25–35 (2013).
561. Vracko, R. Basal lamina scaffold-anatomy and significance for maintenance of orderly tissue structure. *Am. J. Pathol.* **77,** 314–46 (1974).
562. Miner, J. H. & Yurchenco, P. D. Laminin functions in tissue morphogenesis. *Annu. Rev. Cell Dev. Biol.* **20,** 255–284 (2004).
563. Elizabeth, D. H. *Cell Biology of Extracellular matrix*. (1991).
564. Kelley, L. C., Lohmer, L. L., Hagedorn, E. J. & Sherwood, D. R. Traversing the basement membrane in vivo: A diversity of strategies. *J. Cell Biol.* **204,** 291–302 (2014).
565. LeBleu, V. S., Macdonald, B. & Kalluri, R. Structure and function of basement membranes. *Exp. Biol. Med. (Maywood).* **232,** 1121–9 (2007).
566. Miner, J. H. *Current topics in membranes. Volume seventy six, Basement membranes*.
567. Yurchenco, P. D. & Schittny, J. C. Molecular architecture of basement membranes. *FASEB J.* **4,** 1577–90 (1990).
568. Yurchenco, P. D. Basement membranes: Cell scaffoldings and signaling platforms. *Cold Spring Harb. Perspect. Biol.* **3,** 1–27 (2011).
569. Blouw, B. *et al.* The invadopodia scaffold protein Tks5 is required for the growth of human breast cancer cells in vitro and in vivo. *PLoS One* **10,** e0121003 (2015).
570. Gligorijevic, B., Bergman, A. & Condeelis, J. Multiparametric classification links tumor microenvironments with tumor cell phenotype. *PLoS Biol.* **12,** e1001995 (2014).
571. Leong, H. S. *et al.* Invadopodia are required for cancer cell extravasation and are a therapeutic target for metastasis. *Cell Rep.* **8,** 1558–1570 (2014).
572. Lohmer, L. L. *et al.* A sensitized screen for genes promoting invadopodia function in vivo: CDC-42 and Rab GDI-1 direct distinct aspects of invadopodia formation. *PLoS Genet.* **12,** e1005786 (2016).
573. Schoumacher, M. *et al.* Conditional expression of fascin increases tumor progression in a mouse model of intestinal cancer. *Eur. J. Cell Biol.* **93,** 388–395 (2014).
574. Yang, H. *et al.* Mechanosensitive caveolin-1 activation-induced PI3K/Akt/mTOR signaling pathway promotes breast cancer motility, invadopodia formation and metastasis in vivo. *Oncotarget* **7,** 16227–47 (2016).
575. Nicholas A., K. & Jacques P., B. in *Current Topics in Membranes* **56,** 79–111 (2005).
576. Schenk, S. & Quaranta, V. Tales from the crypt[ic] sites of the extracellular matrix. *Trends Cell Biol.* **13,** 366–375 (2003).
577. Altroff, H. *et al.* Interdomain tilt angle determines integrin-dependent function of the ninth and tenth FIII domains of human fibronectin. *J. Biol. Chem.* **279,** 55995–6003 (2004).
578. Brown, A. C., Rowe, J. A. & Barker, T. H. Guiding epithelial cell phenotypes with

engineered integrin-specific recombinant fibronectin fragments. *Tissue Eng Part A* **17,** 139–150 (2011).
579. Yurchenco, P. D., Tsilibary, E. C., Charonis, A. S. & Furthmayr, H. Models for the self-assembly of basement membrane. *J. Histochem. Cytochem.* **34,** 93–102 (1986).
580. Yurchenco, P. D., Smirnov, S. & Mathus, T. Analysis of basement membrane self-assembly and cellular interactions with native and recombinant glycoproteins. *Methods Cell Biol.* **2002,** 111–144 (2002).
581. Fässler, R. & Meyer, M. Consequences of lack of beta 1 integrin gene expression in mice. *Genes Dev.* **9,** 1896–908 (1995).
582. Stephens, L. E. *et al.* Deletion of beta1 integrins in mice results in inner cell mass failure and peri-implantation lethality. *Genes Dev.* **9,** 1883–1895 (1995).
583. Henry, M. D. & Campbell, K. P. A role for dystroglycan in basement membrane assembly. *Cell* **95,** 859–870 (1998).
584. McKee, K. K., Harrison, D., Capizzi, S. & Yurchenco, P. D. Role of laminin terminal globular domains in basement membrane assembly. *J. Biol. Chem.* **282,** 21437–21447 (2007).
585. Willem, M. *et al.* Specific ablation of the nidogen-binding site in the laminin γ1 chain interferes with kidney and lung development. *Development* **129,** 2711–2722 (2002).
586. Hohenester, E. & Yurchenco, P. D. Laminins in basement membrane assembly. *Cell Adhes. Migr.* **7,** 56–63 (2013).
587. Engvall, E. Structure and function of basement membranes. *Int. J. Dev. Biol.* **39,** 781–7 (1995).
588. Glentis, A., Gurchenkov, V. & Vignjevic, D. M. Assembly, heterogeneity, and breaching of the basement membranes. *Cell Adhes. Migr.* **8,** 236–245 (2014).
589. Kalluri, R. Basement membranes: Structure, assembly and role in tumour angiogenesis. *Nat. Rev. Cancer* **3,** 422–433 (2003).
590. Folkman, J. *et al.* A heparin-binding angiogenic protein-basic fibroblast growth factor-is stored within basement membrane. *Am. J. Pathol.* **130,** 393–400 (1988).
591. Vukicevic, S. *et al.* Identification of multiple active growth factors in basement membrane matrigel suggests caution in interpretation of cellular activity related to extracellular matrix components. *Exp. Cell Res.* **202,** 1–8 (1992).
592. Hagedorn, E. J. & Sherwood, D. R. Cell invasion through basement membrane: The anchor cell breaches the barrier. *Curr. Opin. Cell Biol.* **23,** 589–596 (2011).
593. Singh, B., Fleury, C., Jalalvand, F. & Riesbeck, K. Human pathogens utilize host extracellular matrix proteins laminin and collagen for adhesion and invasion of the host. *FEMS Microbiol. Rev.* **36,** 1122–1180 (2012).
594. Nakaya, Y., Sukowati, E. W., Wu, Y. & Sheng, G. RhoA and microtubule dynamics control cell-basement membrane interaction in EMT during gastrulation. *Nature* **10,** 765–775 (2008).
595. Even-Ram, S. & Yamada, K. M. Cell migration in 3D matrix. *Curr. Opin. Cell Biol.* **17,** 524–532 (2005).
596. Sherwood, D. R. & Sternberg, P. W. Anchor cell invasion into the vulval epithelium in C. elegans. *Dev. Cell* **5,** 21–31 (2003).
597. Hagedorn, E. J. *et al.* The netrin receptor DCC focuses invadopodia-driven basement membrane transmigration in vivo. *J. Cell Biol.* **201,** 903–913 (2013).
598. Sharma-Kishore, R., White, J. G., Southgate, E. & Podbilewicz, B. Formation of the vulva in Caenorhabditis elegans: A paradigm for organogenesis. *Development* **126,** 691–699

(1999).
599. Ziel, J. W., Hagedorn, E. J., Audhya, A. & Sherwood, D. R. UNC-6 (netrin) orients the invasive membrane of the anchor cell in C. elegans. *Nat. Cell Biol.* **11,** 183–189 (2009).
600. Hotary, K., Li, X. Y., Allen, E., Stevens, S. L. & Weiss, S. J. A cancer cell metalloprotease triad regulates the basement membrane transmigration program. *Genes Dev.* **20,** 2673–2686 (2006).
601. Cheung, M. *et al.* The transcriptional control of trunk neural crest induction, survival, and delamination. *Dev. Cell* **8,** 179–192 (2005).
602. Bort, R., Signore, M., Tremblay, K., Barbera, J. P. M. & Zaret, K. S. Hex homeobox gene controls the transition of the endoderm to a pseudostratified, cell emergent epithelium for liver bud development. *Dev. Biol.* **290,** 44–56 (2006).
603. Gouzi, M., Kim, Y. H., Katsumoto, K., Johansson, K. & Grapin-Botton, A. Neurogenin3 initiates stepwise delamination of differentiating endocrine cells during pancreas development. *Dev. Dyn.* **240,** 589–604 (2011).
604. Ihara, S. *et al.* Basement membrane sliding and targeted adhesion remodels tissue boundaries during uterine-vulval attachment in Caenorhabditis elegans. *Nat. Cell Biol.* **13,** 641–651 (2011).
605. Hiramatsu, R. *et al.* External mechanical cues trigger the establishment of the anterior-posterior axis in early mouse embryos. *Dev. Cell* **27,** 131–144 (2013).
606. Overall, C. M. & Kleifeld, O. Tumour microenvironment - opinion: validating matrix metalloproteinases as drug targets and anti-targets for cancer therapy. *Nat. Rev. Cancer* **6,** 227–39 (2006).
607. Cavallo-Medved, D. *et al.* Live-cell imaging demonstrates extracellular matrix degradation in association with active cathepsin B in caveolae of endothelial cells during tube formation. *Exp. Cell Res.* **315,** 1234–1246 (2009).
608. Valastyan, S. & Weinberg, R. A. Tumor metastasis: Molecular insights and evolving paradigms. *Cell* **147,** 275–292 (2011).
609. Matus, D. Q. *et al.* Supplementary materials for in vivo identification of regulators of cell invasion across basement membranes. *Sci. Signal.* **3,** ra35 (2010).
610. Löffek, S., Schilling, O. & Franzke, C. W. Biological role of matrix metalloproteinases: A critical balance. *Eur. Respir. J.* **38,** 191–208 (2011).
611. Byron, A. *et al.* A proteomic approach reveals integrin activation state-dependent control of microtubule cortical targeting. *Nat. Commun.* **6,** 6135 (2015).
612. Paul, N. R., Jacquemet, G. & Caswell, P. T. Endocytic trafficking of integrins in cell migration. *Curr. Biol.* **25,** R1092–R1105 (2015).
613. Humphries, J. D., Paul, N. R., Humphries, M. J. & Morgan, M. R. Emerging properties of adhesion complexes: What are they and what do they do? *Trends Cell Biol.* **25,** 388–397 (2015).
614. Kleifeld, O. *et al.* Identifying and quantifying proteolytic events and the natural N terminome by terminal amine isotopic labeling of substrates. *Nat. Protoc.* **6,** 1578–611 (2011).
615. Kleifeld, O. *et al.* Isotopic labeling of terminal amines in complex samples identifies protein N-termini and protease cleavage products. *Nat. Biotechnol.* **28,** 281–8 (2010).
616. Butler, G. S. & Overall, C. M. Proteomic identification of multitasking proteins in unexpected locations complicates drug targeting. *Nat. Rev. Drug Discov.* **8,** 935–48 (2009).
617. Dovas, A. *et al.* Visualization of actin polymerization in invasive structures of

macrophages and carcinoma cells using photoconvertible β-actin - Dendra2 fusion proteins. *PLoS One* **6,** e16485 (2011).
618. Marchesin, V. *et al.* ARF6-JIP3/4 regulate endosomal tubules for MT1-MMP exocytosis in cancer invasion. *J. Cell Biol.* **211,** 339–358 (2015).
619. Aumailley, M. & Smyth, N. The role of laminins in basement membrane function. *J. Anat.* **193 (Pt 1,** 1–21 (1998).
620. Domogatskaya, A., Rodin, S. & Tryggvason, K. Functional diversity of laminins. *Annu. Rev. Cell Dev. Biol.* **28,** 523–553 (2012).
621. Aumailley, M. The laminin family. *Cell Adh. Migr.* **7,** 48–55 (2013).
622. Sasaki, T., Fässler, R. & Hohenester, E. Laminin. *J. Cell Biol.* **164,** 959–963 (2004).
623. Li, S., Edgar, D., Fässler, R., Wadsworth, W. & Yurchenco, P. D. The role of laminin in embryonic cell polarization and tissue organization. *Dev. Cell* **4,** 613–624 (2003).
624. Giannelli, G. Induction of cell migration by matrix metalloprotease-2 cleavage of laminin-5. *Science (80-.).* **277,** 225–228 (1997).
625. Shapiro, S. D. Matrix metalloproteinase degradation of extracellular matrix: biological consequences. *Curr. Opin. Cell Biol.* **10,** 602–608 (1998).
626. Mydel, P. *et al.* Neutrophil elastase cleaves laminin-332 (laminin-5) generating peptides that are chemotactic for neutrophils. *J. Biol. Chem.* **283,** 9513–22 (2008).
627. Faisal Khan, K. M., Laurie, G. W., McCaffrey, T. A. & Falcone, D. J. Exposure of cryptic domains in the alpha 1-chain of laminin-1 by elastase stimulates macrophages urokinase and matrix metalloproteinase-9 expression. *J. Biol. Chem.* **277,** 13778–86 (2002).
628. Koshikawa, N., Giannelli, G., Cirulli, V., Miyazaki, K. & Quaranta, V. Role of cell surface metalloprotease MT1-MMP in epithelial cell migration over laminin 5. *J Cell Biol* **148,** 615–624 (2000).
629. Pulido, D., Hussain, S. A. & Hohenester, E. Crystal structure of the heterotrimeric integrin-binding region of laminin-111. *Structure* **25,** 530–535 (2017).
630. Myllyharju, J. & Kivirikko, K. I. Collagens, modifying enzymes and their mutations in humans, flies and worms. *Trends Genet.* **20,** 33–43 (2004).
631. Ricard-Blum, S. & Ruggiero, F. The collagen superfamily: From the extracellular matrix to the cell membrane. *Pathol. Biol.* **53,** 430–442 (2005).
632. Brodsky, B. & Persikov, A. V. Molecular structure of the collagen triple helix. *Adv. Protein Chem.* **70,** 301–339 (2005).
633. Fratzl, P. *et al.* Fibrillar structure and mechanical properties of collagen. *J. Struct. Biol.* **122,** 119–122 (1997).
634. Hulmes, D. J. S. Building collagen molecules, fibrils, and suprafibrillar structures. *J. Struct. Biol.* **137,** 2–10 (2002).
635. Wenstrup, R. J. *et al.* Type V collagen controls the initiation of collagen fibril assembly. *J. Biol. Chem.* **279,** 53331–53337 (2004).
636. Bruckner, P. Suprastructures of extracellular matrices: Paradigms of functions controlled by aggregates rather than molecules. *Cell Tissue Res.* **339,** 7–18 (2010).
637. Molnar, J. *et al.* Structural and functional diversity of lysyl oxidase and the LOX-like proteins. *Biochim. Biophys. Acta - Proteins Proteomics* **1647,** 220–224 (2003).
638. Eyre, D. R. & Glimcher, M. J. Collagen cross-linking. Isolation of cross-linked peptides from collagen of chicken bone. *Biochem. J.* **135,** 393–403 (1973).
639. Lucero, H. A. & Kagan, H. M. Lysyl oxidase: An oxidative enzyme and effector of cell function. *Cell. Mol. Life Sci.* **63,** 2304–2316 (2006).

640. Ross, A. S., Farrimond, P., Erdmann, M. & Larter, S. R. Geochemical compositional gradients in a mixed oil reservoir indicative of ongoing biodegradation. *Org. Geochem.* **41,** 307–320 (2010).
641. Wess, T. J. in *Advances in Protein Chemistry* **70,** 341–374 (2005).
642. Halfter, W. *et al.* Protein composition and biomechanical properties of in vivo-derived basement membranes. *Cell Adhes. Migr.* **7,** 64–71 (2013).
643. Khoshnoodi, J., Pedchenko, V. & Hudson, B. G. Mammalian collagen IV. *Microsc. Res. Tech.* **71,** 357–370 (2008).
644. Fidler, A. L. *et al.* A unique covalent bond in basement membrane is a primordial innovation for tissue evolution. *Proc. Natl. Acad. Sci. U. S. A.* **111,** 331–6 (2014).
645. Margadant, C. & Sonnenberg, A. Integrin–TGF-β crosstalk in fibrosis, cancer and wound healing. *EMBO Rep.* **11,** 97–105 (2010).
646. González-Mariscal, L., Betanzos, A., Nava, P. & Jaramillo, B. E. Tight junction proteins. *Prog. Biophys. Mol. Biol.* **81,** 1–44 (2003).
647. Polette, M. *et al.* β-catenin and ZO-1: Shuttle molecules involved in tumor invasion-associated epithelial-mesenchymal transition processes. *Cells Tissues Organs* **185,** 61–65 (2007).
648. Gottardi, C. J., Arpin, M., Fanning, a S. & Louvard, D. The junction-associated protein, zonula occludens-1, localizes to the nucleus before the maturation and during the remodeling of cell-cell contacts. *Proc. Natl. Acad. Sci. U. S. A.* **93,** 10779–10784 (1996).
649. Lamouille, S., Xu, J. & Derynck, R. Molecular mechanisms of epithelial–mesenchymal transition. *Nat. Rev. Mol. Cell Biol.* **15,** 178–196 (2014).
650. Bhowmick, N. A., Zent, R., Ghiassi, M., McDonnell, M. & Moses, H. L. Integrin β1 Signaling is Necessary for Transforming Growtn Factor-β Activation of p38MAPK and Epithelial Plasticity. *J. Biol. Chem.* **276,** 46707–46713 (2001).
651. Prunier, C. & Howe, P. H. Disabled-2 (Dab2) is required for transforming growth factor β-induced epithelial to mesenchymal transition (EMT). *J. Biol. Chem.* **280,** 17540–17548 (2005).
652. Balzac, F. *et al.* E-cadherin endocytosis regulates the activity of Rap1: A traffic light GTPase at the crossroads between cadherin and integrin function. *J. Cell Sci.* **118,** 4765–4783 (2005).
653. McPhee, T. R., McDonald, P. C., Oloumi, A. & Dedhar, S. Integrin-linked kinase regulates E-cadherin expression through PARP-1. *Dev. Dyn.* **237,** 2737–2747 (2008).
654. Gimond, C. *et al.* Induction of cell scattering by expression of beta1 integrins in beta1-deficient epithelial cells requires activation of members of the rho family of GTPases and downregulation of cadherin and catenin function. *J Cell Biol* **147,** 1325–1340 (1999).
655. Wiesner, S., Legate, K. R. & Fässler, R. Integrin-actin interactions. *Cell. Mol. Life Sci.* **62,** 1081–1099 (2005).
656. Kim, K. K. *et al.* Alveolar epithelial cell mesenchymal transition develops in vivo during pulmonary fibrosis and is regulated by the extracellular matrix. *Proc. Natl. Acad. Sci. U. S. A.* **103,** 13180–5 (2006).
657. Kim, Y. *et al.* Integrin alpha3beta1 - dependent beta-catenin phosphorylation links epithelial smad signaling to cell contacts. *J. Cell Biol.* **184,** 309–322 (2009).
658. Kim, K. K. *et al.* Epithelial cell α3β1 integrin links β-catenin and Smad signaling to promote myofibroblast formation and pulmonary fibrosis. *J. Clin. Invest.* **119,** 213–224 (2009).

659. NAGASE, H., VISSE, R. & MURPHY, G. Structure and function of matrix metalloproteinases and TIMPs. *Cardiovasc. Res.* **69,** 562–573 (2006).
660. Murphy, G. & Nagase, H. Progress in matrix metalloproteinase research. *Mol. Aspects Med.* **29,** 290–308 (2009).
661. Sternlicht, M. D. & Werb, Z. How matrix metalloproteinases regulate cell behavior. *Annu. Rev. Cell Dev. Biol.* **17,** 463–516 (2001).
662. Duarte, S., Baber, J., Fujii, T. & Coito, A. J. Matrix metalloproteinases in liver injury, repair and fibrosis. *Matrix Biol.* **44–46,** 147–156 (2015).
663. Gaggar, a *et al.* The role of matrix metalloproteinases in cystic fibrosis lung disease. *Eur. Respir. J.* **38,** 721–7 (2011).
664. Yu, X. & Machesky, L. M. Cells assemble invadopodia-like structures and invade into matrigel in a matrix metalloprotease dependent manner in the circular invasion assay. *PLoS One* **7,** e30605 (2012).
665. Mott, J. D. & Werb, Z. Regulation of matrix biology by matrix metalloproteinases. *Curr. Opin. Cell Biol.* **16,** 558–564 (2004).
666. Lin, C. Y. *et al.* Matrix metalloproteinase-9 cooperates with transcription factor Snail to induce epithelial-mesenchymal transition. *Cancer Sci.* **102,** 815–827 (2011).
667. Clark, I. M., Swingler, T. E., Sampieri, C. L. & Edwards, D. R. The regulation of matrix metalloproteinases and their inhibitors. *Int. J. Biochem. Cell Biol.* **40,** 1362–1378 (2008).
668. Murphy, G. Tissue inhibitors of metalloproteinases. *Genome Biol.* **12,** 233 (2011).
669. Mannello, F. & Medda, V. Nuclear localization of matrix metalloproteinases. *Prog. Histochem. Cytochem.* **47,** 27–58 (2012).
670. Van Wart, H. E. & Birkedal-Hansen, H. The cysteine switch: a principle of regulation of metalloproteinase activity with potential applicability to the entire matrix metalloproteinase gene family. *Proc. Natl. Acad. Sci. U. S. A.* **87,** 5578–82 (1990).
671. Brew, K. & Nagase, H. The tissue inhibitors of metalloproteinases (TIMPs): An ancient family with structural and functional diversity. *Biochim. Biophys. Acta - Mol. Cell Res.* **1803,** 55–71 (2010).
672. Bourboulia, D. & Stetler-Stevenson, W. G. Matrix metalloproteinases (MMPs) and tissue inhibitors of metalloproteinases (TIMPs): Positive and negative regulators in tumor cell adhesion. *Semin. Cancer Biol.* **20,** 161–168 (2010).
673. Itoh, Y. Membrane-type matrix metalloproteinases: Their functions and regulations. *Matrix Biol.* **44,** 207–223 (2015).
674. Itoh, Y. MT1-MMP: A key regulator of cell migration in tissue. *IUBMB Life (International Union Biochem. Mol. Biol. Life)* **58,** 589–596 (2006).
675. Seiki, M. The cell surface: The stage for matrix metalloproteinase regulation of migration. *Curr. Opin. Cell Biol.* **14,** 624–632 (2002).
676. Chen, L., Nakai, M., Belton, R. J. & Nowak, R. a. Expression of extracellular matrix metalloproteinase inducer and matrix metalloproteinases during mouse embryonic development. *Reproduction* **133,** 405–414 (2007).
677. Coyle, R. C., Latimer, A. & Jessen, J. R. Membrane-type 1 matrix metalloproteinase regulates cell migration during zebrafish gastrulation: Evidence for an interaction with non-canonical Wnt signaling. *Exp. Cell Res.* **314,** 2150–2162 (2008).
678. Du, X. *et al.* Involvement of matrix metalloproteinase-2 in the development of renal interstitial fibrosis in mouse obstructive nephropathy. *Lab. Investig.* **92,** 1149–1160 (2012).
679. Duong, T. D. & Erickson, C. A. MMP-2 plays an essential role in producing epithelial-

mesenchymal transformations in the avian embryo. *Dev. Dyn.* **229,** 42–53 (2004).
680. Egeblad, M. & Werb, Z. New functions for the matrix metalloproteinases in cancer progression. *Nat Rev Cancer* **2,** 161–174 (2002).
681. Giannandrea, M. & Parks, W. C. Diverse functions of matrix metalloproteinases during fibrosis. *Dis. Model. Mech.* **7,** 193–203 (2014).
682. Kinoh, H. *et al.* MT-MMP, the cell surface activator of proMMP-2 (pro-gelatinase A), is expressed with its substrate in mouse tissue during embryogenesis. *J. Cell Sci.* 953–9 (1996).
683. Lemaître, V. & D'Armiento, J. Matrix metalloproteinases in development and disease. *Birth Defects Res. Part C - Embryo Today Rev.* **78,** 1–10 (2006).
684. Mogi, K. & Toyoizumi, R. Invasion by matrix metalloproteinase-expressing cells is important for primitive streak formation in early chick blastoderm. *Cells Tissues Organs* **192,** 1–16 (2010).
685. Nisticò, P., Bissell, M. J. & Radisky, D. C. Epithelial-mesenchymal transition: General principles and pathological relevance with special emphasis on the role of matrix metalloproteinases. *Cold Spring Harb. Perspect. Biol.* **4,** a011908–a011908 (2012).
686. Orlichenko, L. S. & Radisky, D. C. Matrix metalloproteinases stimulate epithelial-mesenchymal transition during tumor development. *Clin. Exp. Metastasis* **25,** 593–600 (2008).
687. Poincloux, R., Lizárraga, F. & Chavrier, P. Matrix invasion by tumour cells: A focus on MT1-MMP trafficking to invadopodia. *J. Cell Sci.* **122,** 3015–24 (2009).
688. Wiseman, B. S. *et al.* Site-specific inductive and inhibitory activities of MMP-2 and MMP-3 orchestrate mammary gland branching morphogenesis. *J. Cell Biol.* **162,** 1123–1133 (2003).
689. Kargozaran, H. *et al.* A role for endothelial-derived matrix metalloproteinase-2 in breast cancer cell transmigration across the endothelial-basement membrane barrier. *Clin. Exp. Metastasis* **24,** 495–502 (2007).
690. Hirahara, I. *et al.* The potential of matrix metalloproteinase-2 as a marker of peritoneal injury, increased solute transport, or progression to encapsulating peritoneal sclerosis during peritoneal dialysis - A multicentre study in Japan. *Nephrol. Dial. Transplant.* **22,** 560–567 (2007).
691. Corbel, M. *et al.* Repeated endotoxin exposure induces interstitial fibrosis associated with enhanced gelatinase (MMP-2 and MMP-9) activity. *Inflamm. Res.* **50,** 129–135 (2001).
692. Dangi-Garimella, S., Strouch, M. J., Grippo, P. J., Bentrem, D. J. & Munshi, H. G. Collagen regulation of let-7 in pancreatic cancer involves TGF-β1-mediated membrane type 1-matrix metalloproteinase expression. *Oncogene* **30,** 1002–8 (2011).
693. Pang, L. *et al.* Membrane type 1-matrix metalloproteinase induces epithelial-to-mesenchymal transition in esophageal squamous cell carcinoma: Observations from clinical and in vitro analyses. *Sci. Rep.* **6,** 22179 (2016).
694. Radisky, D. C. *et al.* Rac1b and reactive oxygen species mediate MMP-3-induced EMT and genomic instability. *Nature* **436,** 123–7 (2005).
695. Ries, C. *et al.* MMP-2, MT1-MMP, and TIMP-2 are essential for the invasive capacity of human mesenchymal stem cells: Differential regulation by inflammatory cytokines. *Blood* **109,** 4055–4063 (2007).
696. Shields, M. A., Dangi-Garimella, S., Krantz, S. B., Bentrem, D. J. & Munshi, H. G. Pancreatic cancer cells respond to type I collagen by inducing snail expression to

promote membrane type 1 matrix metalloproteinase-dependent collagen invasion. *J. Biol. Chem.* **286,** 10495–10504 (2011).
697. Song, W., Jackson, K. & McGuire, P. G. Degradation of type IV collagen by matrix metalloproteinases is an important step in the epithelial-mesenchymal transformation of the endocardial cushions. *Dev. Biol.* **227,** 606–17 (2000).
698. Walsh, L. A., Cooper, C. A. & Damjanovski, S. Soluble membrane-type 3 matrix metalloproteinase causes changes in gene expression and increased gelatinase activity during Xenopus laevis development. *Int. J. Dev. Biol.* **51,** 389–395 (2007).
699. Park, B. K., Zeng, X. & Glazer, R. I. Akt1 induces extracellular matrix invasion and matrix metalloproteinase-2 activity in mouse mammary epithelial cells. *Cancer Res* **61,** 7647–7653 (2001).
700. Lochter, A. *et al.* Matrix metalloproteinase stromelysin-1 triggers a cascade of molecular alterations that leads to stable epithelial-to-mesenchymal conversion and a premalignant phenotype in mammary epithelial cells. *J. Cell Biol.* **139,** 1861–1872 (1997).
701. Sternlicht, M. D. *et al.* The stromal proteinase MMP3/stromelysin-1 promotes mammary carcinogenesis. *Cell* **98,** 137–146 (1999).
702. Cheng, S. & Lovett, D. H. Gelatinase A (MMP-2) is necessary and sufficient for renal tubular cell epithelial-mesenchymal transformation. *Am. J. Pathol.* **162,** 1937–49 (2003).
703. Ota, I., Li, X. Y., Hu, Y. & Weiss, S. J. Induction of a MT1-MMP and MT2-MMP-dependent basement membrane transmigration program in cancer cells by Snail1. *Proc. Natl. Acad. Sci. U. S. A.* **106,** 20318–20323 (2009).
704. Vu, T. H. & Werb, Z. Matrix metalloproteinases: Effectors of development and normal physiology. *Genes Dev.* **14,** 2123–2133 (2000).
705. Gialeli, C., Theocharis, A. D. & Karamanos, N. K. Roles of matrix metalloproteinases in cancer progression and their pharmacological targeting. *FEBS J.* **278,** 16–27 (2011).
706. Coussens, L. M., Fingleton, B. & Matrisian, L. M. Matrix metalloproteinase inhibitors and cancer: trials and tribulations. *Science (80-.).* **295,** 2387–2392 (2002).
707. Sakurai-Yageta, M. *et al.* The interaction of IQGAP1 with the exocyst complex is required for tumor cell invasion downstream of Cdc42 and RhoA. *J. Cell Biol.* **181,** 985–998 (2008).
708. Steffen, A. *et al.* MT1-MMP-dependent invasion is regulated by TI-VAMP/VAMP7. *Curr. Biol.* **18,** 926–931 (2008).
709. Yu, X. *et al.* N-WASP coordinates the delivery and F-actin-mediated capture of MT1-MMP at invasive pseudopods. *J. Cell Biol.* **199,** 527–544 (2012).
710. Yana, I. & Weiss, S. J. Regulation of membrane type-1 matrix metalloproteinase activation by proprotein convertases. *Mol. Biol. Cell* **11,** 2387–401 (2000).
711. Castro-Castro, A. *et al.* Cellular and molecular Mmechanisms of MT1-MMP-dependent cancer cell invasion. *Annu. Rev. Cell Dev. Biol.* **32,** annurev-cellbio-111315-125227 (2016).
712. Monteiro, P. *et al.* Endosomal WASH and exocyst complexes control exocytosis of MT1-MMP at invadopodia. *J. Cell Biol.* **203,** 1063–1079 (2013).
713. Zucker, S., Pei, D., Cao, J. & Lopez-Otin, C. in 1–74 (2003). doi:10.1016/S0070-2153(03)54004-2
714. Itoh, Y. & Nagase, H. Matrix metalloproteinases in cancer. *Essays Biochem.* **38,** 21–36 (2002).

715. Nishida, Y. *et al.* Activation of Matrix Metalloproteinase-2 (MMP-2) by Membrane Type 1 Matrix Metalloproteinase through an Artificial Receptor for ProMMP-2 Generates Active MMP-2. *Cancer Res.* **68,** 9096–9104 (2008).
716. Knäuper, V. *et al.* Cellular mechanisms for human procollagenase-3 (MMP-13) activation. Evidence that MT1-MMP (MMP-14) and gelatinase a (MMP-2) are able to generate active enzyme. *J. Biol. Chem.* **271,** 17124–31 (1996).
717. Holmbeck, K. *et al.* MT1-MMP-deficient mice develop dwarfism, osteopenia, arthritis, and connective tissue disease due to inadequate collagen turnover. *Cell* **99,** 81–92 (1999).
718. Oblander, S. A. *et al.* Distinctive functions of membrane type 1 matrix-metalloprotease (MT1-MMP or MMP-14) in lung and submandibular gland development are independent of its role in pro-MMP-2 activation. *Dev. Biol.* **277,** 255–269 (2005).
719. Zhou, Z. *et al.* Impaired endochondral ossification and angiogenesis in mice deficient in membrane-type matrix metalloproteinase I. *Proc. Natl. Acad. Sci. U. S. A.* **97,** 4052–7 (2000).
720. Oh, J. *et al.* Mutations in two matrix metalloproteinase genes, MMP-2 and MT1-MMP, are synthetic lethal in mice. *Oncogene* **23,** 5041–8 (2004).
721. Björklund, M. & Koivunen, E. Gelatinase-mediated migration and invasion of cancer cells. *Biochim. Biophys. Acta - Rev. Cancer* **1755,** 37–69 (2005).
722. Kwiatkowska, A., Kijewska, M., Lipko, M., Hibner, U. & Kaminska, B. Downregulation of Akt and FAK phosphorylation reduces invasion of glioblastoma cells by impairment of MT1-MMP shuttling to lamellipodia and downregulates MMPs expression. *Biochim. Biophys. Acta - Mol. Cell Res.* **1813,** 655–667 (2011).
723. Segarra, M. *et al.* Dual function of focal adhesion kinase in regulating integrin-induced MMP-2 and MMP-9 release by human T lymphoid cells. *FASEB J.* **19,** 1875–7 (2005).
724. Sein, T. T. *et al.* A role for FAK in the Concanavalin A-dependent secretion of matrix metalloproteinase-2 and -9. *Oncogene* **19,** 5539–42 (2000).
725. Moon, S. K., Cha, B. Y. & Kim, C. H. ERK1/2 mediates TNF-α-induced matrix etalloproteinase-9 expression in human vascular smooth muscle cells via the regulation of NF-κB and AP-1: Involvement of the Ras dependent pathway. *J. Cell. Physiol.* **198,** 417–427 (2004).
726. Bond, M., Fabunmi, R. P., Baker, A. H. & Newby, A. C. Synergistic upregulation of metalloproteinase-9 by growth factors and inflammatory cytokines: An absolute requirement for transcription factor NF-κB. *FEBS Lett.* **435,** 29–34 (1998).
727. Tan, T. K. *et al.* Matrix metalloproteinase-9 of tubular and macrophage origin contributes to the pathogenesis of renal fibrosis via macrophage recruitment through osteopontin cleavage. *Lab. Invest.* **93,** 434–49 (2013).
728. Bauvois, B. New facets of matrix metalloproteinases MMP-2 and MMP-9 as cell surface transducers: Outside-in signaling and relationship to tumor progression. *Biochim. Biophys. Acta - Rev. Cancer* **1825,** 29–36 (2012).
729. Wang, Z. *et al.* Alpha3beta1 integrin regulates epithelial cytoskeletal organization. *J. Cell Sci.* **112 (Pt 1,** 2925–2935 (1999).
730. Kreidberg, J. A. Functions of α3β1 integrin. *Curr. Opin. Cell Biol.* **12,** 548–553 (2000).
731. Bökel, C. & Brown, N. H. Integrins in Development: Moving on, Responding to, and Sticking to the Extracellular Matrix. *Dev. Cell* **3,** 311–321 (2002).
732. Berditchevski, F., Chang, S., Bodorova, J. & Hemler, M. E. Generation of monoclonal antibodies to integrin-associated proteins. Evidence that alpha3beta1 complexes with

emmprin/basigin/OX47/M6. *J. Biol. Chem.* **272,** 29174–29180 (1997).
733. Zhang, F. *et al.* Distinct ligand binding sites in integrin alpha3beta1 regulate matrix adhesion and cell-cell contact. *J. Cell Biol.* **163,** 177–88 (2003).
734. Iyer, V., Pumiglia, K. & DiPersio, C. M. Alpha3beta1 integrin regulates MMP-9 mRNA stability in immortalized keratinocytes: a novel mechanism of integrin-mediated MMP gene expression. *J. Cell Sci.* **118,** 1185–1195 (2005).
735. Eble, J. A. *et al.* Recombinant soluble human α3β1 integrin: Purification, processing, regulation, and specific binding to laminin-5 and invasin in a mutually exclusive manner. *Biochemistry* **37,** 10945–10955 (1998).
736. Nakamura, K., Iwamoto, R. & Mekada, E. Membrane-anchored heparin-binding EGF-like growth factor (HB-EGF) and diphtheria toxin receptor-associated protein (DRAP27)/CD9 form a complex with integrin alpha3beta1 at cell-cell contact sites. *J. Cell Biol.* **129,** 1691–1705 (1995).
737. Chattopadhyay, N., Wang, Z., Ashman, L. K., Brady-Kalnay, S. M. & Kreidberg, J. A. α3β1 integrin-CD151, a component of the cadherin-catenin complex, regulates PTPμ expression and cell-cell adhesion. *J. Cell Biol.* **163,** 1351–1362 (2003).
738. Lubman, R. L. *et al.* Integrin alpha(3)-subunit expression modulates alveolar epithelial cell monolayer formation. *Am J Physiol Lung Cell Mol Physiol* **279,** L183-93 (2000).
739. Carter, W. G., Wayner, E. a, Bouchard, T. S. & Kaur, P. The role of integrins alpha 2 beta 1 and alpha 3 beta 1 in cell-cell and cell-substrate adhesion of human epidermal cells. *J. Cell Biol.* **110,** 1387–1404 (1990).
740. Nicolaou, N. *et al.* Gain of glycosylation in integrin α3 causes lung disease and nephrotic syndrome. *J. Clin. Invest.* **122,** 4375–4387 (2012).
741. Yalcin, E. G. *et al.* Crucial role of posttranslational modifications of integrin alpha3 in interstitial lung disease and nephrotic syndrome. *Hum. Mol. Genet.* **24,** 3679–3688 (2015).
742. Has, C. *et al.* Integrin α3 mutations with kidney, lung, and skin disease. *N. Engl. J. Med.* **366,** 1508–14 (2012).
743. Kreidberg, J. A. *et al.* Alpha 3 beta 1 integrin has a crucial role in kidney and lung organogenesis. *Development* **122,** 3537–3547 (1996).
744. DiPersio, C. M., Hodivala-Dilke, K. M., Jaenisch, R., Kreidberg, J. A. & Hynes, R. O. alpha3beta1 integrin is required for normal development of the epidermal basement membrane. *J. Cell Biol.* **137,** 729–742 (1997).
745. Sachs, N. *et al.* Loss of integrin α3 prevents skin tumor formation by promoting epidermal turnover and depletion of slow-cycling cells. *Proc. Natl. Acad. Sci. U. S. A.* **109,** 21468–73 (2012).
746. Raymond, K. *et al.* Control of mammary myoepithelial cell contractile function by α3β1 integrin signalling. *EMBO J.* **30,** 1896–906 (2011).
747. Margadant, C. *et al.* Integrin alpha3beta1 inhibits directional migration and wound re-epithelialization in the skin. *J. Cell Sci.* **122,** 278–88 (2009).
748. Rousselle, P., Lunstrum, G. P., Keene, D. R. & Burgeson, R. E. Kalinin: An epithelium-specific basement membrane adhesion molecule that is a component of anchoring filaments. *J. Cell Biol.* **114,** 567–576 (1991).
749. Carter, W. G., Ryan, M. C. & Gahr, P. J. Epiligrin, a new cell adhesion ligand for integrin α3β1 in epithelial basement membranes. *Cell* **65,** 599–610 (1991).
750. Wayner, E. a & Carter, W. G. Identification of multiple cell adhesion receptors for collagen and fibronectin in human fibrosarcoma cells possessing unique alpha and

common beta subunits. *J. Cell Biol.* **105,** 1873–1884 (1987).
751. Gehlsen, K. R., Dickerson, K., Argraves, W. S., Engvall, E. & Ruoslahti, E. Subunit structure of a laminin-binding integrin and localization of its binding site on laminin. *J. Biol. Chem.* **264,** 19034–19038 (1989).
752. Elices, M. J., Urry, L. A. & Hemler, M. E. Receptor functions for the integrin VLA-3: Fibronectin, collagen, and laminin binding are differentially influenced by ARG-GLY-ASP peptide and by divalent cations. *J. Cell Biol.* **112,** 169–181 (1991).
753. Clyman, R. I., Mauray, F. & Kramer, R. H. Beta 1 and beta 3 integrins have different roles in the adhesion and migration of vascular smooth muscle cells on extracellular matrix. *Exp. Cell Res.* **200,** 272–84 (1992).
754. Weitzman, J. B., Pasqualini, R., Takada, Y. & Hemler, M. E. The function and distinctive regulation of the integrin VLA-3 in cell adhesion, spreading, and homotypic cell aggregation. *J. Biol. Chem.* **268,** 8651–8657 (1993).
755. Delwel, G. O. *et al.* Distinct and overlapping ligand specificities of the alpha 3A beta 1 and alpha 6A beta 1 integrins: recognition of laminin isoforms. *Mol. Biol. Cell* **5,** 203–215 (1994).
756. DiPersio, C. M., Shah, S. & Hynes, R. O. alpha 3A beta 1 integrin localizes to focal contacts in response to diverse extracellular matrix proteins. *J. Cell Sci.* **108 (Pt 6,** 2321–36 (1995).
757. Cheresh, D. A. Human endothelial cells synthesize and express an Arg-Gly-Asp-directed adhesion receptor involved in attachment to fibrinogen and von Willebrand factor. *Proc. Natl. Acad. Sci. U. S. A.* **84,** 6471–5 (1987).
758. Dogic, D., Rousselle, P. & Aumailley, M. Cell adhesion to laminin 1 or 5 induces isoform-specific clustering of integrins and other focal adhesion components. *J. Cell Sci.* **111 (Pt 6,** 793–802 (1998).
759. Tang, W., Chang, S. B. & Hemler, M. E. Links between CD147 function, glycosylation, and caveolin-1. *Mol. Biol. Cell* **15,** 4043–50 (2004).
760. Weidle, U. H., Scheuer, W., Eggle, D., Klostermann, S. & Stockinger, H. Cancer-related issues of CD147. *Cancer Genomics and Proteomics* **7,** 157–169 (2010).
761. Iacono, K. T., Brown, A. L., Greene, M. I. & Saouaf, S. J. CD147 immunoglobulin superfamily receptor function and role in pathology. *Exp. Mol. Pathol.* **83,** 283–295 (2007).
762. Curtin, K. D., Meinertzhagen, I. a & Wyman, R. J. Basigin (EMMPRIN/CD147) interacts with integrin to affect cellular architecture. *J. Cell Sci.* **118,** 2649–2660 (2005).
763. Tang, J. *et al.* Overexpression of HAb18G/CD147 promotes invasion and metastasis via alpha3beta1 integrin mediated FAK-paxillin and FAK-PI3K-Ca2+ pathways. *Cell. Mol. Life Sci.* **65,** 2933–2942 (2008).
764. Lawrence, D. A. Transforming growth factor-beta: a general review. *Eur. Cytokine Netw.* **7,** 363–74 (1996).
765. Roberts, A. B. *et al.* Type beta transforming growth factor: A bifunctional regulator of cellular growth. *Proc. Natl. Acad. Sci. U. S. A.* **82,** 119–23 (1985).
766. Coffey, R. J. *et al.* Selective inhibition of growth-related gene expression in murine keratinocytes by transforming growth factor beta. *Mol. Cell. Biol.* **8,** 3088–93 (1988).
767. Annes, J. P., Munger, J. S. & Rifkin, D. B. Making sense of latent TGFbeta activation. *J. Cell Sci.* **116,** 217–24 (2003).
768. Munger, J. S. & Sheppard, D. Cross talk among TGF-β signaling pathways, integrins, and the extracellular matrix. *Cold Spring Harb. Perspect. Biol.* **3,** a005017–a005017 (2011).

769. Robertson, I. B. & Rifkin, D. B. Unchaining the beast; insights from structural and evolutionary studies on TGFβ secretion, sequestration, and activation. *Cytokine Growth Factor Rev.* **24,** 355–372 (2013).
770. Wrana, J. L. *et al.* TGFβ signals through a heteromeric protein kinase receptor complex. *Cell* **71,** 1003–1014 (1992).
771. Edlund, S. *et al.* Transforming growth factor-beta1 (TGF-beta)-induced apoptosis of prostate cancer cells involves Smad7-dependent activation of p38 by TGF-beta-activated kinase 1 and mitogen-activated protein kinase kinase 3. *Mol.Biol.Cell* **14,** 529–544 (2003).
772. Travis, M. A. & Sheppard, D. TGF-β activation and function in immunity. *Annu. Rev. Immunol.* **32,** 51–82 (2014).
773. Massagué, J. TGFβ signalling in context. *Nat. Rev. Mol. Cell Biol.* **13,** 616–30 (2012).
774. Macias, M. J., Martin-Malpartida, P. & Massagué, J. Structural determinants of Smad function in TGF-β signaling. *Trends Biochem. Sci.* **40,** 296–308 (2015).
775. Massagué, J. & Wotton, D. Transcriptional control by the TGF-beta/Smad signaling system. *EMBO J.* **19,** 1745–1754 (2000).
776. Massagué, J. & Chen, Y. G. Controlling TGF-β signaling. *Genes Dev.* **14,** 627–644 (2000).
777. Massagué, J., Blain, S. W. & Lo, R. S. TGFbeta signaling in growth control, cancer, and heritable disorders. *Cell* **103,** 295–309 (2000).
778. Roberts, A. B., McCune, B. K. & Sporn, M. B. TGF-β: Regulation of extracellular matrix. *Kidney Int.* **41,** 557–559 (1992).
779. Sporn, M. B. & Roberts, A. B. Transforming growth factor-beta: Recent progress and new challenges. *J. Cell Biol.* **119,** 1017–21 (1992).
780. Ikushima, H. & Miyazono, K. TGFβ signalling: A complex web in cancer progression. *Nat. Rev. Cancer* **10,** 415–424 (2010).
781. Kitisin, K. *et al.* TGF-beta signaling in development. *Sci. STKE* **2007,** cm1-cm1 (2007).
782. Meulmeester, E. & ten Dijke, P. The dynamic roles of TGF-β in cancer. *J. Pathol.* **223,** 206–219 (2011).
783. Schmierer, B. & Hill, C. S. TGFβ–SMAD signal transduction: Molecular specificity and functional flexibility. *Nat. Rev. Mol. Cell Biol.* **8,** 970–982 (2007).
784. Zhang, L., Zhou, F. & ten Dijke, P. Signaling interplay between transforming growth factor-beta receptor and PI3K/AKT pathways in cancer. *Trends Biochem. Sci.* **38,** 612–620 (2013).
785. Piek, E., Moustakas, A., Kurisaki, A., Heldin, C. H. & ten Dijke, P. TGF-(beta) type I receptor/ALK-5 and Smad proteins mediate epithelial to mesenchymal transdifferentiation in NMuMG breast epithelial cells. *J. Cell Sci.* 4557–68 (1999).
786. Poniatowski, L. A., Wojdasiewicz, P., Gasik, R. & Szukiewicz, D. Transforming growth factor beta family: Insight into the role of growth factors in regulation of fracture healing biology and potential clinical applications. *Mediators Inflamm.* **2015,** 1–17 (2015).
787. Van Roy, F. & Berx, G. The cell-cell adhesion molecule E-cadherin. *Cell. Mol. Life Sci.* **65,** 3756–3788 (2008).
788. Harrison, O. J. *et al.* Two-step adhesive binding by classical cadherins. *Nat. Struct. Mol. Biol.* **17,** 348–57 (2010).
789. Yonemura, S., Wada, Y., Watanabe, T., Nagafuchi, A. & Shibata, M. alpha-Catenin as a tension transducer that induces adherens junction development. *Nat. Cell Biol.* **12,** 533–42 (2010).

790. Yao, M. *et al.* Force-dependent conformational switch of α-catenin controls vinculin binding. *Nat. Commun.* **5,** 4525 (2014).
791. Monteleone, G., Caruso, R. & Pallone, F. Role of Smad7 in inflammatory bowel diseases. *World J. Gastroenterol.* **18,** 5664–8 (2012).
792. Kleeff, J. *et al.* The TGF-β signaling inhibitor Smad7 enhances tumorigenicity in pancreatic cancer. *Oncogene* **18,** 5363–5372 (1999).
793. Nakao, A. *et al.* Identification of Smad7, a TGFbeta-inducible antagonist of TGF-beta signalling. *Nature* **389,** 631–635 (1997).
794. Zhang, S. *et al.* Smad7 antagonizes transforming growth factor beta signaling in the nucleus by interfering with functional Smad-DNA complex formation. *Mol. Cell. Biol.* **27,** 4488–4499 (2007).
795. Zhang, W. *et al.* MAPK signal pathways in the regulation of cell proliferation in mammalian cells. *Cell Res.* **12,** 9–18 (2002).
796. Guo, X. & Wang, X.-F. Signaling cross-talk between TGF-beta/BMP and other pathways. *Cell Res.* **19,** 71–88 (2009).
797. Roux, P. P. & Blenis, J. ERK and p38 MAPK-activated protein kinases: a family of protein kinases with diverse biological functions. *Microbiol. Mol. Biol. Rev.* **68,** 320–44 (2004).
798. Zhang, Y. E. Non-Smad pathways in TGF-β signaling. *Cell Res.* **19,** 128–39 (2009).
799. Lee, K. & Nelson, C. M. in *International Review of Cell and Molecular Biology* **294,** 171–221 (2012).
800. Watanabe-Takano, H., Takano, K., Hatano, M., Tokuhisa, T. & Endo, T. DA-Raf-mediated suppression of the Ras-ERK pathway is essential for TGF-β1-induced epithelial-mesenchymal transition in alveolar epithelial type 2 cells. *PLoS One* **10,** e0127888 (2015).
801. Xie, L. *et al.* Activation of the Erk pathway is required for TGF-beta1-induced EMT in vitro. *Neoplasia* **6,** 603–610 (2004).
802. Zavadil, J. *et al.* Genetic programs of epithelial cell plasticity directed by transforming growth factor-beta. *Proc. Natl. Acad. Sci. U. S. A.* **98,** 6686–91 (2001).
803. Davies, M. *et al.* Induction of an epithelial to mesenchymal transition in human immortal and malignant keratinocytes by TGF-beta1 involves MAPK, Smad and AP-1 signalling pathways. *J. Cell. Biochem.* **95,** 918–931 (2005).
804. Kretzschmar, M., Doody, J. & Massagué, J. Opposing BMP and EGF signalling pathways converge on the TGF-beta family mediator Smad1. *Nature* **389,** 618–22 (1997).
805. Kretzschmar, M., Doody, J., Timokhina, I. & Massagué, J. A mechanism of repression of TGFbeta/ Smad signaling by oncogenic Ras. *Genes Dev.* **13,** 804–16 (1999).
806. Funaba, M., Zimmerman, C. M. & Mathews, L. S. Modulation of Smad2-mediated signaling by extracellular signal-regulated kinase. *J. Biol. Chem.* **277,** 41361–41368 (2002).
807. Matsuura, I., Wang, G., He, D. & Liu, F. Identification and characterization of ERK MAP kinase phosphorylation sites in Smad3. *Biochemistry* **44,** 12546–12553 (2005).
808. Derynck, R., Zhang, Y. & Feng, X.-H. Smad3 and Smad4 cooperate with c-Jun/c-Fos to mediate TGF-β-induced transcription. *Nature* **394,** 909–913 (1998).
809. Hall, M. C. *et al.* The comparative role of activator protein 1 and Smad factors in the regulation of Timp-1 and MMP-1 gene expression by transforming growth factor-??1. *J. Biol. Chem.* **278,** 10304–10313 (2003).
810. Yu, L., Hebert, M. C. & Zhang, Y. E. TGF-beta receptor-activated p38 MAP kinase mediates smad-independent TGF-beta responses. *EMBO J.* **21,** 3749–3759 (2002).

811. Bakin, A. V, Rinehart, C., Tomlinson, A. K. & Arteaga, C. L. p38 mitogen-activated protein kinase is required for TGFbeta-mediated fibroblastic transdifferentiation and cell migration. *J. Cell Sci.* **115,** 3193–3206 (2002).
812. Yamashita, M. *et al.* TRAF6 mediates Smad-independent activation of JNK and p38 by TGF-beta. *Mol. Cell* **31,** 918–924 (2008).
813. Leask, A. Focal adhesion kinase: a key mediator of transforming growth factor beta signaling in fibroblasts. *Adv. wound care* **2,** 247–249 (2013).
814. McLean, G. W. *et al.* The role of focal-adhesion kinase in cancer — a new therapeutic opportunity. *Nat. Rev. Cancer* **5,** 505–515 (2005).
815. Hao, H. *et al.* Focal adhesion kinase as potential target for cancer therapy. *Oncol. Rep.* **22,** 973–9 (2009).
816. Lagares, D. *et al.* Inhibition of focal adhesion kinase prevents experimental lung fibrosis and myofibroblast formation. *Arthritis Rheum.* **64,** 1653–1664 (2012).
817. DeMali, K. A., Wennerberg, K. & Burridge, K. Integrin signaling to the actin cytoskeleton. *Curr. Opin. Cell Biol.* **15,** 572–582 (2003).
818. Carragher, N. O., Westhoff, M. A., Fincham, V. J., Schaller, M. D. & Frame, M. C. A novel role for FAK as a protease-targeting adaptor protein: Regulation by p42 ERK and Src. *Curr. Biol.* **13,** 1442–1450 (2003).
819. Hauck, C. R., Hsia, D. A., Puente, X. S., Cheresh, D. A. & Schlaepfer, D. D. FRNK blocks v-Src-stimulated invasion and experimental metastases without effects on cell motility or growth. *EMBO J.* **21,** 6289–6302 (2002).
820. Hsia, D. A. *et al.* Differential regulation of cell motility and invasion by FAK. *J. Cell Biol.* **160,** 753–767 (2003).
821. Hauck, C. R. *et al.* Inhibition of focal adhesion kinase expression or activity disrupts epidermal growth factor-stimulated signaling promoting the migration of invasive human carcinoma cells. *Cancer Res.* **61,** 7079–7090 (2001).
822. Avizienyte, E. & Frame, M. C. Src and FAK signalling controls adhesion fate and the epithelial-to-mesenchymal transition. *Curr. Opin. Cell Biol.* **17,** 542–547 (2005).
823. Maa, M. C. & Leu, T. H. Vanadate-dependent FAK activation is accomplished by the sustained FAK Tyr-576/577 phosphorylation. *Biochem. Biophys. Res. Commun.* **251,** 344–9 (1998).
824. Schlaepfer, D. D., Mitra, S. K. & Ilic, D. Control of motile and invasive cell phenotypes by focal adhesion kinase. *Biochim. Biophys. Acta - Mol. Cell Res.* **1692,** 77–102 (2004).
825. Bhaskar, P. T. & Hay, N. The two TORCs and Akt. *Dev. Cell* **12,** 487–502 (2007).
826. Bozulic, L. & Hemmings, B. A. PIKKing on PKB: regulation of PKB activity by phosphorylation. *Curr. Opin. Cell Biol.* **21,** 256–261 (2009).
827. Hers, I., Vincent, E. E. & Tavaré, J. M. Akt signalling in health and disease. *Cell. Signal.* **23,** 1515–1527 (2011).
828. Lan, A. & Du, J. Potential role of Akt signaling in chronic kidney disease. *Nephrol. Dial. Transplant* **30,** 1–10 (2014).
829. Xu, J., Lamouille, S. & Derynck, R. TGF-beta-induced epithelial to mesenchymal transition. *Cell Res.* **19,** 156–172 (2009).
830. Wilkes, M. C. & Leof, E. B. Transforming growth factor beta activation of c-Abl is independent of receptor internalization and regulated by phosphatidylinositol 3-kinase and PAK2 in mesenchymal cultures. *J. Biol. Chem.* **281,** 27846–27854 (2006).
831. Hong, M. *et al.* Non-Smad transforming growth factor-beta signaling regulated by focal adhesion kinase binding the p85 subunit of phosphatidylinositol 3-kinase. *J. Biol. Chem.*

286, 17841–17850 (2011).
832. Bakin, A. V., Tomlinson, A. K., Bhowmick, N. A., Moses, H. L. & Arteaga, C. L. Phosphatidylinositol 3-kinase function is required for transforming growth factor beta-mediated epithelial to mesenchymal transition and cell migration. *J. Biol. Chem.* **275,** 36803–36810 (2000).
833. Chien, A. J. *et al.* Activated Wnt/beta-catenin signaling in melanoma is associated with decreased proliferation in patient tumors and a murine melanoma model. *Proc. Natl. Acad. Sci. U. S. A.* **106,** 1193–8 (2009).
834. Henderson, N. C. & Sheppard, D. Integrin-mediated regulation of TGF-beta in fibrosis. *Biochim. Biophys. Acta - Mol. Basis Dis.* **1832,** 891–896 (2013).
835. Oeckinghaus, A. & Ghosh, S. The NF-kappaB family of transcription factors and its regulation. *Cold Spring Harb. Perspect. Biol.* **1,** a000034 (2009).
836. Ghosh, S. & Karin, M. Missing pieces in the NF-κB puzzle. *Cell* **109,** S81-96 (2002).
837. Karin, M. & Lin, A. NF-κB at the crossroads of life and death. *Nat. Immunol.* **3,** 221–227 (2002).
838. Maier, H. J. *et al.* NF-kB promotes epithelial-mesenchymal transition, migration and invasion of pancreatic carcinoma cells. *Cancer Lett.* **295,** 214–228 (2010).
839. Orlowski, R. Z. & Baldwin, A. S. NF-κB as a therapeutic target in cancer. *Trends Mol. Med.* **8,** 385–389 (2002).
840. Brantley, D. M. *et al.* Nuclear factor-kappaB (NF-kappaB) regulates proliferation and branching in mouse mammary epithelium. *Mol. Biol. Cell* **12,** 1445–55 (2001).
841. Hoesel, B. & Schmid, J. a. The complexity of NF-κB signaling in inflammation and cancer. *Mol. Cancer* **12,** 86 (2013).
842. Baldwin, A. S. The NF-κB and IκB proteins: New discoveries and insights. *Annu. Rev. Immunol.* **14,** 649–681 (1996).
843. Bitzer, M. *et al.* A mechanism of suppression of TGF-β/SMAD signaling by NF-κB/RelA. *Genes Dev.* **14,** 187–197 (2000).
844. Huber, M. A. *et al.* NF-kappaB is essential for epithelial-mesenchymal transition and metastasis in a model of breast cancer progression. *J. Clin. Invest.* **114,** 569–81 (2004).
845. Pires, B. R. B. *et al.* NF-kappaB is involved in the regulation of EMT genes in breast cancer cells. *PLoS One* **12,** e0169622 (2017).
846. Guaita, S. *et al.* Snail induction of epithelial to mesenchymal transition in tumor cells is accompanied by MUC1 repression and ZEB1 expression. *J. Biol. Chem.* **277,** 39209–39216 (2002).
847. Comijn, J. *et al.* The two-handed E box binding zinc finger protein SIP1 downregulates E-cadherin and induces invasion. *Mol. Cell* **7,** 1267–1278 (2001).
848. Freudlsperger, C. *et al.* TGF-β and NF-κB signal pathway cross-talk is mediated through TAK1 and SMAD7 in a subset of head and neck cancers. *Oncogene* **32,** 1549–59 (2013).
849. Jaffe, A. B. & Hall, A. Rho GTPases: Biochemistry and Biology. *Annu. Rev. Cell Dev. Biol.* **21,** 247–269 (2005).
850. Bhowmick, N. a *et al.* Transforming growth factor-beta1 mediates epithelial to mesenchymal transdifferentiation through a RhoA-dependent mechanism. *Mol. Biol. Cell* **12,** 27–36 (2001).
851. Edlund, S. Transforming growth factor-beta -induced mobilization of actin cytoskeleton requires signaling by small GTPases Cdc42 and RhoA. *Mol. Biol. Cell* **13,** 902–914 (2002).
852. Wilkes, M. C., Murphy, S. J., Garamszegi, N. & Leof, E. B. Cell-type-specific activation of PAK2 by transforming growth factor beta independent of Smad2 and Smad3. *Mol. Cell.*

Biol. **23,** 8878–89 (2003).
853. Ozdamar, B. Receptors controls epithelial cell plasticity regulation of the polarity protein Par6 by TGFb receptors controls epithelial cell plasticity. *Science (80-.).* **1603,** 1603–1610 (2008).
854. Davis, G. E., Bayless, K. J., Davis, M. J. & Meininger, G. A. Regulation of tissue injury responses by the exposure of matricryptic sites within extracellular matrix molecules. *Am. J. Pathol.* **156,** 1489–1498 (2000).
855. Jean Baptiste Oudart, J. C. M. Control of tumor progression by extracellular matrix molecule fragments, the matrikines. *J. Carcinog. Mutagen.* **4,** 1–8 (2013).
856. Ricard-Blum, S. & Salza, R. Matricryptins and matrikines: Biologically active fragments of the extracellular matrix. *Exp. Dermatol.* **23,** 457–463 (2014).
857. Wells, J. M., Gaggar, A. & Blalock, J. E. MMP generated matrikines. *Matrix Biol.* **44–46,** 122–129 (2015).
858. Purvis, A. & Hohenester, E. Laminin network formation studied by reconstitution of ternary nodes in solution. *J. Biol. Chem.* **287,** 44270–44277 (2012).
859. Miettinen, P. J., Ebner, R., Lopez, A. R. & Derynck, R. TGF-beta induced transdifferentiation of mammary epithelial cells to mesenchymal cells: involvement of type I receptors. *J. Cell Biol.* **127,** 2021–36 (1994).
860. Braghirolli, D. I., Steffens, D. & Pranke, P. Electrospinning for regenerative medicine: A review of the main topics. *Drug Discov. Today* **19,** 743–753 (2014).
861. Lee, H., Dellatore, S. M., Miller, W. M. & Messersmith, P. B. Mussel-inspired surface chemistry for multifunctional coatings. *Science (80-.).* **318,** 426–430 (2007).
862. Carpenter, A. E. *et al.* CellProfiler: image analysis software for identifying and quantifying cell phenotypes. *Genome Biol.* **7,** R100 (2006).
863. Kamentsky, L. *et al.* Improved structure, function and compatibility for CellProfiler: modular high-throughput image analysis software. *Bioinformatics* **27,** 1179–1180 (2011).
864. Van Noort, V. *et al.* Novel drug candidates for the treatment of metastatic colorectal cancer through global inverse gene-expression profiling. *Cancer Res.* **74,** 5690–5699 (2014).
865. Silvestri, C., Bose, R., Attisano, L. & Wrana, J. L. TGFβ signal transduction. *Handb. Cell Signaling, 2/e* **2,** 521–532 (2010).
866. Liddington, R. C. & Ginsberg, M. H. Integrin activation takes shape. *J Cell Biol* **158,** 833–839 (2002).
867. Galbraith, C. G., Davidson, M. W. & Galbraith, J. A. A cautionary tail: Changes in integrin behavior with labeling. *bioRxiv* (2017).
868. Helbig, G. *et al.* NF-κ B promotes breast cancer cell migration and metastasis by inducing the expression of the chemokine receptor CXCR4. *J. Biol. Chem.* **278,** 21631–21638 (2003).
869. Rossé, C. *et al.* Control of MT1-MMP transport by atypical PKC during breast-cancer progression. *Proc. Natl. Acad. Sci. U. S. A.* **111,** E1872-9 (2014).
870. Feinberg, T. Y., Rowe, R. G., Saunders, T. L. & Weiss, S. J. Functional roles of MMP14 and MMP15 in early postnatal mammary gland development. *Development* **143,** 3956–3968 (2016).
871. Weaver, A. M. Cortactin in tumor invasiveness. *Cancer Lett.* **265,** 157–166 (2008).
872. Parsons, S. L., Watson, S. A., Brown, P. D., Collins, H. M. & Steele, R. J. Matrix metalloproteinases. *Br. J. Surg.* **84,** 160–166 (1997).

873. Attisano, L. & Lee-Hoeflich, S. T. The Smads. *Genome Biol.* **2,** 3010.1-3010.8 (2001).
874. Jackson-Bernitsas, D. G. *et al.* Evidence that TNF-TNFR1-TRADD-TRAF2-RIP-TAK1-IKK pathway mediates constitutive NF-kappaB activation and proliferation in human head and neck squamous cell carcinoma. *Oncogene* **26,** 1385–97 (2007).
875. Sakurai, H., Miyoshi, H., Toriumi, W. & Sugita, T. Functional interactions of transforming growth factor beta-activated kinase 1 with IkappaB kinases to stimulate NF-kappaB activation. *J. Biol. Chem.* **274,** 10641–10648 (1999).
876. Takaesu, G. *et al.* TAB2, a novel adaptor protein, mediates activation of TAK1 MAPKKK by linking TAK1 to TRAF6 in the IL-1 signal transduction pathway. *Mol. Cell* **5,** 649–658 (2000).
877. Thannickal, V. J. *et al.* Myofibroblast differentiation by transforming growth factor-beta1 is dependent on cell adhesion and integrin signaling via focal adhesion kinase. *J. Biol. Chem.* **278,** 12384–12389 (2003).
878. Edwards, D. R. *et al.* Differential effects of transforming growth factor-beta 1 on the expression of matrix metalloproteinases and tissue inhibitors of metalloproteinases in young and old human fibroblasts. *Exp. Gerontol.* **31,** 207–23 (1996).
879. Satish, L., Babu, M., Tran, K. T., Hebda, P. A. & Wells, A. Keloid fibroblast responsiveness to epidermal growth factor and activation of downstream intracellular signaling pathways. *Wound Repair Regen.* **12,** 183–192 (2004).
880. Krstic, J. & Santibanez, J. F. Transforming growth factor-beta and matrix metalloproteinases: Functional interactions in tumor stroma-infiltrating myeloid cells. *Sci. World J.* **2014,** 521754 (2014).
881. Wahl, S. M., Allen, J. B., Weeks, B. S., Wong, H. L. & Klotman, P. E. Transforming growth factor beta enhances integrin expression and type IV collagenase secretion in human monocytes. *Proc. Natl. Acad. Sci. USA* **90,** 4577–81 (1993).
882. Brassart-Pasco, S. *et al.* Tetrastatin, the NC1 domain of the alpha4(IV) collagen chain: A novel potent anti-tumor matrikine. *PLoS One* **7,** e29587 (2012).
883. Colorado, P. C. *et al.* Anti-angiogenic cues from vascular basement membrane collagen. *Cancer Res.* **60,** 2520–2526 (2000).
884. Hamano, Y. *et al.* Physiological levels of tumstatin, a fragment of collagen IV α3 chain, are generated by MMP-9 proteolysis and suppress angiogenesis via αVβ3 integrin. *Cancer Cell* **3,** 589–601 (2003).
885. Kamphaus, G. D. *et al.* Canstatin, a novel matrix-derived inhibitor of angiogenesis and tumor growth. *J. Biol. Chem.* **275,** 1209–1215 (2000).
886. Luo, Y.-Q. Q. *et al.* Development of an ELISA for quantification of tumstatin in serum samples and tissue extracts of patients with lung carcinoma. *Clin. Chim. Acta* **411,** 510–515 (2010).
887. Maeshima, Y. *et al.* Distinct antitumor properties of a type IV collagen domain derived from basement membrane. *J. Biol. Chemestry* **275,** 21340 –21348 (2000).
888. Ortega, N. & Werb, Z. New functional roles for non-collagenous domains of basement membrane collagens. *J. Cell Sci.* **115,** 4201–14 (2002).
889. Pasco, S. *et al.* A specific sequence of the noncollagenous domain of the alpha3(IV) chain of type IV collagen inhibits expression and activation of matrix metalloproteinases by tumor cells. *Cancer Res.* **60,** 467–473 (2000).
890. Sand, J. M. *et al.* MMP mediated degradation of type IV collagen alpha 1 and alpha 3 chains reflects basement membrane remodeling in experimental and clinical fibrosis - Validation of two novel biomarker assays. *PLoS One* **8,** e84934 (2013).

891. Borza, C. M. *et al.* Integrin α3β1, a novel receptor for α(IV) noncollagenous domain and a trans-dominant inhibitor for integrin αvβ3. *J. Biol. Chem.* **281,** 20932–20939 (2006).
892. Zeisberg, M. *et al.* Collagen composition and assembly regulates epithelial-mesenchymal transdifferentiation. *Am. J. Pathol.* **159,** 1313–1321 (2001).
893. Varelas, X. *et al.* The crumbs complex couples cell density sensing to Hippo-dependent control of the TGF-β-Smad pathway. *Dev. Cell* **19,** 831–844 (2010).
894. Varelas, X. *et al.* TAZ controls Smad nucleocytoplasmic shuttling and regulates human embryonic stem-cell self-renewal. *Nat. Cell Biol.* **10,** 837–848 (2008).
895. Beyer, T. A. *et al.* Switch enhancers interpret TGF-β and hippo signaling to control cell fate in human embryonic stem cells. *Cell Rep.* **5,** 1611–1624 (2013).
896. Szeto, S. G. *et al.* YAP/TAZ Are Mechanoregulators of TGF- -Smad Signaling and Renal Fibrogenesis. *J. Am. Soc. Nephrol.* **27,** 1–12 (2016).
897. Enomoto, M. I., Boettiger, D. & Menko, A. S. Alpha 5 integrin is a critical component of adhesion plaques in myogenesis. *Dev Biol* **155,** 180–197 (1993).
898. Carter, W. G., Kaur, P., Gil, S. G., Gahr, P. J. & Wayner, E. A. Distinct functions for integrins α3β1 in focal adhesions and α6β4/bullous pemphigoid antigen in a new stable anchoring contact (SAC) of keratinocytes: Relation to hemidesmosomes. *J. Cell Biol.* **111,** 3141–3154 (1990).
899. Grenz, H., Carbonetto, S. & Goodman, S. L. alpha3beta1 integrin is moved into focal contacts in kidney mesangial cells. *J. Cell Sci.* **105,** 739–751 (1993).
900. Hein, B., Willig, K. I. & Hell, S. W. Stimulated emission depletion (STED) nanoscopy of a fluorescent protein-labeled organelle inside a living cell. *Proc. Natl. Acad. Sci.* **105,** 14271–14276 (2008).
901. Toneff, M. J. *et al.* The Z-cad dual fluorescent sensor detects dynamic changes between the epithelial and mesenchymal cellular states. *BMC Biol.* **14,** 1–16 (2016).
902. Ohji, M., SundarRaj, N., Hassell, J. R. & Thoft, R. a. Basement membrane synthesis by human corneal epithelial cells in vitro. *Invest. Ophthalmol. Vis. Sci.* **35,** 479–485 (1994).
903. Furuyama, a & Mochitate, K. Assembly of the exogenous extracellular matrix during basement membrane formation by alveolar epithelial cells in vitro. *J. Cell Sci.* **113 (Pt 5,** 859–868 (2000).
904. Rosso, F., Giordano, A., Barbarisi, M. & Barbarisi, A. From cell-ECM interactions to tissue engineering. *J. Cell. Physiol.* **199,** 174–180 (2004).
905. Cosgrove, B. D. *et al.* N-cadherin adhesive interactions modulate matrix mechanosensing and fate commitment of mesenchymal stem cells. *Nat. Mater.* **15,** 1297–1306 (2016).
906. Rosner, M., Schipany, K. & Hengstschläger, M. Merging high-quality biochemical fractionation with a refined flow cytometry approach to monitor nucleocytoplasmic protein expression throughout the unperturbed mammalian cell cycle. *Nat. Protoc.* **8,** 602–626 (2013).
907. Friedman, S. L., Sheppard, D., Duffield, J. S. & Violette, S. Therapy for fibrotic diseases: Nearing the starting line. *Sci. Transl. Med.* **5,** 167sr1 (2013).
908. Wynn, T. A. Common and unique mechanisms regulate fibrosis in various fibroproliferative diseases. *J. Clin. Invest.* **117,** 524–529 (2007).
909. Selgas, R. *et al.* Epithelial-to-mesenchymal transition of the mesothelial cell - Its role in the response of the peritoneum to dialysis. *Nephrol. Dial. Transplant.* **21,** ii2-ii7 (2006).
910. Loureiro, J. *et al.* BMP-7 blocks mesenchymal conversion of mesothelial cells and prevents peritoneal damage induced by dialysis fluid exposure. *Nephrol. Dial.*

Transplant. **25,** 1098–1108 (2010).
911. Strippoli, R. *et al.* Caveolin-1 deficiency induces a MEK-ERK1/2- Snail-1-dependent epithelial–mesenchymal transition and fibrosis during peritoneal dialysis. *EMBO Mol. Med.* **7,** 102–123 (2015).
912. Seoane, J. & Gomis, R. R. TGF-β family signaling in tumor suppression and cancer progression. *Cold Spring Harb. Perspect. Biol.* a022277 (2017). doi:10.1101/cshperspect.a022277
913. Katsuno, Y., Lamouille, S. & Derynck, R. TGF-β signaling and epithelial–mesenchymal transition in cancer progression. *Curr. Opin. Oncol.* **25,** 76–84 (2013).
914. Brabletz, T., Jung, A., Spaderna, S., Hlubek, F. & Kirchner, T. Opinion: Migrating cancer stem cells - an integrated concept of malignant tumour progression. *Nat. Rev. Cancer* **5,** 744–749 (2005).
915. Scheel, C. & Weinberg, R. A. Phenotypic plasticity and epithelial-mesenchymal transitions in cancer and normal stem cells? *Int. J. Cancer* **129,** 2310–2314 (2011).
916. Xia, W. *et al.* Smad inhibitor induces CSC differentiation for effective chemosensitization in cyclin D1- and TGF-β/Smad-regulated liver cancer stem cell-like cells. *Oncotarget* **8,** 38811–38824 (2017).
917. Udayakumar, T. S. *et al.* Membrane type-1-matrix metalloproteinase expressed by prostate carcinoma cells cleaves human laminin-5 β3 chain and induces cell migration. *Cancer Res.* **63,** 2292–2299 (2003).
918. Bair, E. L. *et al.* Membrane type 1 matrix metalloprotease cleaves laminin-10 and promotes prostate cancer cell migration. *Neoplasia* **7,** 380–9 (2005).
919. Ricard-Blum, S. & Ballut, L. Matricryptins derived from collagens and proteoglycans. *Front. Biosci. (Landmark Ed.* **16,** 674–97 (2011).
920. Veidal, S. S. *et al.* Assessment of proteolytic degradation of the basement membrane: a fragment of type IV collagen as a biochemical marker for liver fibrosis. *Fibrogenesis Tissue Repair* **4,** 22 (2011).
921. Hangai, M. *et al.* Matrix metalloproteinase-9-dependent exposure of a cryptic migratory control site in collagen is required before retinal angiogenesis. *Am. J. Pathol.* **161,** 1429–1437 (2002).
922. Xu, J. *et al.* Proteolytic exposure of a cryptic site within collagen type IV is required for angiogenesis and tumor growth in vivo. *J. Cell Biol.* **154,** 1069–1080 (2001).
923. Monaco, S. *et al.* Enzymatic processing of collagen IV by MMP-2 (gelatinase A) affects neutrophil migration and it is modulated by extracatalytic domains. *Protein Sci.* **15,** 2805–2815 (2006).
924. Yong, H. E. J. *et al.* Anti-angiogenic collagen fragment arresten is increased from 16 weeks' gestation in pre-eclamptic plasma. *Placenta* **36,** 1300–1309 (2015).
925. Katayama, M., Sanzen, N., Funakoshi, A. & Sekiguchi, K. Laminin gamma2-chain fragment in the circulation: A prognostic indicator of epithelial tumor invasion. *Cancer Res.* **63,** 222–9 (2003).

6 Appendices

6.1 Figure reproduction permissions

ELSEVIER LICENSE
TERMS AND CONDITIONS

Aug 23, 2017

This Agreement between Imperial College -- Catherine Hansel ("You") and Elsevier ("Elsevier") consists of your license details and the terms and conditions provided by Elsevier and Copyright Clearance Center.

License Number	4174810279195
License date	Aug 23, 2017
Licensed Content Publisher	Elsevier
Licensed Content Publication	Cell Stem Cell
Licensed Content Title	Material Cues as Potent Regulators of Epigenetics and Stem Cell Function
Licensed Content Author	Spencer W. Crowder,Vincent Leonardo,Thomas Whittaker,Peter Papathanasiou,Molly M. Stevens
Licensed Content Date	Jan 7, 2016
Licensed Content Volume	18
Licensed Content Issue	1
Licensed Content Pages	14
Start Page	39
End Page	52
Type of Use	reuse in a thesis/dissertation
Intended publisher of new work	other
Portion	figures/tables/illustrations
Number of figures/tables/illustrations	1
Format	both print and electronic
Are you the author of this Elsevier article?	No
Will you be translating?	No
Original figure numbers	Figure 2
Title of your thesis/dissertation	Microscopy of interactions at the cell-material and call-matrix interface
Expected completion date	Oct 2017
Estimated size (number of pages)	200
Requestor Location	Imperial College Imperial College London Imperial College Rd Kensington, London SW7 2AZ United Kingdom Attn: Imperial College
Publisher Tax ID	GB 494 6272 12
Total	0.00 GBP
Terms and Conditions	

INTRODUCTION

1. The publisher for this copyrighted material is Elsevier. By clicking "accept" in connection with completing this licensing transaction, you agree that the following terms and conditions apply to this transaction (along with the Billing and Payment terms and conditions established by Copyright Clearance Center, Inc. ("CCC"), at the time that you opened your Rightslink account and that are available at any time at http://myaccount.copyright.com).

GENERAL TERMS

2. Elsevier hereby grants you permission to reproduce the aforementioned material subject to the terms and conditions indicated.

3. Acknowledgement: If any part of the material to be used (for example, figures) has appeared in our publication with credit or acknowledgement to another source, permission must also be sought from that source. If such permission is not obtained then that material may not be included in your publication/copies. Suitable acknowledgement to the source must be made, either as a footnote or in a reference list at the end of your publication, as follows:

"Reprinted from Publication title, Vol /edition number, Author(s), Title of article / title of chapter, Pages No., Copyright (Year), with permission from Elsevier [OR APPLICABLE SOCIETY COPYRIGHT OWNER]." Also Lancet special credit - "Reprinted from The Lancet, Vol. number, Author(s), Title of article, Pages No., Copyright (Year), with permission from Elsevier."

4. Reproduction of this material is confined to the purpose and/or media for which permission is hereby given.

5. Altering/Modifying Material: Not Permitted. However figures and illustrations may be altered/adapted minimally to serve your work. Any other abbreviations, additions, deletions and/or any other alterations shall be made only with prior written authorization of Elsevier Ltd. (Please contact Elsevier at permissions@elsevier.com). No modifications can be made to any Lancet figures/tables and they must be reproduced in full.

6. If the permission fee for the requested use of our material is waived in this instance, please be advised that your future requests for Elsevier materials may attract a fee.

7. Reservation of Rights: Publisher reserves all rights not specifically granted in the combination of (i) the license details provided by you and accepted in the course of this licensing transaction, (ii) these terms and conditions and (iii) CCC's Billing and Payment terms and conditions.

8. License Contingent Upon Payment: While you may exercise the rights licensed immediately upon issuance of the license at the end of the licensing process for the transaction, provided that you have disclosed complete and accurate details of your proposed use, no license is finally effective unless and until full payment is received from you (either by publisher or by CCC) as provided in CCC's Billing and Payment terms and conditions. If full payment is not received on a timely basis, then any license preliminarily granted shall be deemed automatically revoked and shall be void as if never granted. Further, in the event that you breach any of these terms and conditions or any of CCC's Billing and Payment terms and conditions, the license is automatically revoked and shall be void as if never granted. Use of materials as described in a revoked license, as well as any use of the materials beyond the scope of an unrevoked license, may constitute copyright infringement and publisher reserves the right to take any and all action to protect its copyright in the materials.

9. Warranties: Publisher makes no representations or warranties with respect to the licensed material.

10. Indemnity: You hereby indemnify and agree to hold harmless publisher and CCC, and their respective officers, directors, employees and agents, from and against any and all claims arising out of your use of the licensed material other than as specifically authorized pursuant to this license.

11. No Transfer of License: This license is personal to you and may not be sublicensed, assigned, or transferred by you to any other person without publisher's written permission.

12. No Amendment Except in Writing: This license may not be amended except in a writing signed by both parties (or, in the case of publisher, by CCC on publisher's behalf).

13. Objection to Contrary Terms: Publisher hereby objects to any terms contained in any purchase order, acknowledgment, check endorsement or other writing prepared by you, which terms are inconsistent with these terms and conditions or CCC's Billing and Payment

NATURE PUBLISHING GROUP LICENSE TERMS AND CONDITIONS

Aug 23, 2017

This Agreement between Imperial College -- Catherine Hansel ("You") and Nature Publishing Group ("Nature Publishing Group") consists of your license details and the terms and conditions provided by Nature Publishing Group and Copyright Clearance Center.

License Number	4174780827512
License date	Aug 23, 2017
Licensed Content Publisher	Nature Publishing Group
Licensed Content Publication	Nature Reviews Molecular Cell Biology
Licensed Content Title	The final steps of integrin activation: the end game
Licensed Content Author	Sanford J. Shattil,Chungho KimandMark H. Ginsberg
Licensed Content Date	Apr 1, 2010
Licensed Content Volume	11
Licensed Content Issue	4
Type of Use	reuse in a dissertation / thesis
Requestor type	academic/educational
Format	print and electronic
Portion	figures/tables/illustrations
Number of figures/tables/illustrations	1
High-res required	no
Figures	Box 2
Author of this NPG article	no
Your reference number	
Title of your thesis / dissertation	Microscopy of interactions at the cell-material and call-matrix interface
Expected completion date	Oct 2017
Estimated size (number of pages)	200
Requestor Location	Imperial College Imperial College London Imperial College Rd Kensington, London SW7 2AZ United Kingdom Attn: Imperial College
Billing Type	Invoice
Billing Address	Imperial College Imperial College London Imperial College Rd Kensington, United Kingdom SW7 2AZ Attn: Imperial College
Total	0.00 GBP
Terms and Conditions	

Terms and Conditions for Permissions

Nature Publishing Group hereby grants you a non-exclusive license to reproduce this material for this purpose, and for no other use,subject to the conditions below:

1. NPG warrants that it has, to the best of its knowledge, the rights to license reuse of this material. However, you should ensure that the material you are requesting is original to Nature Publishing Group and does not carry the copyright of another entity (as credited in the published version). If the credit line on any part of the material you have requested indicates that it was reprinted or adapted by NPG with permission from another source, then you should also seek permission from that source to reuse the material.

2. Permission granted free of charge for material in print is also usually granted for any electronic version of that work, provided that the material is incidental to the work as a whole and that the electronic version is essentially equivalent to, or substitutes for, the print version.Where print permission has been granted for a fee, separate permission must be obtained for any additional, electronic re-use (unless, as in the case of a full paper, this has already been accounted for during your initial request in the calculation of a print run).NB: In all cases, web-based use of full-text articles must be authorized separately through the 'Use on a Web Site' option when requesting permission.

3. Permission granted for a first edition does not apply to second and subsequent editions and for editions in other languages (except for signatories to the STM Permissions Guidelines, or where the first edition permission was granted for free).

4. Nature Publishing Group's permission must be acknowledged next to the figure, table or abstract in print. In electronic form, this acknowledgement must be visible at the same time as the figure/table/abstract, and must be hyperlinked to the journal's homepage.

5. The credit line should read:
   Reprinted by permission from Macmillan Publishers Ltd: [JOURNAL NAME] (reference citation), copyright (year of publication)
   For AOP papers, the credit line should read:
   Reprinted by permission from Macmillan Publishers Ltd: [JOURNAL NAME], advance online publication, day month year (doi: 10.1038/sj.[JOURNAL ACRONYM].XXXXX)

   Note: For republication from the *British Journal of Cancer*, the following credit lines apply.
   Reprinted by permission from Macmillan Publishers Ltd on behalf of Cancer Research UK: [JOURNAL NAME] (reference citation), copyright (year of publication)For AOP papers, the credit line should read:
   Reprinted by permission from Macmillan Publishers Ltd on behalf of Cancer Research UK: [JOURNAL NAME], advance online publication, day month year (doi: 10.1038/sj.[JOURNAL ACRONYM].XXXXX)

6. Adaptations of single figures do not require NPG approval. However, the adaptation should be credited as follows:

   Adapted by permission from Macmillan Publishers Ltd: [JOURNAL NAME] (reference citation), copyright (year of publication)

   Note: For adaptation from the *British Journal of Cancer*, the following credit line applies.
   Adapted by permission from Macmillan Publishers Ltd on behalf of Cancer Research UK: [JOURNAL NAME] (reference citation), copyright (year of publication)

7. Translations of 401 words up to a whole article require NPG approval. Please visit http://www.macmillanmedicalcommunications.com for more information.Translations of up to a 400 words do not require NPG approval. The translation should be credited as follows:

   Translated by permission from Macmillan Publishers Ltd: [JOURNAL NAME] (reference citation), copyright (year of publication).

   Note: For translation from the *British Journal of Cancer*, the following credit line applies.
   Translated by permission from Macmillan Publishers Ltd on behalf of Cancer Research UK: [JOURNAL NAME] (reference citation), copyright (year of publication)

NATURE PUBLISHING GROUP LICENSE TERMS AND CONDITIONS

Aug 23, 2017

This Agreement between Imperial College -- Catherine Hansel ("You") and Nature Publishing Group ("Nature Publishing Group") consists of your license details and the terms and conditions provided by Nature Publishing Group and Copyright Clearance Center.

License Number	4174780974875
License date	Aug 23, 2017
Licensed Content Publisher	Nature Publishing Group
Licensed Content Publication	Nature Reviews Molecular Cell Biology
Licensed Content Title	Focal adhesion kinase: in command and control of cell motility
Licensed Content Author	Satyajit K. Mitra,Daniel A. HansonandDavid D. Schlaepfer
Licensed Content Date	Jan 1, 2005
Licensed Content Volume	6
Licensed Content Issue	1
Type of Use	reuse in a dissertation / thesis
Requestor type	academic/educational
Format	print and electronic
Portion	figures/tables/illustrations
Number of figures/tables/illustrations	1
High-res required	no
Figures	Box 1
Author of this NPG article	no
Your reference number	
Title of your thesis / dissertation	Microscopy of interactions at the cell-material and call-matrix interface
Expected completion date	Oct 2017
Estimated size (number of pages)	200
Requestor Location	Imperial College Imperial College London Imperial College Rd Kensington, London SW7 2AZ United Kingdom Attn: Imperial College
Billing Type	Invoice
Billing Address	Imperial College Imperial College London Imperial College Rd Kensington, United Kingdom SW7 2AZ Attn: Imperial College
Total	0.00 GBP
Terms and Conditions	

Terms and Conditions for Permissions

Nature Publishing Group hereby grants you a non-exclusive license to reproduce this material for this purpose, and for no other use,subject to the conditions below:

1. NPG warrants that it has, to the best of its knowledge, the rights to license reuse of this material. However, you should ensure that the material you are requesting is original to Nature Publishing Group and does not carry the copyright of another entity (as credited in the published version). If the credit line on any part of the material you have requested indicates that it was reprinted or adapted by NPG with permission from another source, then you should also seek permission from that source to reuse the material.

2. Permission granted free of charge for material in print is also usually granted for any electronic version of that work, provided that the material is incidental to the work as a whole and that the electronic version is essentially equivalent to, or substitutes for, the print version.Where print permission has been granted for a fee, separate permission must be obtained for any additional, electronic re-use (unless, as in the case of a full paper, this has already been accounted for during your initial request in the calculation of a print run).NB: In all cases, web-based use of full-text articles must be authorized separately through the 'Use on a Web Site' option when requesting permission.

3. Permission granted for a first edition does not apply to second and subsequent editions and for editions in other languages (except for signatories to the STM Permissions Guidelines, or where the first edition permission was granted for free).

4. Nature Publishing Group's permission must be acknowledged next to the figure, table or abstract in print. In electronic form, this acknowledgement must be visible at the same time as the figure/table/abstract, and must be hyperlinked to the journal's homepage.

5. The credit line should read:
   Reprinted by permission from Macmillan Publishers Ltd: [JOURNAL NAME] (reference citation), copyright (year of publication)
   For AOP papers, the credit line should read:
   Reprinted by permission from Macmillan Publishers Ltd: [JOURNAL NAME], advance online publication, day month year (doi: 10.1038/sj.[JOURNAL ACRONYM].XXXXX)

   Note: For republication from the *British Journal of Cancer*, the following credit lines apply.
   Reprinted by permission from Macmillan Publishers Ltd on behalf of Cancer Research UK: [JOURNAL NAME] (reference citation), copyright (year of publication)For AOP papers, the credit line should read:
   Reprinted by permission from Macmillan Publishers Ltd on behalf of Cancer Research UK: [JOURNAL NAME], advance online publication, day month year (doi: 10.1038/sj.[JOURNAL ACRONYM].XXXXX)

6. Adaptations of single figures do not require NPG approval. However, the adaptation should be credited as follows:

   Adapted by permission from Macmillan Publishers Ltd: [JOURNAL NAME] (reference citation), copyright (year of publication)

   Note: For adaptation from the *British Journal of Cancer*, the following credit line applies.
   Adapted by permission from Macmillan Publishers Ltd on behalf of Cancer Research UK: [JOURNAL NAME] (reference citation), copyright (year of publication)

7. Translations of 401 words up to a whole article require NPG approval. Please visit http://www.macmillanmedicalcommunications.com for more information.Translations of up to a 400 words do not require NPG approval. The translation should be credited as follows:

   Translated by permission from Macmillan Publishers Ltd: [JOURNAL NAME] (reference citation), copyright (year of publication).

   Note: For translation from the *British Journal of Cancer*, the following credit line applies.
   Translated by permission from Macmillan Publishers Ltd on behalf of Cancer Research UK: [JOURNAL NAME] (reference citation), copyright (year of publication)

NATURE PUBLISHING GROUP LICENSE TERMS AND CONDITIONS

Aug 23, 2017

This Agreement between Imperial College -- Catherine Hansel ("You") and Nature Publishing Group ("Nature Publishing Group") consists of your license details and the terms and conditions provided by Nature Publishing Group and Copyright Clearance Center.

License Number	4174781243164
License date	Aug 23, 2017
Licensed Content Publisher	Nature Publishing Group
Licensed Content Publication	Nature Reviews Molecular Cell Biology
Licensed Content Title	The 'ins' and 'outs' of podosomes and invadopodia: characteristics, formation and function
Licensed Content Author	Danielle A. Murphy and Sara A. Courtneidge
Licensed Content Date	Jul 1, 2011
Licensed Content Volume	12
Licensed Content Issue	7
Type of Use	reuse in a dissertation / thesis
Requestor type	academic/educational
Format	print and electronic
Portion	figures/tables/illustrations
Number of figures/tables/illustrations	1
High-res required	no
Figures	Table 1
Author of this NPG article	no
Your reference number	
Title of your thesis / dissertation	Microscopy of interactions at the cell-material and call-matrix interface
Expected completion date	Oct 2017
Estimated size (number of pages)	200
Requestor Location	Imperial College Imperial College London Imperial College Rd Kensington, London SW7 2AZ United Kingdom Attn: Imperial College
Billing Type	Invoice
Billing Address	Imperial College Imperial College London Imperial College Rd Kensington, United Kingdom SW7 2AZ Attn: Imperial College
Total	0.00 GBP
Terms and Conditions	

Nature Publishing Group hereby grants you a non-exclusive license to reproduce this material for this purpose, and for no other use,subject to the conditions below:

1. NPG warrants that it has, to the best of its knowledge, the rights to license reuse of this material. However, you should ensure that the material you are requesting is original to Nature Publishing Group and does not carry the copyright of another entity (as credited in the published version). If the credit line on any part of the material you have requested indicates that it was reprinted or adapted by NPG with permission from another source, then you should also seek permission from that source to reuse the material.

2. Permission granted free of charge for material in print is also usually granted for any electronic version of that work, provided that the material is incidental to the work as a whole and that the electronic version is essentially equivalent to, or substitutes for, the print version.Where print permission has been granted for a fee, separate permission must be obtained for any additional, electronic re-use (unless, as in the case of a full paper, this has already been accounted for during your initial request in the calculation of a print run).NB: In all cases, web-based use of full-text articles must be authorized separately through the 'Use on a Web Site' option when requesting permission.

3. Permission granted for a first edition does not apply to second and subsequent editions and for editions in other languages (except for signatories to the STM Permissions Guidelines, or where the first edition permission was granted for free).

4. Nature Publishing Group's permission must be acknowledged next to the figure, table or abstract in print. In electronic form, this acknowledgement must be visible at the same time as the figure/table/abstract, and must be hyperlinked to the journal's homepage.

5. The credit line should read:
   Reprinted by permission from Macmillan Publishers Ltd: [JOURNAL NAME] (reference citation), copyright (year of publication)
   For AOP papers, the credit line should read:
   Reprinted by permission from Macmillan Publishers Ltd: [JOURNAL NAME], advance online publication, day month year (doi: 10.1038/sj.[JOURNAL ACRONYM].XXXXX)

   Note: For republication from the *British Journal of Cancer*, the following credit lines apply.
   Reprinted by permission from Macmillan Publishers Ltd on behalf of Cancer Research UK: [JOURNAL NAME] (reference citation), copyright (year of publication)For AOP papers, the credit line should read:
   Reprinted by permission from Macmillan Publishers Ltd on behalf of Cancer Research UK: [JOURNAL NAME], advance online publication, day month year (doi: 10.1038/sj.[JOURNAL ACRONYM].XXXXX)

6. Adaptations of single figures do not require NPG approval. However, the adaptation should be credited as follows:

   Adapted by permission from Macmillan Publishers Ltd: [JOURNAL NAME] (reference citation), copyright (year of publication)

   Note: For adaptation from the *British Journal of Cancer*, the following credit line applies.
   Adapted by permission from Macmillan Publishers Ltd on behalf of Cancer Research UK: [JOURNAL NAME] (reference citation), copyright (year of publication)

7. Translations of 401 words up to a whole article require NPG approval. Please visit http://www.macmillanmedicalcommunications.com for more information.Translations of up to a 400 words do not require NPG approval. The translation should be credited as follows:

   Translated by permission from Macmillan Publishers Ltd: [JOURNAL NAME] (reference citation), copyright (year of publication).

   Note: For translation from the *British Journal of Cancer*, the following credit line applies.
   Translated by permission from Macmillan Publishers Ltd on behalf of Cancer Research UK: [JOURNAL NAME] (reference citation), copyright (year of publication)

Reply all | Delete Junk ...

Permission to use figure for PhD thesis

HS Hansel, Katie S
Wed 23/08, 14:16
permissions@portlandpress.com

Reply all |

Sent Items

Dear Portland Press,

I am completing my PhD thesis at Imperial College London entitled "Microscopy of interactions at the cell-material and cell-matrix interface".

I seek your permission to reprint, in my thesis an extract from:*P. Meinke et al. Biochem. Soc. Trans. 39, (2011)* . The extract to be reproduced (by myself using powerpoint) is Figure 1.

I would like to include the extract in my thesis which will be added to Spiral, Imperial's institutional repository http://spiral.imperial.ac.uk/

and made available to the public under a Creative Commons Attribution-NonCommercial-NoDerivs licence.

If you are happy to grant me all the permissions requested, please return a signed copy of this letter. If you wish to grant only some of the permissions requested, please list these and then sign.

Yours sincerely,



Catherine Hansel

Permission granted for the use requested above:
I confirm that I am the copyright holder of the extract above and hereby give permission to include it in your thesis which will be made available, via the internet, for non-commercial purposes under the terms of the user licence.
[please edit the text above if you wish to grant more specific permission]
Signed:
Name:
Organisation:
Job title:

FW: Permission to use figure for PhD thesis

Malavika Legge <Malavika.Legge@portlandpress.com>

Fri 01/09/2017 10:42

To:Hansel, Katie S <c.hansel13@imperial.ac.uk>;

Dear Catherine Hansel

You are welcome to reuse figure 1 from this 2011 Biochem. Soc. Trans. article http://www.biochemsoctrans.org/content/39/6/1693, at no charge, subject to the following:

1. Your reproduced figure in the thesis must cite the article and author, both in the reference list and in the figure legend
2. Please include a hyperlink to the article on the journal site when referencing/citing it
3. If you modify the original figure in any way, please ensure that it is labelled as a modified version of the original; in addition, the modified version should not imply approval from the original authors unless such approval is separately and expressly sought
4. Yes, it is fine for the thesis, including this reproduced figure, to be included in the Institutional Repository; however, please note that the re-used figure **may NOT** be licensed under a CC BY-NC-ND licence.

Please use this email as permission to proceed on the basis of the above. If you need a formal licence above and beyond this email, please visit copyright.com and make your request following the steps on this site. (Note that although we do not make a charge for the re-use you have requested, you may be charged the small admin fee of $3.50 USD by the Copyright Clearance Center if seeking permission via the copyright.com site.)

Best wishes,

Malavika

Biochemical Society | Portland Press
Charles Darwin House, 12 Roger Street, London WC1N 2JU

T+44 (0)20 7685 2420
malavika.legge@biochemistry.org

BIOCHEMICAL SOCIETY PORTLAND PRESS

From: Portland Press – Production
Sent: 01 September 2017 10:26
To: Malavika Legge <Malavika.Legge@portlandpress.com>
Subject: FW: Permission to use figure for PhD thesis

From: Hansel, Katie S [mailto:c.hansel13@imperial.ac.uk]
Sent: 23 August 2017 14:17
To: Portland Press – Production <production@portlandpress.com>
Subject: Permission to use figure for PhD thesis

ELSEVIER ORDER DETAILS

Aug 30, 2017

Order Number	501300704
Order date	Aug 23, 2017
Licensed Content Publisher	Elsevier
Licensed Content Publication	Elsevier Books
Licensed Content Title	Semiconducting Silicon Nanowires for Biomedical Applications
Licensed Content Author	C. Chiappini,C. Almeida
Licensed Content Date	2014
Licensed Content Volume	n/a
Licensed Content Issue	n/a
Licensed Content Pages	24
Start Page	144
End Page	167
Type of Use	reuse in a thesis/dissertation
Intended publisher of new work	other
Portion	figures/tables/illustrations
Number of figures/tables/illustrations	1
Format	both print and electronic
Are you the author of this Elsevier chapter?	No
Will you be translating?	No
Original figure numbers	Figure 1
Title of your thesis/dissertation	Microscopy of interactions at the cell-material and call-matrix interface
Expected completion date	Oct 2017
Estimated size (number of pages)	200
Requestor Location	Imperial College Imperial College London Imperial College Rd Kensington, London SW7 2AZ United Kingdom Attn: Imperial College
Publisher Tax ID	GB 494 6272 12
Total	Not Available

NATURE PUBLISHING GROUP LICENSE TERMS AND CONDITIONS

Aug 23, 2017

This Agreement between Imperial College -- Catherine Hansel ("You") and Nature Publishing Group ("Nature Publishing Group") consists of your license details and the terms and conditions provided by Nature Publishing Group and Copyright Clearance Center.

License Number	4170631161061
License date	Aug 16, 2017
Licensed Content Publisher	Nature Publishing Group
Licensed Content Publication	Nature Nanotechnology
Licensed Content Title	Vertical nanopillars for in situ probing of nuclear mechanics in adherent cells
Licensed Content Author	Lindsey Hanson, Wenting Zhao, Hsin-Ya Lou, Ziliang Carter Lin, Seok Woo Lee, Praveen Chowdary
Licensed Content Date	May 18, 2015
Licensed Content Volume	10
Licensed Content Issue	6
Type of Use	reuse in a dissertation / thesis
Requestor type	academic/educational
Format	print and electronic
Portion	figures/tables/illustrations
Number of figures/tables/illustrations	1
High-res required	no
Figures	1
Author of this NPG article	no
Your reference number	
Title of your thesis / dissertation	Microscopy of interactions at the cell-material and call-matrix interface
Expected completion date	Oct 2017
Estimated size (number of pages)	200
Requestor Location	Imperial College Imperial College London Imperial College Rd Kensington, London SW7 2AZ United Kingdom Attn: Imperial College
Billing Type	Invoice
Billing Address	Imperial College Imperial College London Imperial College Rd Kensington, United Kingdom SW7 2AZ Attn: Imperial College
Total	0.00 GBP
Terms and Conditions	

Nature Publishing Group hereby grants you a non-exclusive license to reproduce this material for this purpose, and for no other use,subject to the conditions below:

1. NPG warrants that it has, to the best of its knowledge, the rights to license reuse of this material. However, you should ensure that the material you are requesting is original to Nature Publishing Group and does not carry the copyright of another entity (as credited in the published version). If the credit line on any part of the material you have requested indicates that it was reprinted or adapted by NPG with permission from another source, then you should also seek permission from that source to reuse the material.

2. Permission granted free of charge for material in print is also usually granted for any electronic version of that work, provided that the material is incidental to the work as a whole and that the electronic version is essentially equivalent to, or substitutes for, the print version.Where print permission has been granted for a fee, separate permission must be obtained for any additional, electronic re-use (unless, as in the case of a full paper, this has already been accounted for during your initial request in the calculation of a print run).NB: In all cases, web-based use of full-text articles must be authorized separately through the 'Use on a Web Site' option when requesting permission.

3. Permission granted for a first edition does not apply to second and subsequent editions and for editions in other languages (except for signatories to the STM Permissions Guidelines, or where the first edition permission was granted for free).

4. Nature Publishing Group's permission must be acknowledged next to the figure, table or abstract in print. In electronic form, this acknowledgement must be visible at the same time as the figure/table/abstract, and must be hyperlinked to the journal's homepage.

5. The credit line should read:
   Reprinted by permission from Macmillan Publishers Ltd: [JOURNAL NAME] (reference citation), copyright (year of publication)
   For AOP papers, the credit line should read:
   Reprinted by permission from Macmillan Publishers Ltd: [JOURNAL NAME], advance online publication, day month year (doi: 10.1038/sj.[JOURNAL ACRONYM].XXXXX)

   Note: For republication from the *British Journal of Cancer*, the following credit lines apply.
   Reprinted by permission from Macmillan Publishers Ltd on behalf of Cancer Research UK: [JOURNAL NAME] (reference citation), copyright (year of publication)For AOP papers, the credit line should read:
   Reprinted by permission from Macmillan Publishers Ltd on behalf of Cancer Research UK: [JOURNAL NAME], advance online publication, day month year (doi: 10.1038/sj.[JOURNAL ACRONYM].XXXXX)

6. Adaptations of single figures do not require NPG approval. However, the adaptation should be credited as follows:

   Adapted by permission from Macmillan Publishers Ltd: [JOURNAL NAME] (reference citation), copyright (year of publication)

   Note: For adaptation from the *British Journal of Cancer*, the following credit line applies.
   Adapted by permission from Macmillan Publishers Ltd on behalf of Cancer Research UK: [JOURNAL NAME] (reference citation), copyright (year of publication)

7. Translations of 401 words up to a whole article require NPG approval. Please visit http://www.macmillanmedicalcommunications.com for more information.Translations of up to a 400 words do not require NPG approval. The translation should be credited as follows:

   Translated by permission from Macmillan Publishers Ltd: [JOURNAL NAME] (reference citation), copyright (year of publication).

   Note: For translation from the *British Journal of Cancer*, the following credit line applies.
   Translated by permission from Macmillan Publishers Ltd on behalf of Cancer Research UK: [JOURNAL NAME] (reference citation), copyright (year of publication)

Copyright Clearance Center

Note: Copyright.com supplies permissions but not the copyrighted content itself.

1 PAYMENT 2 REVIEW 3 CONFIRMATION

Step 3: Order Confirmation

Thank you for your order! A confirmation for your order will be sent to your account email address. If you have questions about your order, you can call us 24 hrs/day, M-F at +1.855.239.3415 Toll Free, or write to us at info@copyright.com. **This is not an invoice.**

Confirmation Number: 11665054
Order Date: 08/23/2017

If you paid by credit card, your order will be finalized and your card will be charged within 24 hours. If you choose to be invoiced, you can change or cancel your order until the invoice is generated.

Payment Information

Catherine Hansel
Imperial College
c.hansel13@imperial.ac.uk
+44 7947506370
Payment Method: n/a

Order Details

Nanotechnology

Order detail ID:	70650932
Order License Id:	4174791383367
ISSN:	0957-4484
Publication Type:	Journal
Volume:	
Issue:	
Start page:	
Publisher:	IOP Publishing

Permission Status: Granted
Permission type: Republish or display content
Type of use: Thesis/Dissertation

Requestor type	Academic institution
Format	Print, Electronic
Portion	image/photo
Number of images/photos requested	1
Title or numeric reference of the portion(s)	Figure 2b(ii-v)
Title of the article or chapter the portion is from	Fluorescence labelling and imaging strategy
Editor of portion(s)	N/A
Author of portion(s)	N/A
Volume of serial or monograph	N/A
Page range of portion	3

Publication date of portion	September 2012
Rights for	Main product
Duration of use	Life of current edition
Creation of copies for the disabled	no
With minor editing privileges	no
For distribution to	Worldwide
In the following language(s)	Original language of publication
With incidental promotional use	no
Lifetime unit quantity of new product	Up to 499
Made available in the following markets	Education
The requesting person/organization	Imperial College
Order reference number	
Author/Editor	Katie Hansel
The standard identifier of New Work	N/A
The proposed price	0
Title of New Work	Microscopy of cell-material and cell-matrix interactions
Publisher of New Work	Imperial College
Expected publication date	Oct 2017
Estimated size (pages)	200

Note: This item will be invoiced or charged separately through CCC's **RightsLink** service. More info **$ 0.00**

This is not an invoice.

Total order items: 1 **Order Total: 0.00 USD**

Confirmation Number: 11665054

Special Rightsholder Terms & Conditions

The following terms & conditions apply to the specific publication under which they are listed

Nanotechnology
Permission type: Republish or display content
Type of use: Thesis/Dissertation

TERMS AND CONDITIONS

The following terms are individual to this publisher:

Other Terms and Conditions:

STANDARD TERMS AND CONDITIONS

1. Description of Service; Defined Terms. This Republication License enables the User to obtain licenses for republication of one or more copyrighted works as described in detail on the relevant Order Confirmation (the "Work(s)"). Copyright Clearance Center, Inc. ("CCC") grants licenses through the Service on behalf of the rightsholder identified on the Order Confirmation (the "Rightsholder"). "Republication", as used herein, generally means the inclusion of a Work, in whole or in part, in a new work or works, also as described on the Order Confirmation. "User", as used herein, means the person or entity making such republication.

2. The terms set forth in the relevant Order Confirmation, and any terms set by the Rightsholder with respect to a particular Work, govern the terms of use of Works in connection with the Service. By using the Service, the person transacting for a republication license on behalf of the User represents and warrants that he/she/it (a) has been duly authorized by the User to accept, and hereby does accept, all such terms and conditions on behalf of User, and (b) shall inform User of all such terms and conditions. In the event such person is a "freelancer" or other third party independent of User and CCC, such party shall be deemed jointly a "User" for purposes of these terms and conditions. In any event, User shall be deemed to have accepted and agreed to all such terms and conditions if User republishes the Work in any fashion.

3. Scope of License; Limitations and Obligations.

3.1 All Works and all rights therein, including copyright rights, remain the sole and exclusive property of the Rightsholder. The license created by the exchange of an Order Confirmation (and/or any invoice) and payment by User of the full amount set forth on that document includes only those rights expressly set forth in the Order Confirmation and in these terms and conditions, and conveys no other rights in the Work(s) to User. All rights not expressly granted are hereby reserved.

3.2 General Payment Terms: You may pay by credit card or through an account with us payable at the end of the month. If you and we agree that you may establish a standing account with CCC, then the following terms apply: Remit Payment to: Copyright Clearance Center, 29118 Network Place, Chicago, IL 60673-1291. Payments Due: Invoices are payable upon their delivery to you (or upon our notice to you that they are available to you for downloading). After 30 days, outstanding amounts will be subject to a service charge of 1-1/2% per month or, if less, the maximum rate allowed by applicable law. Unless otherwise specifically set forth in the Order Confirmation or in a separate written agreement signed by CCC, invoices are due and payable on "net 30" terms. While User may exercise the rights licensed immediately upon issuance of the Order Confirmation, the license is automatically revoked and is null and void, as if it had never been issued, if complete payment for the license is not received on a timely basis either from User directly or through a payment agent, such as a credit card company.

3.3 Unless otherwise provided in the Order Confirmation, any grant of rights to User (i) is "one-time" (including the editions and product family specified in the license), (ii) is non-exclusive and non-transferable and (iii) is subject to any and all limitations and restrictions (such as, but not limited to, limitations on duration of use or circulation) included in the Order Confirmation or invoice and/or in these terms and conditions. Upon completion of the licensed use, User shall either secure a new permission for further use of the Work(s) or immediately cease any new use of the Work(s) and shall render inaccessible (such as by deleting or by removing or severing links or other locators) any further copies of the Work (except for copies printed on paper in accordance with this license and still in User's stock at the end of such period).

3.4 In the event that the material for which a republication license is sought includes third party materials (such as photographs, illustrations, graphs, inserts and similar materials) which are identified in such material as having been used by permission, User is responsible for identifying, and seeking separate licenses (under this Service or otherwise) for, any of such third party materials; without a separate license, such third party materials may not be used.

3.5 Use of proper copyright notice for a Work is required as a condition of any license granted under the Service. Unless otherwise provided in the Order Confirmation, a proper copyright notice will read substantially as follows: "Republished with permission of [Rightsholder's name], from [Work's title, author, volume, edition number and year of copyright]; permission conveyed through Copyright Clearance Center, Inc. " Such notice must be provided in a reasonably legible font size and must be placed either immediately adjacent to the Work as used (for example, as part of a by-line or footnote but not as a separate electronic link) or in the place where substantially all other credits or notices for the new work containing the republished Work are located. Failure to include the required notice results in loss to the Rightsholder and CCC, and the User shall be liable to pay liquidated damages for each such failure equal to twice the use fee specified in the Order Confirmation, in addition to the use fee itself and any other fees and charges specified.

3.6 User may only make alterations to the Work if and as expressly set forth in the Order Confirmation. No Work may be used in any way that is defamatory, violates the rights of third parties (including such third parties' rights of copyright, privacy, publicity, or other tangible or intangible property), or is otherwise illegal, sexually explicit or obscene. In addition, User may not conjoin a Work with any other material that may result in damage to the reputation of the

Rightsholder. User agrees to inform CCC if it becomes aware of any infringement of any rights in a Work and to cooperate with any reasonable request of CCC or the Rightsholder in connection therewith.

4. Indemnity. User hereby indemnifies and agrees to defend the Rightsholder and CCC, and their respective employees and directors, against all claims, liability, damages, costs and expenses, including legal fees and expenses, arising out of any use of a Work beyond the scope of the rights granted herein, or any use of a Work which has been altered in any unauthorized way by User, including claims of defamation or infringement of rights of copyright, publicity, privacy or other tangible or intangible property.

5. Limitation of Liability. UNDER NO CIRCUMSTANCES WILL CCC OR THE RIGHTSHOLDER BE LIABLE FOR ANY DIRECT, INDIRECT, CONSEQUENTIAL OR INCIDENTAL DAMAGES (INCLUDING WITHOUT LIMITATION DAMAGES FOR LOSS OF BUSINESS PROFITS OR INFORMATION, OR FOR BUSINESS INTERRUPTION) ARISING OUT OF THE USE OR INABILITY TO USE A WORK, EVEN IF ONE OF THEM HAS BEEN ADVISED OF THE POSSIBILITY OF SUCH DAMAGES. In any event, the total liability of the Rightsholder and CCC (including their respective employees and directors) shall not exceed the total amount actually paid by User for this license. User assumes full liability for the actions and omissions of its principals, employees, agents, affiliates, successors and assigns.

6. Limited Warranties. THE WORK(S) AND RIGHT(S) ARE PROVIDED "AS IS". CCC HAS THE RIGHT TO GRANT TO USER THE RIGHTS GRANTED IN THE ORDER CONFIRMATION DOCUMENT. CCC AND THE RIGHTSHOLDER DISCLAIM ALL OTHER WARRANTIES RELATING TO THE WORK(S) AND RIGHT(S), EITHER EXPRESS OR IMPLIED, INCLUDING WITHOUT LIMITATION IMPLIED WARRANTIES OF MERCHANTABILITY OR FITNESS FOR A PARTICULAR PURPOSE. ADDITIONAL RIGHTS MAY BE REQUIRED TO USE ILLUSTRATIONS, GRAPHS, PHOTOGRAPHS, ABSTRACTS, INSERTS OR OTHER PORTIONS OF THE WORK (AS OPPOSED TO THE ENTIRE WORK) IN A MANNER CONTEMPLATED BY USER; USER UNDERSTANDS AND AGREES THAT NEITHER CCC NOR THE RIGHTSHOLDER MAY HAVE SUCH ADDITIONAL RIGHTS TO GRANT.

7. Effect of Breach. Any failure by User to pay any amount when due, or any use by User of a Work beyond the scope of the license set forth in the Order Confirmation and/or these terms and conditions, shall be a material breach of the license created by the Order Confirmation and these terms and conditions. Any breach not cured within 30 days of written notice thereof shall result in immediate termination of such license without further notice. Any unauthorized (but licensable) use of a Work that is terminated immediately upon notice thereof may be liquidated by payment of the Rightsholder's ordinary license price therefor; any unauthorized (and unlicensable) use that is not terminated immediately for any reason (including, for example, because materials containing the Work cannot reasonably be recalled) will be subject to all remedies available at law or in equity, but in no event to a payment of less than three times the Rightsholder's ordinary license price for the most closely analogous licensable use plus Rightsholder's and/or CCC's costs and expenses incurred in collecting such payment.

8. **Miscellaneous.**

8.1 User acknowledges that CCC may, from time to time, make changes or additions to the Service or to these terms and conditions, and CCC reserves the right to send notice to the User by electronic mail or otherwise for the purposes of notifying User of such changes or additions; provided that any such changes or additions shall not apply to permissions already secured and paid for.

8.2 Use of User-related information collected through the Service is governed by CCC's privacy policy, available online here: http://www.copyright.com/content/cc3/en/tools/footer/privacypolicy.html.

8.3 The licensing transaction described in the Order Confirmation is personal to User. Therefore, User may not assign or transfer to any other person (whether a natural person or an organization of any kind) the license created by the Order Confirmation and these terms and conditions or any rights granted hereunder; provided, however, that User may assign such license in its entirety on written notice to CCC in the event of a transfer of all or substantially all of User's rights in the new material which includes the Work(s) licensed under this Service.

8.4 No amendment or waiver of any terms is binding unless set forth in writing and signed by the parties. The Rightsholder and CCC hereby object to any terms contained in any writing prepared by the User or its principals, employees, agents or affiliates and purporting to govern or otherwise relate to the licensing transaction described in the Order Confirmation, which terms are in any way inconsistent with any terms set forth in the Order Confirmation and/or in these terms and conditions or CCC's standard operating procedures, whether such writing is prepared prior to, simultaneously with or subsequent to the Order Confirmation, and whether such writing appears on a copy of the Order Confirmation or in a separate instrument.

8.5 The licensing transaction described in the Order Confirmation document shall be governed by and construed under the law of the State of New York, USA, without regard to the principles thereof of conflicts of law. Any case, controversy, suit, action, or proceeding arising out of, in connection with, or related to such licensing transaction shall be brought, at CCC's sole discretion, in any federal or state court located in the County of New York, State of New York, USA, or in any federal or state court whose geographical jurisdiction covers the location of the Rightsholder set forth in the Order Confirmation. The parties expressly submit to the personal jurisdiction and venue of each such federal or state court.If you have any comments or questions about the Service or Copyright Clearance Center, please contact us at 978-750-8400 or send an e-mail to info@copyright.com.

v 1.1

Close

NATURE PUBLISHING GROUP LICENSE TERMS AND CONDITIONS

Aug 23, 2017

This Agreement between Imperial College -- Catherine Hansel ("You") and Nature Publishing Group ("Nature Publishing Group") consists of your license details and the terms and conditions provided by Nature Publishing Group and Copyright Clearance Center.

License Number	4170640212874
License date	Aug 16, 2017
Licensed Content Publisher	Nature Publishing Group
Licensed Content Publication	Nature Materials
Licensed Content Title	Biodegradable silicon nanoneedles delivering nucleic acids intracellularly induce localized in vivo neovascularization
Licensed Content Author	C. Chiappini, E. De Rosa, J. O. Martinez, X. Liu, J. Steele, M. M. Stevens
Licensed Content Date	Mar 30, 2015
Licensed Content Volume	14
Licensed Content Issue	5
Type of Use	reuse in a dissertation / thesis
Requestor type	academic/educational
Format	print and electronic
Portion	figures/tables/illustrations
Number of figures/tables/illustrations	1
High-res required	no
Figures	2
Author of this NPG article	no
Your reference number	
Title of your thesis / dissertation	Microscopy of interactions at the cell-material and call-matrix interface
Expected completion date	Oct 2017
Estimated size (number of pages)	200
Requestor Location	Imperial College Imperial College London Imperial College Rd Kensington, London SW7 2AZ United Kingdom Attn: Imperial College
Billing Type	Invoice
Billing Address	Imperial College Imperial College London Imperial College Rd Kensington, United Kingdom SW7 2AZ Attn: Imperial College
Total	0.00 GBP
Terms and Conditions	

Nature Publishing Group hereby grants you a non-exclusive license to reproduce this material for this purpose, and for no other use,subject to the conditions below:

1. NPG warrants that it has, to the best of its knowledge, the rights to license reuse of this material. However, you should ensure that the material you are requesting is original to Nature Publishing Group and does not carry the copyright of another entity (as credited in the published version). If the credit line on any part of the material you have requested indicates that it was reprinted or adapted by NPG with permission from another source, then you should also seek permission from that source to reuse the material.

2. Permission granted free of charge for material in print is also usually granted for any electronic version of that work, provided that the material is incidental to the work as a whole and that the electronic version is essentially equivalent to, or substitutes for, the print version.Where print permission has been granted for a fee, separate permission must be obtained for any additional, electronic re-use (unless, as in the case of a full paper, this has already been accounted for during your initial request in the calculation of a print run).NB: In all cases, web-based use of full-text articles must be authorized separately through the 'Use on a Web Site' option when requesting permission.

3. Permission granted for a first edition does not apply to second and subsequent editions and for editions in other languages (except for signatories to the STM Permissions Guidelines, or where the first edition permission was granted for free).

4. Nature Publishing Group's permission must be acknowledged next to the figure, table or abstract in print. In electronic form, this acknowledgement must be visible at the same time as the figure/table/abstract, and must be hyperlinked to the journal's homepage.

5. The credit line should read:
   Reprinted by permission from Macmillan Publishers Ltd: [JOURNAL NAME] (reference citation), copyright (year of publication)
   For AOP papers, the credit line should read:
   Reprinted by permission from Macmillan Publishers Ltd: [JOURNAL NAME], advance online publication, day month year (doi: 10.1038/sj.[JOURNAL ACRONYM].XXXXX)

   Note: For republication from the *British Journal of Cancer*, the following credit lines apply.
   Reprinted by permission from Macmillan Publishers Ltd on behalf of Cancer Research UK: [JOURNAL NAME] (reference citation), copyright (year of publication)For AOP papers, the credit line should read:
   Reprinted by permission from Macmillan Publishers Ltd on behalf of Cancer Research UK: [JOURNAL NAME], advance online publication, day month year (doi: 10.1038/sj.[JOURNAL ACRONYM].XXXXX)

6. Adaptations of single figures do not require NPG approval. However, the adaptation should be credited as follows:

   Adapted by permission from Macmillan Publishers Ltd: [JOURNAL NAME] (reference citation), copyright (year of publication)

   Note: For adaptation from the *British Journal of Cancer*, the following credit line applies.
   Adapted by permission from Macmillan Publishers Ltd on behalf of Cancer Research UK: [JOURNAL NAME] (reference citation), copyright (year of publication)

7. Translations of 401 words up to a whole article require NPG approval. Please visit http://www.macmillanmedicalcommunications.com for more information.Translations of up to a 400 words do not require NPG approval. The translation should be credited as follows:

   Translated by permission from Macmillan Publishers Ltd: [JOURNAL NAME] (reference citation), copyright (year of publication).

   Note: For translation from the *British Journal of Cancer*, the following credit line applies.
   Translated by permission from Macmillan Publishers Ltd on behalf of Cancer Research UK: [JOURNAL NAME] (reference citation), copyright (year of publication)

ELSEVIER LICENSE
TERMS AND CONDITIONS

Sep 18, 2017

This Agreement between Imperial College -- Catherine Hansel ("You") and Elsevier ("Elsevier") consists of your license details and the terms and conditions provided by Elsevier and Copyright Clearance Center.

License Number	4191980895339
License date	Sep 18, 2017
Licensed Content Publisher	Elsevier
Licensed Content Publication	Biophysical Journal
Licensed Content Title	Penetration of Cell Membranes and Synthetic Lipid Bilayers by Nanoprobes
Licensed Content Author	Matthew R. Angle,Andrew Wang,Aman Thomas,Andreas T. Schaefer,Nicholas A. Melosh
Licensed Content Date	Nov 4, 2014
Licensed Content Volume	107
Licensed Content Issue	9
Licensed Content Pages	10
Start Page	2091
End Page	2100
Type of Use	reuse in a thesis/dissertation
Portion	figures/tables/illustrations
Number of figures/tables/illustrations	1
Format	both print and electronic
Are you the author of this Elsevier article?	No
Will you be translating?	No
Original figure numbers	Figure 1 part d
Title of your thesis/dissertation	Microscopy of interactions at the cell-material and call-matrix interface
Expected completion date	Oct 2017
Estimated size (number of pages)	200
Requestor Location	Imperial College Imperial College London Imperial College Rd Kensington, London SW7 2AZ United Kingdom Attn: Imperial College
Publisher Tax ID	GB 494 6272 12
Total	0.00 GBP
Terms and Conditions	

INTRODUCTION

1. The publisher for this copyrighted material is Elsevier. By clicking "accept" in connection with completing this licensing transaction, you agree that the following terms and conditions

1. The publisher for this copyrighted material is Elsevier. By clicking "accept" in connection with completing this licensing transaction, you agree that the following terms and conditions apply to this transaction (along with the Billing and Payment terms and conditions established by Copyright Clearance Center, Inc. ("CCC"), at the time that you opened your Rightslink account and that are available at any time at http://myaccount.copyright.com).

GENERAL TERMS

2. Elsevier hereby grants you permission to reproduce the aforementioned material subject to the terms and conditions indicated.

3. Acknowledgement: If any part of the material to be used (for example, figures) has appeared in our publication with credit or acknowledgement to another source, permission must also be sought from that source. If such permission is not obtained then that material may not be included in your publication/copies. Suitable acknowledgement to the source must be made, either as a footnote or in a reference list at the end of your publication, as follows:

"Reprinted from Publication title, Vol /edition number, Author(s), Title of article / title of chapter, Pages No., Copyright (Year), with permission from Elsevier [OR APPLICABLE SOCIETY COPYRIGHT OWNER]." Also Lancet special credit - "Reprinted from The Lancet, Vol. number, Author(s), Title of article, Pages No., Copyright (Year), with permission from Elsevier."

4. Reproduction of this material is confined to the purpose and/or media for which permission is hereby given.

5. Altering/Modifying Material: Not Permitted. However figures and illustrations may be altered/adapted minimally to serve your work. Any other abbreviations, additions, deletions and/or any other alterations shall be made only with prior written authorization of Elsevier Ltd. (Please contact Elsevier at permissions@elsevier.com). No modifications can be made to any Lancet figures/tables and they must be reproduced in full.

6. If the permission fee for the requested use of our material is waived in this instance, please be advised that your future requests for Elsevier materials may attract a fee.

7. Reservation of Rights: Publisher reserves all rights not specifically granted in the combination of (i) the license details provided by you and accepted in the course of this licensing transaction, (ii) these terms and conditions and (iii) CCC's Billing and Payment terms and conditions.

8. License Contingent Upon Payment: While you may exercise the rights licensed immediately upon issuance of the license at the end of the licensing process for the transaction, provided that you have disclosed complete and accurate details of your proposed use, no license is finally effective unless and until full payment is received from you (either by publisher or by CCC) as provided in CCC's Billing and Payment terms and conditions. If full payment is not received on a timely basis, then any license preliminarily granted shall be deemed automatically revoked and shall be void as if never granted. Further, in the event that you breach any of these terms and conditions or any of CCC's Billing and Payment terms and conditions, the license is automatically revoked and shall be void as if never granted. Use of materials as described in a revoked license, as well as any use of the materials beyond the scope of an unrevoked license, may constitute copyright infringement and publisher reserves the right to take any and all action to protect its copyright in the materials.

9. Warranties: Publisher makes no representations or warranties with respect to the licensed material.

10. Indemnity: You hereby indemnify and agree to hold harmless publisher and CCC, and their respective officers, directors, employees and agents, from and against any and all claims arising out of your use of the licensed material other than as specifically authorized pursuant to this license.

11. No Transfer of License: This license is personal to you and may not be sublicensed, assigned, or transferred by you to any other person without publisher's written permission.

12. No Amendment Except in Writing: This license may not be amended except in a writing signed by both parties (or, in the case of publisher, by CCC on publisher's behalf).

13. Objection to Contrary Terms: Publisher hereby objects to any terms contained in any purchase order, acknowledgment, check endorsement or other writing prepared by you, which terms are inconsistent with these terms and conditions or CCC's Billing and Payment

NATURE PUBLISHING GROUP LICENSE TERMS AND CONDITIONS

Aug 23, 2017

This Agreement between Imperial College -- Catherine Hansel ("You") and Nature Publishing Group ("Nature Publishing Group") consists of your license details and the terms and conditions provided by Nature Publishing Group and Copyright Clearance Center.

License Number	4170640600647
License date	Aug 16, 2017
Licensed Content Publisher	Nature Publishing Group
Licensed Content Publication	Nature Communications
Licensed Content Title	Quantification of nanowire penetration into living cells
Licensed Content Author	Alexander M. Xu, Amin Aalipour, Sergio Leal-Ortiz, Armen H. Mekhdjian, Xi Xie et al.
Licensed Content Date	Apr 7, 2014
Licensed Content Volume	5
Type of Use	reuse in a dissertation / thesis
Requestor type	academic/educational
Format	print and electronic
Portion	figures/tables/illustrations
Number of figures/tables/illustrations	1
High-res required	no
Figures	1b&c
Author of this NPG article	no
Your reference number	
Title of your thesis / dissertation	Microscopy of interactions at the cell-material and call-matrix interface
Expected completion date	Oct 2017
Estimated size (number of pages)	200
Requestor Location	Imperial College Imperial College London Imperial College Rd Kensington, London SW7 2AZ United Kingdom Attn: Imperial College
Billing Type	Invoice
Billing Address	Imperial College Imperial College London Imperial College Rd Kensington, United Kingdom SW7 2AZ Attn: Imperial College
Total	0.00 GBP
Terms and Conditions	

Terms and Conditions for Permissions

Nature Publishing Group hereby grants you a non-exclusive license to reproduce this material for this purpose, and for no other use,subject to the conditions below:

1. NPG warrants that it has, to the best of its knowledge, the rights to license reuse of this material. However, you should ensure that the material you are requesting is original to Nature Publishing Group and does not carry the copyright of another entity (as credited in the published version). If the credit line on any part of the material you have requested indicates that it was reprinted or adapted by NPG with permission from another source, then you should also seek permission from that source to reuse the material.

2. Permission granted free of charge for material in print is also usually granted for any electronic version of that work, provided that the material is incidental to the work as a whole and that the electronic version is essentially equivalent to, or substitutes for, the print version.Where print permission has been granted for a fee, separate permission must be obtained for any additional, electronic re-use (unless, as in the case of a full paper, this has already been accounted for during your initial request in the calculation of a print run).NB: In all cases, web-based use of full-text articles must be authorized separately through the 'Use on a Web Site' option when requesting permission.

3. Permission granted for a first edition does not apply to second and subsequent editions and for editions in other languages (except for signatories to the STM Permissions Guidelines, or where the first edition permission was granted for free).

4. Nature Publishing Group's permission must be acknowledged next to the figure, table or abstract in print. In electronic form, this acknowledgement must be visible at the same time as the figure/table/abstract, and must be hyperlinked to the journal's homepage.

5. The credit line should read:
   Reprinted by permission from Macmillan Publishers Ltd: [JOURNAL NAME] (reference citation), copyright (year of publication)
   For AOP papers, the credit line should read:
   Reprinted by permission from Macmillan Publishers Ltd: [JOURNAL NAME], advance online publication, day month year (doi: 10.1038/sj.[JOURNAL ACRONYM].XXXXX)

   Note: For republication from the *British Journal of Cancer*, the following credit lines apply.
   Reprinted by permission from Macmillan Publishers Ltd on behalf of Cancer Research UK: [JOURNAL NAME] (reference citation), copyright (year of publication)For AOP papers, the credit line should read:
   Reprinted by permission from Macmillan Publishers Ltd on behalf of Cancer Research UK: [JOURNAL NAME], advance online publication, day month year (doi: 10.1038/sj.[JOURNAL ACRONYM].XXXXX)

6. Adaptations of single figures do not require NPG approval. However, the adaptation should be credited as follows:

   Adapted by permission from Macmillan Publishers Ltd: [JOURNAL NAME] (reference citation), copyright (year of publication)

   Note: For adaptation from the *British Journal of Cancer*, the following credit line applies.
   Adapted by permission from Macmillan Publishers Ltd on behalf of Cancer Research UK: [JOURNAL NAME] (reference citation), copyright (year of publication)

7. Translations of 401 words up to a whole article require NPG approval. Please visit http://www.macmillanmedicalcommunications.com for more information.Translations of up to a 400 words do not require NPG approval. The translation should be credited as follows:

   Translated by permission from Macmillan Publishers Ltd: [JOURNAL NAME] (reference citation), copyright (year of publication).

   Note: For translation from the *British Journal of Cancer*, the following credit line applies.
   Translated by permission from Macmillan Publishers Ltd on behalf of Cancer Research UK: [JOURNAL NAME] (reference citation), copyright (year of publication)

ELSEVIER LICENSE
TERMS AND CONDITIONS

Aug 23, 2017

This Agreement between Imperial College -- Catherine Hansel ("You") and Elsevier ("Elsevier") consists of your license details and the terms and conditions provided by Elsevier and Copyright Clearance Center.

License Number	4170770947329
License date	Aug 16, 2017
Licensed Content Publisher	Elsevier
Licensed Content Publication	Biomaterials
Licensed Content Title	The control of cell adhesion and viability by zinc oxide nanorods
Licensed Content Author	Jiyeon Lee,B.S. Kang,Barrett Hicks,Thomas F. Chancellor,Byung Hwan Chu,Hung-Ta Wang,Benjamin G. Keselowsky,F. Ren,Tanmay P. Lele
Licensed Content Date	Sep 1, 2008
Licensed Content Volume	29
Licensed Content Issue	27
Licensed Content Pages	7
Start Page	3743
End Page	3749
Type of Use	reuse in a thesis/dissertation
Portion	figures/tables/illustrations
Number of figures/tables/illustrations	1
Format	both print and electronic
Are you the author of this Elsevier article?	No
Will you be translating?	No
Original figure numbers	Figure 2
Title of your thesis/dissertation	Microscopy of interactions at the cell-material and call-matrix interface
Expected completion date	Oct 2017
Estimated size (number of pages)	200
Requestor Location	Imperial College Imperial College London Imperial College Rd Kensington, London SW7 2AZ United Kingdom Attn: Imperial College
Publisher Tax ID	GB 494 6272 12
Total	0.00 GBP
Terms and Conditions	

INTRODUCTION

1. The publisher for this copyrighted material is Elsevier. By clicking "accept" in connection with completing this licensing transaction, you agree that the following terms and conditions

1. The publisher for this copyrighted material is Elsevier. By clicking "accept" in connection with completing this licensing transaction, you agree that the following terms and conditions apply to this transaction (along with the Billing and Payment terms and conditions established by Copyright Clearance Center, Inc. ("CCC"), at the time that you opened your Rightslink account and that are available at any time at http://myaccount.copyright.com).

GENERAL TERMS

2. Elsevier hereby grants you permission to reproduce the aforementioned material subject to the terms and conditions indicated.

3. Acknowledgement: If any part of the material to be used (for example, figures) has appeared in our publication with credit or acknowledgement to another source, permission must also be sought from that source. If such permission is not obtained then that material may not be included in your publication/copies. Suitable acknowledgement to the source must be made, either as a footnote or in a reference list at the end of your publication, as follows:

"Reprinted from Publication title, Vol /edition number, Author(s), Title of article / title of chapter, Pages No., Copyright (Year), with permission from Elsevier [OR APPLICABLE SOCIETY COPYRIGHT OWNER]." Also Lancet special credit - "Reprinted from The Lancet, Vol. number, Author(s), Title of article, Pages No., Copyright (Year), with permission from Elsevier."

4. Reproduction of this material is confined to the purpose and/or media for which permission is hereby given.

5. Altering/Modifying Material: Not Permitted. However figures and illustrations may be altered/adapted minimally to serve your work. Any other abbreviations, additions, deletions and/or any other alterations shall be made only with prior written authorization of Elsevier Ltd. (Please contact Elsevier at permissions@elsevier.com). No modifications can be made to any Lancet figures/tables and they must be reproduced in full.

6. If the permission fee for the requested use of our material is waived in this instance, please be advised that your future requests for Elsevier materials may attract a fee.

7. Reservation of Rights: Publisher reserves all rights not specifically granted in the combination of (i) the license details provided by you and accepted in the course of this licensing transaction, (ii) these terms and conditions and (iii) CCC's Billing and Payment terms and conditions.

8. License Contingent Upon Payment: While you may exercise the rights licensed immediately upon issuance of the license at the end of the licensing process for the transaction, provided that you have disclosed complete and accurate details of your proposed use, no license is finally effective unless and until full payment is received from you (either by publisher or by CCC) as provided in CCC's Billing and Payment terms and conditions. If full payment is not received on a timely basis, then any license preliminarily granted shall be deemed automatically revoked and shall be void as if never granted. Further, in the event that you breach any of these terms and conditions or any of CCC's Billing and Payment terms and conditions, the license is automatically revoked and shall be void as if never granted. Use of materials as described in a revoked license, as well as any use of the materials beyond the scope of an unrevoked license, may constitute copyright infringement and publisher reserves the right to take any and all action to protect its copyright in the materials.

9. Warranties: Publisher makes no representations or warranties with respect to the licensed material.

10. Indemnity: You hereby indemnify and agree to hold harmless publisher and CCC, and their respective officers, directors, employees and agents, from and against any and all claims arising out of your use of the licensed material other than as specifically authorized pursuant to this license.

11. No Transfer of License: This license is personal to you and may not be sublicensed, assigned, or transferred by you to any other person without publisher's written permission.

12. No Amendment Except in Writing: This license may not be amended except in a writing signed by both parties (or, in the case of publisher, by CCC on publisher's behalf).

13. Objection to Contrary Terms: Publisher hereby objects to any terms contained in any purchase order, acknowledgment, check endorsement or other writing prepared by you, which terms are inconsistent with these terms and conditions or CCC's Billing and Payment

Copyright Clearance Center RightsLink®

Home | Account Info | Help

ACS Publications
Most Trusted. Most Cited. Most Read.

Title: Fine-Tuning the Degree of Stem Cell Polarization and Alignment on Ordered Arrays of High-Aspect-Ratio Nanopillars
Author: Michael A. Bucaro, Yolanda Vasquez, Benjamin D. Hatton, et al
Publication: ACS Nano
Publisher: American Chemical Society
Date: Jul 1, 2012
Copyright © 2012, American Chemical Society

Logged in as:
Catherine Hansel
Imperial College
Account #:
3001174884
LOGOUT

PERMISSION/LICENSE IS GRANTED FOR YOUR ORDER AT NO CHARGE

This type of permission/license, instead of the standard Terms & Conditions, is sent to you because no fee is being charged for your order. Please note the following:

- Permission is granted for your request in both print and electronic formats, and translations.
- If figures and/or tables were requested, they may be adapted or used in part.
- Please print this page for your records and send a copy of it to your publisher/graduate school.
- Appropriate credit for the requested material should be given as follows: "Reprinted (adapted) with permission from (COMPLETE REFERENCE CITATION). Copyright (YEAR) American Chemical Society." Insert appropriate information in place of the capitalized words.
- One-time permission is granted only for the use specified in your request. No additional uses are granted (such as derivative works or other editions). For any other uses, please submit a new request.

If credit is given to another source for the material you requested, permission must be obtained from that source.

BACK | CLOSE WINDOW

Copyright © 2017 Copyright Clearance Center, Inc. All Rights Reserved. Privacy statement. Terms and Conditions.
Comments? We would like to hear from you. E-mail us at customercare@copyright.com

Copyright Clearance Center RightsLink®

Home | Account Info | Help

ACS Publications
Most Trusted. Most Cited. Most Read.

Title: Tuning InAs Nanowire Density for HEK293 Cell Viability, Adhesion, and Morphology: Perspectives for Nanowire-Based Biosensors
Author: Sara Bonde, Trine Berthing, Morten Hannibal Madsen, et al
Publication: Applied Materials
Publisher: American Chemical Society
Date: Nov 1, 2013
Copyright © 2013, American Chemical Society

Logged in as:
Catherine Hansel
Imperial College
Account #:
3001174884
LOGOUT

PERMISSION/LICENSE IS GRANTED FOR YOUR ORDER AT NO CHARGE

This type of permission/license, instead of the standard Terms & Conditions, is sent to you because no fee is being charged for your order. Please note the following:

- Permission is granted for your request in both print and electronic formats, and translations.
- If figures and/or tables were requested, they may be adapted or used in part.
- Please print this page for your records and send a copy of it to your publisher/graduate school.
- Appropriate credit for the requested material should be given as follows: "Reprinted (adapted) with permission from (COMPLETE REFERENCE CITATION). Copyright (YEAR) American Chemical Society." Insert appropriate information in place of the capitalized words.
- One-time permission is granted only for the use specified in your request. No additional uses are granted (such as derivative works or other editions). For any other uses, please submit a new request.

If credit is given to another source for the material you requested, permission must be obtained from that source.

BACK | CLOSE WINDOW

Copyright © 2017 Copyright Clearance Center, Inc. All Rights Reserved. Privacy statement. Terms and Conditions.
Comments? We would like to hear from you. E-mail us at customercare@copyright.com

JOHN WILEY AND SONS LICENSE TERMS AND CONDITIONS

Aug 23, 2017

This Agreement between Imperial College -- Catherine Hansel ("You") and John Wiley and Sons ("John Wiley and Sons") consists of your license details and the terms and conditions provided by John Wiley and Sons and Copyright Clearance Center.

License Number	4170780285778
License date	Aug 16, 2017
Licensed Content Publisher	John Wiley and Sons
Licensed Content Publication	Small
Licensed Content Title	Fibroblasts Cultured on Nanowires Exhibit Low Motility, Impaired Cell Division, and DNA Damage
Licensed Content Author	Henrik Persson,Carsten Købler,Kristian Mølhave,Lars Samuelson,Jonas O. Tegenfeldt,Stina Oredsson,Christelle N. Prinz
Licensed Content Date	Jun 27, 2013
Licensed Content Pages	11
Type of use	Dissertation/Thesis
Requestor type	University/Academic
Format	Print and electronic
Portion	Figure/table
Number of figures/tables	1
Original Wiley figure/table number(s)	Figure 1
Will you be translating?	No
Title of your thesis / dissertation	Microscopy of interactions at the cell-material and call-matrix interface
Expected completion date	Oct 2017
Expected size (number of pages)	200
Requestor Location	Imperial College Imperial College London Imperial College Rd Kensington, London SW7 2AZ United Kingdom Attn: Imperial College
Publisher Tax ID	EU826007151
Billing Type	Invoice
Billing Address	Imperial College Imperial College London Imperial College Rd Kensington, United Kingdom SW7 2AZ Attn: Imperial College
Total	0.00 GBP
Terms and Conditions	

TERMS AND CONDITIONS

This copyrighted material is owned by or exclusively licensed to John Wiley & Sons, Inc. or one of its group companies (each a"Wiley Company") or handled on behalf of a society with which a Wiley Company has exclusive publishing rights in relation to a particular work (collectively "WILEY"). By clicking "accept" in connection with completing this licensing transaction, you agree that the following terms and conditions apply to this transaction (along with the billing and payment terms and conditions established by the Copyright Clearance Center Inc., ("CCC's Billing and Payment terms and conditions"), at the time that you opened your RightsLink account (these are available at any time at http://myaccount.copyright.com).

Terms and Conditions

- The materials you have requested permission to reproduce or reuse (the "Wiley Materials") are protected by copyright.
- You are hereby granted a personal, non-exclusive, non-sub licensable (on a stand-alone basis), non-transferable, worldwide, limited license to reproduce the Wiley Materials for the purpose specified in the licensing process. This license, **and any CONTENT (PDF or image file) purchased as part of your order,** is for a one-time use only and limited to any maximum distribution number specified in the license. The first instance of republication or reuse granted by this license must be completed within two years of the date of the grant of this license (although copies prepared before the end date may be distributed thereafter). The Wiley Materials shall not be used in any other manner or for any other purpose, beyond what is granted in the license. Permission is granted subject to an appropriate acknowledgement given to the author, title of the material/book/journal and the publisher. You shall also duplicate the copyright notice that appears in the Wiley publication in your use of the Wiley Material. Permission is also granted on the understanding that nowhere in the text is a previously published source acknowledged for all or part of this Wiley Material. Any third party content is expressly excluded from this permission.
- With respect to the Wiley Materials, all rights are reserved. Except as expressly granted by the terms of the license, no part of the Wiley Materials may be copied, modified, adapted (except for minor reformatting required by the new Publication), translated, reproduced, transferred or distributed, in any form or by any means, and no derivative works may be made based on the Wiley Materials without the prior permission of the respective copyright owner.**For STM Signatory Publishers clearing permission under the terms of the STM Permissions Guidelines only, the terms of the license are extended to include subsequent editions and for editions in other languages, provided such editions are for the work as a whole in situ and does not involve the separate exploitation of the permitted figures or extracts,** You may not alter, remove or suppress in any manner any copyright, trademark or other notices displayed by the Wiley Materials. You may not license, rent, sell, loan, lease, pledge, offer as security, transfer or assign the Wiley Materials on a stand-alone basis, or any of the rights granted to you hereunder to any other person.
- The Wiley Materials and all of the intellectual property rights therein shall at all times remain the exclusive property of John Wiley & Sons Inc, the Wiley Companies, or their respective licensors, and your interest therein is only that of having possession of and the right to reproduce the Wiley Materials pursuant to Section 2 herein during the continuance of this Agreement. You agree that you own no right, title or interest in or to the Wiley Materials or any of the intellectual property rights therein. You shall have no rights hereunder other than the license as provided for above in Section 2. No right, license or interest to any trademark, trade name, service mark or other branding ("Marks") of WILEY or its licensors is granted hereunder, and you agree that you shall not assert any such right, license or interest with respect thereto

- NEITHER WILEY NOR ITS LICENSORS MAKES ANY WARRANTY OR REPRESENTATION OF ANY KIND TO YOU OR ANY THIRD PARTY, EXPRESS, IMPLIED OR STATUTORY, WITH RESPECT TO THE MATERIALS OR THE ACCURACY OF ANY INFORMATION CONTAINED IN THE MATERIALS, INCLUDING, WITHOUT LIMITATION, ANY IMPLIED WARRANTY OF MERCHANTABILITY, ACCURACY, SATISFACTORY QUALITY, FITNESS FOR A PARTICULAR PURPOSE, USABILITY, INTEGRATION OR NON-INFRINGEMENT AND ALL SUCH WARRANTIES ARE HEREBY EXCLUDED BY WILEY AND ITS LICENSORS AND WAIVED BY YOU.

- WILEY shall have the right to terminate this Agreement immediately upon breach of this Agreement by you.

- You shall indemnify, defend and hold harmless WILEY, its Licensors and their respective directors, officers, agents and employees, from and against any actual or threatened claims, demands, causes of action or proceedings arising from any breach of this Agreement by you.

- IN NO EVENT SHALL WILEY OR ITS LICENSORS BE LIABLE TO YOU OR ANY OTHER PARTY OR ANY OTHER PERSON OR ENTITY FOR ANY SPECIAL, CONSEQUENTIAL, INCIDENTAL, INDIRECT, EXEMPLARY OR PUNITIVE DAMAGES, HOWEVER CAUSED, ARISING OUT OF OR IN CONNECTION WITH THE DOWNLOADING, PROVISIONING, VIEWING OR USE OF THE MATERIALS REGARDLESS OF THE FORM OF ACTION, WHETHER FOR BREACH OF CONTRACT, BREACH OF WARRANTY, TORT, NEGLIGENCE, INFRINGEMENT OR OTHERWISE (INCLUDING, WITHOUT LIMITATION, DAMAGES BASED ON LOSS OF PROFITS, DATA, FILES, USE, BUSINESS OPPORTUNITY OR CLAIMS OF THIRD PARTIES), AND WHETHER OR NOT THE PARTY HAS BEEN ADVISED OF THE POSSIBILITY OF SUCH DAMAGES. THIS LIMITATION SHALL APPLY NOTWITHSTANDING ANY FAILURE OF ESSENTIAL PURPOSE OF ANY LIMITED REMEDY PROVIDED HEREIN.

- Should any provision of this Agreement be held by a court of competent jurisdiction to be illegal, invalid, or unenforceable, that provision shall be deemed amended to achieve as nearly as possible the same economic effect as the original provision, and the legality, validity and enforceability of the remaining provisions of this Agreement shall not be affected or impaired thereby.

- The failure of either party to enforce any term or condition of this Agreement shall not constitute a waiver of either party's right to enforce each and every term and condition of this Agreement. No breach under this agreement shall be deemed waived or excused by either party unless such waiver or consent is in writing signed by the party granting such waiver or consent. The waiver by or consent of a party to a breach of any provision of this Agreement shall not operate or be construed as a waiver of or consent to any other or subsequent breach by such other party.

- This Agreement may not be assigned (including by operation of law or otherwise) by you without WILEY's prior written consent.

- Any fee required for this permission shall be non-refundable after thirty (30) days from receipt by the CCC.

- These terms and conditions together with CCC's Billing and Payment terms and conditions (which are incorporated herein) form the entire agreement between you and WILEY concerning this licensing transaction and (in the absence of fraud) supersedes all prior agreements and representations of the parties, oral or written. This Agreement

may not be amended except in writing signed by both parties. This Agreement shall be binding upon and inure to the benefit of the parties' successors, legal representatives, and authorized assigns.

- In the event of any conflict between your obligations established by these terms and conditions and those established by CCC's Billing and Payment terms and conditions, these terms and conditions shall prevail.
- WILEY expressly reserves all rights not specifically granted in the combination of (i) the license details provided by you and accepted in the course of this licensing transaction, (ii) these terms and conditions and (iii) CCC's Billing and Payment terms and conditions.
- This Agreement will be void if the Type of Use, Format, Circulation, or Requestor Type was misrepresented during the licensing process.
- This Agreement shall be governed by and construed in accordance with the laws of the State of New York, USA, without regards to such state's conflict of law rules. Any legal action, suit or proceeding arising out of or relating to these Terms and Conditions or the breach thereof shall be instituted in a court of competent jurisdiction in New York County in the State of New York in the United States of America and each party hereby consents and submits to the personal jurisdiction of such court, waives any objection to venue in such court and consents to service of process by registered or certified mail, return receipt requested, at the last known address of such party.

WILEY OPEN ACCESS TERMS AND CONDITIONS

Wiley Publishes Open Access Articles in fully Open Access Journals and in Subscription journals offering Online Open. Although most of the fully Open Access journals publish open access articles under the terms of the Creative Commons Attribution (CC BY) License only, the subscription journals and a few of the Open Access Journals offer a choice of Creative Commons Licenses. The license type is clearly identified on the article.

The Creative Commons Attribution License

The Creative Commons Attribution License (CC-BY) allows users to copy, distribute and transmit an article, adapt the article and make commercial use of the article. The CC-BY license permits commercial and non-

Creative Commons Attribution Non-Commercial License

The Creative Commons Attribution Non-Commercial (CC-BY-NC)License permits use, distribution and reproduction in any medium, provided the original work is properly cited and is not used for commercial purposes.(see below)

Creative Commons Attribution-Non-Commercial-NoDerivs License

The Creative Commons Attribution Non-Commercial-NoDerivs License (CC-BY-NC-ND) permits use, distribution and reproduction in any medium, provided the original work is properly cited, is not used for commercial purposes and no modifications or adaptations are made. (see below)

Use by commercial "for-profit" organizations

Use of Wiley Open Access articles for commercial, promotional, or marketing purposes requires further explicit permission from Wiley and will be subject to a fee.

Further details can be found on Wiley Online Library

http://olabout.wiley.com/WileyCDA/Section/id-410895.html

Other Terms and Conditions:

v1.10 Last updated September 2015

Copyright Clearance Center RightsLink®

Home | Account Info | Help

ACS Publications
Most Trusted. Most Cited. Most Read.

Title: Biodegradable Nanoneedles for Localized Delivery of Nanoparticles in Vivo: Exploring the Biointerface
Author: Ciro Chiappini, Jonathan O. Martinez, Enrica De Rosa, et al
Publication: ACS Nano
Publisher: American Chemical Society
Date: May 1, 2015
Copyright © 2015, American Chemical Society

Logged in as:
Catherine Hansel
Imperial College
Account #:
3001174884
LOGOUT

PERMISSION/LICENSE IS GRANTED FOR YOUR ORDER AT NO CHARGE

This type of permission/license, instead of the standard Terms & Conditions, is sent to you because no fee is being charged for your order. Please note the following:

- Permission is granted for your request in both print and electronic formats, and translations.
- If figures and/or tables were requested, they may be adapted or used in part.
- Please print this page for your records and send a copy of it to your publisher/graduate school.
- Appropriate credit for the requested material should be given as follows: "Reprinted (adapted) with permission from (COMPLETE REFERENCE CITATION). Copyright (YEAR) American Chemical Society." Insert appropriate information in place of the capitalized words.
- One-time permission is granted only for the use specified in your request. No additional uses are granted (such as derivative works or other editions). For any other uses, please submit a new request.

If credit is given to another source for the material you requested, permission must be obtained from that source.

BACK | CLOSE WINDOW

Copyright © 2017 Copyright Clearance Center, Inc. All Rights Reserved. Privacy statement. Terms and Conditions.
Comments? We would like to hear from you. E-mail us at customercare@copyright.com

ELSEVIER LICENSE
TERMS AND CONDITIONS

Aug 24, 2017

This Agreement between Imperial College -- Catherine Hansel ("You") and Elsevier ("Elsevier") consists of your license details and the terms and conditions provided by Elsevier and Copyright Clearance Center.

License Number	4175230442238
License date	Aug 24, 2017
Licensed Content Publisher	Elsevier
Licensed Content Publication	European Journal of Cell Biology
Licensed Content Title	Basement membrane fragments in the context of the epithelial-to-mesenchymal transition
Licensed Content Author	Christine-Maria Horejs
Licensed Content Date	Nov 1, 2016
Licensed Content Volume	95
Licensed Content Issue	11
Licensed Content Pages	14
Start Page	427
End Page	440
Type of Use	reuse in a thesis/dissertation
Portion	figures/tables/illustrations
Number of figures/tables/illustrations	2
Format	both print and electronic
Are you the author of this Elsevier article?	No
Will you be translating?	No
Original figure numbers	Figure 1, 2
Title of your thesis/dissertation	Microscopy of interactions at the cell-material and call-matrix interface
Expected completion date	Oct 2017
Estimated size (number of pages)	200
Requestor Location	Imperial College Imperial College London Imperial College Rd Kensington, London SW7 2AZ United Kingdom Attn: Imperial College
Publisher Tax ID	GB 494 6272 12
Total	0.00 GBP
Terms and Conditions	

INTRODUCTION

1. The publisher for this copyrighted material is Elsevier. By clicking "accept" in connection with completing this licensing transaction, you agree that the following terms and conditions apply to this transaction (along with the Billing and Payment terms and conditions

1. The publisher for this copyrighted material is Elsevier. By clicking "accept" in connection with completing this licensing transaction, you agree that the following terms and conditions apply to this transaction (along with the Billing and Payment terms and conditions established by Copyright Clearance Center, Inc. ("CCC"), at the time that you opened your Rightslink account and that are available at any time at http://myaccount.copyright.com).

GENERAL TERMS

2. Elsevier hereby grants you permission to reproduce the aforementioned material subject to the terms and conditions indicated.

3. Acknowledgement: If any part of the material to be used (for example, figures) has appeared in our publication with credit or acknowledgement to another source, permission must also be sought from that source. If such permission is not obtained then that material may not be included in your publication/copies. Suitable acknowledgement to the source must be made, either as a footnote or in a reference list at the end of your publication, as follows:

"Reprinted from Publication title, Vol /edition number, Author(s), Title of article / title of chapter, Pages No., Copyright (Year), with permission from Elsevier [OR APPLICABLE SOCIETY COPYRIGHT OWNER]." Also Lancet special credit - "Reprinted from The Lancet, Vol. number, Author(s), Title of article, Pages No., Copyright (Year), with permission from Elsevier."

4. Reproduction of this material is confined to the purpose and/or media for which permission is hereby given.

5. Altering/Modifying Material: Not Permitted. However figures and illustrations may be altered/adapted minimally to serve your work. Any other abbreviations, additions, deletions and/or any other alterations shall be made only with prior written authorization of Elsevier Ltd. (Please contact Elsevier at permissions@elsevier.com). No modifications can be made to any Lancet figures/tables and they must be reproduced in full.

6. If the permission fee for the requested use of our material is waived in this instance, please be advised that your future requests for Elsevier materials may attract a fee.

7. Reservation of Rights: Publisher reserves all rights not specifically granted in the combination of (i) the license details provided by you and accepted in the course of this licensing transaction, (ii) these terms and conditions and (iii) CCC's Billing and Payment terms and conditions.

8. License Contingent Upon Payment: While you may exercise the rights licensed immediately upon issuance of the license at the end of the licensing process for the transaction, provided that you have disclosed complete and accurate details of your proposed use, no license is finally effective unless and until full payment is received from you (either by publisher or by CCC) as provided in CCC's Billing and Payment terms and conditions. If full payment is not received on a timely basis, then any license preliminarily granted shall be deemed automatically revoked and shall be void as if never granted. Further, in the event that you breach any of these terms and conditions or any of CCC's Billing and Payment terms and conditions, the license is automatically revoked and shall be void as if never granted. Use of materials as described in a revoked license, as well as any use of the materials beyond the scope of an unrevoked license, may constitute copyright infringement and publisher reserves the right to take any and all action to protect its copyright in the materials.

9. Warranties: Publisher makes no representations or warranties with respect to the licensed material.

10. Indemnity: You hereby indemnify and agree to hold harmless publisher and CCC, and their respective officers, directors, employees and agents, from and against any and all claims arising out of your use of the licensed material other than as specifically authorized pursuant to this license.

11. No Transfer of License: This license is personal to you and may not be sublicensed, assigned, or transferred by you to any other person without publisher's written permission.

12. No Amendment Except in Writing: This license may not be amended except in a writing signed by both parties (or, in the case of publisher, by CCC on publisher's behalf).

13. Objection to Contrary Terms: Publisher hereby objects to any terms contained in any purchase order, acknowledgment, check endorsement or other writing prepared by you, which terms are inconsistent with these terms and conditions or CCC's Billing and Payment

6.2 List of publications

E. Thomas Pashuck, Benoît J R Duchet, Catherine S Hansel, Stephanie A Maynard, Lesley W Chow, and Molly M Stevens, Controlled sub-nanometer epitope spacing in a three dimensional self-assembled peptide hydrogel, *ACS Nano*, 2016, 10 (12), 11096-11104.

Eunjung Kim, Limor Zwi-Dantsis, Natalie Reznikov, Catherine S Hansel, Shih-Ting Wang, and Molly M Stevens, One-pot synthesis of multiple protein-encapsulated DNA flowers for intracellular protein delivery, *Adv. Mater, 2017*, 1701086.

Christine-Maria Horejs, Jean-Philippe St-Pierre, Juha RM Ojala, Joseph A.M. Steele, Patricia Barros da Silva, Angela Rynne-Vidal, Stephanie Maynard, Catherine S Hansel, Clara Rodríguez-Fernández, Manuel M. Mazo, Amanda YF You, Alex J Wang, Thomas von Erlach, Karl Tryggvason, Manuel López-Cabrera and Molly M Stevens, Preventing tissue fibrosis by local biomaterials-interfacing of specific cryptic extracellular matrix information, *Nat. Commun.,* 2017, 8, 15509.

Catherine S Hansel, Spencer W Crowder, Samuel Cooper, Sahana Gopal, Maria João Pardelha da Cruz, Leonardo de Oliveira Martins, Stephen Rothery, Michele Becce, Anthony E G Cass, Chris Bakal, Ciro Chiappini and Molly M Stevens, Nanoneedle stimulation of mechanoresponsive organelles reveals divergent lamin and YAP regulation, under review.